

DEVELOPMENT OF MICROSCALE IMMUNOASSAYS USING  
AQUEOUS TWO-PHASE SYSTEMS

by

Alyne Grasiela Teixeira

Submitted in partial fulfillment of the requirements  
for the degree of Doctor of Philosophy

at

Dalhousie University  
Halifax, Nova Scotia  
September 2021

© Copyright by Alyne Grasiela Teixeira, 2021

## **DEDICATION**

To my parents, Teresinha and João, in loving memory.

# TABLE OF CONTENTS

LIST OF TABLES .....	vii
LIST OF FIGURES .....	viii
ABSTRACT .....	x
LIST OF ABBREVIATIONS AND SYMBOLS USED .....	xi
ACKNOWLEDGEMENTS .....	xiv
CHAPTER 1 INTRODUCTION .....	1
CHAPTER 2 AQUEOUS TWO-PHASE SYSTEM (ATPS) .....	19
2.1 ABSTRACT .....	19
2.2 INTRODUCTION .....	20
2.3 ATPS PROPERTIES .....	21
2.3.1 The Separation of Phases .....	22
2.3.2 The Physicochemical Properties of The Bulk Phases .....	25
2.3.2.1 Viscosity .....	25
2.3.2.2 Density .....	26
2.3.2.3 Osmolarity .....	26
2.3.2.4 Hydrophobicity .....	27
2.4 THE ATPS INTERFACE .....	28
2.5 PARTITIONING OF MOLECULES AND PARTICLES .....	30
2.6 EMERGING APPLICATIONS OF ATPS .....	32
2.6.1 Cell Micropatterning and Microtissue Engineering with ATPS .....	32
2.6.1.1 Cell Micropatterning for Analysis of Growth and Differentiation .....	33
2.6.1.2 Cell Micropatterning for Engineering Mammalian Cell-Cell Interactions .....	35
2.6.1.3 Cell Micropatterning for Engineering Microbial Growth Microenvironments .....	37
2.6.1.4 Self-Assembly of Cell and Tissue Constructs in ATPSs .....	41
2.6.2 Solution Microarrays for Biochemical Analysis .....	45
2.6.3 Microfluidics .....	51
2.6.3.1 Continuous Microfluidic Devices .....	53
2.6.3.2 Droplet Microfluidics .....	56
2.6.4 ATPSs in Synthetic Biology .....	60
2.7 SUMMARY AND OUTLOOK .....	61
CHAPTER 3 ATPS SCALABILITY – FROM FEMTOLITERS TO LITERS .....	64

3.1	ABSTRACT .....	64
3.2	INTRODUCTION.....	65
3.3	MATERIALS AND METHODS .....	69
3.3.1	Materials and Methods.....	69
3.3.1.1	ATPS Formulations .....	69
3.3.1.2	Microchannel Fabrication.....	69
3.3.1.3	Imaging.....	70
3.3.1.4	Droplet Volume Quantification .....	70
3.4	RESULTS AND DISCUSSION .....	71
3.5	CONCLUSIONS.....	79
3.6	ATPS APPLICATIONS USING VOLUMES RANGING FROM nL TO $\mu$ L .....	79
3.6.1	Biomolecule and Cell Encapsulation .....	79
3.6.2	Multiplexed ATPS-ELISA and ATPS-AlphaLISA .....	84
3.6.3	Cost-Effective Single ATPS-ELISA and ATPS-ELISpot .....	86
3.7	ATPS APPLICATIONS USING VOLUMES RANGING FROM mL TO L .....	89
3.8	CONCLUSIONS.....	93
CHAPTER 4 DEVELOPMENT AND OPTIMIZATION OF A COST-EFFECTIVE SINGLE ATPS-ELISA .....		95
4.1	ABSTRACT .....	95
4.2	INTRODUCTION.....	96
4.3	MATERIALS AND METHODS .....	99
4.3.1	Aqueous Two-Phase System Formulations .....	99
4.3.2	Optimization of Polymer Concentrations .....	100
4.3.3	Confinement of Antibodies in the PEG-Dextran System for ELISA.....	100
4.3.4	Optical Crosstalk Analysis.....	102
4.3.5	Analysis of Assay Performance Characteristics .....	102
4.3.6	Statistical Analysis.....	103
4.4	RESULTS AND DISCUSSION .....	103
4.4.1	Sandwich ELISA using the PEG-Dextran ATPS.....	103
4.4.2	The PEG-Dextran System Minimizes Consumption of Capture and Detection Antibodies in Sandwich ELISA .....	105
4.4.3	ATPS-ELISA Produces Comparable Performance Characteristics to Conventional Sandwich ELISA, while Requiring Lower Capture and Detection Antibody Volumes.....	110
4.4.4	Cost Comparisons Between ELISA Methods.....	114
4.5	CONCLUSIONS.....	117

CHAPTER 5	DEVELOPMENT AND CHARACTERIZATION OF A NOVEL <i>IN VITRO</i> ATPS-BASED VACCINE SCREENING PLATFORM .....	118
5.1	ABSTRACT .....	118
5.2	INTRODUCTION .....	119
5.3	MATERIALS AND METHODS .....	121
5.3.1	PEG- and PEO-BSA Binodals .....	121
5.3.2	Microdroplet Characterization .....	122
5.3.3	Effects of Salt on Phase Separation .....	123
5.3.4	Jurkat T Cell Culture.....	123
5.3.5	RPMI-8226 B Cell Culture .....	124
5.3.6	Cell Viability Assessment.....	124
5.3.7	Jurkat T Cell Activation.....	125
5.3.8	RPMI-8226 B Cell Activation .....	126
5.3.9	Measurement of IL-2 and IL-6 Secretion.....	126
5.3.10	Confinement of Cells in the PEG-BSA System for ELISpot Assay .....	127
5.3.11	Measurement of IL-6 Confinement.....	128
5.4	RESULTS AND DISCUSSION .....	129
5.5	CONCLUSIONS.....	147
CHAPTER 6	SCREENING VACCINE FORMULATIONS IN THE ATPS-ELISpot ASSAY .....	148
6.1	ABSTRACT .....	148
6.2	INTRODUCTION.....	149
6.3	MATERIALS AND METHODS .....	157
6.3.1	HA Titration.....	157
6.3.2	Single Adjuvant Screening.....	159
6.3.3	Statistical Analysis.....	161
6.4	RESULTS AND DISCUSSION .....	161
6.4.1	HA Titration.....	161
6.4.2	Single Adjuvant Screening.....	162
6.4.2.1	Pam3CSK4 (TLR2/1 Agonist) .....	163
6.4.2.3	LPS (TLR4 Agonist) .....	165
6.4.2.4	Imiquimod (TLR7 Agonist).....	166
6.4.2.5	CpG (TLR9 Agonist).....	167
6.4.3	Single Adjuvant Screening using ATPS-ELISpot versus Conventional ELISpot.....	172

6.4.4	Partitioning of TLR Agonists in the PEG-BSA System .....	173
6.4.5	Cost-Effective ATPS-ELISpot versus Other Cell-Based Immunoassays .....	177
6.5	CONCLUSION .....	180
CHAPTER 7 CONCLUSIONS AND FUTURE DIRECTIONS .....		181
7.1	SUMMARY AND CONCLUSIONS .....	181
7.2	NOVEL CONTRIBUTIONS TO SCIENCE .....	183
7.3	RECOMMENDATIONS FOR FUTURE WORK .....	184
BIBLIOGRAPHY .....		186
APPENDIX A: COPYRIGHT PERMISSION LETTERS .....		216

## LIST OF TABLES

<b>Table 1</b>	Examples of proteins partitioned in various two-phase systems ..... 7
<b>Table 2</b>	Examples of bioproduct purification using ATPS at various scales ..... 92
<b>Table 3</b>	TLR agonists as potential adjuvants to influenza vaccines ..... 154
<b>Table 4</b>	TLR agonists used in the single adjuvant screening assay ..... 160
<b>Table 5</b>	Hypotheses to which phase each TLR agonist may partition ..... 176

## LIST OF FIGURES

Figure 1	The evolution of ATPS-based technologies .....	21
Figure 2	Binodal phase diagram.....	23
Figure 3	Overview of ATPS cell micropatterning techniques .....	34
Figure 4	Applications of ATPSs in microbial culture.....	39
Figure 5	Overview of ATPS-facilitated microtissue engineering .....	43
Figure 6	ATPS-based immunoassay techniques .....	47
Figure 7	Applications of ATPSs in continuous and droplet microfluidic systems .....	52
Figure 8	Areas of future growth for applied ATPS research .....	63
Figure 9	Binodal phase diagram and images of PEG-dextran emulsions .....	66
Figure 10	Schematic diagram of the microfluidic device and images of PEG-dextran emulsions within microchannels.....	73
Figure 11	Distribution of droplet volumes at each channel position for 3 different ATPS formulations .....	75
Figure 12	Size comparison between vaccine delivery systems and the size range of microfluidic ATPS droplets.....	77
Figure 13	Microencapsulation of biomolecules and cells using ATPS.....	83
Figure 14	ATPS-based immunoassays.....	88
Figure 15	Schematic representation of molecule purification using ATPS .....	89
Figure 16	Monoclonal antibody clarification and purification via membrane-based separation and ATPS extraction.....	91
Figure 17	Comparison of the ATPS-ELISA method to conventional sandwich ELISA .....	105
Figure 18	Optimization of polymer concentrations .....	106
Figure 19	Optimization of antibody solution volumes.....	108
Figure 20	Comparison of standard curves for TGF- $\beta$ 1 and CRP between conventional sandwich ELISA and ATPS-ELISA .....	109
Figure 21	Performance characteristics of ATPS-ELISA compared to conventional sandwich ELISA using blank wells next to the lowest standard concentration.....	111
Figure 22	Performance characteristics of ATPS-ELISA compared to conventional sandwich ELISA using blank wells next to the highest standard concentration.....	112



Figure 23	Bland–Altman analysis of agreement between conventional sandwich ELISA and ATPS-ELISA.....	113
Figure 24	Comparison of optical crosstalk between ATPS-ELISA and conventional sandwich ELISA .....	114
Figure 25	Comparison of assay costs .....	116
Figure 26	Binodal curves for PEG- and PEO-BSA systems.....	131
Figure 27	Representative images (10X) of microdroplet emulsions in PEO 900 kDa-BSA systems with addition of NaCl (A), HEPES (B), NaHCO <sub>3</sub> (C), NAH <sub>2</sub> PO <sub>4</sub> (D).....	134
Figure 28	Jurkat T cell and RPMI-8226 B cell viability in ATPS-polymer solutions .....	136
Figure 29	Cytokine secretion by Jurkat T cells and RPMI-8226 B cells .....	138
Figure 30	Schematic diagram of the PEG-BSA system for compartmentalized immune cell culture .....	140
Figure 31	Screening immune cells in the PEG-BSA system by ELISpot.....	142
Figure 32	Global burden of infectious diseases .....	150
Figure 33	Examples of emerging and re-emerging infectious diseases worldwide .....	151
Figure 34	Influenza virus structure .....	151
Figure 35	HA titration using ATPS-ELISpot versus conventional ELISpot assay.....	159
Figure 36	Titration of HA (A) and Bland-Altman analysis of agreement between ATPS-ELISpot and conventional ELISpot (B).....	162
Figure 37	IFN- $\gamma$ secretion from PBMCs exposed to HA alone (orange bars) or in combination with one of five TLR-agonists (black bars) .....	164
Figure 38	IFN- $\gamma$ secretion from PBMCs in the presence (black bars) or in the absence (white bars) of HA combined with one of the five TLR-agonists ..	167
Figure 39	Stimulation of TLR9 signaling pathways by CpG.....	170
Figure 40	Variation of IFN- $\gamma$ secretion across PBMC lots .....	171
Figure 41	Single adjuvant screening using ATPS-ELISpot versus conventional ELISpot.....	173
Figure 42	FTIR spectra of TLR agonists in 10% BSA solution (A) and 7% PEG solution (B) .....	174
Figure 43	Cost comparisons between ELISpot assays.....	179

## ABSTRACT

Aqueous two-phase systems (ATPSs) have been traditionally applied in liquid-liquid extraction processes to purify and recover biological products. Due to their high biocompatibility, easy handling, and potential to be scaled up, ATPSs have also been applied in nonconventional innovative applications, such as solution microarrays to improve performance and cost-effectiveness of immunoassays.

The enzyme linked immunoassay (ELISA) has numerous applications in clinics, industrial R&D, environmental surveillance, forensics, and academic research. However, the high cost of biologic reagents, such as antibodies, and relatively time-consuming protocols represent significant drawbacks. The enzyme-linked immunospot (ELISpot) is a cell-based assay widely used to evaluate vaccine formulations *in vitro*. However, it requires considerable amounts of expensive vaccine reagents.

In this thesis, two innovative ATPS-based platforms were developed to reduce the amount of capture and detection antibodies required for single sandwich ELISA and to minimize the amount of vaccine reagents required for vaccine formulation screening by ELISpot. An ATPS composed of poly (ethylene glycol) (PEG) and dextran was used to confine antibodies for multiplex analyte detection in the so-called ATPS-ELISA, which consumed 3-fold less capture and 2.5-fold detection antibodies compared to conventional sandwich ELISA. The novel PEG-bovine serum albumin (BSA) system was used to confine immune cells and vaccine reagents in microdroplet reactors, which enabled screening hemagglutinin (antigen) and Toll-like receptors (TLR) agonists (adjuvants), using only a fifth of the amounts required by conventional ELISpot.

Therefore, the ATPS-based techniques presented in this thesis can improve the cost-effectiveness of immunoassays such as ELISA and ELISpot. In both cases, the consumption of expensive reagents has been significantly reduced, while producing comparable performance characteristics compared to conventional assays. Thus, ATPS-based methods have high potential for the development of innovative immunoassay technologies.

## LIST OF ABBREVIATIONS AND SYMBOLS USED

ABPA	Allergic bronchopulmonary aspergillosis
ACM	Antibody colocalization microarray
ANOVA	Analysis of variance
APC	Antigen-presenting cells
ASL	Adenyl succinate lyase
ATIC	5-aminoimidazole-4-carboxamide ribonucleotide transformylase/inosine monophosphate cyclohydrolase
ATPS	Aqueous two-phase system
BCIP/NBT	5-Bromo-4-chloro-3-indolyl phosphate/nitro blue tetrazolium
BSA	Bovine serum albumin
C-AM	Calcein-AM
CCD	Charge-coupled device
CD	Cluster of differentiation
CH <sub>2</sub>	Hydrocarbons
CO <sub>2</sub>	Carbon dioxide
COOH	Carboxylic acid
COVID-19	Coronavirus disease 2019
CPG ODN	CpG oligodeoxynucleotides
CRP	C-reactive protein
CXCL	C-X-C motif chemokine ligand
CXCR	C-X-C motif chemokine receptor
D <sub>2</sub> O	Heavy water
DEX	Dextran
MyD88	Myeloid differentiation factor 88
DAMP	Damage-associated molecular patterns
DMEM	Dulbecco's modified eagle's medium
ECM	Extracellular matrix
ELISA	Enzyme-linked immunosorbent assay

ELISpot	Enzyme-linked immunospot
EO/PO	Ethylene oxide/propylene oxide
FBS	Fetal bovine serum
FITC	Fluorescein isothiocyanate
FTIR	Fourier-transform infrared spectroscopy
GLA-SE	Glucopyranosyl lipid adjuvant–stable emulsion
GLM	General linear model
GVHD	Graft versus host disease
HA	Hemagglutinin
HEPES	4-(2-hydroxyethyl)-1-piperazineethanesulfonic acid
HRP	Horse radish peroxidase
IBBC	Integrated blood barcode chip
IDO	Indoleamine 2,3-dioxygenase
IFN-g	Interferon gamma
IL	Interleukin
IMDM	Iscove's modified Dulbecco's media
K	Partitioning coefficient
K <sub>3</sub> PO <sub>4</sub>	Potassium phosphate
LDR	Linear dynamic range
LFA	Lateral-flow immunoassay
LOD	Limit of detection
LPS	Lipopolysaccharide
mPAD	Microfluidic paper-based analytical devices
MPL	Monophosphoryl lipid A
MW	Molecular weight
NaHCO <sub>3</sub>	Sodium bicarbonate
NaH <sub>2</sub> PO <sub>4</sub>	Monosodium phosphate
NaCl	Sodium chloride
Pam3CSK4	Pam3CysSerLys4

PAMP	Pathogen-associated molecular patterns
PBMC	Peripheral blood mononuclear cells
PBS	Phosphate buffered saline
PBST	PBS with Tween 20
PDMS	Polydimethylsiloxane
PEG	Poly(ethylene glycol)
PEGDA	Poly(ethylene glycol) diacrylate
PEO	Poly(ethylene oxide)
PI	Propidium iodide
PLGA	Poly(lactide-co-glycolide)
PMA	Phorbol-12-myristate-13-acetate
POC	Point-of-care
PRR	Pattern-recognition receptors
PSA	Prostate-specific antigen
RANTES	Regulated on activation, normal T expressed and secreted
RPMI	Roswell Park Memorial Institute medium
SARS	Severe acute respiratory syndrome
SCN	Sodium thiocyanate
SD	Standard deviation
SIA	Solvent interaction analysis
SPRi	Surface plasmon resonance imaging
TGF- $\beta$	Transforming growth factor beta
TLL	Tie line length
TLR	Toll-like receptor
TMAO	Trimethylamine N-oxide
TNF	Tumor necrosis factor
TRIF	TIR-domain-containing adapter-inducing interferon- $\beta$
UV	Ultraviolet

## ACKNOWLEDGEMENTS

I sincerely appreciate the great mentorship from my supervisor, Dr. John Frampton, throughout my PhD project. I am grateful for your support, time, optimism, encouragement, and opportunities provided over the last five years. Additionally, I'd like to thank my supervisory committee members: Dr. Brendan Leung, Dr. Mark Filiaggi, and Dr. Jun Wang for their insightful feedback and advice towards the development of my project. Your guidance has led me to grow significantly as a researcher.

I would like to express my sincere gratitude for my lab mates, past and present, for their friendship, support and encouragement throughout the years: Rishima Agarwal, Kristin Ko, Angela Tsai, Leo Liu, Maia Kvas, Nicky Tam, Jonathan Tjong, Dr. Sam Baldwin, Mady Thompson, Dr. Swomitra Palit, Dr. Surendra Verma, among others.

In special, I'd like to thank my lovey friend (and ex-roomie) Rishima Agarwal, who opened her heart and her house and empathetically helped in a very difficult moment of my life. You are a very caring person, and your kindness is your superpower! I'd like also to give special thanks to my friend Kristin Ko, who has always been available to help me in and out the lab, and for being someone who I can always count on. Thank you both for all the support and such a warm welcome when I started in the lab five years ago.

I acknowledge the Nova Scotia Graduate Scholarship and the Scotia Scholars Award from the Nova Scotia Provincial Government for the financial support of my graduate studies and this project.

Finally, I want to thank my family and friends (from far and near) for their amazing support and encouragement. In special, I'd like to thank Tim MacDonald for his continuous support and healthy snacks. And the MacDonald family for being my Canadian family and for supporting me since I arrived in Canada.

## CHAPTER 1

## INTRODUCTION

Immunoassays play an essential role in clinical analysis, industrial R&D, environmental surveillance, forensics, and academic research<sup>1</sup>. Between 2010 and 2020, there were more than 128,000 scientific articles published that mention immunoassay as the main method of analysis<sup>2,3</sup>. The global immunoassay market is expected to reach 27 billion dollars by 2023 from 20 billion dollars in 2018. The market growth is mainly driven by the increasing incidence of chronic and infectious diseases, technological advancements in immunoassay instruments and introduction of novel automated systems, growth in the biotechnology and biopharmaceutical industries, increasing adoption of immunoassay-based point-of-care and testing<sup>4,5</sup>.

These assays are highly adaptable and can be applied to many formats depending on the needs of the end-user, which includes hospitals, clinical laboratories, blood banks, research institutes, academic institutes, pharmaceutical, and biotechnology companies<sup>4,5</sup>. Sandwich immunoassays are very specific and sensitive due to the use of monoclonal antibodies (mAb) which can recognize only one epitope on an antigen. Labels attached to antibodies may be radioactive, enzymes, chemiluminescent, fluorescent, and metallic ions<sup>6</sup>. Among enzymatic immunoassays, the enzyme linked-immunosorbent assay (ELISA) has been widely used to detect several biomarkers, including hormones, antigens, and antibodies secreted in response to allergies and infections<sup>7-10</sup>. However, conventional ELISA platforms have limited detection sensitivity, which may hinder the detection of small concentrations of biomarkers in the early stages of many diseases. Over the last decade, ELISA has become more sophisticated to the point of being able to

detect clinically relevant proteins, such as prostate-specific antigen (PSA), at sub-femtomolar concentrations<sup>11</sup>.

Another key immunoassay in biomedical research is the enzyme-linked-immunospot (ELISpot). ELISpot has gained much attention over the last years due to its high sensitivity, functionality, and relative simplicity. These characteristics have made it one of the most attractive immunoassays for different applications in the field of infectious diseases, allergy, transplantation diagnostics, autoimmune disorders, and vaccination studies<sup>12-19</sup>. The ELISpot assay enables detection of cytokine or antibody secretion on a single-cell level, with a higher sensitivity than ELISA or intracellular staining, improving measurement of very low densities of analyte-producing cells<sup>20</sup>. In addition, cells used in ELISpot can be further characterized afterward, because they are not fixed or killed during the procedure<sup>21</sup>. FluoroSpot, an advanced assay derived from ELISpot, measures several analytes at the single-cell level simultaneously, because it uses fluorescent detection reagents rather than chromogenic substrates<sup>21</sup>.

The main limitations of immunoassays are the time associated with performing the assays and the cost associated with biologic reagents. These limitations have motivated the development of a large variety of microscale immunoassays that reduce the number of steps, shorten incubation times, lower the volumes of reagents and samples, or allow the assay to be multiplexed to measure multiple analytes from the same sample. In attempt to reduce assay time and cost, higher throughput technologies have been developed. Microfluidic systems have enabled reduction of cost and time by increasing surface-to-volume ratio for mass transport within microchannels, and by integrating the procedure with other functions, such as valves, pumps, mixers, and detectors<sup>22,23</sup>.



Microfluidic immunoassays have recently attracted much attention due to their portability arising from their compact format, which is an essential aspect for point-of-care (POC) applications. For example, an integrated blood barcode chip (IBBC) has been designed to perform blood separation and plasma protein measurement from a finger prick. The IBBC enabled measurement of a panel of 12 protein biomarkers from microliter volumes of whole human blood within 10 min of sample collection<sup>24</sup>. Another microfluidic platform has been developed to monitor cytokine secretion upon continued long-term cell culture of T lymphocytes. Previously stimulated T cells were injected on antibody-based biochip, where they were captured by specific antibodies that recognized their surface differentiation markers. Then, the cytokines secreted by the T cells were detected by their specific antibodies. Cytokine secretions were analyzed either by immunofluorescence after 24 hours of on-chip cell culture or by direct measurement using Surface Plasmon Resonance Imaging (SPRi) for up to 65 hours<sup>25</sup>. More recently, a point-of-care microfluidic immunoassay has been developed for the diagnosis of coronavirus disease 2019 (COVID-19). The microfluidic device integrates a fluorescence detection analyzer and multiple immunoassay microchips, specifically designed to detect three COVID-19 biomarkers (IgG, IgM, and antigen). This platform is portable, easy-to-use, sensitive, fast (<15 min), and can detect the three biomarkers simultaneously<sup>26</sup>.

However, these platforms are not available for most life science laboratories and clinical chemistry laboratories. In this respect, a polymer-based system is a versatile technology that can address these drawbacks, contributing to the development of cost-effective assays that require simple sample manipulation. These systems are based on the colocalization of antibodies, which have been achieved by depositing capture antibodies

(cAbs) and detection antibodies (dAbs) at precise locations on nitrocellulose films or nitrocellulose coated slides using a snap chip device<sup>27-29</sup>.

Antibody colocalization can also be achieved using an aqueous two-phase system (ATPS) composed of two thermodynamically incompatible polymers that phase-separate from each other. ATPS phase-separation enables the confinement of both cells and reagents into microdroplets, without affecting cell viability and proliferation. ATPS-based platforms require a lower amount of reagents in comparison to conventional assays. Therefore, they can contribute to decreasing costs while allowing simple sample manipulation<sup>30</sup>.

ATPS has been exploited for a wide variety of biotechnology applications since when the phenomenon was first recognized by the microbiologist Martinus Beijerinck in 1896. However, ATPS application began in the 1950s, when Per-Åke Albertsson used a variety of polymer-polymer and polymer-salt solutions for isolating biomolecules, viruses, cells, and cell fragments by exploiting the preferential distribution of materials between phases, according to their physicochemical properties, a phenomenon known as partitioning<sup>31</sup>. Physicochemical characteristics of the target molecule (e.g., hydrophobicity, charge, molecular weight), and their interactions with the liquid-liquid system (e.g., composition, ionic strength, pH) are determinants of their partition coefficient<sup>32</sup>. Separation of biomolecules in aqueous two-phase systems can be achieved by manipulating these physicochemical properties to increase partition coefficient (K-value) from one phase to another<sup>33</sup>. K-value is defined as the ratio of the solute concentration in the top phase to the solute concentration in the bottom phase. Aqueous polymer-polymer and polymer-salt systems have been extensively studied and used for

several years<sup>34</sup>. Due to their high biocompatibility, high-water content, and low interfacial tension, ATPS provides a suitable environment for partitioning biological materials<sup>32</sup>. The phases of an ATPS can be viewed as two different solvents of the same aqueous nature, which can be tuned to favor partitioning to the bottom or top phase<sup>35,36</sup>. Partitioning of peptides with different CH<sub>2</sub> chain lengths in PEG-dextran systems was investigated, and as expected, peptides with longer chain lengths (greater hydrophobicity) presented higher K-values<sup>33</sup>. The effect of hydrophobicity of proteins was also investigated using polymer-salt systems: PEG 4,000-phosphate, sulfate, and citrate in the presence of low and high levels of NaCl (0.6 to 8.8% w/w). At high concentrations of NaCl, the partition coefficient, K, was higher for all systems, with the resolution (the ability of the system to discriminate between proteins with different hydrophobicities) increased 3 to 4 times. These results suggested that the presence of NaCl in the systems increased protein partitioning to the more hydrophobic phase (PEG)<sup>37</sup>. This can be explained by the fact that adding NaCl to the systems increases the tie line length (TLL), which means that the water content is reduced and, therefore, the system becomes more hydrophobic<sup>38</sup>. Particularly, the PEG-citrate system showed a higher hydrophobic resolution compared to the other systems, suggesting that system hydrophobicity had greater relevance in protein partitioning in PEG-citrate systems<sup>37</sup>. The larger the TLL, the more hydrophobic the ATPS compositions are, i.e., higher polymer/salt concentrations mean lower water content in the system<sup>38</sup>.

In general, larger differences in hydrophobicity between the two ATPS-forming polymers increase the likelihood of the system to phase separate. For example, adding hydrophilic side chains to dextran intensifies its separation from PEG<sup>31</sup>. Another example

can also illustrate this feature: the system composed of the copolymer ethylene oxide/propylene oxide (EO/PO) and dextran. Compared to the PEG-dextran system, EO/PO-dextran system has a larger hydrophobicity difference, because EO/PO is more hydrophobic than PEG, which is, therefore, more likely to phase separate<sup>39</sup>. Therefore, in polymer-polymer systems, it is possible to favor partitioning to one of the phases by increasing the difference of hydrophobicity between them.

In polymer-salt systems, PEG is often used as one of the phase-forming components because it is unexpansive and easily separates from salts. Phosphates and sulfates are salts with ATPS forming capabilities, however, they are not eco-friendly. It has been suggested to use organic salts such as citrates and tartrates due to their biodegradability and non-toxicity<sup>40,41</sup>. One strategy to manipulate the hydrophobicity of both polymer-polymer and polymer-salt systems is by varying the TLL. The composition of the two phases is represented by points on the binodal curve. Above the binodal are the polymer/salt concentrations that phase separate and form ATPS. Each tie line connects two points on the binodal that represent the composition of the bottom and the top phase in equilibrium<sup>42</sup>.

The partitioning in ATPSs can also be tuned by altering the type of ions in the system or adding a salt such as NaCl. Studies have shown that hydrophobic proteins can be separated from their contaminants extremely efficiently in PEG-salt systems with the addition of NaCl at different concentrations<sup>33</sup>. When a salt dissolves in polymer-polymer systems, it generates ions that are charged and can influence the solute-solvent interactions. As a result, the distribution of charged molecules, such as proteins, between the phases is also affected. In polymer-salt systems, the addition of NaCl changes the

ratio between the ions, which also affects the partition of charged molecules<sup>43</sup>. Franco et al.<sup>44</sup> showed that adding 6% of NaCl in a PEG 1,500-phosphate system increased the resolution for separating hydrophobic proteins from 10.2 to 25.5 (2.5-fold) and an increase in log K from -0.8 to 1.4. The addition of 6% NaCl in a PEG 4,000-phosphate promoted an increase in resolution from 22.6 to 29.0 (1.3-fold) and in log K from  $\sim -2.8$  to  $\sim 0.5$ . The addition of 9% NaCl in the PEG-dextran system increased log K from  $\sim 0$  to  $\sim 0.8$  and promoted the same resolution increase (1.3-fold) observed in the PEG 4,000-phosphate system with only 6% NaCl, which indicates that PEG 4,000-dextran systems require higher concentrations of NaCl than PEG-salt systems to promote an increase in resolution. The effect observed in the improvement of resolution and increase of log K was due to the increase in hydrophobic differences between the phases promoted by the addition of NaCl.

**Table 1** Examples of proteins partitioned in various two-phase systems

Protein	Top Phase	Bottom Phase	Salt Additive	K-value	Ref.
Thaumatococcus	PEG 10,000 (10%, w/w)	Sodium sulfate (18%, w/w)	NaCl (1%, w/w)	20.0	45
	PEG 3,000 (10%, w/w)	Potassium phosphate (17%, w/w)	NaCl (1%, w/w)	15.2	
BSA	EO-PO (8.9%, w/w)	Maltodextrin (22.5% w/w)	Na <sub>3</sub> PO <sub>4</sub> (50 mM) + NaClO <sub>4</sub> (100mM)	0.1	48
			Glutamic acid, (10 mM) + NaClO <sub>4</sub> (100mM)	1.4	
Lysozyme	PEG 8,000 (13.95%, w/w)	Sodium sulfate (8.06%, w/w)	-	0.236	51
	PEG 8,000 (15.70%, w/w)	Sodium sulfate (9.47%, w/w)	NaSCN (0.40M)	93.7	

PEG-sulfate and PEG-phosphate have been successfully optimized to separate the hydrophobic protein thaumatin<sup>45</sup>. Thaumatin is a very sweet tasting protein with a molecular weight of 22.0 kDa, and an isoelectric point (pI) of 12 (twelve)<sup>46</sup>. They found that in both systems PEG-sulfate and PEG-phosphate the main factors influencing thaumatin partitioning were the phase-forming salt and NaCl concentrations. As expected, high concentrations of NaCl favored the partitioning of thaumatin to the PEG phase. The highest thaumatin partition coefficient in the PEG-sulfate system was 20.00 (log K 1.301) and 15.24 (log K 1.183) for the PEG-phosphate system (Table 1). Because the partitioning in the PEG-sulfate system was higher, a more detailed analysis was carried out and it was observed that high salt concentration was the main factor affecting thaumatin partitioning with a 70-fold increase of K value. This effect could be associated with the presence of NaCl in the system, which increased the hydrophobicity difference between the phases and drove the hydrophobic protein from the salt phase to the PEG phase. Also, NaCl promoted an electrical potential between the phases, partitioning the protein from the bottom phase to the top phase. It has been reported that positively charged proteins are preferentially partitioned to the top phase<sup>47</sup>. Since the pH of the system was maintained at 7.0 and thaumatin pI is 12, this protein was positively charged during the partitioning, which favored its partition to the top phase. After optimization, they found that the optimal condition for thaumatin partitioning in the PEG-sulfate system was 10% PEG 3,000 (w/w), 17.76% sodium sulfate (w/w), and 0.95 M NaCl, with a K value of 24.15 (log K 1.383) and 96.02% recovery<sup>45</sup>.

The use of pH values above the pI of proteins may induce an additional affinity towards the PEG-rich phase. Bolognese and co-workers<sup>48</sup> described the partition of

bovine serum albumin (BSA) in an ATPS formed by maltodextrin and the copolymer EO/PO with different buffer solutions. The partitioning of BSA in the system showed to be very sensitive to pH changes and lyotropic ion presence. The separation was dramatically increased with the addition of glutamic acid, pH 3.1 NaClO<sub>4</sub>. Since BSA has a pI of 5.0 and the bulk phases had a pH of 3.1, BSA was positively charged during partitioning. The EO/PO phase is more hydrophobic and so is the ClO<sub>4</sub><sup>-</sup> anion, which created a negative potential in the EO/PO phase and drove BSA to the top phase to balance the negative charges carried by the perchlorate ions (Table 1).

It has also been reported that the partitioning of biomolecules in ATPSs can be manipulated by changing the polymer molecular weight (size). Increasing the molecular weight of the ATPS-forming polymers decreases the hydrophilic/hydrophobic groups ratio, and eventually increases the hydrophobicity of the system<sup>49</sup>. It is well established that increasing the polymer molecular weight, the phase diagram is shifted downwards which means that lower concentrations of polymers are required for phase separation<sup>50</sup>. It has been hypothesized that protein partitioning is affected by the volume exclusion effect caused by the larger polymers in the system, i.e., the volume available for the proteins to be partitioned is reduced by increasing polymer size<sup>38</sup>. However, this hypothesis is inconsistent with the results obtained from studies conducted by Ferreira et al.<sup>51</sup>. They showed that protein partition behavior cannot be explained in terms of polymer excluded volume effect, in agreement with other studies<sup>45</sup>. They examined 15 proteins in PEG-sodium sulfate systems using PEG with two different molecular weights, PEG 600 and PEG 8,000. The effect of two salt additives NaCl or NaSCN and different buffers with pH 7.4 on protein partitioning behavior was investigated. They found that the effects of

salt additives and the buffer concentration on the system were much more pronounced compared to PEG molecular weight on the difference between the relative hydrophobicity of the phases (Table 1). In another study, the same group demonstrated that the excluded volume effect is not the only factor that influences biomolecule behavior<sup>52</sup>. Experimental data showed that macromolecular crowding causes additional effects on so-called soft interactions, such as electrostatic, hydrophobic, and van der Waals, between the polymers (crowding agents) and the protein. In addition, they also demonstrated that the partition of both small organic compounds (amino acids) and proteins in a polymer-polymer system is drastically increased with the concentration of a non-ionic additive (trimethylamine N-oxide (TMAO))<sup>53</sup>. These results indicate that the molecular weight/size of a solute should not be considered one of the main factors influencing its partitioning, and the partition behavior of small organic compounds and proteins is governed by the solute-water interactions in the ATPS phases<sup>53</sup>.

It has been established that heavy polymers induce phase separation at low concentrations due to differences in interfacial tension<sup>54</sup>, phase density<sup>55</sup>, and viscosity<sup>56</sup>. According to the second law of thermodynamics, two compounds can mix and form a solution if the Gibbs free energy of the system ( $\Delta G$ ) is negative:  $\Delta G = \Delta H - T\Delta S < 0$ , where  $\Delta H$  represents the change in enthalpy,  $T$  represents the temperature, and  $\Delta S$  represents the change in entropy. Therefore, for phase separation to occur,  $\Delta G$  has to be positive, which means that the entropic contribution ( $T\Delta S$ ) must be smaller than the enthalpic contribution<sup>31</sup>. It is evident that temperature plays an important role in phase separation, and as such, it can also influence the partitioning of biomolecules along with the viscosity and density of the systems. Asenjo et al.<sup>56</sup> investigated the relationships



between densities and viscosities of PEG-phosphate systems with TLL. They showed that the rate of separation is strongly dependent on the viscosity of the top phase (PEG) and the density of the bottom phase (salt). Therefore, the system could be optimized in terms of separation and partitioning by playing with the TLL. It is important to mention that the settling times of the bulk phases increase with viscosity, which may affect separation efficiency and mass transfer between the two phases. The PEG-salt systems have a practical advantage over the polymer-polymer systems due to their low viscosity and, therefore, shorter setting time<sup>35</sup>.

The partitioning of biomolecules and particles is also significantly controlled by the interfacial tension between the two phases of aqueous systems. The interfacial tension of the PEG–dextran systems ranges from  $\sim 1$  to  $100 \mu\text{N/m}$  (against  $\sim 31 \text{ mN/m}$  in oil-water systems)<sup>57</sup>, depending on the molecular weights and concentrations of the polymers<sup>54</sup>. Bamberger et al. used PEG/dextran systems to analyze the influence of dextran molecular weight and temperature on partitioning. They showed that the interfacial tension increased with increasing dextran MW and that systems with the same compositions had their interfacial tensions increased as the temperature decreased. However, for systems on the same TLL, the interfacial tension was shown to increase with the temperature<sup>58</sup>. According to Forciniti et al.<sup>59</sup>, the trend between interfacial tension and temperature is not definite, and depends on the tie line length that has been investigated. For PEG-phosphate systems, de Oliveira et al.<sup>60</sup> showed that the increase in temperature increased interfacial tension values.

Modification of ATPS with biospecific affinity ligands has been used to improve recovery and purification of biological materials<sup>61</sup>. Attaching an affinity ligand to one of

the phase-forming components of the system enhances partitioning of the molecule of interest, similarly to affinity column chromatography<sup>62</sup>. Partitioning of human antibodies (IgG) using several ligands in polymer-polymer and polymer-salt systems has been investigated<sup>63,64</sup>. PEGs with different chain lengths (PEG 150 and PEG 3350) were functionalized with triazine-based ligands, terminal carboxylic acid (-COOH), and amino groups (NH<sub>2</sub>). The functionalized PEG-dextran system with diglutamic acid increased the affinity of IgG to the PEG phase, allowing the recovery of IgG in the top phase. In terms of selectivity, PEG 150-COOH was able to recover 91% of IgG in the presence of serum proteins such as albumin, while IgG did not show affinity to PEG 3350-COOH. In contrast, the functionalized PEG-phosphate system was not appropriate for the affinity partitioning of IgG. The high concentration of salts suppressed the effect of the affinity ligand by interfering in the electrostatic interaction between charged polymers and proteins charges, which agrees with previous studies conducted by Andrews et al.<sup>65</sup>. They investigated purification of thaumatin and trypsin in PEG-dextran and PEG-phosphate systems, by coupling glutathione and trypsin inhibitor as biospecific ligands in PEG molecules. Thaumatin presented a 17-fold increase in K in the PEG-dextran system with PEG-glutathione in the top phase, while the PEG-phosphate system showed a much smaller K (3-fold increase). Trypsin presented an expressive increase in K (32-fold increase) in PEG-dextran systems containing PEG-trypsin inhibitor in the top phase. These studies demonstrated that recovery and purification of these proteins can be considerably increased by modifying APTS with biospecific ligands attached to PEG molecules<sup>65</sup>. Biotinylated microsomal membranes and biotinylated liposomes have been partitioned in a functionalized PEG-dextran system using deglycosylated avidin

(NeutrAvidin) as a bioaffinity ligand in the dextran-rich phase. As a result, both membranes and liposomes were recovered in the bottom dextran phase. Without NeutrAvidin, more than 90% of the liposomes partitioned to the PEG-rich phase. With the addition of NeutrAvidin–dextran, 90% of the biotinylated liposomes partitioned to the dextran phase, suggesting that the biotin-NeutrAvidin interaction in liposomes and membranes influenced the partitioning behavior of these molecules<sup>66</sup>.

Unlike polymer-polymer systems, polymer-salt systems do not offer a good versatility in terms of affinity enhancement. The main disadvantage of these systems is because ionic groups of certain molecules interact with the salt-forming phase<sup>61</sup>. The enzyme penicillin acylase from *E. coli* was partitioned in a functionalized PEG-sulfate system using modified PEG-derivatives as affinity ligands: PEG-benzoate (PEG-Bz), PEG-phosphate (PEG-PO<sub>4</sub>), PEG-trimethylamine (PEG-tma), PEG-palmitate (PEG-pal), and PEG-phenylacetamide (PEG-paa). In the presence of PEG-Bz, the partition coefficient of the enzyme presented a 14-fold increase. Studies conducted in the presence of PEG-PO<sub>4</sub> showed maximum enzyme partitioning to the top functionalized PEG phase at pH 6.8 (K~3). At this pH, the enzyme was below its isoelectric point, therefore it was expected to be positively charged. On the other hand, PEG-PO<sub>4</sub> was expected to be negatively charged at the same pH, which favored selective interaction with the positively charged enzyme. In the presence of PEG-tma, pH 7.3 was considered to be optimum for selectively partitioning the enzyme to the top phase (K~2.2). In the derivative PEG-pal, the enzyme partition coefficient was the highest at or near the isoelectric point (pH 7.1; K 3.2). Being at its isoelectric point, the enzyme is not charged and becomes more responsive to the hydrophobic ligand, improving partitioning to the

top phase. Finally, the greatest enzyme partition coefficient in the presence of PEG-paa was 2.3, corresponding to an 11.5-fold increase. Overall, all PEG derivatives significantly increased enzyme partitioning in the PEG-sulfate affinity system. The affinity interaction between the enzyme and the ligands was attributed to phenyl rings along with either amine or amide groups present in the PEG-derivatives<sup>67</sup>.

Different biotechnology applications have used ATPS for the development of cell-based and biomolecular assays at the microscale. Since the early 2000s, continuous flow microfluidic devices incorporating ATPSs have been used for cell partitioning. By stabilizing the laminar flow and increasing the surface-to-volume ratio within the microchannel, the ATPS interface prevents diffusive mixing and allows continuous partitioning<sup>68</sup>. One of the first applications that integrate ATPS with microfluidics aimed to partition plant cell aggregates to one of the two phases<sup>69</sup>. Using an ATPS composed of PEG and dextran, it was possible to retrieve plant cell aggregates in the dextran-rich phase without the addition of salt (lithium sulfate). Besides, cell migration to the dextran-rich phase increased when the flow rate increased or the width of the PEG-rich phase decreased, regardless of the presence of salt. By increasing the flow rate, the inertial force of the cell movement also increased, which promoted the migration of cell aggregate into the dextran-rich phase. When the width of the PEG-rich phase decreased, cells migrated to the dextran-rich phase more easily because the distance to the interface was decreased<sup>69</sup>. Nam et al. further demonstrated the efficacy of this microfluidic-based ATPS technique to recover animal cells. They were able to recover more than 80% of CHO-K1 (Chinese Hamster Ovary) cells to the PEG-rich top at both weakly acidic and basic conditions, while they were more evenly partitioned at pH 7.0, which is caused by a

change of surface properties of animal cells, such as hydrophobicity and surface net charge. Because the surface of animal cells has a negative net charge at neutral pH, it can be neutralized in a weakly acidic solution. Also, the less charged the cell surface, the more hydrophobic it is. Thus, the partition of animal cells to the PEG-rich phase is favored when the phase is weakly acidic<sup>69</sup>.

ATPSs have also been used to separate leukocytes and erythrocytes from whole blood in continuous flow microfluidic devices. Using a microfluidic ATPS composed of PEG and dextran, it was possible to retrieve both cell types with much greater efficiency compared to conventional ATPS batch procedures<sup>70,71</sup>. In addition to the purification of cells, microfluidic ATPSs have been used to pattern different populations of cells within microfluidic channels, as well as to selectively deliver biochemical treatments to cells. This approach enabled precise laminar patterns of four adherent cell populations simultaneously, and enhanced selectivity of trypsin delivery to cells<sup>72</sup>. Similarly, Tavana et al. demonstrated the efficacy of delivering transfection agents to mammalian cells in a PEG-dextran system<sup>73</sup>. More recently, ATPS has been exploited to generate microdroplets in a microfluidic device for cell encapsulation<sup>74,75</sup>. For example, a passive microfluidic platform has been used to generate particle-stabilized water-in-water droplets that encapsulate cells. In this work, researchers used carboxylated particles to stabilize dextran droplets containing cells in the continuous phase of PEG<sup>74</sup>. In another study, microcapsules with an aqueous core and a hydrogel shell have been generated using a simple microfluidic approach. This process generated droplets with a dextran-rich core and a tetra-PEG hydrogel shell. Droplets were stabilized by spontaneous cross-linking by a cross-end coupling reaction between tetra-PEG macromonomers in the shell,

resulting in the formation of hydrogel microcapsules<sup>75</sup>. Although the microencapsulation of drug or cells has not been demonstrated, the platform developed in this work can be a suitable alternative to traditional water-in-oil emulsions used for drug encapsulation. Owing to its intrinsic biocompatibility, ATPS has been exploited in several biomedical applications, which have gradually become more sophisticated over the last years. However, there has been little to no exploration of applying ATPS for screening vaccine formulations *in vitro*, where primary cells can be cultured in ATPS for a day or longer and the system can be directly used in a cell-based assay.

Therefore, the overall goal of this project was to develop a novel ATPS-based platform for screening drugs and vaccine formulations against infectious diseases. This innovative method enabled screening immune responses using extremely small quantities of reagents. To achieve this aim, the research objectives were to:

i) To utilize optimized ATPS-polymers to confine cells and reagents into microdroplets, and to determine the effect of individual polymer solutions on immune cell viability, proliferation, immunological phenotype, and functionality to enable long term cell culture;

ii) To determine the baseline of activation of RPMI 8226 B cells and Jurkat T cells in the ATPS systems selected in objective 1 such that they can be employed to screen immune responses to vaccine formulations;

iii) To demonstrate the utility of ATPS as bioassays by improving the performance and cost-effectiveness of sandwich enzyme-linked immunosorbent assay (ELISA) and enzyme-linked immunospot (ELISpot);

iv) To demonstrate the ability of the novel ATPS-ELISpot to screen vaccine formulations while consuming up to 5-fold lower reagent volumes compared to conventional ELISpot.

This thesis follows a format where most chapters are composed of materials that have been already published or submitted to peer-reviewed journals. In these chapters, there is evidence from the literature to support the approach proposed in the thesis. This is followed by the summary and discussion of research results, conclusions, and recommendations.

**Chapter 2** is a literature review of emerging biotechnology applications of ATPSs. An overview of key properties of ATPSs are critically reviewed, which lent context to how these systems have progressed to modern applications in the Biotechnology field. Also, future directions, limitations, and design considerations are presented and discussed.

**Chapter 3** presents the scalability of ATPS, ranging from platforms handling femtoliter volumes to large-scale operations. In this context, the application of ATPS for drug and cell encapsulation, and for the development of cost-effective immunoassays is summarized. This chapter also reviews ATPS scale-up strategies to enable its industrial adoption, including different phase separation procedures, optimization of techniques to improve recovery and purity of bioproducts.

In **Chapter 4**, the application of ATPS to improve the performance and cost-effectiveness of ELISA is demonstrated. This chapter describes a cost-effective single ATPS-ELISA technique that requires reduced reagent volumes while decreasing optical crosstalk between neighboring wells.

**Chapter 5** describes the development and characterization of a cost-effective ATPS-ELISpot that requires lower amounts of stimulants in comparison with conventional ELISpot.

**Chapter 6** describes the application of the novel ATPS-ELISpot for screening vaccine formulations. The adjuvants are examined individually or combined with an influenza-specific antigen (hemagglutinin), by confining them in microdroplets with primary human peripheral blood mononuclear cells (PBMCs).

**Chapter 7** summarizes and concludes the research results in this project with future recommendations.



## CHAPTER 2      AQUEOUS TWO-PHASE SYSTEM (ATPS)

Materials of this chapter have been published in **Advanced Healthcare Materials** and are being reproduced in this thesis with permission from the publisher Wiley.

Teixeira, A. G., Agarwal, R., Ko, K. R., Grant-Burt, J., Leung, B.M., Frampton, J. P. (2017). Emerging biotechnology applications of aqueous two-phase systems. *Advanced Healthcare Materials*, vol. 7, issue 6, 1701036.

### 2.1      ABSTRACT

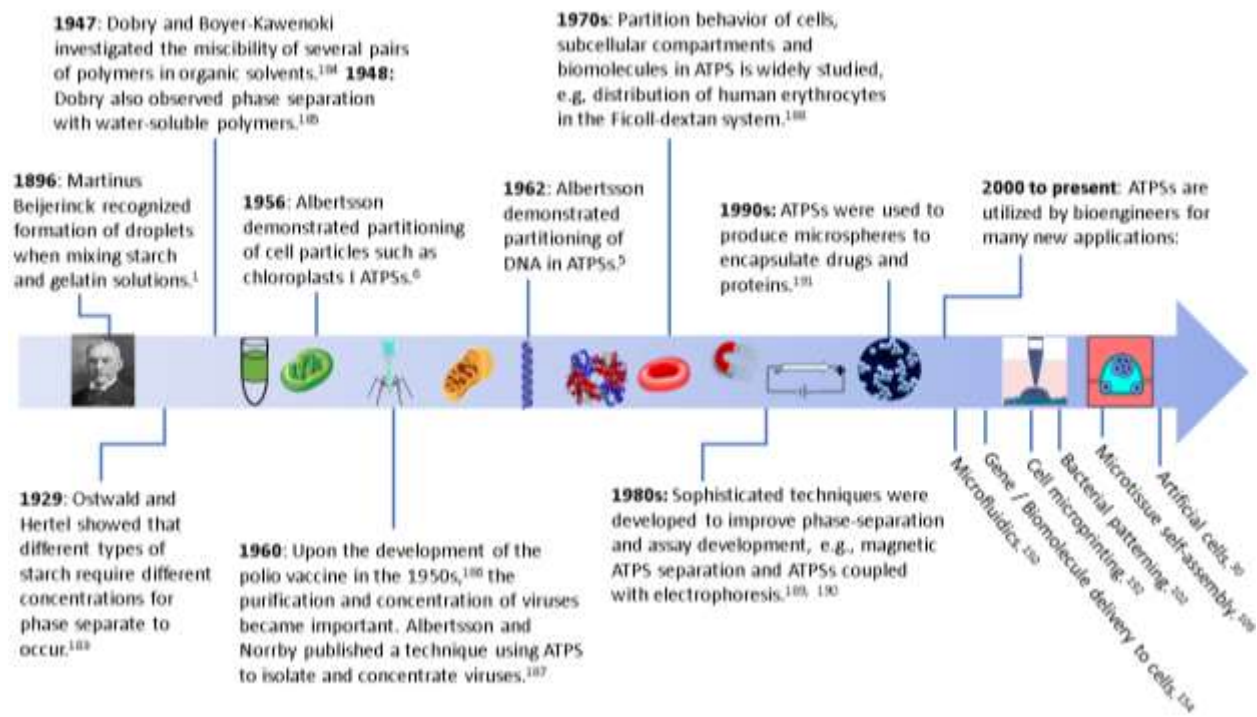
Liquid-liquid phase separation between aqueous solutions containing two incompatible polymers, a polymer and a salt, or a polymer and a surfactant has been exploited for a wide variety of biotechnology applications throughout the years. While many applications for aqueous two-phase systems fall within the realm of separation science, the ability to partition many different materials within these systems, coupled with recent advances in materials science and liquid handling, has allowed bioengineers to imagine new applications. This progress report provides an overview of the history and key properties of aqueous two-phase systems to lend context to how these materials have progressed to modern applications such as cellular micropatterning and bioprinting, high-throughput three-dimensional tissue assembly, microscale biomolecular assay development, facilitation of cell separation and microcapsule production using microfluidic devices, and synthetic biology. Future directions and present limitations and design considerations of this adaptable and promising toolkit for biomolecule and cellular manipulation are further evaluated.

## 2.2 INTRODUCTION

Aqueous two-phase systems (ATPSs) form when two incompatible polymers, a polymer and a salt, or a polymer and a surfactant exceed threshold concentrations in a water-based solvent, resulting in liquid-liquid phase separation<sup>76,77</sup>. This phenomenon was first recognized by the microbiologist Martinus Beijerinck in 1896. While preparing an aqueous solution of starch for culturing bacteria, he noticed that droplets formed as the concentrated starch solution mixed with gelatin<sup>78,79</sup>. This emergent property was later appreciated for a variety of different long chain polymer mixtures. However, the utility of ATPSs was not appreciated until the 1950s, when Per-Åke Albertsson began utilizing a variety of polymer-polymer and polymer-salt solutions for isolation of proteins, viruses, cells, and cell fragments (e.g., chloroplasts from green algae) by exploiting the preferential distribution of materials between phases, a phenomenon known as partitioning<sup>31,80,81</sup>. Partitioning occurs when molecules or particles are mixed into the polymeric system, but do not contribute to phase-separation. After equilibration, these materials distribute to the phase for which they have the greatest relative affinity<sup>82</sup>.

Since these pioneering discoveries, ATPSs have been used extensively in the field of separation science for isolation and recovery of antibodies<sup>83,84</sup>, proteins<sup>81,85,86</sup>, virus-like particles<sup>87,88</sup>, antibiotics<sup>89-91</sup>, DNA<sup>92-94</sup>, cells<sup>95,96</sup>, extracellular vesicles<sup>97,98</sup>, and hormones<sup>99,100</sup>. More recently, bioengineers have begun exploiting the properties of ATPSs in a wide variety of novel applications including solution micropatterning of cells to investigate cell migration and cell-cell interactions<sup>101</sup>, confinement of antibodies and other reagents into solution-patterned microarrays<sup>102</sup>, microfluidic devices<sup>103</sup>, and even to generate synthetic cell-like structures<sup>104</sup>. A timeline highlighting important events in the

development of this growing field is presented in Figure 1. The purpose of this progress report is to highlight some of the most promising emerging applications for ATPSs.



**Figure 1 The evolution of ATPS-based technologies.** Applications of ATPSs date back to at least the 1950s, when they were first exploited for purification of biological materials. Progress in the characterization and application of these materials has accelerated since the early 2000s, giving rise to many new technologies. Reproduced with permission<sup>30</sup>. Copyright 2017, Advanced Healthcare Materials.

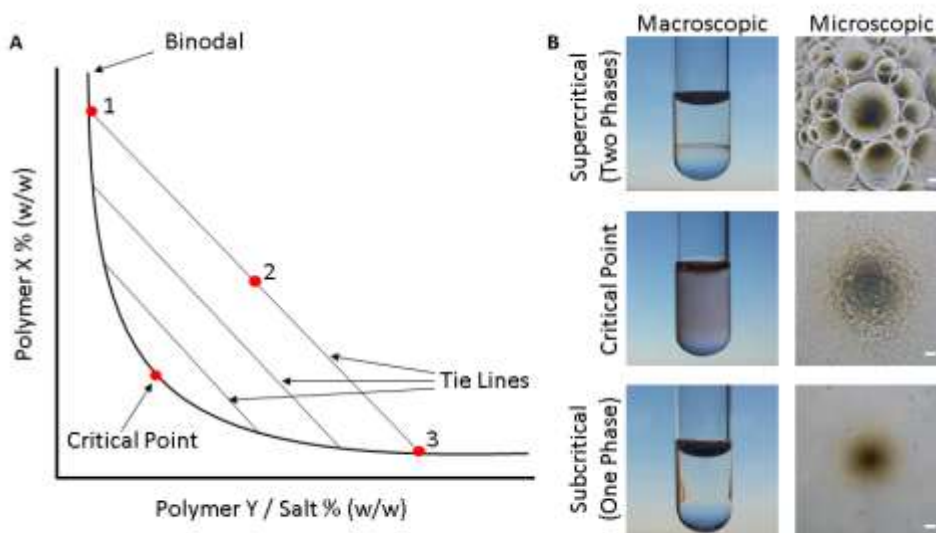
## 2.3 ATPS PROPERTIES

Before describing the emerging applications of ATPSs in detail, it is necessary to review some of the key properties of these materials. An ATPS contains three zones: the two bulk phases, which often separate by density into a top phase and a bottom phase, and the interface. Each of these zones can have distinct properties (as discussed below), which dictate their performance in various applications.

### 2.3.1 The Separation of Phases

Phase-separation can be explained by the thermodynamic properties of incompatible solutions, which result in formation of immiscible liquid phases<sup>78,79</sup>. To further understand the thermodynamic process of ATPS formation, one must consider the free energy of the system:  $\Delta G = \Delta H - T\Delta S$ , where  $\Delta G$  represents the change in Gibbs free energy of the system,  $\Delta H$  represents the change in enthalpy,  $T$  represents the temperature and  $\Delta S$  represents the change in entropy. When  $\Delta G < 0$ , the process is spontaneous, which means that ATPSs cannot form because the polymers will mix. For phase separation to occur, the entropic contribution must be smaller than the enthalpic contribution such that  $\Delta G > 0$ <sup>31,103,105</sup>. Although attempts have been made to develop thermodynamic models capable of predicting the concentrations at which phase separation occurs<sup>42,106–108</sup>, it is customary to empirically determine the concentrations required for phase separation due to the number of factors such as pH, temperature and ionic concentration that may influence the tendency of solutions to phase-separate<sup>101,106</sup>. These concentrations are typically plotted on a binodal phase diagram, with the concentration of the polymer occupying the top phase on the ordinate and the concentration of the polymer occupying the bottom phase on the abscissa. Supercritical concentrations represented by points above the binodal curve yield two immiscible phases. The binodal curve also gives information about the relative volumes of the two phases and the concentrations of the two-polymer species in the respective phases at equilibrium. A detailed description of how to interpret these diagrams, including information about how to interpret critical points and tie lines, can be found in the classic work by Albertsson<sup>31</sup>. However, when utilizing ATPSs for practical applications, it is

important to consider that systems closer to the critical point and other points along the binodal curve are less stable and more sensitive to environmental fluctuations than supercritical systems far from the binodal curve. A fictitious binodal phase diagram is presented in Figure 2, along with representative images of poly (ethylene glycol) (PEG)-dextran systems formed from supercritical concentrations of polymers, near-critical concentrations of polymers and subcritical concentrations of polymers.



**Figure 2 Binodal phase diagram.** A) The bottom phase is represented on the abscissa and the top phase is represented on the ordinate. The binodal curve divides the ATPS forming polymer concentrations (above the curve) from those concentrations that do not form ATPS (below the curve). The tie lines connect two points on the binodal which represent the final concentration of the bottom and the top phase. Points 1, 2, and 3 represent three compositions of ATPS lying on the same tie line. Point 1 indicates the composition of the top phase, point 2 has equal volumes for the top and the bottom phases, and point 3 indicates the composition of the bottom phase. At the critical point, the composition and the volume of the two phases are the same. B) Images of supercritical polymer solutions forming two phases (top), near-critical point concentrations (middle), and subcritical polymer solutions (bottom) contained in test tubes (left) and imaged by bright field microscopy. Scale bar = 100  $\mu\text{m}$ . Reproduced with permission<sup>30</sup>. Copyright 2017, Advanced Healthcare Materials.

The most common method for determining the binodal phase diagram, turbidimetric titration, is performed by analyzing a series of polymer systems of known concentrations before and after dilution. The point at which a given system becomes clear

upon mixing, indicating an absence of immiscible microscopic droplets, is taken as a point on the binodal curve. Another commonly used method, the cloud-point method, is performed by adding a concentrated stock solution of one of the two components of the system (e.g., dextran) to a known volume of a concentrated stock solution of the second component (e.g., PEG). After a certain amount of the second component has been added, the cloud-point is reached and the mixture becomes turbid, which indicates the formation of a two-phase system. The composition preceding ATPS formation is taken as a point on the binodal curve<sup>42</sup>. Although these methods are commonly used for determination of the binodal phase diagram, they consume large amounts of reagents and tend to be tedious and time-consuming.

To address these limitations, Silva et al. developed a microfluidic platform for high-throughput screening of ATPS-forming polymer mixtures. This method is based on the diffusion of different solutions through three microchannels: one for the polymer present in the top phase, another for the polymer/salt present in the bottom phase, and the last for water. In the microchannel, the fluids flow in a laminar regime with only diffusive mixing. To evaluate phase separation, optical microscopy is performed at the distal end of the microchannel<sup>106</sup>. Another alternative method for efficient phase diagram determination was developed by Ruthven et al. Using a simplified technique based on 96-well microplate titration, it was possible to analyze up to 64 binodal compositions in several hours using only widely available laboratory pipettes and plastic ware. In this assay, the presence or absence of phase separation (droplets) is also determined by light microscopy<sup>101</sup>.

### 2.3.2 The Physicochemical Properties of The Bulk Phases

Many of the applications discussed below involve manipulation of ATPSs at the micro- to nano-liter scales. As one would expect for these scales, material properties such as fluid viscosity and hydrophobicity, as well as density (i.e., specific gravity) and osmolarity are important to consider when implementing or evaluating novel ATPS applications.

#### 2.3.2.1 Viscosity

Viscosity is an important parameter in the phase separation process because it determines the settling time of the phases following emulsion<sup>56,109</sup>, as well as the fluid dynamics of micropatterned droplets<sup>110</sup>. For polymer-polymer ATPSs (e.g., the PEG-dextran system), the viscosity of the phases increases with polymer content and molecular weight, implying that this property cannot be manipulated independently of the fluid densities, relative-phase volumes at equilibrium and affinity for partitioned materials<sup>56,111</sup>. For any ATPS containing a polymer, the viscosity of the entire system will increase as a function of polymer content. However, if we consider the viscosities of the phases individually as a function of increasing dextran content for the PEG-dextran system, the viscosity of the dextran-rich phase will increase proportionally to the tie line length as the dextran content increases, while the viscosity of the PEG-rich phase will remain nearly constant. Similarly, if we consider a series of PEG-dextran ATPSs formed from varying molecular weights of dextran for a constant molecular weight of PEG and constant total polymer content, the dextran-rich phase viscosity will increase relative to the PEG-rich phase viscosity as the molecular weight of dextran is increased.

### 2.3.2.2 Density

ATPSs can separate mixtures of particles by differences in density through the formation of three stable interfaces: air/top phase, top phase/bottom phase, and bottom phase/container. The densities of individual phases can be modulated by alteration of the concentrations of the polymers or the surfactants<sup>77</sup>, as well as by addition of salts (e.g., cesium bromide)<sup>112</sup>, ionic liquids<sup>113</sup>, paramagnetic solutes (e.g., Mn(II)Cl<sub>2</sub>)<sup>114</sup>, and co-solutes (e.g., D<sub>2</sub>O)<sup>77</sup>. In addition, phase-separating polymers may be selected to optimize differences in polymer densities among the phases or to create multi-phase systems with more than one liquid-liquid interface<sup>77,114,115</sup>. In the commonly used PEG-dextran system, the dextran-rich phase is always denser than the PEG-phase. However, in the dextran-Ficoll system, the denser phase can be either the dextran-rich phase or the Ficoll-rich phase, depending on the polymer concentrations. For dextran-Ficoll ATPSs far from the critical point on the binodal curve, the dextran-rich phase is denser than the Ficoll-rich phase, whereas for compositions close to the critical point on the binodal curve, the Ficoll-rich phase is the denser of the two phases<sup>31</sup>.

### 2.3.2.3 Osmolarity

The two liquid phases have the same osmotic pressure at equilibrium regardless of polymer molecular weight<sup>31,116</sup>. In practice, it is not common to adjust the osmolarity of ATPSs prior to use because the polymers are typically dissolved in a physiological buffer. However, it is possible to adjust the osmotic pressure or tonicity of an ATPS by addition of salts or sugars. For example, it has been demonstrated that when an ATPS vesicle is encapsulated by a semipermeable membrane, phase separation can be



modulated by addition of osmolytes such as sucrose to the external solution. As the external osmotic pressure increases, the interfacial tension also increases, leading to vesicle budding<sup>117,118</sup>. From the perspective of biomolecule separation, the ionic composition of a polymer-polymer system plays a significant role in partitioning of materials between the phases. This occurs due to electrostatic potential differences between the two phases at equilibrium resulting from non-uniform distribution of ions between the phases. In addition, the presence of salt modifies the intramolecular forces between the material of interest and the polymers. For example, partitioning of pectinase in a PEG-dextran system can be enhanced by addition of low concentrations of sulfate salts<sup>119</sup>. Finally, by adding salts, phase separation can be achieved at lower total polymer concentrations due to the entropic effect of salt addition. Consequently, the binodal curve is shifted towards the origin on the phase diagram<sup>120</sup>.

#### **2.3.2.4 Hydrophobicity**

The difference in hydrophobicity between two ATPS-forming polymers is correlated with their tendency to phase separate into an ATPS. For example, PEG is more compatible (and therefore less likely to phase-separate) with dextran polymers modified to contain hydrophobic side chains<sup>31</sup>. Another example is the system composed of the copolymer ethylene oxide/propylene oxide (EO-PO) and dextran. EO-PO is slightly more hydrophobic than PEG, leading to a larger hydrophobicity difference between the EO-PO-rich phase and the dextran-rich phase compared to the PEG-dextran system.<sup>121</sup> In general, the larger the difference in hydrophobicity between the two polymers of interest, the more likely the system will be to phase separate.

Hydrophobicity is also one of the most important factors influencing the partitioning of proteins in both polymer-salt and polymer-polymer ATPSs<sup>33</sup>. In a PEG-dextran system, highly hydrophobic proteins are more likely to partition to the more hydrophobic top phase (i.e., the PEG-rich phase) as opposed to the dextran-rich phase. On the other hand, hydrophilic proteins tend to partition to the less hydrophobic of the two phases<sup>122</sup>. Hydrophobic interactions of materials with ATPS-forming polymers may also depend on the surface properties of the biomolecules. For example, the surface net hydrophobicity of tRNA (transfer RNA) has been evaluated by partitioning within the PEG-dextran system. As the difference in hydrophobicity between the PEG and dextran phases increases, the partition coefficient of the tRNA decreases, indicating increased affinity for the dextran phase<sup>123</sup>. As the surface net hydrophobicity of the tRNA increases with temperature, partitioning shifts from the dextran phase to the PEG phase. ATPSs have also been used to evaluate surface net hydrophobicity of proteins<sup>124,125</sup>. Finally, in addition to the effects of ATPS hydrophobicity on partitioning, it is also important to consider the interaction of the fluid phases with solid substrates based on surface chemistry<sup>39</sup>. The surface chemistry of the container holding the ATPS will influence the wettability by one or both of the phase-forming polymers. In the case of the solution micropatterning applications discussed later, this has the effect of lowering the droplet contact angle, i.e., droplets will have the tendency to spread more.

## **2.4 THE ATPS INTERFACE**

The interface between the bulk phases of an ATPS has very low interfacial tension compared to the interface of an oil-water system. For example, the interfacial

tension of the PEG-dextran system ranges from approximately 1 to 100  $\mu\text{N/m}$ , depending on the molecular weights and concentrations of the polymers<sup>54,126</sup>. ATPS formulations close to the binodal curve have smaller interfacial tensions compared to supercritical formulations far from the binodal curve<sup>31</sup>. It has also been observed that the adsorption of particles to the interface increases as supercritical concentrations of ATPS forming-polymers increase<sup>58,126</sup>. When particles are adsorbed at the interface between the two aqueous phases, the interfacial area is reduced proportionally to the number of adsorbed particles. Hence, there is a loss of interfacial area that leads to a decrease in free energy. For this reason, the interfacial tension is an important determinant of partitioning behavior of biomolecules and cells since these materials normally distribute themselves within the bulk phases, but in some cases, they can be trapped at the interface if there is sufficient interfacial tension present<sup>58</sup>. In addition, polymer molecular weight, salt content and temperature all play a role in determining the interfacial tension of an ATPS. Bamberger et al. observed that interfacial tension increased proportionally to phosphate concentration. Addition of NaCl, however, had less of an effect on interfacial tension<sup>58,109</sup>. Interfacial tension is also affected by temperature. In general, lowering the temperature favors phase separation of two-polymer systems and polymer-salt systems, thereby increasing the interfacial tension<sup>127</sup>. However, it has been noted by Forciniti et al. that the correlation between the interfacial tension and temperature is less clear than with polymer molecular weight<sup>59</sup>. Others have noted that pH can affect the interfacial tension of an ATPS<sup>48</sup>, particularly in the case of polymer-salt ATPSs<sup>128</sup>.

## 2.5 PARTITIONING OF MOLECULES AND PARTICLES

Partitioning of a wide variety of materials is influenced by their physicochemical properties such as their electrochemical charge<sup>119</sup>, size (molecular weight)<sup>37</sup>, bio-specific affinity<sup>129</sup>, and surface hydrophobicity<sup>33</sup>. As stated previously, in a PEG-dextran ATPS, most hydrophilic materials will distribute to the bottom dextran-rich phase, which is less hydrophobic than the top PEG-rich phase. In contrast, hydrophobic molecules<sup>130</sup> (e.g., proteins containing large numbers of non-polar amino acids) will partition to the more hydrophobic PEG-rich top phase. Choosing ATPS-forming materials based on their hydrophobicity can improve the separation of a specific protein according to the protein's hydrophobic interactions with the phase-separating materials<sup>38,131</sup>. Due to their versatility in partitioning a wide-range of materials (in particular proteins and cells), as well as their low cost, scalability, easy implementation and environmental-friendliness, ATPSs have started to replace traditional organic solvent extraction techniques<sup>78,132,133</sup>. In addition, ATPSs do not cause denaturing effects on biomolecules or cells<sup>134,135</sup>. Moreover, due to their low interfacial tension, ATPS have been reported to prevent damage to fragile cell structures, and in some cases, can even stabilize sensitive biological materials<sup>31</sup>.

In recent years, these capabilities have allowed ATPSs to overcome challenges encountered in the biotechnology industry in addition to enabling the confinement of materials in polymeric droplets for the emerging application that we will discuss in detail in the following sections<sup>134</sup>. One example of an application of ATPS technology for advanced biomolecule purification is the separation and purification of Zera® fusion proteins in the PEG-phosphate system. Extraction of Zera® fusion proteins was optimized by modulating the PEG molecular weight, tie line length, pH, sample load, and

salt concentration to select the best extraction conditions. Upon optimization of this process, it was possible to reliably partition high-value recombinant proteins<sup>136</sup>. Another example is the partitioning of alpha-amylases. Alpha-amylases are hydrolases used industrially for fermentation, food production, pharmaceutical production, textile processing, and paper processing<sup>137,138</sup>. Alpha-amylases generally interact with the PEG phase in PEG-phosphate systems. However, when higher molecular weight PEGs (e.g., above 8000 g/mol) are used, the proteins partition to the bottom phosphate phase. Although the enzymes can be isolated in either phase, the recovery from the PEG-phase requires further processing for separation from the polymer. Thus, choosing an appropriate polymer molecular weight (i.e., PEG 8000) simplifies the extraction process<sup>137,139</sup>.

Separation and purification of monoclonal antibodies in ATPSs is another important industrial application where the implementation of ATPSs has demonstrated potential as an approach for large scale recovery and purification<sup>140-143</sup>. Azevedo et al. demonstrated that integration of a PEG-citrate system with traditional chromatography techniques improved antibody recovery. Prior to chromatography, the concentration of the antibodies in the citrate-rich phase provided a recovery process with 72% protein purity ( $[\text{IgG}]/[\text{total protein}]$ ) and 97% yield (mass of eluted IgG/ initial mass of IgG). Integration with chromatographic extraction enabled collection of a 100% pure protein solution with 90% yield<sup>142</sup>. This same group developed a method that integrated a PEG-dextran system with cation exchange chromatography for IgG purification. The PEG-dextran system recovered 82% of IgG with up to 96% protein purity. After integration with chromatographic extraction, the overall process resulted in a protein purity of 100%

and a yield of 75%<sup>143</sup>. Subsequently, this process was adapted for microfluidic separation to reduce the operation time without affecting antibody extraction<sup>144</sup>.

## **2.6 EMERGING APPLICATIONS OF ATPS**

Although the majority of applications involving ATPSs focus on the use of relatively large volumes of the two phases (mL to L) for purification of biological materials, here we will focus on how the materials properties and principals of partitioning have been applied at the microliter to nanoliter scale to develop advanced cell-based and biomolecular assays.

### **2.6.1 Cell Micropatterning and Microtissue Engineering with ATPS**

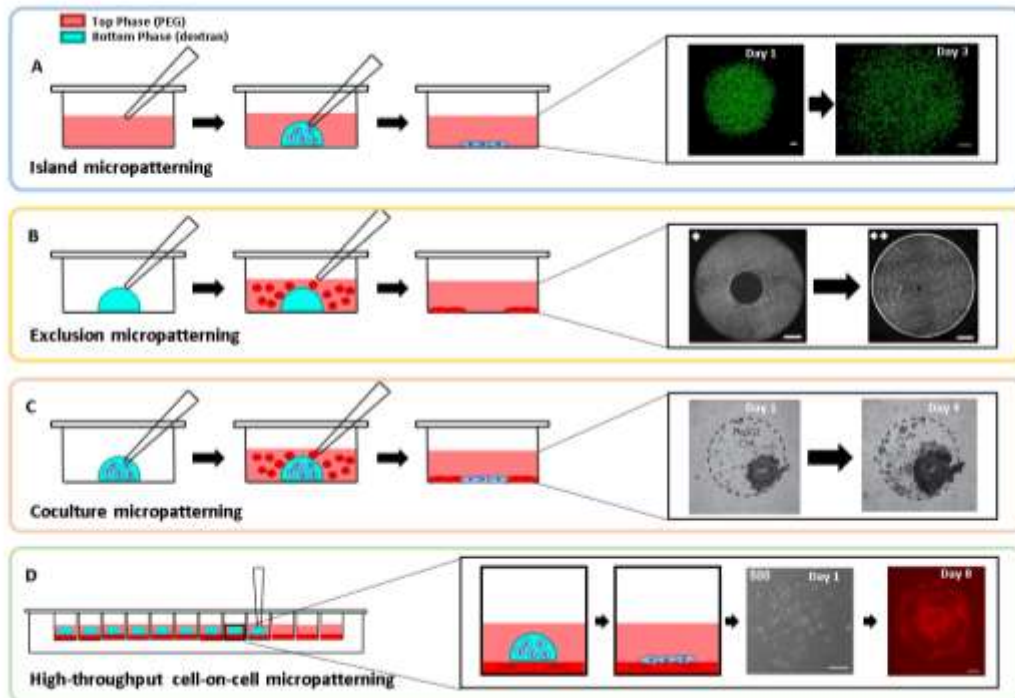
The past two decades of tissue engineering have focused on development of new strategies for restoring damaged tissues and/or organs and understanding the homotypic and heterotypic cell-cell interactions involved in tissue formation and function<sup>145</sup>. Analysis of complex cell-cell, cell-extracellular matrix (ECM), and cell-environment interactions are crucial in understanding these phenomena. A variety of biopatterning approaches for the fabrication of spatially-organized cell cultures including, but not limited to, microcontact printing<sup>146</sup>, microfluidic patterning<sup>147</sup>, stencil-based patterning<sup>148</sup>, inkjet-based bioprinting<sup>149</sup>, and laser-assisted bioprinting<sup>150</sup>, have offered the possibility to explore the intricacies of how cells interact with each other and their extracellular environment in greater depth. Recently, novel ATPS-based patterning techniques have been developed as an alternative to these approaches for versatile non-contact patterning of cells.

### 2.6.1.1 Cell Micropatterning for Analysis of Growth and Differentiation

Using ATPS-based patterning techniques, it is possible to precisely position cells directly on various substrates without the need to selectively pattern or otherwise process the substrate beforehand. This method uses ATPS-forming polymers (e.g., PEG and dextran) such that nano- to micro-liter droplets of dextran containing cells are dispensed onto a substrate coated with a solution of PEG<sup>82,151</sup>. Unlike other techniques that are driven by electrical or thermal energy, ATPS micropatterning takes advantage of the optimal range of interfacial tensions exhibited at the interface between phase-separating polymers to precisely confine cells into the desired configurations without application of harsh forces that may harm cells or damage the substrate. Moreover, this approach is easy to implement and can be performed using simple laboratory tools such as micropipettors<sup>82</sup>.

To perform this approach, low concentrations of phase separating polymers are first dissolved in cell culture medium. Cell islands or colonies are then delivered to a substrate by dispensing dextran droplets containing cells into a PEG solution (Figure 3A)<sup>82</sup>. The interfacial tension-driven patterning mechanism confines the cells within the denser dextran droplets at the surface of the substrate, but allows the cells to attach to the substrate surface with ~ 98-100% viability relative to controls<sup>152,153</sup>. Once the cells attach to the substrate, the polymers are easily removed by rinsing with fresh cell culture media, leaving behind islands of patterned cells. Recent reports highlight the use of this technique for biopatterning keratinocytes in colonies to enhance cell-cell contact and viability compared to non-patterned cells, which may have future applications in wound healing and skin tissue regeneration<sup>153</sup>. In addition to analysing colony growth and

differentiation, similar strategies have been employed to pattern particles and biomolecules atop pre-existing cell monolayers. This strategy has been used to deliver genetic materials, enzymes and even buoyant particles such as microbubbles used for sonoporation to the surfaces of cell monolayers immersed in PEG<sup>134,154</sup>.



**Figure 3 Overview of ATPS cell micropatterning techniques.** A) Island micropatterning. Cell-laden dextran droplets are dispensed onto a plate coated with PEG. Cells are confined within the droplets, resulting in the formation of adherent cell islands as shown in the images to the right (HEK001 cell line, Scale Bar = 100 and 200  $\mu\text{m}$ ). B) Exclusion micropatterning. A cell-laden PEG phase is dispensed onto a plate containing dextran droplets, resulting in the formation of exclusion zones. The images to the right display exclusion zones and migration of MDA MB-231 breast cancer cells (MDA MB-231 cell line, Scale Bar = 1 mm). C) Coculture micropatterning. Cell-laden dextran droplets are pipetted onto standard tissue culture plates. Cell-laden PEG is then slowly added to the plate, resulting in the formation of cocultures after cell attachment to the plate. The images to the right show cocultures of HEPG2 C3A cells and NIH 3T3 fibroblasts. D) Stem cell islands (mESCs) can be printed on a PA6 stromal layer using the ATPS island micropatterning technique to enhance neuronal differentiation. The images to the right show bright field and fluorescence images of printed mESCs. Differentiated mESC cells are stained with the neuron specific class III beta tubulin TuJ1 differentiation marker. (Scale Bar = 250 and 500  $\mu\text{m}$ ). Reproduced with permission<sup>30</sup>. Copyright 2017, Advanced Healthcare Materials.



The interfacial tension between PEG and dextran has also been used to pattern cell exclusion zones by depositing a cell-laden PEG phase on top of patterned cell-free dextran droplets to exclude the cells as they settle around the interface of the dextran droplets (Figure 3B). Cell exclusion zones have been applied to assess cell migration, proliferation rates and wound healing capacity<sup>82,155</sup>. For instance, Tavana et al. used cell exclusion patterning to develop a novel, high-throughput, 96-well format, scratch-free cell migration assay<sup>155</sup>. To achieve this, single-microliter dextran droplets of dextran were printed and dehydrated on the surface of standard microwell plates. A cell-laden PEG phase was then added to the wells, which rehydrated the regions patterned with dextran to form cell-excluding droplets. This generated well-defined, cell-free, circular areas within a monolayer without the need for any specialized instruments or modification of the underlying substrate, overcoming some of the limitations of conventional wound healing and cell migration assays.

#### **2.6.1.2 Cell Micropatterning for Engineering Mammalian Cell-Cell Interactions**

The use of coculture systems with more complex heterocellular interactions can enable more physiologically relevant analysis of cell-cell interactions. By further combining cell exclusion zones and cell islands, ATPS micropatterning technology enables the patterning of multiple types of cells to generate cocultures (Figure 3C). For example, Frampton et al. demonstrated that cocultures of hepatocytes and fibroblasts displayed higher albumin production than monocultures of hepatocytes, which was indicative of enhanced function of the liver cells<sup>82</sup>. Multiplexed patterns of cocultures have also been generated by combining acoustic droplet ejection (ADE) and cell

exclusion patterning. This method uses acoustic radiation pressure to eject uniform cell-laden dextran droplets. A PEG solution containing additional cells is then added to the cultures. ADE of ATPSs has been applied for studying cancer growth by patterning cocultures of MDA MB 231 breast cancer cells (confined in dextran droplets) and HEK 293 cells (applied in PEG) to investigate the effects of CXCL12/CXCR4 signaling (a pathway that mediates cancer metastasis, cell proliferation and migration)<sup>156</sup>.

There has also been increasing interest in generation of heterocellular environments for stem cell research, which has led to the development of many cell patterning techniques specific to stem cells<sup>157-159</sup>. However, success of these techniques is dependent on how well they mimic microenvironmental interactions and regulatory effects on cell fate. Conventional patterning methods rely on adhesive materials to facilitate the adhesion of a second cell type on an existing layer of cells<sup>160</sup>, but the positioning of this second layer can be challenging<sup>135</sup>. Furthermore, some of the techniques used for cell-on-cell patterning require physical contact, which can be damaging to delicate substrates such as cell layers. To address these limitations, ATPSs were used to spatially pattern one type of cells on an existing layer of cells (Figure 3D). Here, a cell-laden dextran droplet was dispensed on an existing layer of cells coated with PEG. Using this technique, it was possible to retain full cellular viability of the printed cells and the pre-existing layer of cells after coculture biopatterning. Moreover, this study revealed enhanced neuronal differentiation of mouse embryonic stem cells (MESC)s printed on PA6 stromal cells<sup>135,152</sup>. The utility of ATPS micropatterning technology was further demonstrated by patterning clusters of feeder cells with predefined spacing on hydrogels and cell monolayers<sup>161</sup>. This study enabled high-throughput production of

embryonic stem cell microenvironments and was able to identify the roles of different feeder cells on stem cell differentiation.

This brief synopsis of ATPS-based cell patterning highlights its future potential in stem cell research and tissue engineering applications. In terms of stem cell research, this gentle, contact-free microprinting technology will be useful for determining the optimal conditions to direct the fate of stem cells towards particular lineages. The ability to generate heterocellular environments will also enable more physiologically realistic analysis of cell proliferation and migration. Finally, high-throughput patterning of complex cellular constructs might one day be used as a tool to optimize microenvironmental interactions and produce more representative lab-grown tissues for physiological modelling of various diseases, as will be described further in section 3.1.4.

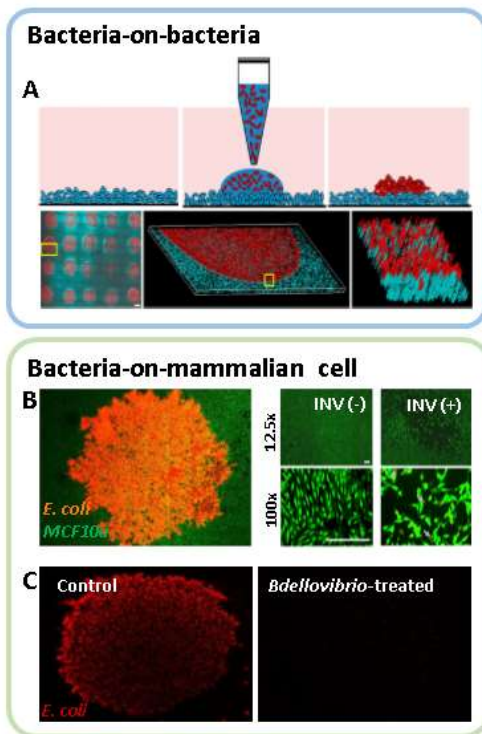
### **2.6.1.3 Cell Micropatterning for Engineering Microbial Growth Microenvironments**

Similar to mammalian cocultures, controlled and standardized *in vitro* coculture platforms for studying the interactions among microbial cell types or between eukaryotic and prokaryotic cells have been explored. One challenge in the development of these systems has been to overcome incompatible growth conditions between these cell types<sup>162</sup>. Other challenges include balancing the growth kinetics among microbial species and/or mammalian cells when using replication competent microbial cells and promoting the dynamics that occur during natural microbial colonization, such as biofilm formation and quorum sensing. By depositing and culturing bacteria within ATPSs, it is possible to overcome some of these limitations, as living replication-competent bacteria can be deposited at precise locations in a format that enables direct cell-cell and soluble factor-

mediated intercellular signalling. In addition, the interfacial tension between the phases in an ATPS helps maintain physical confinement of the bacterial cells within the droplet phase, thus preventing overgrowth. Meanwhile, small molecules and metabolites can freely diffuse across the interface to mitigate nutrient depletion and excessive waste build-up. This fine balance of coculture microenvironment parameters is difficult to replicate using conventional microbial-mammalian coculture techniques<sup>163–165</sup>.

Yaguchi et al. demonstrated that polymer-based ATPSs can be used to pattern living microbes in a fully aqueous environment<sup>166</sup>. Using a PEG-dextran ATPS, multiple species of bacteria were patterned in adjacent colonies without intermixing. As described above for mammalian cells, this was achieved by suspending the bacteria in separate solutions of dextran before direct deposition by micropipette onto a substrate covered with PEG. This same study demonstrated that bacterial colonies can be patterned to form confined biofilms above a larger pre-formed biofilm (Figure 4A). The patterned bacterial biofilms developed and matured within the confines of the dextran droplets over the course of two days, with the size of the mature biofilm being proportional to the volume of the initial dextran droplet. To demonstrate the transfer of antibiotic resistance between bacteria colonies, the authors also created patterned cultures consisting of two overlapping biofilms from two different strains of *Escherichia coli*. Circular colonies of an ampicillin-sensitive *E. coli* MG1655/pLacCherry strain were patterned over a pre-existing biofilm layer consisting of a  $\beta$ -lactamase producing and ampicillin resistant *E. coli* strain (MG1655/pAmCyan). The presence of ampicillin caused significantly less damage to pLacCherry colonies seeded over the pAmCyan biofilm, compared to similar colonies seeded over a wildtype *E. coli* MG1655 biofilm, or cells cultured on tissue

culture polystyrene. This study recapitulated the commensalistic benefits conferred by one species to another in complex microbial communities found in nature<sup>167–169</sup>.



**Figure 4** Applications of ATPSs in microbial culture. A) Bacterial colonies can be patterned using a PEG–dextran ATPS to deliver cells directly over a pre-existing bacteria biofilm, forming two distinct yet interconnected colonies. Adapted with permission.[102] Copyright 2012, Biomacromolecules. B) Here, mCherry expressing *E. coli* forms a stable biofilm over a monolayer of human mammary epithelial cells (MCF10a). *E. coli* expressing invasin (*inv+*) from *Yersinia pseudotuberculosis* can invade underlying MCF10a cells and cause cell death, thereby demonstrating localized and direct microbe-mammalian cell interaction. C) The presence of a Gram-negative bacteria predator, *Bdellovibrio bacteriovorus*, significantly reduces the density of *inv+**E. coli*, which in turn rescues the underlying MCF10a cells from cell death caused by *E. coli* invasion. Reproduced with permission<sup>30</sup>. Copyright 2017, Advanced Healthcare Materials.

The technique of patterning and confining bacteria colonies to form stable biofilms can be extended to the study of bacterial-mammalian cell interactions. Cultured bacteria can be suspended in the dextran medium, and directly patterned over an epithelial monolayer submerged in PEG medium (Figure 4B)<sup>170</sup>. This system provides physical confinement of the bacterial cells, which resolves the aforementioned issues

related to growth kinetics and nutrient availability. In this system, the bacterial cells are still able to make physical contact with the epithelial monolayer, which can enable detailed analysis of bacterial virulence and the effects of secreted factors on mammalian cells. Using this platform as a functional antimicrobial assay, Dwidar *et al.* demonstrated the rescue of a mammalian epithelial monolayer from invasin-expressing bacteria by *Bdellovibrio bacteriovorus*, a predator specific to Gram-negative bacteria. *E. coli* MG1655/pINVCherry, a strain that expresses the *Yersinia pseudotuberculosis* invasin (*inv*<sup>+</sup>) gene were capable of invasion of the epithelial monolayer via association with  $\beta$ 1-integrin receptors on epithelial cells, leading to deterioration of the integrity of the MFC10a cells directly below the bacterial colony. When cultured in the presence of *B. bacteriovorus*, the survival of *E. coli* MG1655/pINVCherry, along with two other bacterial species (*Shigella. boydii* KACC 10792 and *Pseudomonas sp.* DSM 50906) was markedly lower in comparison to control plates, suggesting that *B. bacteriovorus* could move from the surrounding regions to the bacteria-laden dextran droplets to predate the pathogenic bacterial cells (Figure 4C). Moreover, the clearance of INV<sup>+</sup> bacteria colonies restored the health and integrity of epithelial monolayer, suggesting that *B. bacteriovorus* may be a promising biological agent in the fight against antibiotic-resistant bacterial infection<sup>171,172</sup>. The use of the ATPS coculture platform as a functional assay is an exciting development in this field, as it gives researchers the ability to study interactions between microbes and mammalian cells at a greater level of complexity.

#### 2.6.1.4 Self-Assembly of Cell and Tissue Constructs in ATPSs

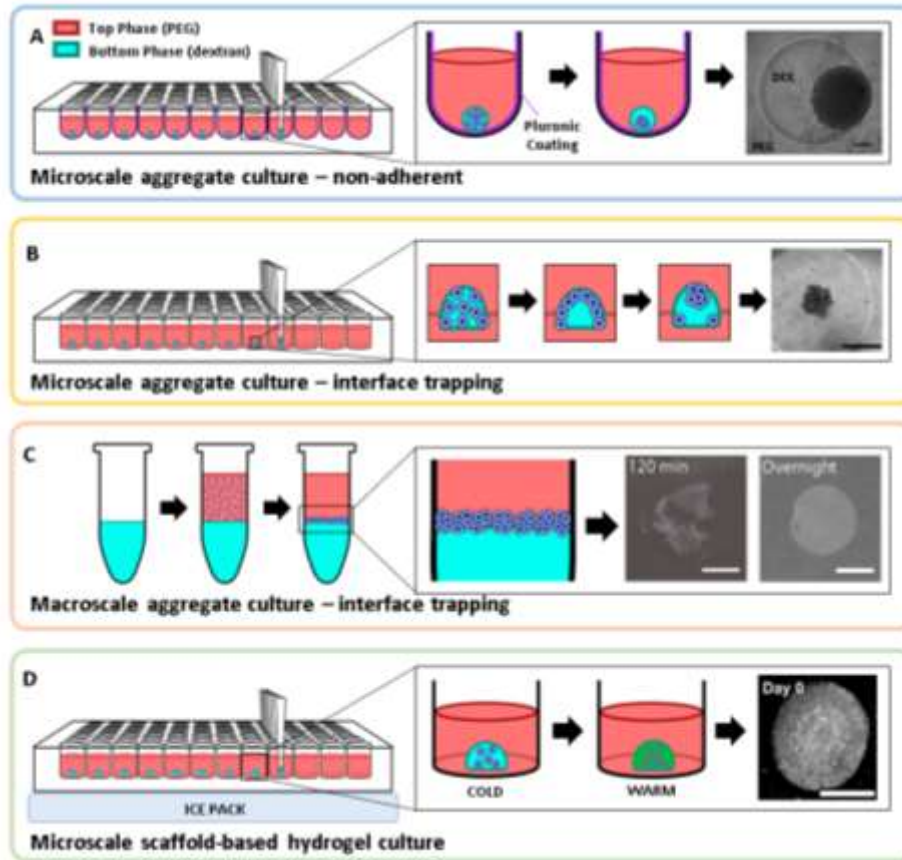
While advancements in cell culture techniques over the past decade have greatly enhanced our ability to analyze complex cellular functions and behaviours, aspects of native tissue architecture, mass transport and cell-cell interaction can be lost in two-dimensional (2D) culture, even under somewhat more complex formats such as those created through ATPS biopatterning. Simple three-dimensional (3D) microtissue models have been proposed as alternative platforms for *in vitro* drug screening and assay development, and ATPS-based microtissue assembly has offered inroads for the fabrication of self-assembling cell-rich constructs<sup>173–175</sup>. Common 3D culture techniques typically fall under two categories: aggregate culture, which relies on the spontaneous self-assembling properties of certain cell types to form 3D structures such as spheroids, or scaffold-based culture, which makes use of a hydrogel or other scaffolding material to act as structural support for cellular adhesion and 3D growth.

In recent years, the partitioning capabilities of ATPSs have been revealed to have unique utility in 3D microtissue engineering. Aggregate culture is conventionally achieved by promoting cell clustering through suspension of cells in hanging drops, continuous uniform mechanical agitation via spinner flasks or rotary orbital suspension culture, and low-attachment, specially designed plates<sup>174,176–180</sup>. However, these techniques can be low-throughput, expensive, technically complex, generate non-uniform aggregates, and/or require specialized equipment. To address these limitations, the Tavana group developed a novel, high-throughput aggregate culture technique facilitated by ATPSs (Figure 5A)<sup>175,181–183</sup>. Using this technique, cells are confined within a microscale, bottom-phase-forming droplet dispensed within a larger volume of a top-

phase solution in a pluronic-coated round bottom plate. This format allows cells within close, controllable proximity to each other to aggregate into spheroids without the risk of evaporation of their liquid medium, which can be problematic for hanging drop methods. While initially presented in a 96-well format, their technique has since been adapted to 384-well plates for advanced high-throughput oncological drug screening using 3D tumor microtissue models<sup>175</sup>.

Other microtissue strategies include the work by Han et al. utilizing ATPS-based phase density manipulation (Figure 5B)<sup>184</sup>. By changing the polymer concentration of the dextran-rich bottom-phase solution, phase density could be increased. The higher bottom-phase liquid density therefore increased the buoyant force acting upon the less dense cells resulting in cells becoming trapped at the interface of the ATPS due to the opposing forces of interfacial tension and buoyancy.





**Figure 5 Overview of ATPS-facilitated microtissue engineering.** A) Nonadherent microscale aggregate culture. Nontreated, round bottom plates are coated with 1% pluronic to prevent cell adhesion. A bottom phase-rich (dextran 500 kDa) cell suspension solution is then dispensed into a pool of top phase solution (PEG 35 kDa), which traps the cells within the bottom phase droplet, resulting in aggregate formation as displayed to the right (MDA-MB-157 cell line; scale bar = 200  $\mu$ m). B,C) Micro- and macroscale aggregate culture. B) When the bottom phase of an ATPS achieves a critical concentration at which the buoyant force acting upon cells is greater than the gravitational force pulling cells in the opposing direction, cells can become trapped at the interface between the two ATPS solutions. Microscale MCF-7 aggregates form at the apex of a droplet when cells rise to the interface (MCF-7 cell line; scale bar = 400  $\mu$ m). C) At the macroscale, cells suspended in a top phase solution settle and collect at the interface of the ATPS, with longer term incubation resulting in increased aggregation and microtissue formation (MCF-10 A cell line; scale bar = 5 mm). (D) Microscale scaffold-based hydrogel cell culture. Cells combined with a scaffold-forming hydrogel and a bottom phase forming solution are dispensed into a pool of top phase solution to prevent hydrogel evaporation. The hydrogel is crosslinked (e.g., by heating type I collagen) to form a scaffold (green) around the cells. Reproduced with permission<sup>30</sup>. Copyright 2017, Advanced Healthcare Materials.

In another study based on a similar concept, cells were instead combined with the PEG-rich top-phase solution and fell towards the interface due to higher gravitational

force relative to the buoyant force (Figure 5C)<sup>185</sup>. The forces acting upon cells at the interface of the ATPS were enough to promote macroscale aggregation to form skin-like constructs. It is important to note, however, that as previous studies have suggested, polymer concentration and cell type-specific surface properties can impact cellular partitioning behaviour<sup>184,186</sup>. ATPS and cell type characterization would be necessary prior to generating aggregate-based assays, especially in cases where cell lines or primary cell sources carry mixed populations that may have differing surface properties and sensitivities to growth conditions.

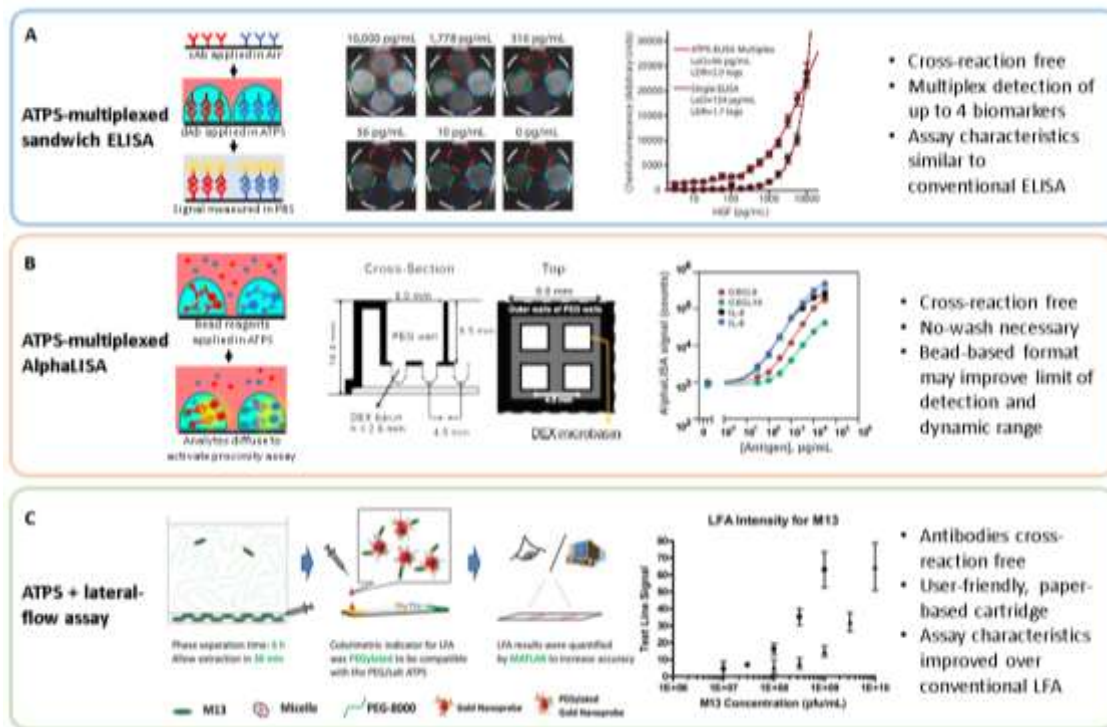
ATPSs provide a useful platform for cellular confinement, but do not always result in desirable aggregation properties depending on the cell type of interest. Cellular behaviours such as extracellular matrix (ECM) remodelling can also be difficult to observe or assess in the compacted aggregate formats. Thus, functional assays targeting cell-matrix interactions (e.g., mechanical contractility assays) have commonly been performed using type I collagen or other hydrogels to encase cells before cross-linking into a scaffold<sup>187,188</sup>. A key weakness of fabricating hydrogel-based microtissue constructs, however, involves the limitations of small-volume liquid-based systems. Large quantities of hydrogel material and cells are required to avoid evaporation and undesirable interfacial tension effects between liquids and air, which is costly, low-throughput, and produces unnecessarily thick cultures with poorer mass transport properties. As ATPSs allow for the manipulation of liquid systems and isolation of the bottom phase from air by the top phase, the Takayama group circumvented evaporation and interfacial tension by combining type I collagen with a dextran-rich bottom phase and trapping it within another aqueous solution (Figure 5D)<sup>189,190</sup>. Further investigation

by our lab revealed that a similar ATPS-based methodology could also be applied to Matrigel, a thermo-responsive, ECM-based hydrogel<sup>191</sup>. While incompatible with the commonly used dextran 500 kDa and PEG 35 kDa ATPS due to immediate precipitate formation when combined with Matrigel, hydroxypropyl methylcellulose (top phase) and a low molecular weight 10 kDa dextran (bottom phase) performed as an effective ATPS for the formation of ~60-110  $\mu\text{m}$  thin disks in a 96-well plate format. There remains a wide range of potential materials with ATPS-forming capabilities that may be useful for future 3D culture applications that have yet to be explored. At present, the simplicity and cost-effectiveness of ATPSs have facilitated promising approaches for accessible, high-throughput, 3D, microtissue assays that have the potential to offer more representative models of various tissues.

### **2.6.2 Solution Microarrays for Biochemical Analysis**

There are many techniques available for the detection of biomolecules in complex specimens, which may be either label-free (e.g., mass spectrometry-based analysis) or may include label-based (or immunometric) approaches<sup>192,193</sup>. However, most of the existing detection methods that are used clinically are based on the enzyme-linked immunosorbent assay (ELISA), which uses capture and detection antibodies to measure the concentration of analytes of interest in a bio-specimen. ELISA is the gold standard technique for clinical immunoassays and is capable of detecting a variety of pathologies ranging from cancer to autoimmune diseases with high sensitivity and specificity<sup>194-196</sup>. However, conventional ELISA platforms may suffer from cross-reactions among antibodies mixed in a common solution, leading to false-positive or false-negative

readouts. This can result in inaccurate diagnosis and treatment of patients, and may also complicate the validation of multi-biomarker panels and downstream development of clinically-applicable assays<sup>197</sup>. To address this drawback, ATPS-based strategies have been developed to eliminate potential antibody cross-reactions in multiplex panels by precisely confining the antibodies at specific locations. Frampton et al. developed a method, referred to as ATPS-ELISA, that prevents antibody cross-reactions, while utilizing lower volumes of antibodies and patient samples than conventional ELISA. This method takes advantage of a PEG-dextran system to facilitate deposition of detection antibody solutions contained in dextran droplets over pre-patterned capture antibody regions (Figure 6A). This procedure follows the standard ELISA workflow and is compatible with commercially available ELISA reagents and laboratory tools such as handheld multi-pipettors.



**Figure 6** ATPS-based immunoassay techniques. A) ATPS-multiplexed sandwich ELISA. Capture antibodies are applied to the ELISA plate. Colocalization of detection antibodies over capture antibodies is performed using a PEG–dextran system. This system confines the antibodies in dextran droplets, preventing cross-reaction. Standard curves are generated for up to four biomarkers (as shown by HGF analyzed by ATPS-ELISA and compared to conventional sandwich ELISA). B) ATPS-multiplexed AlphaLISA. Antibody-bead complexes are confined in dextran droplets, eliminating antibody cross-reactions. Custom plates enable analysis of up to four biomarkers. C) ATPS + lateral flow assay. Analytes are enriched prior to introduction to the lateral flow strip to increase total assay sensitivity. Reproduced with permission<sup>30</sup>. Copyright 2017, Advanced Healthcare Materials.

As with the techniques described above for solution micropatterning of cells, the denser dextran droplets sink within a common PEG solution and remain in contact with the assay plate during incubation. The interfacial tension between the PEG-dextran solutions and PEG-dextran-assay plate interface ensures the formation of stable dextran droplets that remain in place and prevents diffusive dispersion of detection antibodies. In this study, droplet stability was further enhanced through use of a customizable assay plate with micro-indentations designed to increase the surface area contacting the dextran

droplets. This strategy provided detection of four biomarkers associated with acute graft versus host disease (GVHD) without antibody cross-reaction due to diffusion, enabling streamlined analysis of the serum biomarkers<sup>102</sup>.

Although the sandwich ELISA workflow described above is the most widely used method for detection of biomarkers in biological samples, it is difficult to improve it in terms of automation and throughput. To overcome these obstacles, a technique for ATPS-based micropatterning of a homogenous bead-based AlphaLISA® platform was developed (Figure 6B). This choice of a homogenous assay offers the possibility for increased throughput, a reduction in total assay time through elimination of wash steps and superior assay sensitivity and dynamic range<sup>198</sup>. However, in its standard format, this technique typically allows only single protein detection. Similar to the ATPS-ELISA procedure, AlphaLISA was multiplexed with the use of a PEG-dextran system to partition the bead-conjugated antibody reagents within micropatterned arrays of dextran droplets, thus preventing non-specific cross-reaction among the reagents for improved multiplex protein detection. In this study, both human plasma and cell culture supernatants were analyzed<sup>199</sup>.

Recently, these ATPS-based ELISA procedures were further improved to make operation easier for end-users and to reduce pipetting steps. This was accomplished by dehydrating the ATPS during preparation and then rehydrating it with a solution containing the analyte. In this simplified assay, capture antibody solutions were first immobilized on the microplate surface by dehydration in the presence of lyoprotectants. The plates were then prepared by application of a separation layer containing additional lyoprotectants and dextran, before an additional layer containing lyoprotectants, dextran

and horse radish peroxidase (HRP)-conjugated detection antibodies was applied. After complete drying, the antibody microarrays were rehydrated in a PEG solution containing the target analytes. The analytes diffused from the PEG phase into the dextran droplets containing the immobilized capture antibodies and dextran-confined detection antibodies to form capture antibody- analyte-detection antibody complexes that could be detected by development of chemiluminescence in the presence of an appropriate substrate reagent. According to the authors, this method simplifies the ATPS-ELISA procedure and reduces potential user error due to easier droplet placement. It also opens the possibility for automation of the antibody array fabrication process. Cell culture supernatants were analyzed in this study, and the limit of detection (LOD) and signal to noise ratio (S/N) values were compared to the previous ATPS-ELISA. The results showed a comparable LOD between the methods and lower S/N using the dehydrated ATPS technique<sup>200</sup>.

ATPSs have also been applied to improve the sensitivity of the lateral-flow immunoassay (LFA) using a similar strategy to the one employed in ATPS-ELISA to confine biomolecules (Figure 6C)<sup>201</sup>. LFA is a paper-based diagnostic system commonly used to detect disease biomarkers and infectious agents such as the bacterium *Chlamydia trachomatis*<sup>202</sup>. Chlamydia infection is considered the most common sexually transmitted disease worldwide and can cause serious sequelae such as pelvic inflammatory disease in women and permanent damage to the reproductive system if is not treated. For this reason, there is an urgent demand for low-cost, rapid and user-friendly devices that allow early detection of this disease<sup>203</sup>. The improved lateral-flow immunoassay designed for chlamydia diagnosis used a sample solution to rehydrate a dehydrated PEG-phosphate system, concentrating *C. trachomatis* within the LFA paper. The diagnostic device was

designed to integrate a PEG-salt ATPS with standard LFA by applying the *C. trachomatis* samples to the ATPS formation region of the device where they became concentrated, which had the effect of improving the assay sensitivity by enriching the target analytes present in the original sample. In this procedure, once the concentrated samples reached the standard LFA section, detection of the target (e.g., *C. trachomatis*) was significantly enhanced compared to the LFA only version, with a 10-fold improvement in sensitivity. The same group developed other small-scale diagnostic approaches by combining ATPS with LFA, improving the detection of biomolecules such as proteins<sup>204,205</sup>, and viruses<sup>206,207</sup>.

Similar strategies have been applied to detect natural toxin contamination of food, for example mycotoxins<sup>208</sup>. The annual loss of food products due to mycotoxin contamination is considerable, with estimates that up to 25% of the world's food crops contain some level of contamination by mycotoxins. This results in an estimated waste of 1 billion metric tons of food per year that is deemed unfit for human consumption due to probable presence of mycotoxins that may cause serious health problems including cancer, hepatotoxicity, neurotoxicity and immunosuppression<sup>209</sup>. Due to the impact of mycotoxin contamination on the food production sector, the rapid detection of mycotoxins in food samples is extremely important. The traditional technologies developed to improve mycotoxin detection typically use organic solvents and complex multi-step procedures. To improve mycotoxin detection capabilities, a single-step extraction using a PEG-citrate system was developed. The method consists of concentrating and extracting three different mycotoxins from raw feed. The samples are first vigorously mixed with the PEG-citrate extraction solution. After extraction, the



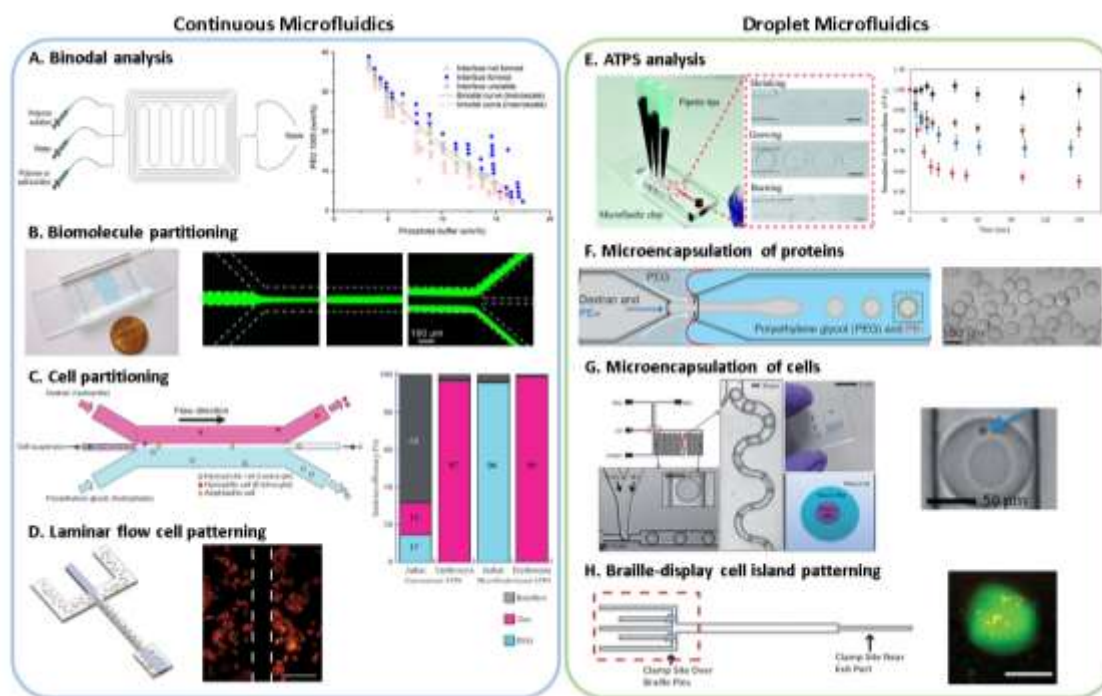
ATPS phases are separated by centrifugation, which leads to partition of the mycotoxin to the top PEG-rich phase. The PEG-rich phase is then collected and diluted with an HRP-labelled anti-mycotoxin antibody solution. This solution is inserted in a microfluidic channel, previously coated with mycotoxin-BSA-conjugate, and blocked with a solution of BSA. Finally, a luminol plus hydrogen peroxide solution is injected in the microchannel to generate a chemiluminescence signal that can be detected by microscopy<sup>210</sup>.

Another example of the utility of ATPSs in immunoassay development pertains to the commonly used prostate cancer diagnostic marker, prostate-specific antigen (PSA). Detection of PSA was improved by partitioning isoforms of PSA in ATPSs. IsoPSA™, previously known as PSA/SIA, is a blood assay that detects each PSA isoform partitioned between the two aqueous phases. The total PSA in both phases is measured by a conventional PSA clinical ELISA. Based on the partition coefficient, a composite structural index of the PSA isoform population can be generated<sup>211,212</sup>. According to a recent multicenter prospective study, IsoPSA has shown to be more sensitive and specific than the current gold standard PSA test, with potential to reduce unnecessary biopsies and decrease the risk of over-detection and overtreatment of nonlethal prostate cancers<sup>212</sup>.

### **2.6.3 Microfluidics**

Microfluidic platforms, such as the LFA technology described above, the microfluidic binodal determination system described in Section 2.1 (Figure 7A), and the microchannel systems described below, are interesting tools for biotechnology because they enable the precise manipulation of small volumes of solvents, reagents and cells,

which can reduce assay costs, improve the throughput and quality of analysis and conserve rare or expensive samples. Advantages such as short reaction times, portability, versatility in design through rapid prototyping, and integration with other miniaturized technologies are also touted for these devices<sup>103,213,214</sup>. Recently, the microfluidic research community has begun to explore how ATPS can be utilized to further enhance the capabilities of microfluidic devices.



**Figure 7 Applications of ATPS in continuous and droplet microfluidic systems.** A) Binodal analysis. Schematic of an ATPS binodal analysis microfluidic device and associated binodal curves. B) Biomolecule partitioning. Representative images of a microfluidic device showing FITC-labeled IgG in a detergent-rich phase entering a PEG-rich phase at the end of the microchannel. C) Cell partitioning. Diagram of a microfluidic device used for extraction of cells with comparison to data from the conventional method at right. D) Laminar flow cell patterning. Diagram of a microfluidic device used to selectively deliver trypsin to a cell population growing within a microchannel as shown at right. E) Passive droplet generation in a microfluidic device. F,G) Microencapsulation using ATPSs. Diagrams of microfluidic devices used to generate protein and cell microcapsules as shown at the right. H) Cell island patterning. Diagram of a Braille-actuated microfluidic device used to generate dextran droplet containing cells as shown at right. Reproduced with permission<sup>30</sup>. Copyright 2017, Advanced Healthcare Materials.

### 2.6.3.1 Continuous Microfluidic Devices

Continuous-flow microfluidic devices refer to devices that generate laminar fluid streams within microchannels that allow separation of small volumes of sample continuously. The laminar flow forms a stable interface between the polymer solutions, through which biomolecules or cells are segregated<sup>215</sup>.

Continuous flow microfluidic devices incorporating ATPSs have been used primarily for biomolecule and cell enrichment (Figure 7B-C). One of the first studies to integrate ATPSs with microfluidics utilized a conventional laminar flow channel designed to separate leukocytes and erythrocytes from whole blood with much greater efficiency compared to conventional batch procedures. Using an ATPS composed of PEG and dextran, it was possible to simultaneously retrieve erythrocytes in the dextran phase and leukocytes in the PEG phase<sup>71,133</sup>. This phenomenon may be explained by the repulsion of the negative charge on the membrane of the leukocytes from the negatively charged dextran phase and by the affinity of the sugar chain on the surface of the erythrocytes to dextran. Tsukamoto et al. further demonstrated the efficacy of this microfluidic-based ATPS technique. They were able to recover up to 99% of erythrocytes and 96% of leukocytes (Jurkat cells), as compared to recovery of 97% of erythrocytes and 15% of leukocytes using a conventional ATPS batch approach.<sup>71</sup> Moreover, SooHoo and Walker used a microfluidic PEG-dextran system to separate both types of cells simultaneously. Their approach resulted in up to a 9.13-fold increase in the concentration of leukocytes over the control (without ATPS)<sup>133</sup>. In addition to the purification of cells in ATPS, microfluidic ATPSs have also enabled micropatterning of different cell populations with minimal cross-contamination among cell populations, as well as

selective chemical delivery within microfluidic channels (Figure 7D). This approach enabled more precise cell patterning in microfluidic devices and more highly localized chemical treatment to cells growing within microchannels compared to conventional laminar flow patterning<sup>72</sup>.

The collection and enrichment of molecules within microfluidic devices can also be enhanced by way of the partitioning effects of ATPSs. By integrating ATPSs with microfluidics, the efficiency of ATPS-based separation of biomolecules is often improved. This can be achieved by increasing the surface area of the interface between the two phases by decreasing the width of the fluid lamellae either by adjusting the width of the microfluidic channel itself or by adjusting the fraction of the channel occupied by one of the phases (an effect that can be achieved by adjusting the relative flow rates of the phases or by design of the channel inlets)<sup>216</sup>. Taking advantage of the short diffusion distances of microfluidic channels and the mild conditions of ATPSs, separation/purification of proteins (e.g., beta-galactosidase and bovine serum albumin (BSA)<sup>217,218</sup>) has been achieved across laminar stream of phase-separating ATPS-based fluids. Due to the hydrophobic characteristic of some proteins (e.g., membrane proteins), their purification is a challenge and requires solubilization with detergent to extract them from the cells. By combining detergent/polymer two-phase systems with microfluidics, it is possible to separate membrane proteins more efficiently and with less denaturation<sup>219</sup>. Furthermore, the purification of protein drugs such as monoclonal antibodies has been conducted in microfluidic devices incorporating ATPSs. This approach has significant potential in the biotechnology industry because it is easily scaled by adjusting the number

of microfluidic channels performing separation and because the production process can be easily monitored and optimized<sup>144</sup>.

Separation processes such as these can also be readily coupled with additional purification modalities. For example, electrokinetic flow, which is a technique that applies an electric field to separate molecules, may be used in conjunction with ATPS partition-based purification. Since many biomolecules are charged, it is faster to transport them by electroextraction than by diffusion. Therefore, this approach can augment the partition of biomolecules, increasing the yield and the selectivity of the method<sup>213</sup>. It has been demonstrated that under the driving force provided by an external electric field, the partition of BSA molecules is enhanced, and that mass transfer is no longer governed by adsorption at the interface, but rather by the electrophoretic mobility and the partitioning of the molecules to the bulk phases<sup>220</sup>. It is also possible to perform biomolecule separations in microfluidic devices according to at least two different properties of the samples, for example, simultaneous affinity-based partitioning in an ATPS and electrophoretic separation<sup>218</sup>.

In general, the transfer of protocols from macroscopic batch processes to ATPS-based microfluidic platforms has been relatively straightforward in comparison to other technologies, opening possibilities for many novel applications<sup>103</sup>. As with most microfluidic designs, the majority of microfluidic systems integrating ATPSs do not exhibit significant turbulence, which means that they readily form laminar streams that mix primarily by diffusion. In the case of laminar flows of ATPS-based fluids, the diffusion of biomolecules and particles takes on a selective quality based on partitioning effects.

Laminar flow can usually be achieved using the conventional methods customary to the field of microfluidics. However, the stability of laminar flows of ATPSs in microchannels is fundamental for many of the above applications. The least complex designs typically involve the use of two channels that meet at a junction to generate the laminar streams. To stabilize laminar flows of ATPSs in microfluidic devices, it is often necessary to optimize channel geometries and fluid viscosities. Another strategy to achieve improved stability is to modify the inlet and outlet design. A trifurcated design can compensate for differences between the flow ratios of the inlets and outlet to improve the stability of continuous ATPS separations in microchannels<sup>221</sup>. The result of instabilities in flow profiles of ATPS-based fluids is the formation of droplets, which is useful for other applications as described below, but can be difficult to control and is not desirable for continuous separations. However, following appropriate optimization of the flow properties, it is possible for the two phases to be recovered with minimum cross-contamination of the phase-separating materials<sup>103</sup>.

### **2.6.3.2 Droplet Microfluidics**

Droplet-microfluidic systems enable the generation and manipulation of size-controlled droplets within microchannels. This approach, which more-commonly is achieved with oil-water systems, has been adapted for bioassays, single cell or drug encapsulation, and high-throughput analysis involving ATPS microdroplets<sup>160-164</sup>.

As mentioned above, microfluidic droplet formation results from instability between the two immiscible flows. Due to the low interfacial tension of most ATPSs, it has been difficult to control the formation of droplets, as the two immiscible fluids tend

to form laminar streams as they flow through most microchannel geometries. Some of the first examples of controlled ATPS droplet formation were achieved using high concentrations of PEG and salts<sup>165</sup>. These approaches produced ATPSs that displayed interfacial tensions much higher than what is typically encountered for ATPSs used in biotechnology applications, but allowed droplets to form spontaneously due to Rayleigh instability. Although these studies represented a first step in the use of ATPSs for droplet microfluidics, the flow regimes required to form droplets generated relatively broad droplet size distributions using materials that were not as conducive to applications involving cells and sensitive biomolecules as other commonly used ATPSs.

Subsequent studies focused on the use of external forces to generate the instabilities required for droplet formation by low interfacial tension ATPSs. Some of the first example of this included devices incorporating piezoelectric bending disks and actuators driven by Braille displays that improved control over droplet size, as well as the frequency of droplet formation<sup>160,166</sup>. Shum et al also demonstrated the effect of adjusting the flow rates and the frequency of external forcing on the ultra-low interfacial tension of PEG/K<sub>3</sub>PO<sub>4</sub> system. After applying different frequencies (from 0.1Hz to 50kHz), they concluded that the interfacial tension could be modified by external perturbation and that the most effective frequency to promote droplet formation in their system was ~4.5Hz. They also observed that the ratio of flow rates of the two phases has considerable influence on the morphology of the jets. As the ratio of the inner fluid flow rate to the outer fluid flow rate increased, the jet became thicker, requiring greater deformation of the interface to promote the transition from a corrugate-interface regime to a droplet regime<sup>167</sup>. In addition, the same group investigated the influence of fluctuations induced

by syringe-pump on ATPS microfluid flows. In this work, they considered the same system used previously (PEG/K<sub>3</sub>PO<sub>4</sub>). The stepper motor inside the syringe pump was used as source of disturbance to the fluid injected in the microdevice. They concluded that the frequency of the ripples only depends on the flow rate of the inner phase and that each ripple is generated by one moving step of the stepper motor, which depends on many parameters including the flow rates and the internal diameter of the syringe. The authors suggested that by manipulating the flow rate in a controlled manner, it is feasible to control the deformation of the interface<sup>168</sup>.

Recently, Moon et al. developed a microfluidic system capable of forming ATPS droplets passively, i.e., without any external forces to perturb the ATPS interface (Figure 7E)<sup>169</sup>. This strategy is based on applying weak hydrostatic pressures through ATPS fluid-filled pipette tips connected to the inlets, promoting low speed flows to a flow focusing junction. Under the optimal conditions, it was possible to form highly uniform droplets with polydispersity less than 3%. Moon et al. also demonstrated that the droplet size along the microfluidic channel can be controlled by modulating ATPS equilibrium, which is not possible with traditional water-in-oil or oil-in-water droplet systems. To achieve this, they introduced a secondary inlet downstream of the PEG-dextran flow focusing junction, whereby a different concentration of PEG solution was injected. The injection of a more concentrated PEG solution through the secondary inlet decreased the droplet volume since the water left the disperse phase (dextran) to reduce the overall concentration of PEG in the continuous phase. To increase droplet volume, water could enter the dextran phase droplets during the re-equilibrium process after a less concentrated PEG solution was infused at a second cross junction<sup>224</sup>.



Applications for microfluidic ATPS droplet formation include the generation of microcapsules with potential cell and drug delivery applications, as well as the ability to perform cellular micropatterning inside microfluidic devices (Figure 7F-H). Polymer microcapsules based on similar materials to those known to form ATPSs have been used for drug delivery, tissue engineering, and biochemical analysis<sup>170,171</sup>. An ATPS composed of Pluronic F127 and dextran was used to produce poly(lactide-co-glycolide) (PLGA) microparticles. When PLGA is emulsified in the Pluronic F127-dextran system, a unique particle is formed due to ATPS assisted self-assembly. These microparticles exhibit amphiphilic characteristics that favor encapsulation of both hydrophobic and hydrophilic molecules. Furthermore, the lower critical solution temperature properties of Pluronic F127 impart temperature responsive properties to the particles. Both features make these PLGA microcapsules well-suited for biomedical applications such as drug delivery<sup>171</sup>. Although this process did not take place inside a microfluidic device, microfluidic droplet generation could offer potential to improve droplet uniformity. For example, by applying ATPS microfluidic technology, it was possible to generate microcapsules with precise control over the morphology, internal structure, and size, as demonstrated using PEGDA-dextran and PEG-dextran systems<sup>172,173</sup>. Both core diameter and shell thickness can be modulated by adjusting the flow rates of the core and the shell phases. By increasing the flow rate of the outer PEG phase, not only can the total droplet diameter and size variation be reduced, but also the required UV exposure time for polymer shell cross-linking. Therefore, PEG-dextran systems can provide production of a wide variety of water-based microcapsules that can be tuned to address specific applications<sup>174</sup>. Frampton et al. demonstrated yet another application of the PEG-dextran system to precisely deliver

cells and biomolecules using droplet dispensing devices (Figure 7H). The cells were encapsulated within dextran droplets and delivered into the PEG phase. Due to the interfacial and partitioning properties of the ATPS, cells were patterned in precise colonies within enclosed microfluidic channels<sup>72</sup>.

#### **2.6.4 ATPSs in Synthetic Biology**

The development and testing of artificial cell-like structures can potentially offer insights into cellular function and provide new modalities to control and manipulate biological systems<sup>175–177</sup>. As such, the design of artificial cells and cytomimetic materials is emerging as a major theme in synthetic biology. Many processes occurring in even the most complex of living cells are influenced by confinement or micro-compartmentalization within both membrane-enclosed and membrane-free structures.<sup>178</sup> The phase separation properties of ATPSs have been exploited to mimic some of these intracellular compartments, such as liquid-like organelles and nucleoli<sup>30,45,179–181</sup>. In addition, research has begun to explore how proteins can be encapsulated within ATPS polymersomes to serve as useful tools for therapeutic delivery and for fundamental research<sup>182</sup>. Some of the first example of this include studies investigating the effect of micro-compartmentalization on enzymatic reactions. It has been demonstrated that enzyme compartmentalization in the PEG-dextran system can model the behavior of two sequential enzymes involved in purine biosynthesis: ASL (adenyl succinate lyase) and ATIC (5-aminoimidazole-4-carboxamide ribonucleotide transformylase/inosine monophosphate cyclohydrolase). These enzymes partitioned to the dextran-rich phase due to their higher affinity for the more hydrophilic of the two polymers. Although

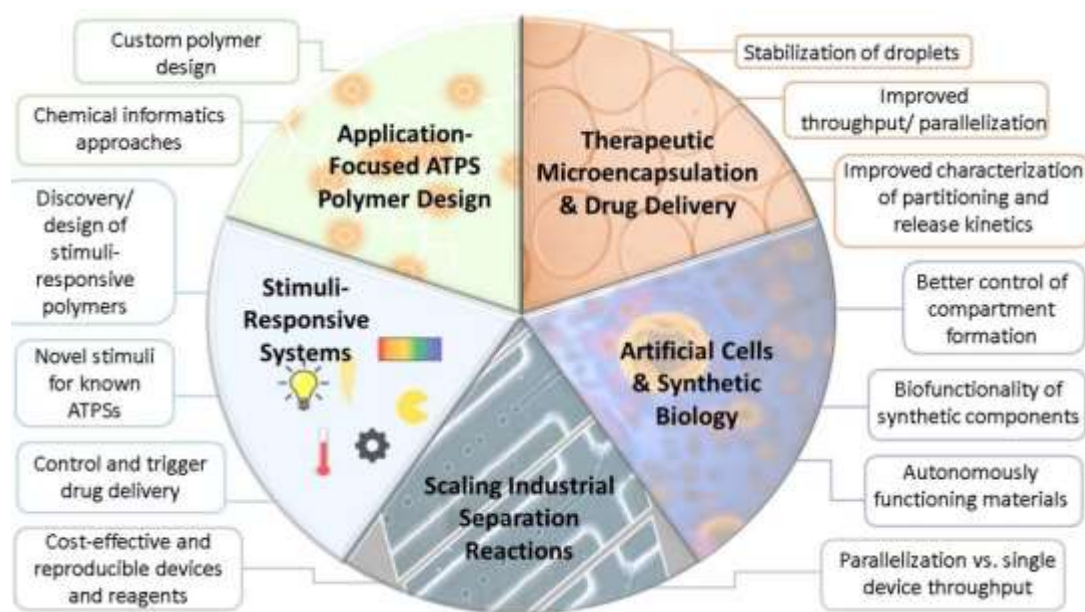
ATPS-based compartmentalization was initially hypothesized to increase the reaction rates of these enzymes, in this case, compartmentalization in an ATPS did not produce a significant increase in reaction rate. The authors reasoned that to enhance metabolic rates it would be necessary to achieve stronger partitioning of the enzymes into one of the compartment-forming phases, which could be achieved by including other purine biosynthetic enzymes to interact with the two enzymes investigated (ASL and ATIC) or by promoting higher local enzyme concentrations<sup>181</sup>. In another experimental model, the rate of RNA cleavage was increased about 70-fold when ribozyme was partitioned into the dextran-rich phase of the PEG-dextran system. In this work RNA catalysis was enhanced by varying the dextran-rich phase volume, consequently providing a 3,000-fold RNA enrichment. The results showed that RNA catalysis was increased by decreasing the compartment size, i.e., the dextran- to PEG-rich phase volume<sup>179</sup>. These studies provide some of the first evidence that ATPSs can be used to model biological compartmentalization, which may have future impact on the generation of synthetic cell-like structures.

## **2.7 SUMMARY AND OUTLOOK**

ATPSs have enabled a variety of simple, cost-effective approaches that take advantage of the low interfacial tension between polymer phases, partitioning effects and high degree of biocompatibility of many ATPS-forming polymers, providing researchers with a valuable tool set for microscale analysis of cell growth and many other biotechnology applications. In terms of micropatterning, ATPS offers a high degree of spatial and temporal control over cell positioning. Moreover, ATPS micropatterning can

be performed using simple laboratory equipment, making it highly transferrable to new users. ATPS has also shown remarkable promise in the field of tissue engineering. This gentle, contact-free microprinting technology will enable researchers to generate cellular microenvironments that can be used to recapitulate *in vivo* stimuli and study homotypic and heterotypic interactions with greater detail. Combining ATPSs with microfluidic platforms has also resulted in development of many novel applications. ATPSs have been utilized to separate biomolecules and cells within microchannels, requiring only small volumes of samples that can be continuously separated and monitored. In addition, formation of ATPS droplets in microfluidic devices has enabled encapsulation of biomolecules and cells, which may be useful for future drug and cell delivery applications. Moreover, ATPSs have been exploited for improvement of multi-biomarker detection, addressing some limitations of the gold standard ELISA. ATPS-ELISA is compatible with standard ELISA reagents but offers the major advantage of preventing antibodies cross-reactions. Transfer of this multiplex biomarker platform from lab to lab or lab to clinic will be possible with the investigation of new systems able to analyze a wider range of diseases. Finally, over the past decade, synthetic biology has grown significantly and has utilized ATPSs to mimic cellular structures. ATPS partitioning properties have been used to develop experimental models for compartmentalization of cellular organelles, which has contributed to understanding of physicochemical mechanisms of fundamental biological processes. Although ATPS technologies hold immense potential for these and other biotechnological applications, they have not been widely exploited in industry yet due to the incomplete understanding of the physicochemical properties of some of these systems and their interactions with

biological specimens. Figure 8 highlights several areas of future growth within the field, indicating important technological barriers and design considerations that need to be addressed before it will be possible to realize the full potential of ATPSs in biotechnology. As this field matures and as more studies fill in gaps in the characterization and performance of ATPS-forming materials, ATPSs are likely to see more widespread use beyond the laboratory.



**Figure 8** Areas of future growth for applied ATPS research. Technological needs and design considerations required to enable future applications are indicated. Reproduced with permission<sup>30</sup>. Copyright 2017, Advanced Healthcare Materials.

## CHAPTER 3

# ATPS SCALABILITY – FROM FEMTOLITERS TO LITERS

Portions of this chapter have been published in **Proceedings of SPIE** and are being reproduced in this thesis with permission from the publisher SPIE.

Alyne G. Teixeira, Meng-Chiao Tsai, John P. Frampton (2018). Microfluidic control of droplet formation from stable emulsions formed by aqueous two-phase systems.

*Proceedings of SPIE*, vol. 10491, Microfluidics, BioMEMS, and Medical Microsystems XVI.

### 3.1 ABSTRACT

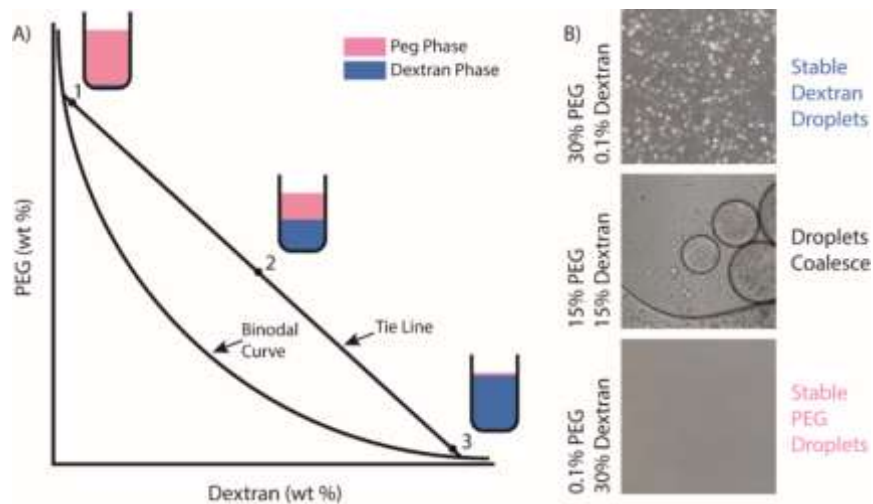
Aqueous two-phase systems (ATPSs) form from the thermodynamic separation of two incompatible solutes, such as two polymers, a polymer and a salt, and a polymer and a surfactant. ATPSs can be applied to numerous applications with individual phases occupying volumes ranging from several fL to several L or more. This chapter will highlight work to explore the lower range of ATPS droplet formation and compare the applications and utility of the polyethylene glycol (PEG)-dextran system across volume scales. At the fL scale, for most supercritical concentrations, ATPS emulsions can be formed by vigorous mixing. These emulsions typically settle into distinct layers in minutes to hours. However, it is also possible to choose ATPS compositions with extremely long settling times that resemble stable emulsions. Here, we generated stable emulsions from a PEG-dextran system by selecting ATPS compositions at the extreme ends of the tie lines connecting the binodal curve delineating phase-separating compositions. Droplets of PEG in a continuous dextran phase did not coalesce appreciably over the course of several days when stored in a conical tube or syringe. However, upon exposure to laminar flow conditions in a microfluidic channel, droplets

were observed to coalesce. Through microscopic characterization of droplet volume, an increase in droplet size and decrease in overall droplet number was observed as a function of channel distance, suggesting a progressive droplet merging phenomenon. This novel approach to control droplet size by encouraging coalescence of stable emulsions under laminar flow in a microfluidic channel enables the production of droplets ranging from fL to several pL, which may enable various future biotechnology applications. Examples of how ATPSs have also been used in biomedical applications using volumes from nL to  $\mu$ L, such as multiplexed assays, and in larger platforms that use ATPS volumes ranging from mL to L, such as purification of biomolecules, are also presented with a focus on applications in immunoassays and isolation of proteins involved in immune responses from complex biological fluids.

### **3.2 INTRODUCTION**

As described previously, ATPSs are formed when incompatible solutes such as two polymers, a polymer and a salt, or a polymer and a surfactant are dissolved in water at sufficiently high concentrations such that the thermodynamic equilibrium favors separation into two distinct liquid phases<sup>151</sup>. Among the many solutes that form ATPSs, the most widely explored are polymer-salt systems (e.g., polyethylene glycol (PEG)-phosphate) and polymer-polymer systems (e.g., PEG-dextran). By applying the Gibbs free energy equation  $\Delta G = \Delta H - T\Delta S$ , where  $\Delta G$  represents the change in free energy of the system,  $\Delta H$  represents the change in enthalpy,  $T$  represents the temperature, and  $\Delta S$  represents the change in entropy, it is possible to understand how the driving forces

operate in these systems. For a two-polymer system such as the PEG-dextran system, phase separation is associated with a gain in enthalpy from interactions between polymer molecules and a loss in entropy from segregation of the phases. The concentrations of two solute species above which an ATPS will form are delineated by the binodal phase diagram<sup>213</sup> (Figure 9). For any system above the binodal curve, there exists a tie line, which describes the polymer concentrations and relative volumes for each phase. As one examines various ATPSs located along a tie line, the polymer concentrations in each of the phases remain the same, but the relative volumes of the phases change. The midpoint of a tie line corresponds to a composition at which 50% of the volume is occupied by each phase, resulting in a bicontinuous system. As one explores compositions farther from the midpoint of the tie line, the phase with the greater relative volume composes the continuous phase and the phase with the lesser relative volume composes the dispersed phase when the system is agitated to generate an emulsion<sup>244</sup>.



**Figure 9** Binodal phase diagram and images of PEG-dextran emulsions. A) Points 1, 2, and 3 represent three hypothetical compositions of ATPS lying on the same line. Point 1 indicates the composition of the PEG-rich top phase, point 2 has equal volumes for the top and the bottom phases, and point 3 indicates the composition of the dextran-rich bottom phase. B) Bright field microscopy images of an emulsion composed of a PEG continuous phase and a dextran dispersed phase (top), bicontinuous emulsion (middle), and an emulsion containing a dextran continuous phase and a PEG dispersed phase (bottom). Reproduced with permission<sup>414</sup>. Copyright 2018, Proceedings of SPIE.



Due to their well-defined physicochemical properties, ease of use, and compatibility with a wide range of sensitive biological materials, ATPSs have started to replace approaches involving other phase-separating liquids (e.g., organic solvent/water and oil/water systems) in a wide range of biotechnology applications<sup>30</sup>. ATPSs have also found increasing use in microfluidics research<sup>103</sup>, with considerable interest as materials for the generation of microfluidic droplets. Most approaches for generating droplets from ATPSs in microfluidic channels involve the use of external forces (e.g., electrohydrodynamic<sup>226,245</sup> or mechanical<sup>222,227</sup> perturbation) to produce the instability necessary for droplet breakup, as most conventional channel designs utilized for generating oil-in-water (O/W) or water-in-oil (W/O) droplets produce laminar streams when ATPSs are introduced. However, these approaches are relatively complex and are restricted in terms of throughput and their ability to produce a wide range of droplet sizes. Recently, Moon et al<sup>230</sup> demonstrated generation of droplets by passive flow focusing using a PEG-dextran ATPS. This simplified approach utilized weak hydrostatic pressures to introduce PEG and dextran solutions into microfluidic channels at very low flow rates. Using this approach, it was possible to produce a dispersed phase of dextran introduced through the center channel of a flow focusing geometry, surrounded by a continuous phase consisting of PEG. Droplet size was dictated by the interfacial tension and viscosity of the ATPS, and by the column heights in the pipette tips used to apply the hydrostatic pressure. The same group also demonstrated that it was possible to either shrink or grow ATPS droplets in microfluidic devices by perturbing the phase-separation equilibrium with a PEG solution injected through a downstream microchannel<sup>224</sup>. Even more recently, Mytnyk et al.<sup>235</sup> developed a microfluidic platform that spontaneously

generated droplets at a flow-focusing junction, using PEG and cross-linkable dextrans. The ATPS solutions were injected at two consecutive flow-focusing junctions, using individual syringe pumps. Once the droplets formed, they were stabilized by downstream crosslinking via ultraviolet irradiation. Although these previous studies represent important steps in the development of ATPSs for droplet microfluidics, they are limited in terms of throughput and the ability to generate droplets smaller than  $\sim 5$  pL. To overcome some of these limitations, we considered whether it would be possible to generate droplets from ATPSs by alternative means. Upon vigorous agitation, an ATPS will typically take the form of an opaque water-in-water (W/W) emulsion. Over time, the droplets dispersed in this emulsion tend to separate into two distinct volumes according to their specific gravity, forming distinct layers. However, when compositions at the extreme ends of a tie line on the binodal phase diagram are selected, it is possible to generate stable emulsions, e.g., droplets of dextran in PEG or droplets of PEG in dextran that do not coalesce<sup>79,246</sup>.

This chapter is divided in three parts: the first part is dedicated to describing a novel approach to generate size selectable droplets (fL to pL) from ATPS emulsions by encouraging normally stable droplets to coalesce under laminar flow conditions in a microfluidic channel. The second part is focused on ATPS applications using volumes from nL to  $\mu$ L in multiplexed immunoassays, enzyme-linked immunosorbent assay (ELISA) and enzyme-linked immunospot (ELISpot); and the last part presents applications that use ATPS volumes ranging from mL to L, such as purification of biomolecules.

### **3.3 MATERIALS AND METHODS**

#### **3.3.1 Materials and Methods**

##### **3.3.1.1 ATPS Formulations**

ATPS solutions were prepared by dissolving 500 kDa dextran and 35 kDa PEG in distilled deionized water to obtain the following systems: 30% (w/w) dextran and 0.025% (w/w) PEG, 30% (w/w) dextran and 0.050% (w/w) PEG, and 30% (w/w) dextran and 0.1% (w/w) PEG. The solutions were vigorously mixed before being introduced into a 1mL syringe connected to a 1mm inner diameter tubing segment that was inserted into the inlet of the microfluidic device.

##### **3.3.1.2 Microchannel Fabrication**

Microchannels were designed using Adobe Illustrator CS6 64 Bit. The final design consisted of a continuous serpentine channel with five bends (inverting direction at each bend), forming six parallel sections with a straight segment length of 20.96 mm and a width of 500  $\mu\text{m}$ . The height of the channel was 75  $\mu\text{m}$ , as determined by the thickness of the masking film. The total distance from the first to the last parallel section was 142.85 mm. Designs were transferred to masking film (Ulano Rubylith RU3 Universal Tack Knifecut Masking Film for Graphic Arts) using a CE6000-60 Graphtec Cutting Plotter. Relief structures were created by peeling regions of masking film from the film backings using tweezers. Film backings containing the desired relief structures were taped to ethanol-cleaned glass slides and wiped clean of any dust using an ethanol-soaked Kim wipe. These structures served as single-use replica molds for curing

polydimethylsiloxane (PDMS; SYLGARD 184 Silicone Elastomer). Once cured, PDMS replicas were cut from the molds and inlet and outlet ports were punched using a 1 mm biopsy punch. PDMS replicas and ethanol-cleaned glass slide were activated by atmospheric gas plasma using a Plasma Etch plasma oxidizer. PDMS replicas and glass slides were then pressed together to bond the devices and baked in a 60°C gravity convection oven for 2 hours before use.

### **3.3.1.3 Imaging**

A Nikon Eclipse T1 Microscope was used to capture bright field images using a 10X objective lens. Ten 640 x 480-pixel images were captured at seven distinct locations – one before each bend, one right after the inlet, and one right before the outlet. A flow rate of 5 nL/min was generated using a KD Scientific Legato 111 syringe pump, such that droplets moved through the channels at a speed that could be captured using the microscope CCD camera without significant image blurring. Consecutive images for each channel position were captured a few seconds apart with an exposure time of 1 msec.

### **3.3.1.4 Droplet Volume Quantification**

ImageJ was used for droplet volume quantification. After converting images to 8-bit format, differences between two consecutive images were extracted to remove any static features (e.g., any non-droplet features such as the channel walls, debris, or imperfections in the PDMS). This was achieved using the Difference operation within the Image Calculator function of Image J. The resulting images contained the moving

droplets present in both images without any extraneous data, yielding 5 images for analysis. These images were then converted to binary via the Auto Threshold function using the Renyi Entropy method. After cropping the modified images to 640 (l) x 380 (w) pixels corresponding to the regions where the features were located, the area of each droplet was measured with the Analyze Particles function in ImageJ. Pooled pixel area data were converted to spherical volumes in  $\mu\text{L}$  for the three different ATPS compositions listed above. Values were plotted as histograms for each channel location and ATPS formulation.

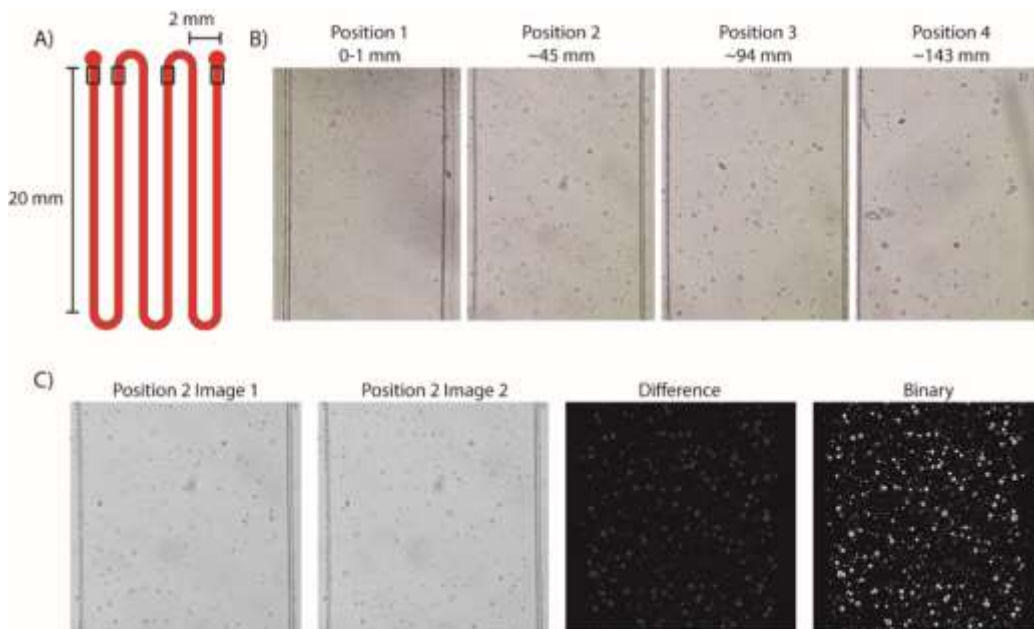
### **3.4 RESULTS AND DISCUSSION**

A fictitious phase diagram describing the phase separation of a PEG-dextran system is illustrated in Figure 9. Each point along the binodal curve represents a critical concentration below which the polymers will be miscible and above which phase separation will occur. The tie line connecting points on the binodal curve gives the polymer concentrations in each of the phases after equilibration and their respective volume fractions for each composition along the tie line. When the volume of one phase is much higher than the other phase, droplets resembling those found in O/W emulsions are formed<sup>246</sup>. At point 1 in Figure 9A, the PEG phase initially forms a continuous phase surrounding dextran droplets. Following sufficient settling time or centrifugation, the dextran droplets coalesce to form two layers (a thin layer of dextran at the bottom of the tube and a thick layer of PEG at the top of the tube). At point 3, the dextran solution forms the continuous phase surrounding PEG droplets, which eventually coalesce to form a thin PEG layer atop a thick layer of dextran. At point 2, PEG and dextran occupy

similar volume fractions, forming bicontinuous structures, as shown in the middle panel of Figure 9B. At extreme compositions on the binodal curve (e.g., 30% PEG/0.1% dextran and 0.1% PEG/30% dextran) the droplets have extremely long settling times, forming stable emulsions that do not readily coalesce over the course of several days, as shown in the top and bottom panels of Figure 9B. Therefore, binodal phase diagrams of an ATPS can be used not only to predict phase separation, but also to identify ATPS compositions suitable for generating stable emulsions. Stable emulsion such as those shown in Figure 9B, take on a slightly clouding appearance when observed by eye following vortex mixing. In some cases, as reported previously<sup>101</sup>, phase-separating compositions are only visible by microscopic analysis. Due to the high viscosity of these polymer mixtures and the dispersed nature of the droplets within the continuous phase, the droplets do not coalesce under static conditions. This may be due to the energy barrier associated with merging of adjacent droplets, as well as the freedom of droplets to move in multiple directions with respect to each other under static conditions in a relatively large vessel<sup>247,248</sup>. We hypothesized that by introducing these emulsions into a microchannel structure, laminar flow would promote droplet coalescence by causing smaller droplets to collide and merge with larger droplets as they move down the channel within the same streamlines, presumably due to inertial effects imposed by the channel geometry<sup>249</sup>. To test this hypothesis, we introduced stable emulsions into serpentine channels of the following dimensions: 500  $\mu\text{m}$  wide, 75  $\mu\text{m}$  in height and  $\sim 140$  mm long. Figure 10A shows a schematic diagram of the microfluidic device used to promote droplet coalescence. Images were acquired at 4 positions to monitor droplet sizes. At position 1, small droplets of similar size to those observed in the original emulsion were

present in abundance. These droplets were of relatively uniform size and moved in laminar streams down the channel. Droplet size increased with distance down the channel, with fewer total droplets and larger droplet sizes observed as a function of channel distance (Figure 10B). Near the outlet, the largest droplets were observed to merge with smaller droplets travelling behind them within the same streamlines.

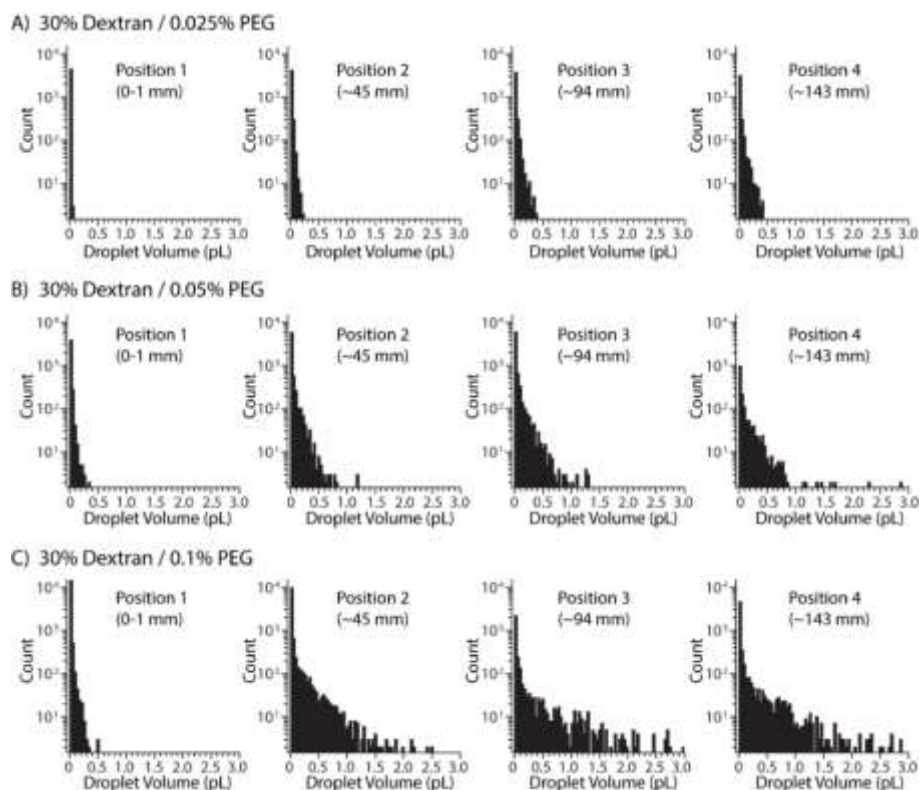
To quantify droplet size as a function of channel position, we recorded a series of images at the positions indicated in Figure 10A. Consecutive images were processed in ImageJ to remove static features associated with the channel walls and non-droplets debris (Figure 10C). Extracted features were submitted to particle analysis in ImageJ to determine droplet size distribution as a function of channel position and ATPS formulation.



**Figure 10** Schematic diagram of the microfluidic device and images of PEG-dextran emulsions within microchannels. A) Schematic diagram of the microfluidic device used to produce ATPS droplets of various sizes. Squares show the positions where images were recorded. B) Brightfield microscopy images of droplets formed at positions 1, 2, 3, and 4. C) Differences between image 1 and 2 of position 2 were displayed by subtracting one image from the other to remove any static and background features. The resulting image was converted to a binary image. Bright spots on the binary image correspond to individual droplets areas that were measured with ImageJ. Reproduced with permission<sup>414</sup>. Copyright 2018, Proceedings of SPIE.

Figure 11A shows the narrow distribution of droplet sizes present for an ATPS composed of 30% dextran and 0.025% PEG. The droplets present near the inlet for this condition were  $\sim 1\text{-}3$  pixel<sup>213</sup>, suggesting the possibility that even smaller droplets were present that could not be detected by our microscope and camera. For this condition, the largest droplets formed at position 4, with a maximum volume of 0.5 pL. Increasing the PEG concentration to 0.05%, resulted in larger droplets at downstream channel positions with a wider distribution of droplet sizes compared to 0.025% PEG (Figure 11B). Further increasing the PEG concentration to 0.1%, resulted in an even greater number of large droplets and an even wider distribution of droplet sizes at downstream channel positions (Figure 11C). For the three ATPS formulations tested, the numbers of large droplets increased at the expense of small droplets as the droplets moved down the channel, suggesting a progressive merging phenomenon that was confirmed by visual observation. Similar droplet dynamics were observed for dextran droplets in a continuous PEG phase (data not shown). This approach allows control of ATPS droplet coalescence to generate a range of droplet sizes smaller than 3 pL. These data suggest that microfluidic manipulation of ATPS emulsions will be useful for simple, high throughput production of droplets for a variety of applications ranging from drug encapsulation to droplet based analytical chemistry, where O/W and W/O systems are currently utilized.



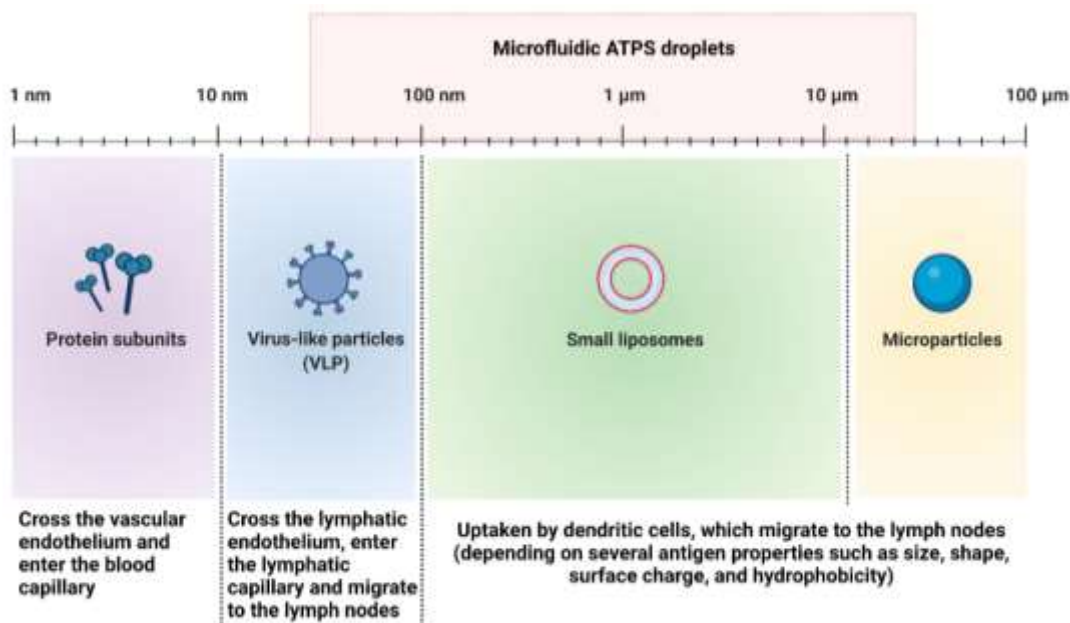


**Figure 11** Distribution of droplet volumes at each channel position for 3 different ATPS formulations. A) 30% dextran/0.025% PEG, B) 30% dextran/0.05% PEG, and C) 30% dextran/0.1% PEG. Reproduced with permission<sup>414</sup>. Copyright 2018, Proceedings of SPIE.

Vaccine delivery systems, for example, have been optimized in terms of size, shape, hydrophobicity and surface properties of the system to optimize antigen delivery and vaccine efficacy<sup>250,251</sup>. The size of a vehicle has a significant impact on antigen uptake and processing. Protein subunits (< 10 nm) can enter both vascular and lymphatic capillaries but can also be rapidly cleared away from the interstitium. Particles with diameter from 10 nm to 100 nm (2 fL to 20 fL range) cannot cross the vascular endothelium, but can diffuse through the lymphatic endothelium, enter the lymphatic capillary and reach the lymph nodes<sup>252</sup>. Although size is an important determinant to allow access to the lymphatic system, charge also plays an essential role here. Due to the

high concentration of negatively charged hyaluronic acid in the interstitium, positively charged vehicles may interact with hyaluronic acid and become trapped before reaching lymphatic capillaries, and for this reason, neutral or negative charge is preferred<sup>253,254</sup>. Regarding hydrophobicity, hydrophilic materials are more efficient transporters in the aqueous environment of the interstitium<sup>255</sup>. In addition to size, charge, and hydrophobicity, the interstitial fluid flow has also been manipulated to potentialize lymphatic transport. This can be achieved by increasing interstitial pressure through addition of agents that increase interstitial oncotic pressure such as albumin and dextrans<sup>256,257</sup>. Vaccine formulations encapsulated in particles larger than 100 nm are unable to enter the lymphatic capillary but can be phagocytosed and transported by antigen-presenting cells (APCs). For effective vaccine uptake by APCs, it is also essential to optimize surface charge and hydrophobicity<sup>250</sup>. In addition to optimizing vehicle properties, co-delivering antigens and adjuvants together to the lymph nodes is important to enhance the adaptive immune response and prevent systemic toxicity<sup>258</sup>. Figure 12 shows a diagram comparing size of different vaccine delivery systems and the size range of ATPS droplets generated by the microfluidic platform described above (section 3.3.1). Due to the large range of sizes, ATPS droplets have potential to be used to encapsulate vaccine formulations in small capsules to be delivered in lymphatic capillaries or in larger capsules that can be taken up by dendritic cells and transported to the lymph nodes. In addition, ATPS has the advantage to be completely water-based, which favors the transport through the water channels in the interstitium. Furthermore, ATPSs composed of PEG and albumin or dextran have an additional advantage, since

both polymers can enhance interstitial oncotic pressure, and promote a more effective transport of vaccine formulations through lymphatic capillaries to the lymph nodes.



**Figure 12** Size comparison between vaccine delivery systems and the size range of microfluidic ATPS droplets. Vaccine delivery systems smaller than 10 nm can cross the vascular endothelium and enter the blood capillary; systems with diameters from 10 to 100 nm can cross the lymphatic endothelium, enter the lymphatic capillary, and be transported to the lymph nodes; systems larger than 100 nm cannot enter the lymphatic capillary, but can be uptaken by dendritic cells, which then migrate to the lymph nodes. Microfluidic ATPS droplet size ranges from 50 nm to 50 μm approximately.

One limitation of the droplets formed from ATPS emulsions is their lack of stability, representing an important challenge to be overcome. Due to the very low interfacial tension at water-water interfaces, amphiphilic molecules are not readily adsorbed to these interfaces. Thus, unlike oil-based emulsions, which display much higher interfacial tensions, the kinetic stability of W/W emulsions cannot be as easily controlled by adding surfactants<sup>259</sup>. Techniques based on adsorption of proteins or latex to the water-water interface have shown promising results for stabilizing W/W

emulsions<sup>260–263</sup>. However, it will be necessary to carefully consider how these, or similar approaches are integrated into our future work, as adsorption of these materials may interfere with droplet coalescence.

The stability of W/W emulsions is also pH- and salt- sensitive. Dextran-polyethylene oxide (PEO) emulsions become relatively more stable between pH 6.5 and pH 8.0, and by addition of salt. At neutral pH, these emulsions can be further stabilized by block copolymers composed of two hydrophilic end chains with different affinities for the two aqueous phases<sup>261</sup>. Thus, there are various strategies available for stabilizing the droplets formed in our system that may be used in conjunction with various cross-linkable ATPS-forming polymers to aid in the production of stable capsules for applications where a liquid droplet is not desirable. Nano- and micro-particulate strategies have been applied to encapsulate vaccine formulations to enhance immune response. These particles can concentrate adjuvants within the lymph nodes for several days by forming a depot that prolongs localized delivery<sup>258</sup>. This approach has been traditionally achieved encapsulating immunomodulatory agents in liposomes or polymeric particles generated by oil/water emulsions<sup>264,265</sup>. Jewell et al<sup>266</sup> encapsulated the toll-like receptor-3 agonist poly(inosinic:cytidylic acid) (poly(I:C)) in microparticles ( $5.4 \pm 0.5 \mu\text{m}$ ) composed of a biodegradable poly(lactide-co-glycolide) (PLGA) core and phospholipid surface coating. After intranodal injection, the microparticles promoted a sustained release of poly(I:C) in the lymph nodes over four days, mediating 3.6-fold increase in poly(I:C) concentration in the lymph nodes compared to animals receiving soluble poly(I:C). PLGA microcapsules have also been generated using ATPS assisted self-assembly, using Pluronic F127 and dextran to emulsify PLGA<sup>232</sup>. These

microcapsules enabled thermo-responsive release of hydrophilic and hydrophobic components, which could be applied in local delivery of immunotherapies encapsulated in thermosensitive microparticles. Therefore, ATPSs have potential to generate particles that can be optimized to encapsulate vaccine formulations for controlled release. However, future work will also be necessary to fully elucidate the fluid mechanics and mechanisms involved in the ATPS droplet generation, as well as to optimize this approach to encapsulate clinically relevant biomolecules.

### **3.5 CONCLUSIONS**

W/W emulsions are very interesting formulations with a wide range of applications. Due to the absence of oil, these emulsions hold promise for encapsulation of hydrophilic components for drug delivery, or fragile biological materials, such as cells. Exploiting the ability of ATPS to form stable emulsions, we demonstrated that it is possible to control droplet coalescence within microchannels, and consequently droplet sizes. For practical applications, this method may require optimizations for precise selection of droplets and efficient crosslinking to obtain stable capsules.

### **3.6 ATPS APPLICATIONS USING VOLUMES RANGING FROM nL TO $\mu$ L**

#### **3.6.1 Biomolecule and Cell Encapsulation**

Microfluidic platforms are interesting tools for biotechnology research because they enable the precise manipulation of small volumes of solvents, reagents, and cells, which can reduce assay costs, improve the throughput and quality of analysis and conserve rare or expensive samples. Short reaction times, portability, versatility in design

through rapid prototyping, and integration with other miniaturized technologies are also advantages of using these devices<sup>101,213,214</sup>. Recently, the microfluidic research community has begun to explore how ATPS can be utilized to further enhance the capabilities of microfluidic devices. Droplet-microfluidic systems enable the generation and manipulation of size-controlled droplets within microchannels. This approach, which more-commonly is achieved with oil-water systems, has been adapted for bioassays, high-throughput analysis, single cell or drug encapsulation involving ATPS microdroplets<sup>222–225,267</sup>.

Microfluidic droplet formation results from instability between the two immiscible flows. Due to the low interfacial tension of most ATPSs, it has been difficult to control the formation of droplets, as the two immiscible fluids tend to form laminar streams as they flow through most microchannel geometries. Some of the first examples of controlled ATPS droplet formation were achieved using high concentrations of PEG and salts<sup>226</sup>. These approaches produced ATPSs that displayed interfacial tensions much higher than what is typically encountered for ATPSs used in biotechnology applications but allowed droplets to form spontaneously due to Plateau-Rayleigh instability. Although these studies represented a first step in the use of ATPSs for droplet microfluidics, the flow regimes required to form droplets generated relatively broad droplet size distributions and high concentrations of salt which is not ideal for applications involving cells and sensitive biomolecules. More recently, Mastiani et al. developed a PEG-magnesium sulfate system able to passively generate ATPS microdroplets to encapsulate cells while maintaining cell viability<sup>268</sup>. The advantage of using PEG-salt systems is the

relatively higher range of interfacial tension compared with PEG-dextran systems, which facilitates droplet generation without applying external perturbations<sup>269</sup>.

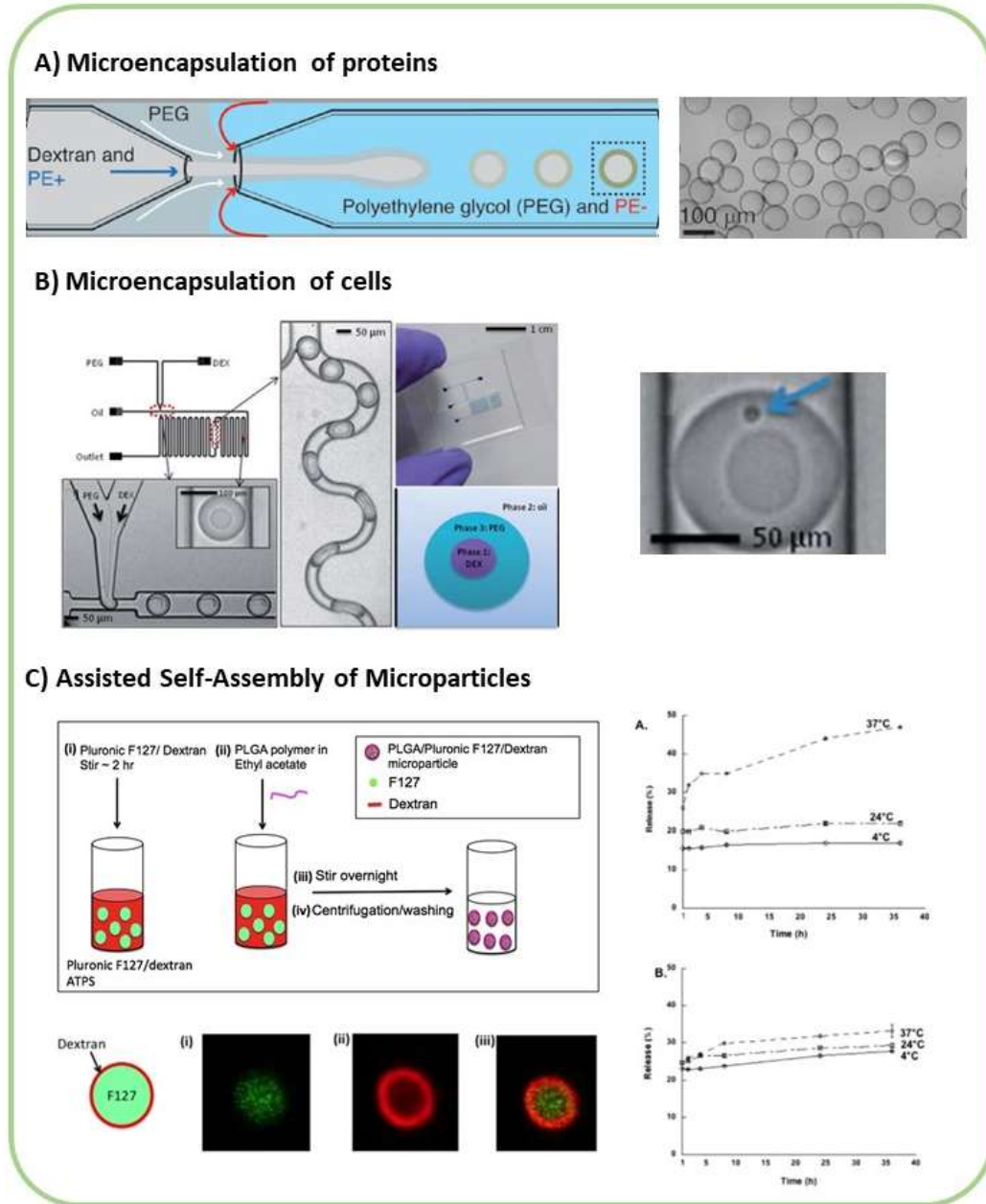
Other studies have focused on the use of external forces to generate the instabilities required for droplet formation by low interfacial tension ATPSs. Some of the first example of this strategy included devices incorporating piezoelectric bending disks and actuators driven by Braille displays that improved control over droplet size, as well as the frequency of droplet formation<sup>222,227</sup>. Sauret et al. also demonstrated the effect of adjusting the flow rates and the frequency of external forcing on the ultra-low interfacial tension of PEG-K<sub>3</sub>PO<sub>4</sub> system. After applying different frequencies (from 0.1Hz to 50kHz), they concluded that the interfacial tension could be modified by external perturbation and that the most effective frequency to promote droplet formation in their system was ~4.5Hz. They also observed that the ratio of flow rates of the two phases has considerable influence on the morphology of the jets. As the ratio of the inner fluid flow rate to the outer fluid flow rate increased, the jet became thicker, requiring greater deformation of the interface to promote the transition from a corrugate-interface regime to a droplet regime<sup>228</sup>. In addition, the same group investigated the influence of fluctuations induced by syringe-pump on ATPS microfluid flows. In this work, they considered the same system used previously (PEG-K<sub>3</sub>PO<sub>4</sub>). A stepper motor inside the syringe pump was used as source of disturbance to the fluid injected in the microdevice. They concluded that the frequency of the ripples only depends on the flow rate of the inner phase and that each ripple is generated by one moving step of the stepper motor, which depends on many parameters including the flow rates and the internal diameter of

the syringe. The authors suggested that by manipulating the flow rate in a controlled manner, it is feasible to control the deformation of the interface<sup>229</sup>.

Applications for microfluidic ATPS droplet formation include the generation of microcapsules with potential drug delivery applications, as well as the ability to perform cellular micropatterning inside microfluidic devices (Figures 13A and 13B). Polymer microcapsules based on similar materials to those known to form ATPSs have been used for drug delivery, tissue engineering, and biochemical analysis<sup>231,232</sup>. An ATPS composed of Pluronic F127 and dextran was used to produce poly(lactide-co-glycolide) (PLGA) microparticles (Figure 13C). When PLGA is emulsified in the Pluronic F127-dextran system, a unique particle is formed due to ATPS assisted self-assembly. These microparticles exhibit amphiphilic characteristics that favor encapsulation of both hydrophobic and hydrophilic molecules. Furthermore, the lower critical solution temperature properties of Pluronic F127 impart temperature responsive properties to the particles. Both features make these PLGA microcapsules well-suited for biomedical applications such as drug delivery<sup>232</sup>. Although this process did not take place inside a microfluidic device, microfluidic droplet generation could offer potential to improve droplet uniformity. For example, by applying ATPS microfluidic technology, it was possible to generate microcapsules with precise control over the morphology, internal structure, and size, as demonstrated using UV polymerizable PEG-DA (PEG diacrylate) and dextran<sup>233</sup>. Both core diameter and shell thickness can be modulated by adjusting the flow rates of the core and the shell phases. By increasing the flow rate of the outer PEG phase, not only can the total droplet diameter and size variation be reduced, but also the required UV exposure time for polymer shell crosslinking. Therefore, PEG-dextran



systems can produce a wide variety of water-based microcapsules that can be tuned to address specific applications<sup>235</sup>.



**Figure 13** Microencapsulation of biomolecules and cells using ATPS. A) Diagram of microfluidic encapsulation of protein using ATPS. Adapted with permission<sup>225</sup>. Copyright 2016, Angewandte Chemie. B) Diagram of a microfluidic device for cell encapsulation. Adapted with permission<sup>267</sup>. Copyright 2010, Chemical Science. C) Schematic representation of Pluronic F127-dextran ATPS assisted self-assembly to produce PLGA microparticles. Images are reproduced under a Creative Commons Attribution 4.0 International license<sup>232</sup>.

Frampton et al. demonstrated yet another application of the PEG-dextran system to precisely deliver cells and biomolecules using droplet dispensing devices. The cells were encapsulated within dextran droplets and delivered into the PEG phase. Due to the interfacial and partitioning properties of the APTS, cells were patterned in precise colonies within enclosed microfluidic channels<sup>72</sup>.

Dumas et al.<sup>270</sup> developed a novel process to stabilize APTS microparticles using a Pickering-like emulsion technique. An APTS composed of polyethylene oxide (PEO) and dextran was prepared, and semi-solid particles (chitosan-grafted lipid nanocapsules) were adsorbed at the interface between the two aqueous phases to form microparticles via polyelectrolyte complexation and gelation. This process led to microparticles smaller than 10  $\mu\text{m}$  with stability in solution at 4°C for at least 28 days, which are interesting carriers for oral drug delivery. Such a strategy can significantly improve oral bioavailability of hydrophilic drugs with low permeability, and may be an alternative to protect drugs that easily undergo denaturation or degradation in the gastrointestinal tract<sup>271</sup>.

### **3.6.2 Multiplexed APTS-ELISA and APTS-AlphaLISA**

The enzyme-linked immunosorbent assay (ELISA) is the gold standard technique for quantification of biomarkers present in complex biological samples. It is used to detect several clinical relevant analytes, such as proteins and antibodies, with high sensitivity and specificity<sup>194,195</sup>. However, conventional ELISA formats may lead to inaccurate results due to antibody cross-reactivity, affecting diagnosis and treatments of patients, and validation of clinically relevant multi-biomarkers<sup>197</sup>. To address this issue,

Frampton et al.<sup>102</sup> developed an ATPS-based platform able to prevent antibody cross-reactions in multiplexed ELISA by confining antibodies within polymer microdroplets. This method, referred to as ATPS-ELISA (Figure 14A), applies a PEG–dextran system to confine detection antibodies in dextran droplets over previously deposited capture antibodies. The interfacial tension between PEG and dextran solutions, and between dextran solution and the assay plate stabilizes the dextran droplets, which are held in place by four droplet insets within a sample well. This strategy allowed detection of four analytes simultaneously, while preventing antibody cross-reactions.

The amplified luminescent proximity homogeneous assay (AlphaLISA) is a no-wash platform designed to increase ELISA throughput, reduce total assay time, and improve assay sensitivity and dynamic range<sup>198</sup>. However, it was developed to detect only single analytes. To address this issue, Simon et al. multiplexed AlphaLISA using a PEG–dextran system to confine the bead-conjugated antibody pairs in specific dextran microdroplets and, therefore, prevent nonspecific antibody cross-reactions. In the multiplexed ATPS-AlphaLISA (Figure 14B), human plasma or cell supernatant are mixed in the PEG phase, from where the target analytes diffuse into the dextran microdroplets to interact with confined antibody pairs. The utility of the multiplexed ATPS-AlphaLISA was demonstrated by detecting four analytes (C-X-C motif chemokine) ligand 10 (CXCL10), and ligand 9 (CXCL9), interleukin 8 (IL-8) and interleukin 6 (IL-6) in the same sample. An ATPS composed of 18% PEG 35 kDa and 18% dextran 10 kDa (w/w%) was used to facilitate analytes and antibody-conjugated beads to partition to the dextran phase. Due to the higher hydrophilicity and lower molecular weight of dextran compared to PEG, cytokines and chemokines in the PEG-

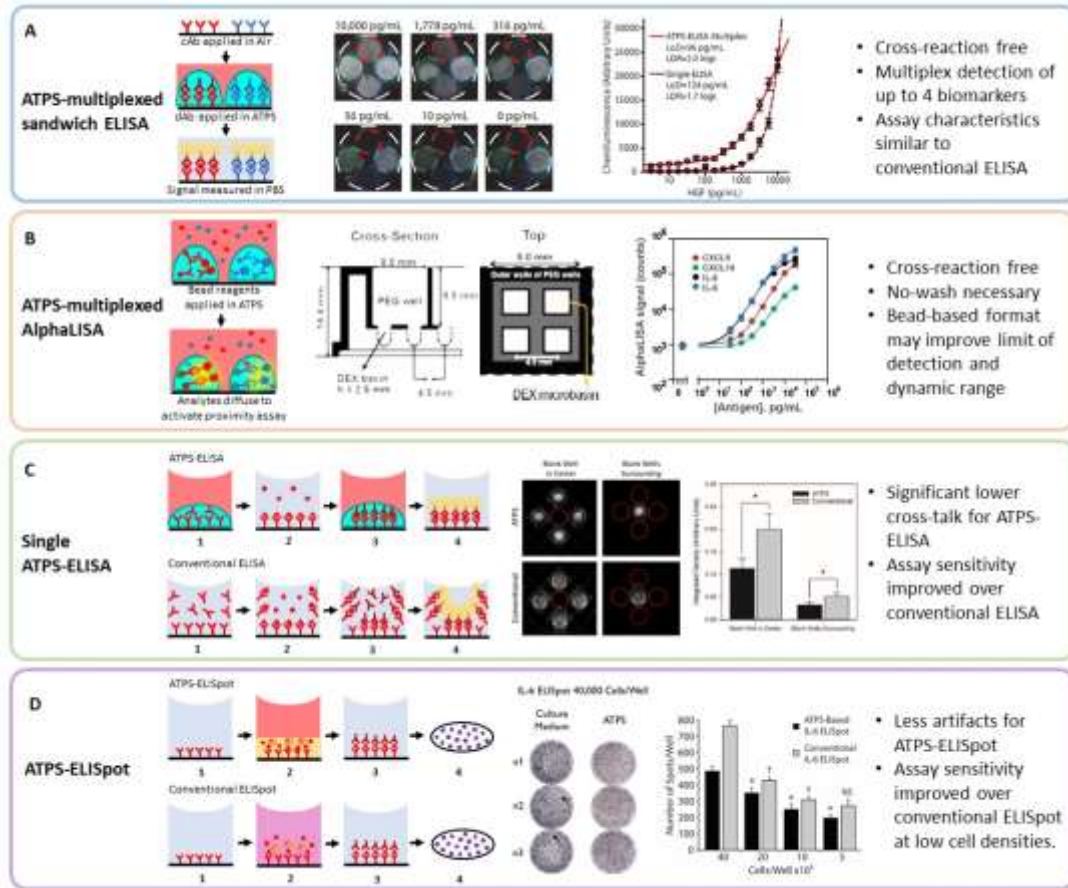
phase preferentially partition to the dextran phase. The assay beads also partitioned to the dextran phase because of their dextran coating. The multiplexed ATPS-AlphaLISA was performed in custom 96-well plates containing four microbasins per well, which is necessary for dextran droplet stabilization, since each dextran droplet is dispensed into a specific microbasin<sup>199</sup>.

### **3.6.3 Cost-Effective Single ATPS-ELISA and ATPS-ELISpot**

The conventional single sandwich ELISA has been adapted for confining antibodies using ATPS to reduce reagent volumes and optical crosstalk between neighboring wells of transparent microplates<sup>272</sup> (Figure 14C). We developed a cost-effective single ATPS-ELISA that requires smaller reagent volumes compared to conventional assay. ATPS-ELISA confines antibodies within 20  $\mu$ L of dextran solution overlaid with 100  $\mu$ L of PEG solution, which represents up to 3-fold lower capture antibody quantities compared to conventional ELISA. Because ATPS-ELISA confines antibody solutions in the center of each well, it prevents antibody solutions from coming into contact with the well edges and walls and formation of detectable signal at these regions. Therefore, ATPS-ELISA provides lower optical crosstalk compared to conventional ELISA when using transparent plates, thereby preventing false positives in surrounding wells, expanding limits of detection, and increasing assay sensitivity. The complete study is presented in Chapter 4.

In addition to the widely used PEG-dextran systems, there are several other ATPSs which properties can be exploited for specific biomedical applications. The ATPS composed of PEG and bovine serum albumin (BSA) is one of these underexplored

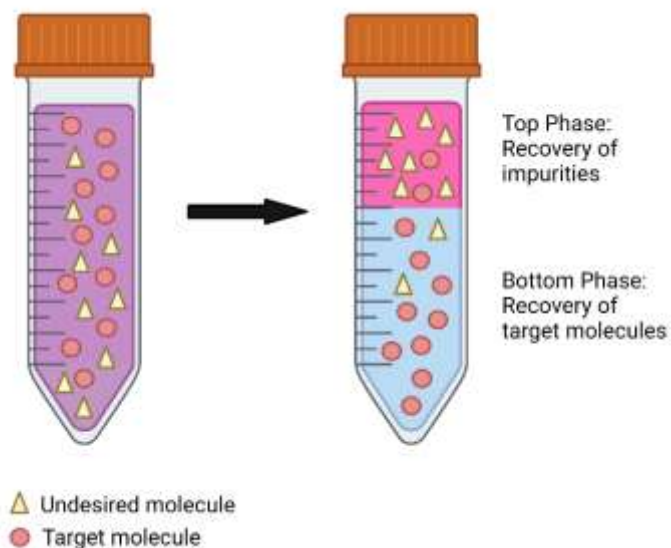
systems. We characterized the new PEG-BSA system and demonstrated that it can be used to confine suspension-cultured cells (Jurkat T cells and RPMI-8226 B cells). We also showed that the new system is able to retain high cell viability and low levels of baseline cell activation up to 72 hours<sup>273</sup>. To demonstrate the utility of the PEG-BSA system, we screened immune responses using enzyme-linked immunospot (ELISpot) assay, by confining immune cells and lipopolysaccharide (LPS) in the BSA phase (Figure 14D). We were able to measure secretion of interleukin-6 (IL-6) from RPMI-8226 B cells confined in a 20- $\mu$ L BSA droplet beneath an 80- $\mu$ L PEG solution overlay, which improved the reaction efficiency and reduced reagent consumption of the assay by 5-fold. In comparison to conventional ELISpot, results obtained from ATPS-ELISpot produced less artifacts resulted from cell movement. The overall number of spots from ATPS-ELISpot was smaller compared to the conventional assay because the BSA solution blocked non-specific binding and consequently improved the assay sensitivity, specially at low cell densities. The complete study is presented in Chapter 5.



**Figure 14** ATPS-based immunoassays. A) ATPS-multiplexed sandwich ELISA. Capture antibodies are applied to an ELISA plate, followed by colocalization of detection antibodies over capture antibodies using a PEG–dextran system. Detection antibodies remain confined in dextran droplets, preventing cross-reaction and enabling detection of up to four biomarkers. Adapted with permission<sup>274</sup>. Copyright 2018, Adv. Healthcare Materials. B) ATPS-multiplexed AlphaLISA. Bead-conjugated antibodies are confined in dextran droplets, preventing antibody cross-reactions, and enabling analysis of up to four biomarkers simultaneously. Adapted with permission<sup>274</sup>. Copyright 2018, Adv. Healthcare Materials. C) Single ATPS-ELISA. Capture or detection antibodies are confined in dextran droplets and covered with a PEG solution (Steps 1 and 3 respectively, top panel). Steps 2 and 4 are the same as the conventional sandwich ELISA protocol (bottom panel). ATPS-ELISA workflow significantly reduces optical crosstalk compared to conventional assay. Adapted with permission<sup>272</sup>. Copyright 2020, Analyst. D) ATPS-ELISpot. ATPS-ELISpot follows the same conventional ELISpot protocol, except for Step 2, where the ATPS-ELISpot confines cells and cytokines in the bottom BSA phase, which prevents artifacts from cell movement and improves assay sensitivity at low cell densities. Images are reproduced under a Creative Commons Attribution 4.0 International license<sup>232</sup>.

### 3.7 ATPS APPLICATIONS USING VOLUMES RANGING FROM mL TO L

Traditionally, ATPS has been successfully used to purify biomolecules such as proteins, antibiotics, and DNA<sup>30</sup>. Over the last decades, ATPS has been applied to improve efficiency and cost-effectiveness of the purification process of biopharmaceuticals, such as monoclonal antibodies (mAb)<sup>274</sup>. These systems have proved to be an interesting alternative to established chromatography separation methods because they are highly biocompatible, environmentally friendly, ease of scaling-up, and capable of continuous mode operation<sup>275</sup>. As mentioned in Chapter 2, the partition of molecules to a particular phase depends on several factors such as molecular weight and hydrophobicity of the solute and the ATPS polymers, electrochemical charge of the system, and isoelectric point of the solute, which is represented in Figure 15.



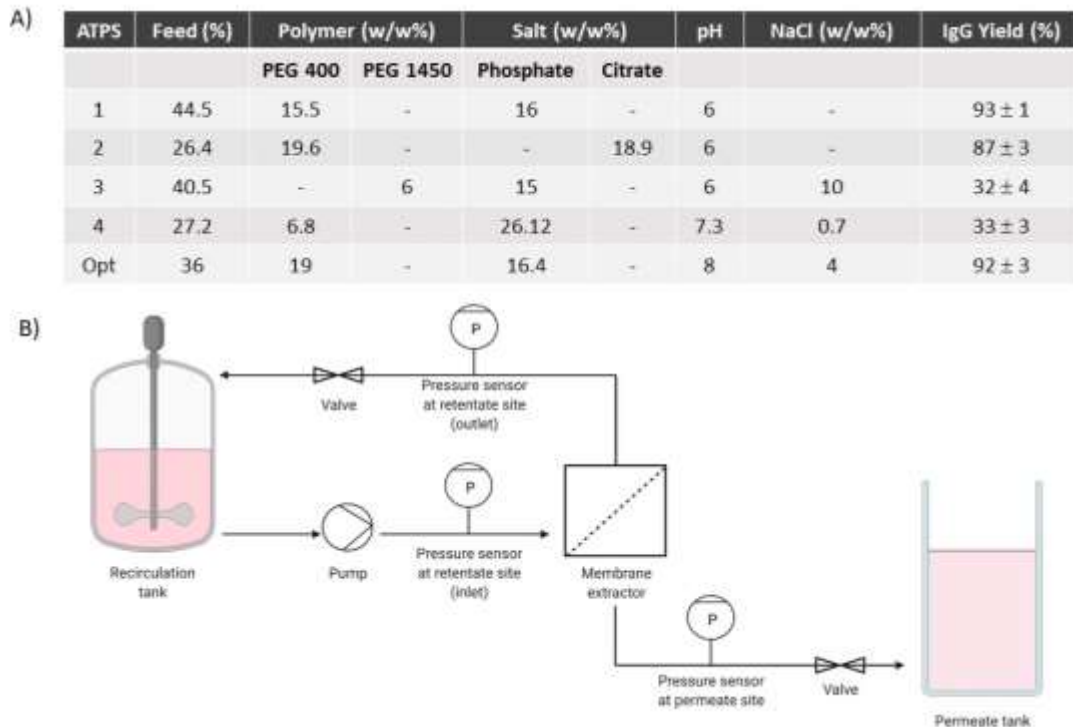
**Figure 15** Schematic representation of molecule purification using ATPS. First, a sample containing target molecules and impurities is mixed with the aqueous system. Then, the two aqueous phases separate over time, and the molecules are recovered in the phase for which they have more affinity.

Although ATPSs can enhance recovery of commercially relevant biomolecules at large scales (10 to 10,000 L), industrial adoption of these systems has been limited<sup>276</sup>. One of the reasons for its limited industrial application is the high costs associated with some polymers used in ATPS, which makes these systems less cost-competitive than other extraction processes that employ organic solvents. However, ATPS offers a much milder environment for biomolecules due to its aqueous nature. Although large scale ATPS has not been widely applied at large scale, several ATPS extractions have been developed over the last decades, for example, for the recovery of human insulin-like growth factor I (IGF-I) from *E. coli*. Hart et al.<sup>277</sup> performed *in situ* purification of IGF-I in a 14% PEG 8000 and 5% sodium sulphate system from fermentations ranging in size from 10 to 1000 liters. Their results showed that the ATPS extraction recovered 70% of non-native IGF-I in the hydrophobic PEG-rich phase, and its recovery yield remained consistent across batch sizes.

Besides being a time-consuming process, downstream purification of biopharmaceuticals has other challenges to be overcome, such as limited capacity and high cost of chromatographic methods<sup>278–280</sup>. To address these drawbacks, Kruse et al. developed a new method that integrates mAb clarification and purification steps via membrane-based separation and ATPS extraction<sup>280</sup>. The approach consists of extracting mAb (Immunoglobulin type G (IgG)) directly from the cultivation broth of Chinese hamster ovary (CHO) cell line, which was performed in a single-use bioreactor (200 mL). Figure 16A shows ATPS compositions tested and their respective IgG yield. The process is based on transferring the ATPS into a stirred recirculation tank and collecting the PEG phase in the permeate tank (Figure 16B) using a hydrophobic polypropylene membrane



modified with Tween 20 to allow higher permeate flow rate and purity. The highest IgG yield was obtained for ATPS1 (Figure 16A), with 93% IgG collected in the PEG phase. The optimized ATPS (Opt) (Figure 16A) had a similar IgG yield, but a more efficient impurity removal compared to ATPS1. The same research group further optimized the previously proposed downstream processing by applying diafiltration and ion-exchange chromatography for removal of impurities<sup>279</sup>. The ATPS extraction step yielded 97% mAb, but the whole alternative downstream process had an overall mAb yield of 74%.



**Figure 16** Monoclonal antibody clarification and purification via membrane-based separation and ATPS extraction. A) ATPS compositions and respective IgG yields. B) Schematic representation of the benchtop crossflow system used for mAb purification combined with ATPS extraction<sup>280</sup>. Opt: optimized ATPS.

Persson et al. developed a primary extraction using ATPS to purify a recombinant human growth hormone (hGH) expressed in *E. coli*<sup>281</sup>. This system is composed of a random copolymer of ethylene oxide and propylene oxide (EOPO) and starch with final weight ranging from 5 to 1,000 g. The aqueous two-phase extraction enabled robust hGH purification and efficient removal of undesired molecules and cell debris. They also demonstrated that the two-phase extraction was compatible with further downstream chromatography steps and kept hGH stable at room temperature, which is an important factor to consider at large-scale operations because it may be longer than bench scale processes. Table 1 summarizes some of the ATPSs used for bioproduct purification.

**Table 2** Examples of bioproduct purification using ATPS at various scales

<b>Bioproducts</b>	<b>ATPS Composition (w/w)</b>	<b>Scale</b>
Monoclonal antibodies <sup>279</sup>	19% PEG 400, 16.4% phosphate buffer and 4% NaCl	< 500 mL
Recombinant human growth hormone (hGH) <sup>281</sup>	8.2% EOPO and 5.5% starch 20% EOPO and 5.5% starch	5 g to 1 Kg
Recombinant cutinase <sup>282</sup>	5% PEG 3350 and 15% phosphate buffer	10 ml, 1 L and 30 L
Xylose reductase <sup>283,284</sup>	19.3% PEG 1000 and 12.4% phosphate buffer	10 g
Monoclonal antibodies <sup>285</sup>	8% PEG 3350, 8% citrate buffer and 15% NaCl	5 g
Monoclonal antibodies <sup>286</sup>	12% PEG 6000, 10% phosphate buffer and 15% NaCl	5 g
Interleukin-18-binding protein <sup>287</sup>	11.25% PEG 10,000 and 11.25% sodium sulfate	-

Although ATPS platforms have shown industrial potential for the recovery of several biomolecules, they have not been widely adopted yet, mainly because a general lack of confidence associated with applying materials that are still under discovery and examination.

### **3.8 CONCLUSIONS**

The remarkable versatility of ATPSs have enabled the development of several simple and cost-effective platforms ranging from microscale analysis to purification of biomolecules at large scale. At microscale level, ATPS offers a highly biocompatible environment for confining cells and reagents at precise regions of ELISA and ELISpot microplates, which can be performed using simple laboratory equipment, available to any life science laboratory. For optimal delivery in the lymphatic capillaries, particles require a size ranging from 10 nm to 100 nm. Particle with size ranging from 100 nm and 20  $\mu$ m can be internalized by dendritic cells and transported to the lymph nodes, but this route is less efficient<sup>251</sup>.

For generating cost-effective multiplexed ATPS-ELISA and ATPS-AlphaLISA, the volume of ATPS droplets must be 1  $\mu$ L to confine antibodies within microbasins. For a cost-effective single ATPS-ELISA, the droplet volume must be 20  $\mu$ L to uniformly coat the bottom of a standard 96-well plate. A cost-effective ATPS-ELISpot also requires a 20- $\mu$ L droplet, which enables confinement of immune cells and vaccine reagents without compromising spot development.

At large scale, ATPSs have not been widely applied yet because they need to be further investigated, optimized, and validated before industrial implementation. However,

studies have shown that ATPS can be reliably scaled up. The *in situ* solubilization and aqueous two-phase extraction conducted by Hart et al.<sup>277</sup> demonstrated that IGF-I recovery yield and purity remained almost the same at 10, 100, and 1000 L volumes. Recombinant cutinase has been extracted using a PEG-phosphate system and scaled from 10 mL to 1 L and 30 L with a recovery yield of 95% at all scales<sup>282</sup>. Persson et al.<sup>281</sup> showed the advantages of using aqueous two-phase extraction for the initial recovery of recombinant hGH over the traditional clarification performed by centrifugation. In conclusion, these studies showed the feasibility of scaling-up ATPS-based extraction using traditional operation units and provided evidence that ATPS-based processes can improve the overall cost-efficiency in the downstream purification of biopharmaceuticals.

## CHAPTER 4 DEVELOPMENT AND OPTIMIZATION OF A COST-EFFECTIVE SINGLE ATPS-ELISA

Materials of this chapter have been published in **Analyst** and are being reproduced in this thesis with permission from the publisher The Royal Society of Chemistry.

Kvas M\*, Teixeira AG\*, Chiang B, Frampton JP (2020). Aqueous two-phase system antibody confinement enables cost-effective analysis of protein analytes by sandwich enzyme-linked immunosorbent assay with minimal optical crosstalk. *Analyst*.

\* These authors contributed equally to the work.

### 4.1 ABSTRACT

An aqueous two-phase system formed from polyethylene glycol and dextran was used to uniformly coat the bottom surfaces of the wells of standard 96-well assay plates with capture and detection antibodies to improve the performance and cost-effectiveness of sandwich enzyme-linked immunosorbent assay (ELISA). Using this approach, limits of detection and linear dynamic range values comparable to those obtained for conventional sandwich ELISA were obtained using considerably lower antibody quantities due to the much lower reagent volumes required when antibodies are applied in a dextran solution beneath a polyethylene glycol overlay. Confinement of the antibody reagents to the bottom surfaces of the wells within the dextran phase also dramatically decreased the optical crosstalk present between neighboring wells when using transparent microplates. Adaptation of the conventional single sandwich ELISA for aqueous two-phase system antibody confinement was demonstrated by analysis of standard curves for C-reactive protein, transforming growth factor beta 1, and the chemokine CXCL10.

## 4.2 INTRODUCTION

The enzyme-linked immunosorbent assay (ELISA) is the gold standard method for quantification of specific protein analytes present in complex biological fluids<sup>1</sup>. ELISA accounts for the largest segment of the immunoassay market, which is currently valued at between 19 and 27 billion USD, due to its widespread use in clinics, industrial R&D, environmental surveillance, forensics, and academic research<sup>4,5</sup>. Between 2010 and 2019, there were more than 79,000 scientific articles published that mention ELISA, which further highlights the extent to which academic laboratories rely on this technique<sup>2,3</sup>. The main factors that limit more widespread adoption of ELISA in research settings are the time associated with performing the assay, which varies accordingly with the number of required washing and incubation steps, and the cost associated with well-validated biologic reagents, which in the case of sandwich ELISA, include a recombinant protein standard, two antibodies that recognize different epitopes on the protein of interest, and an enzyme conjugate<sup>288</sup>.

Limitations associated with the time and cost required to perform ELISA have motivated the development of modified ELISA approaches that reduce the number of wash steps, shorten incubation times, lower the volumes of reagents and samples required for analysis, or allow the assay to be multiplexed to measure multiple analytes from the same sample. In attempt to reduce assay time and cost, recent advances in miniaturizing multiwell plates and high-throughput technologies have been developed. For example, ELISA can be performed in 384-well plates with reaction volumes as low as 10  $\mu\text{L}$ <sup>289,290</sup>. However, in practice it can be difficult to accurately pipette reagents into individual wells of a 384-well plate. To address these drawbacks, another miniaturized platform that uses

an intelligent multifunctional analytical plate (IMAPlate 5RC96) was developed. Although the IMAPlate works with reaction volumes as low as 5 $\mu$ L, it requires an additional transfer plate to facilitate transfer of reagents to the assay plate<sup>291</sup>.

Microfluidic systems have also been designed to either miniaturize the reaction vessel in which the ELISA is carried out or automate the procedure using either active flow control<sup>292–296</sup> or passive capillary action<sup>297</sup>. For example, Safaviéh and Juncker developed a low-cost passive microfluidic system comprised of microchannels, fluidic resistors, vents, capillary pumps, trigger valves, capillary retention valves, retention burst valves, and closed and open reservoirs to measure C-reactive protein concentration<sup>298</sup>. Similarly, Kim et al. developed an integrated microfluidic system to passively regulate the flow of up to 10 reagents required for ELISA in a sequential and synchronous manner<sup>299,300</sup>. To further improve ease-of-use and reduce assay costs, microfluidic paper-based analytical devices ( $\mu$ PADs), also known as lateral flow assays (LFAs), have been developed. These systems utilize micropatterned chromatography paper to control fluid transport by way of capillary action, thus eliminating the need for active fluid displacement driven by external devices such as syringe pumps and the design of complex integrated microfluidic channels<sup>202,301</sup>.

In addition to the emerging microfluidic options available for ELISA, bead-based assays such as the wash-free Amplified Luminescent Proximity Homogeneous Assay (AlphaLISA) marketed by Perkin-Elmer and Luminex xMAP technology enable efficient multi-analyte detection within carefully validated panels<sup>198,302</sup>. Bead-based antibody assays are usually as sensitive as conventional ELISAs, offer a wide dynamic range, and have high inter-assay reproducibility<sup>303</sup>, but are typically expensive, require relatively

large sample volumes, and do not always reduce the time required to complete the assay<sup>304</sup>. Moreover, human sera may contain antibodies that directly bind to the beads of the Luminex system, resulting in non-specific background signal<sup>305</sup>. Finally, it can sometimes be difficult to obtain custom panels for specific applications due to the extensive validation that must be performed for each panel to prevent cross-reactions from occurring between antibodies, which can lead to false-positive or false-negative results<sup>306</sup>.

To address these drawbacks in multiplex analyte detection, strategies based on colocalizing capture antibodies (cAbs) and detection antibodies (dAbs) have been developed. Antibody colocalization has been achieved by depositing cAbs and dAbs at precise locations on nitrocellulose films or nitrocellulose-coated slides using a snap chip device<sup>27-29</sup>. Antibody colocalization can also be achieved using an aqueous two-phase system (ATPS) comprised of polyethylene glycol (PEG) and dextran, in which dextran droplets containing dAbs are deposited above a pre-patterned cAb array<sup>102</sup>. Simon et al. later demonstrated that a similar approach could be used to reduce the consumption of AlphaLISA reagent for multiplex analyte detection by colocalizing the antibody-conjugated AlphaLISA beads within a PEG-dextran ATPS<sup>199</sup>. ATPS-based ELISA platforms have been further improved to make the procedure more user-friendly by dehydrating the ELISA reagents prior to adding a PEG solution containing the target analytes<sup>200</sup>. After rehydration, the analytes diffuse from the PEG phase into the dextran droplets containing the immobilized capture antibodies and dextran-confined detection antibodies to form cAb-analyte-dAb complexes.



Overall, these antibody colocalization techniques show comparable limit of detection and signal to noise ratio values to the conventional sandwich ELISA, while providing substantial benefits to the end user by suppressing antibody cross-reactivity and reducing the consumption of expensive cAbs and dAbs. However, the utility of the ATPS approach for reducing the consumption of assay reagents in the single ELISA format, which is by far the most widely used ELISA format in industry and academic research, has not been explored in term of its performance characteristics and cost. Here, we describe a cost-effective single ATPS-ELISA technique that requires reduced reagent volumes without compromising the signal readout. By depositing antibody reagents in conventional 96-well microplates using a PEG-dextran ATPS, similar limits of detection and linear dynamic range values can be obtained using up to 3-fold lower capture antibody quantities compared to conventional sandwich ELISA, while limiting optical crosstalk between neighboring wells. The utility of this platform is demonstrated through quantitative measurements of C-reactive protein (CRP), transforming growth factor beta 1 (TGF- $\beta$ 1), and the chemokine CXCL10.

## **4.3 MATERIALS AND METHODS**

### **4.3.1 Aqueous Two-Phase System Formulations**

Technical grade dextran 500 kDa (Pharmacosmos) and PEG 35 kDa (Sigma-Aldrich) were dissolved in phosphate-buffered saline (PBS) for capture antibody deposition. Dextran 500 kDa and PEG 35 kDa were dissolved in PBS containing 1%

bovine serum albumin (BSA; Sigma-Aldrich) for detection antibody deposition. Unless otherwise noted, dextran 500 kDa and PEG 35 kDa were dissolved separately to achieve stock solution of 20 wt% for each polymer.

#### **4.3.2 Optimization of Polymer Concentrations**

Various concentrations (wt%) of PEG 35 kDa and dextran 500 kDa were examined to assess their stability for antibody deposition. FITC-dextran (final concentration of 0.1%) was added to the dextran solution to facilitate droplet visualization. A volume of 100  $\mu\text{L}$  of PEG was added in each well of a 96-well plate. Droplets of dextran solution ranging from 8  $\mu\text{L}$  to 30  $\mu\text{L}$  were then dispensed into the wells beneath the PEG solution. Images were acquired using an Azure Biosystems c300 imager immediately following droplet deposition and after 24 hours to observe droplet stability. The area of the droplet covering the bottom of the each well was measured using the tracing tool in ImageJ.

#### **4.3.3 Confinement of Antibodies in the PEG-Dextran System for ELISA**

To demonstrate the cost-effectiveness of depositing ELISA antibodies in an ATPS, the cost of the conventional sandwich ELISA protocol was compared with the modified ATPS-ELISA protocol. The ELISA kits used were the following: CRP (R&D Systems cat # DY1707), TGF- $\beta$ 1 (R&D Systems cat # DY240) or CXCL10 (R&D Systems cat # DY266). The conventional sandwich ELISA protocol was performed as recommended by R&D Systems for conventional ELISA. Briefly, 96-well plates were

coated with 60  $\mu\text{L}$  of the working concentration of the capture antibody diluted in PBS. Next, the plates were incubated at room temperature overnight. The next day, the plates were washed five times with wash buffer consisting of PBS containing 0.1% Tween (PBST) and blocked for 1 hour with 1% BSA. After blocking, the plates were washed three times. Then, 50  $\mu\text{L}$  of standard diluted in reagent diluent (PBST + 1% BSA) was added to each well and incubated for 2 hours. Next, the wells were washed three times with wash buffer. Then, 25  $\mu\text{L}$  of detection antibodies diluted in reagent diluent was added and incubated at room temperature for 2 hours. After five washes with PBST, before a volume of 100  $\mu\text{L}$  of streptavidin-conjugated horseradish peroxidase was added to each well and incubated for 20 minutes in the dark. Next, the plates were washed in PBST, before 100  $\mu\text{L}$  of chemiluminescent substrate (Thermo Scientific Super Signal ELISA Pico Substrate cat # 37069) was added to each well to develop the assay. Plates were imaged using an Azure Biosystems c300 imager and then immediately analyzed using a Molecular Devices FilterMax F5 plate reader. The ATPS-ELISA protocol differed from the conventional sandwich ELISA protocol for the capture and detection antibody deposition steps only. For the capture antibody step, the wells were first filled with 100  $\mu\text{L}$  of PEG solution and then 20  $\mu\text{L}$  of dextran solution diluted in PBS containing capture antibodies with final concentration of 16.7% and 3.3% respectively was deposited in the center of the well. For the detection antibody step, the wells were again filled with 100  $\mu\text{L}$  of PEG solution and then 10  $\mu\text{L}$  of dextran solution diluted in reagent diluent containing detection antibodies with final concentration of 18.2% and 1.8% respectively was deposited in the center of the well. Dispense and aspirations for

ATPS-ELISA capture and antibody steps were accomplished using a Hudson Robotics Solo automated liquid handling robot.

#### **4.3.4 Optical Crosstalk Analysis**

To reproduce the effect of optical crosstalk within a blank well surrounded by wells with intense signal, four 500 pg/mL TGF- $\beta$ 1 standards were applied via both the ATPS-ELISA technique and conventional ELISA technique within the wells surrounding the blank well. To reproduce the effect of optical crosstalk within blank wells surrounding a central well with intense signal, the central well was treated with 500 pg/mL of TGF- $\beta$ 1 standard for both the ATPS-ELISA technique and conventional ELISA technique. Only three internal replicates for both ATPS and conventional ELISA were performed per plate to minimize optical crosstalk between internal replicates.

#### **4.3.5 Analysis of Assay Performance Characteristics**

Assay plate wells were observed using either an Azure Biosystems c300 imager or a Molecular Devices FilterMax F5 plate reader. For images acquired using the c300 imager, integrated density values were obtained using ImageJ. Maximum linear response was determined using the range of standard concentrations that yielded an  $R^2$  value for a linear fit of above either 0.95 or 0.99. Two limits of blanks (LoB) were calculated using the average and standard deviation of blank wells beside both the most highly concentrated standards and least concentrated standards according to  $LoB = \text{mean blank} + 1.645(\text{SD blank})$ . The limit of detection (LoD) was calculated according to  $LoD = LoB +$

1.645(SD low concentration sample). The linear dynamic range (LDR) values were calculated according to  $LDR = \log((\text{maximum linear response})/LoD)$ .

#### **4.3.6 Statistical Analysis**

Unless otherwise noted, all data were compared in terms of mean +/- SD. Two-tailed unpaired Student's t-tests assuming equal variance were used to compare the ATPS-ELISA and conventional ELISA techniques. A p-value <0.05 (denoted by \*) was considered significant. The Brown-Forsythe equal variance test and Shapiro-Wilk normality test were performed using Sigmaplot 14.0 to determine to verify equal variance and normality assumptions, respectively. At least three internal replicates and three external replicates were performed for each experiment.

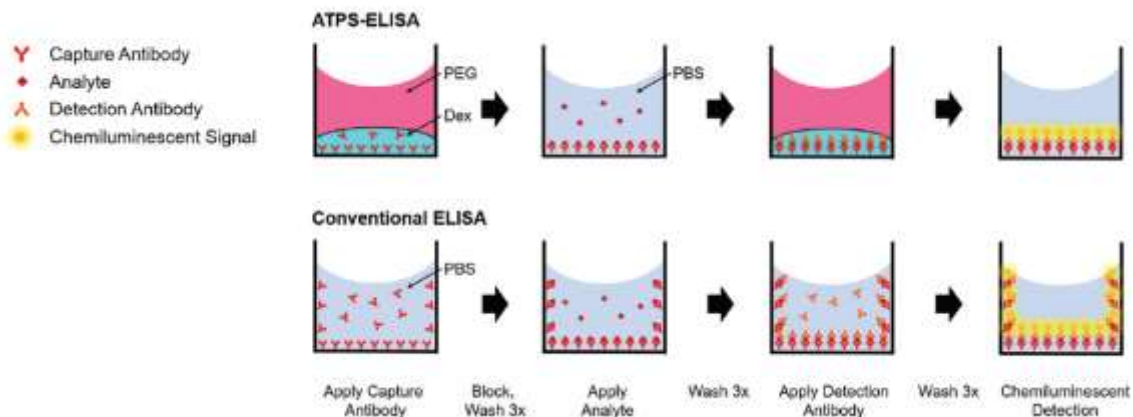
### **4.4 RESULTS AND DISCUSSION**

#### **4.4.1 Sandwich ELISA using the PEG-Dextran ATPS**

The conventional sandwich ELISA is performed by first coating the wells of a 96-well assay plate with 100  $\mu$ L of cAb (Figure 17, bottom panel). During this process, the cAb can adsorb to both the bottom of the wells and the walls of the wells. Next, the plate is blocked and washed before 100  $\mu$ L of the sample containing the analyte of interest is applied. After the analyte binds specifically to the cAb, the plate is washed again, and 100  $\mu$ L of biotinylated dAb is applied. The dAb can then bind to the analyte, which is indirectly bound to the bottom and walls of the assay well via interaction with the cAb.

The plate is then washed again, incubated in 100  $\mu\text{L}$  of streptavidin-conjugated horseradish peroxidase, washed a final time, and developed using a chemiluminescent substrate. The relatively large assay volumes used in the conventional sandwich ELISA are recommended to prevent inconsistent results that arise from air-liquid interface meniscus effects that take place when the assay is performed using lower volumes.

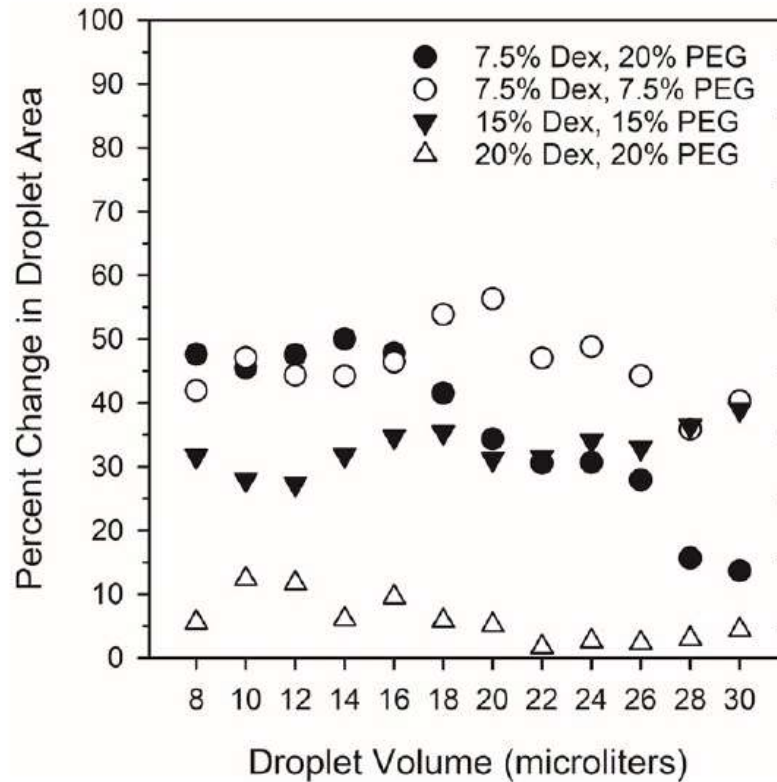
ATPS-ELISA follows almost the same assay workflow as conventional sandwich ELISA, but allows much smaller volumes of reagents such as cAb and dAb to be used to conduct the assay by confining the antibodies with the dextran phase of a PEG-dextran ATPS (Figure 17, top panel). In this format, the PEG phase serves as a liquid overlay that limits evaporation of the antibody solution contained within the dextran phase, eliminates exposure of antibodies to the air-liquid interface which can denature a small fraction of antibodies near the surface of the liquid, and prevents air-liquid meniscus effects that arise from surface tension. The relatively low interfacial tension between the aqueous PEG and dextran phases (from  $\sim 1$  to  $100 \mu\text{N/m}$ )<sup>54</sup> compared to that of oil and water ( $\sim 31.0 \text{ mN/m}$ )<sup>57</sup> and air and water ( $\sim 72.0 \text{ mN/m}$ )<sup>307</sup> produces a nearly flat interface that evenly coats the bottom of the wells, but not the walls of the wells, with the cAb and dAb.



**Figure 17 Comparison of the ATPS-ELISA method to conventional sandwich ELISA.** In ATPS-ELISA (top), the capture and/or detection antibodies are diluted in dextran solution and dispensed beneath a PEG solution overlay designed to confine the antibodies to the microplate surface. This allows the user to conserve antibodies and lower total assay costs, because lower volumes of antibody solution are required to cover the bottom surface of the microplate. All other steps including blocking, washing and chemiluminescent detection are the same as the conventional sandwich ELISA workflow (bottom). Reproduced with permission<sup>272</sup>. Copyright 2020, Analyst.

#### 4.4.2 The PEG-Dextran System Minimizes Consumption of Capture and Detection Antibodies in Sandwich ELISA

We first sought to determine the minimum dextran volumes required to uniformly cover the bottom of a well of a 96-well plate to assess the impact that this strategy could have on the cost of a typical sandwich ELISA for a single analyte. The volumes and concentration of polymer solution were optimized to minimize changes in the area of the dextran phase covering the bottom of each well as measured using a FITC-dextran tracer in the dextran phase of the PEG-dextran ATPS (Figure 18).



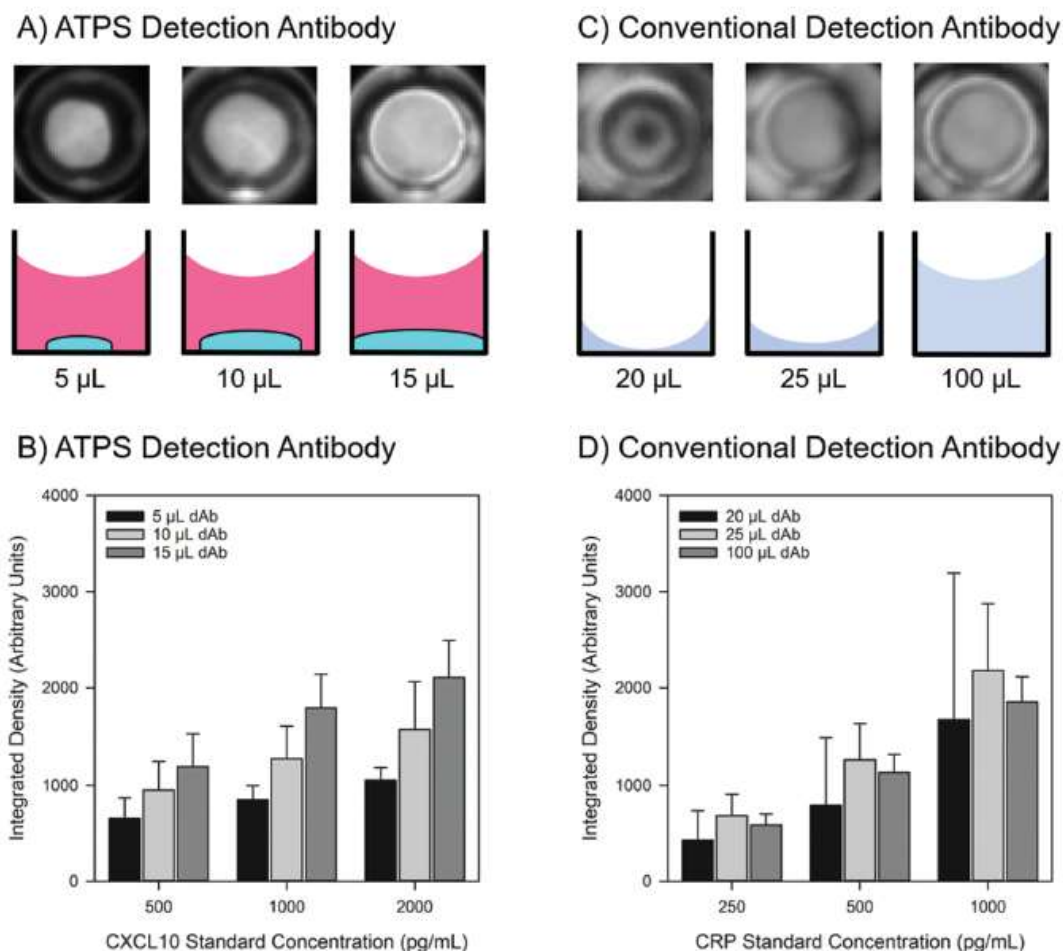
**Figure 18 Optimization of polymer concentrations.** Dextran droplet volumes for various ATPS formulations were varied and the percentage change in area of the dextran droplets after 24 hours was recorded. Area coverage decreased for a fixed volume as polymer concentration increased due to the larger liquid-liquid-plate interfacial tension present. For equal concentrations of polymers, droplet area remained consistent over time. However, for the 7.5% dextran, 20% PEG system, the droplet gradually shrunk due to equilibration of the two polymer solutions. Reproduced with permission<sup>272</sup>. Copyright 2020, Analyst.

From these data, we also inferred that a fixed volume of 20  $\mu\text{L}$  of cAb confined within the dextran phase of a 20% dextran/ 20% PEG ATPS was required to uniformly coat the bottom of a standard 96-well assay plate, whereas a minimum volume of 60  $\mu\text{L}$  of cAb was required for conventional sandwich ELISA in the absence of an ATPS. Using a fixed concentration of cAb recommended by the R&D Systems applied in either 20  $\mu\text{L}$  of dextran solution for ATPS-ELISA or 100  $\mu\text{L}$  of PBS for conventional sandwich ELISA (as recommended by the R&D Systems), we next sought to minimize the volume



of dAb solution required for the assay. The minimum -dAb volume required to completely coat the bottom of a well in a 96-well assay plate was 10  $\mu\text{L}$  for ATPS-ELISA (Figure 19, A and B) and 25  $\mu\text{L}$  for conventional sandwich ELISA (Figure 19, C and D), although air-liquid interface meniscus effects and subtle signal artefacts from non-uniform coating were apparent for conventional sandwich ELISA. It is important to note that R&D Systems recommends a dAb volume of 100  $\mu\text{L}$  to ensure uniform signal. In comparison with the cAb coating steps for both ATPS-ELISA and conventional sandwich ELISA, lower volumes of dAb were required to coat the wells due to the lower surface energy from previous cAb and analyte coatings steps and the presence of surfactant in the dAb solution.

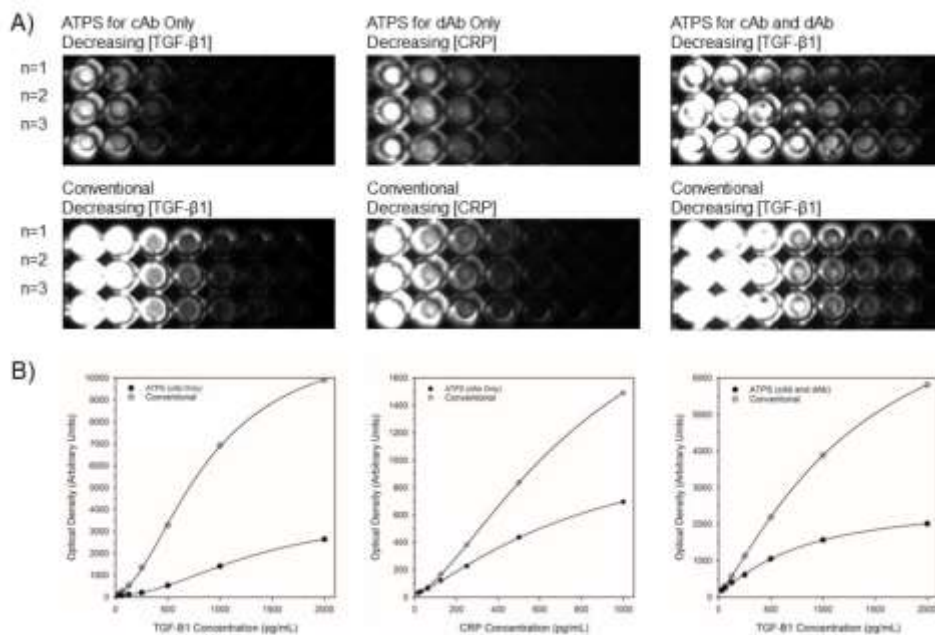
An important distinction between ATPS-ELISA and conventional sandwich ELISA is that ATPS-ELISA produced uniform signal at the bottom of the well but did not produce discernable signal at the edge or on the wall of the well (Figure 19A). When antibody solutions come into contact with the edges and walls of the wells as they do in conventional sandwich ELISA, this produces non-uniform signals in the form of bright rings at the well edges and halos on the wells of the walls from signal that is outside of the focal plane of the detector (Figure 19B). When data are recorded as optical images, this leads to greater variation in standard curve data for conventional CXCL10 sandwich ELISA as compared to CXCL10 ATPS-ELISA (Figure 19, B and D).



**Figure 19 Optimization of antibody solution volumes.** (A) Representative images and schematic diagrams of ATPS-ELISA for wells treated with 2000  $\text{pg mL}^{-1}$  CXCL10 detection antibody using 5, 10, and 15  $\mu\text{L}$  dextran droplets dispensed beneath a PEG overlay. (B) The mean integrated density values for 5, 10, and 15  $\mu\text{L}$  dextran droplets for three different CXCL10 standard concentrations. (C) Representative images and schematic diagrams of conventional sandwich ELISA for wells containing 1000  $\text{pg mL}^{-1}$  CRP detection antibody using 20, 25, and 100  $\mu\text{L}$  solutions of PBST. (D) The mean integrated density values for 20, 25, and 100  $\mu\text{L}$  droplets for three different CRP standard concentrations. Error bars represent standard deviation of the mean. Reproduced with permission<sup>272</sup>. Copyright 2020, Analyst.

When data are recorded using a plate reader, these effects are not as apparent but may lead to significant optical crosstalk depending on the type of plate that is chosen for the assay. Using the optimal cAb and dAb volumes obtained from this analysis, we also

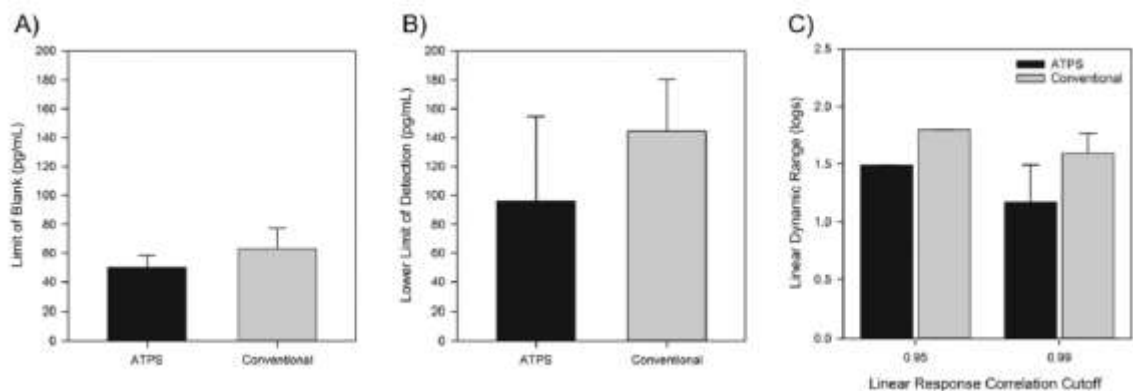
compared standard curves for TGF- $\beta$ 1 and CRP between conventional sandwich ELISA and ATPS-ELISA when only the cAb was applied using an ATPS, when only the dAb was applied using an ATPS and when both the cAb and dAb were applied using an ATPS and noted qualitatively similar standard curves across assay formats (Figure 20).



**Figure 20 Comparison of standard curves for TGF- $\beta$ 1 and CRP between conventional sandwich ELISA and ATPS-ELISA.** A) Representative images for assays in which an ATPS is used to dispense just the capture antibody (cAb), just the detection antibody (dAb) or both the capture and detection antibodies. Images of the conventional ELISA performed within the same plate are shown for comparison. For the trials using only ATPS for the cAb step, the TGF- $\beta$ 1 ELISA kit was used. The capture and detection antibody concentrations used for the TGF- $\beta$ 1 kit were 2  $\mu$ g/mL and 300 ng/mL, respectively. The volumes used for the capture antibody in the ATPS condition was 20  $\mu$ L whereas, the volume of the capture antibody for the conventional condition was 60  $\mu$ L. The detection antibody volume for both ATPS and conventional conditions was 50  $\mu$ L. For the trials using only ATPS for the dAb step, the CRP ELISA kit was used. The capture and detection antibody concentrations used for the CRP kit were 2  $\mu$ g/mL and 90 ng/mL, respectively. The volume of capture antibody used for both the conventional and ATPS conditions was 50  $\mu$ L. The volume of detection antibody used for the conventional condition was 25  $\mu$ L whereas, the volume of detection antibody used for the ATPS condition was 10  $\mu$ L. For the trials using ATPS for both the cAb and dAb step, the TGF- $\beta$ 1 kit was used. The capture and detection antibody concentrations used for the TGF- $\beta$ 1 kit were 2  $\mu$ g/mL and 300 ng/mL, respectively. The volumes used for the capture and detection antibody solutions for the ATPS conditions were 20  $\mu$ L and 10  $\mu$ L, respectively. The volumes used for the capture and detection antibody solutions for the conventional conditions were 60  $\mu$ L and 25  $\mu$ L, respectively. B) Representative standard curves comparing signal versus concentration between ATPS-ELISA and conventional sandwich ELISA. Reproduced with permission<sup>272</sup>. Copyright 2020, Analyst.

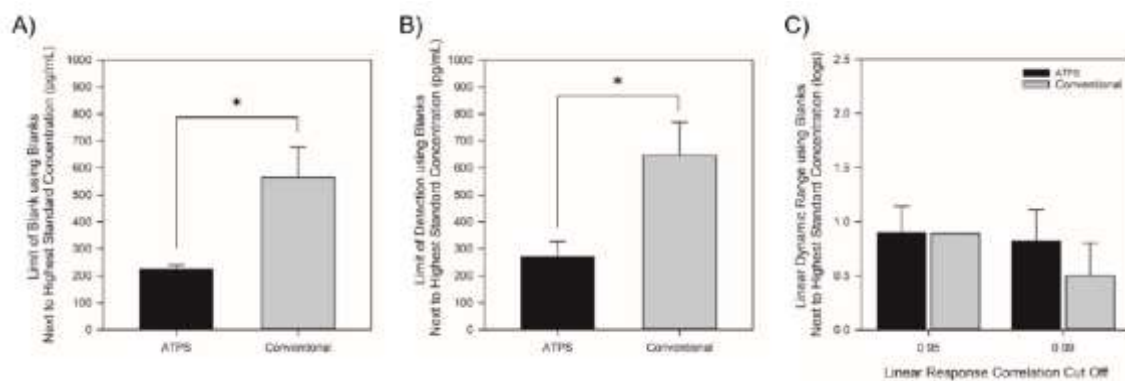
#### **4.4.3 ATPS-ELISA Produces Comparable Performance Characteristics to Conventional Sandwich ELISA, while Requiring Lower Capture and Detection Antibody Volumes**

In order to assess the performance characteristics of ATPS-ELISA relative to conventional sandwich ELISA, standard curves were fit with 4-parameter logistic functions and values for limit of blank, limit of detection, and linear dynamic range were calculated. The limit of blank was similar for ATPS-ELISA and conventional sandwich ELISA when using the wells next to the low concentration standards as blanks (Figure 21A). Similarly, limits of detection were comparable between ATPS-ELISA and conventional sandwich ELISA (Figure 21B). The linear dynamic range for ATPS-ELISA was lower than for conventional sandwich ELISA when an R-squared cut-off value of 0.95 was applied (Figure 21C). The smaller linear dynamic range was due primarily to the diminished response of ATPS-ELISA at high protein standard concentration. Although the linear dynamic range is slightly smaller for ATPS-ELISA, this can be easily adjusted for by diluting samples containing high concentrations of the protein analyte before performing the assay. When a more stringent R-squared cut-off value of 0.99 was applied, linear dynamic range values were equivalent between ATPS-ELISA and conventional sandwich ELISA.



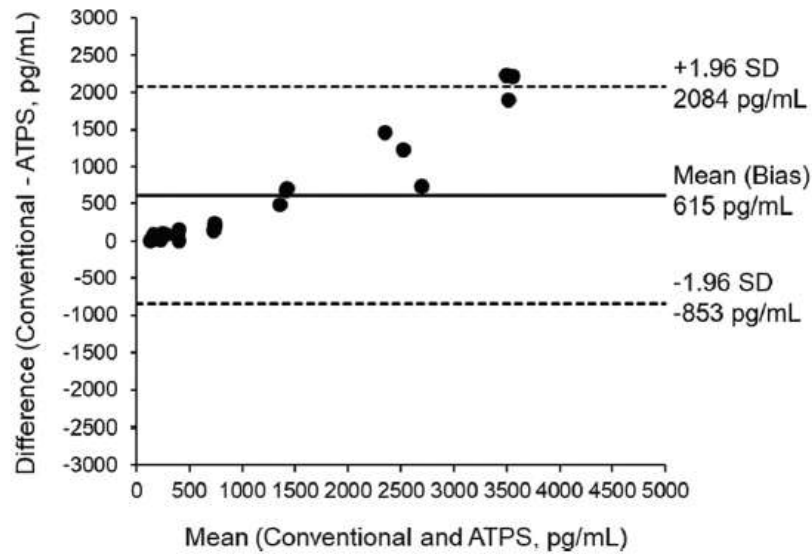
**Figure 21 Performance characteristics of ATPS-ELISA compared to conventional sandwich ELISA using blank wells next to the lowest standard concentration.** The limit of blank (A) and limit of detection (B) were calculated using blank wells next to the lowest standard concentration of TGF- $\beta$ 1 ( $31.6 \text{ pg mL}^{-1}$ ) for both ATPS-ELISA and conventional ELISA. (C) Average linear dynamic ranges of TGF- $\beta$ 1 standard curves for ATPS-ELISA and conventional sandwich ELISA were determined using different correlation coefficients as maximum linear response cut offs using the integrated densities of wells adjacent to the lowest standard concentration of TGF- $\beta$ 1 ( $31.3 \text{ pg mL}^{-1}$ ). For the ATPS conditions, both the capture and detection antibodies were dispensed in dextran. Capture and detection antibody volumes for ATPS-ELISA were 20 and 10  $\mu\text{L}$ , respectively. Capture and detection antibody volumes for conventional ELISA were 60  $\mu\text{L}$  and 25  $\mu\text{L}$ , respectively. As per the TGF- $\beta$ 1 kit, the concentration of the capture antibody used was  $2 \mu\text{g mL}^{-1}$  and the concentration of the detection antibody was  $300 \text{ ng mL}^{-1}$ . Error bars represent standard deviation of the mean. Reproduced with permission<sup>272</sup>. Copyright 2020, Analyst.

We also compared the performance characteristics of ATPS-ELISA and conventional sandwich ELISAs using blank wells next to high concentration standards (Figure 22). When using the wells next to the high concentration standards as blanks, the limit of blank was significantly lower for ATPS-ELISA compared to conventional sandwich ELISA (Figure 22A), as was the limit of detection (Figure 22B). When using blank wells next to high concentration standards, linear dynamic range values for ATPS-ELISA were equivalent to those of conventional sandwich ELISA for R-squared cut-off values of 0.95 and 0.99.



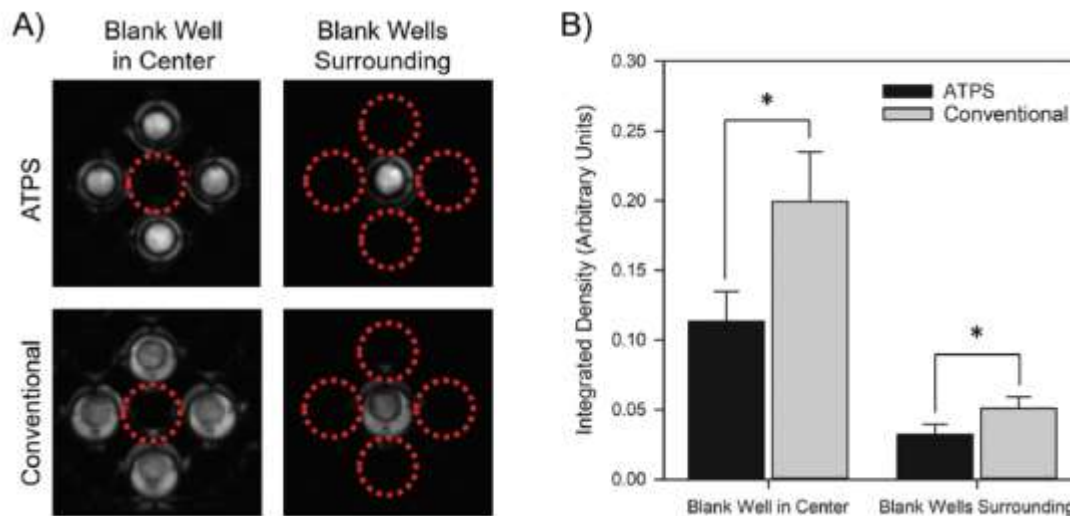
**Figure 22 Performance characteristics of ATPS-ELISA compared to conventional sandwich ELISA using blank wells next to the highest standard concentration.** The limit of blank (A) and limit of detection (B) were calculated using blank wells next to the highest standard concentration of TGF- $\beta$ 1 (2000 pg/mL) for both ATPS-ELISA (using capture and detection antibody in ATPS) and conventional sandwich ELISA. C) Average linear dynamic ranges of TGF- $\beta$ 1 standard curves for ATPS-ELISA and conventional sandwich ELISA determined using different correlation coefficients as maximum linear response cut offs using the integrated densities of wells adjacent to the highest standard concentration of TGF- $\beta$ 1 (2000 pg/mL). For the ATPS conditions, both the capture and detection antibodies were dispensed in dextran. Capture and detection antibody concentrations used were 2  $\mu$ g/mL and 300 ng/mL, respectively. The volumes used for the capture and detection antibody solutions for the ATPS conditions were 20  $\mu$ L and 10  $\mu$ L, respectively. The volumes used for the capture and detection antibody solutions for the conventional conditions were 60  $\mu$ L and 25  $\mu$ L, respectively. Error bars represent standard deviation of the mean. The \* indicates  $p < 0.05$ . Reproduced with permission<sup>272</sup>. Copyright 2020, Analyst.

To further compare ATPS-ELISA and conventional sandwich ELISA we assessed assay agreement using Bland-Altman analysis. We found that ATPS-ELISA and conventional sandwich ELISAs agreed more closely at lower protein standard concentrations as compared to higher protein standard concentrations (Figure 23). This is partially accounted for by the lower dynamic range observed for ATPS-ELISA compared to conventional sandwich ELISA but may also be explained by higher levels of optical crosstalk at higher protein standard concentrations for conventional sandwich ELISA.



**Figure 23 Bland–Altman analysis of agreement between conventional sandwich ELISA and ATPS-ELISA.** Individual data points correspond to measured values of TGF- $\beta$ 1 standards recorded for both assays. At low standard concentrations the two assays are in close agreement. At higher concentrations, there is a bias that may be attributable to the slightly lower dynamic range of ATPS-ELISA compared to conventional ELISA and significant levels of optical crosstalk at higher standard concentration for conventional sandwich ELISA. Reproduced with permission<sup>272</sup>. Copyright 2020, Analyst.

Here, we define optical crosstalk as the proportion of signal originating from one well that is detected in adjacent wells. We compared optical crosstalk between ATPS-ELISA and conventional sandwich ELISA using a central blank well surrounded by wells with intense signal and using a central well with intense signal surrounded by blank wells (Figure 24A). The optical crosstalk was significantly lower for ATPS-ELISA compared to conventional sandwich ELISA in both configurations (Figure 24B). This is important because optical crosstalk produced by highly concentrated samples may produce false positives in surrounding wells. In addition, optical crosstalk can contribute to higher limits of detection, thus decreasing the sensitivity of the assay.



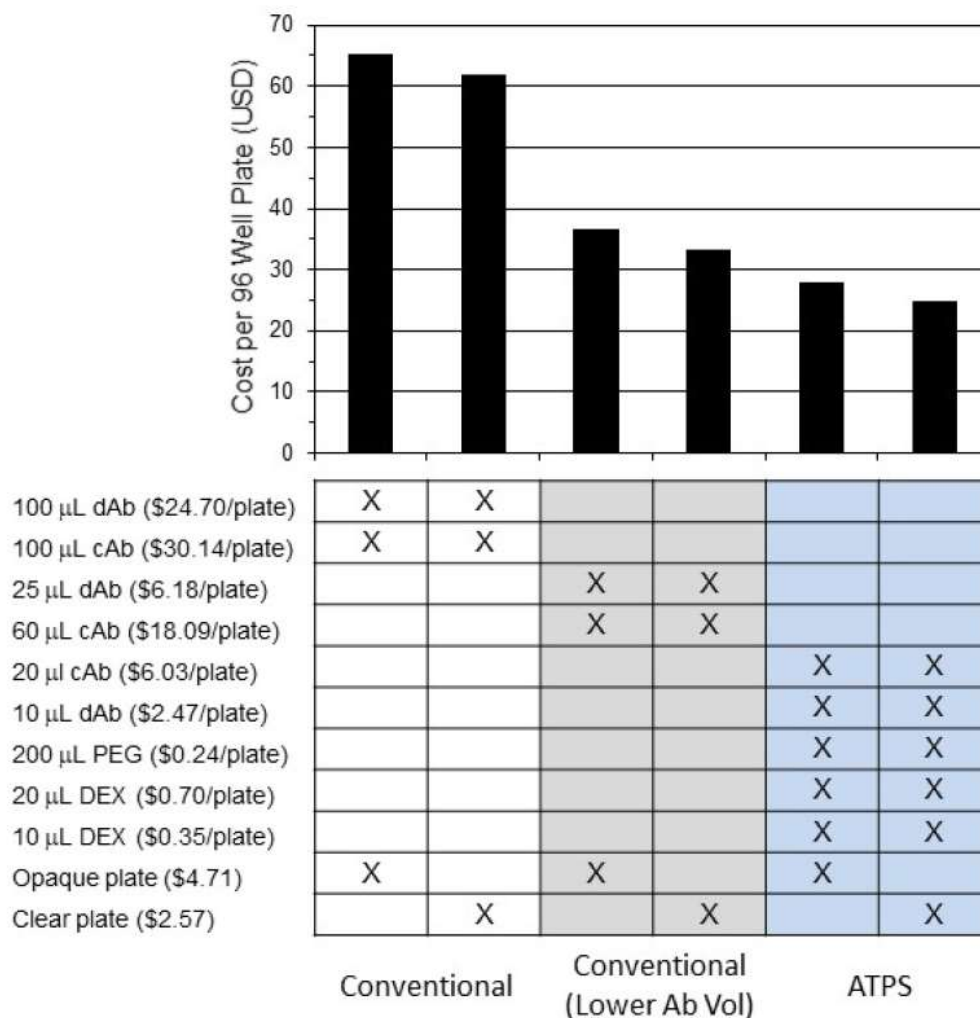
**Figure 24 Comparison of optical crosstalk between ATPS-ELISA and conventional sandwich ELISA.** (A) Representative images showing optical crosstalk for blank wells surrounded by well containing intense chemiluminescent signal and wells in which blank wells surround a central well with an intense chemiluminescent signal. (B) ATPS-ELISA results in lower levels of optical crosstalk because antibodies are present only at the bottom surface of the microplate, whereas for conventional sandwich ELISA, antibodies can associate with both the bottom and walls of the microplate. For the ATPS condition, both the capture and detection antibodies were dispensed in ATPS. Data are for TGF- $\beta$ 1 protein at 500 pg mL<sup>-1</sup> using capture antibody concentration of 2  $\mu$ g mL<sup>-1</sup> and detection antibody concentration of 300 ng mL<sup>-1</sup>. Error bars represent standard deviation of the mean. The \* indicates p < 0.05. Reproduced with permission<sup>272</sup>. Copyright 2020, Analyst.

#### 4.4.4 Cost Comparisons Between ELISA Methods

The differences in the cost between the optimized ATPS-ELISA protocol and conventional sandwich ELISA were considerable when compared using antibody prices for the TGF- $\beta$ 1 duo set (Figure 24). The two bars representing conventional sandwich ELISA on the far left represent the costs associated with the conventional sandwich ELISA protocol when using the antibody volumes recommended by R&D Systems and differ only by the type of plate used in the assay. The opaque and clear plate prices were included in the cost analysis because it is more likely that an opaque plate will be needed to reduce optical crosstalk when using the conventional sandwich ELISA protocol, as



previously suggested<sup>308</sup>. However, as shown in Figure 25, opaque plates are more expensive than clear plates, and therefore contribute to increase costs for sandwich ELISA. Although conventional sandwich ELISA costs can be reduced slightly by using antibody volumes lower than those recommended by the manufacturer, this is not advisable due to meniscus effects that can occasionally produce signal artefacts. The ATPS-ELISA method was the most cost-effective option in our analysis because of the significant reduction in antibody volumes without sacrificing uniformity of the measure signal. To further reduce assay costs in the ATPS ELISA format, it should be possible to determine the minimum amount of antibody required to be added to the dextran phase to approximately cover the bottom surface of each well by quartz crystal piezogravimetry or by estimating the coverage from antibody molecular dimensions and molecular mass<sup>309,310</sup>.



**Figure 25 Comparison of assay costs.** Each bar in the graph (x-axis) corresponds to a column in the table and represents the costs (shown on the left) by varying the volumes of capture/detection antibodies, with/without ATPS polymers, and using different type of plates. Reproduced with permission<sup>272</sup>. Copyright 2020, Analyst.

In comparison to other ELISA systems designed to reduce antibody consumption, the ATPS-ELISA system provides comparable performance, but in a format that is likely more easily translated to life science and clinical chemistry laboratories. It is important to note, however, that microscale ELISA systems, such as the antibody colocalization microarray (ACM) systems, are highly tuned for specific applications, although they may also be adapted for single sandwich ELISA<sup>102,298</sup>. For example, the ACM systems are

perhaps best suited for tests that required a high level of specificity, as they enable multiplex protein analyte detection with minimal cross-reactivity between antibody reagents. However, ACMs may not be advisable in settings where complex infrastructure for precision antibody colocalization is unavailable or when measurement of a single protein analyte is sufficient. For situations where assay cost is an issue and end users have limited capacity to adjust their workflow, we therefore recommend the ATPS-ELISA system described here as it provides comparable performance characteristics to conventional sandwich ELISA, while consuming 3-fold less cAb and 2.5-fold less dAb compared to conventional sandwich ELISA, while mitigating effects of optical crosstalk that can contribute to false-positive readouts and inaccurate standard curves. Finally, ATPS-ELISA may be advantageous for developing assays with custom-made antibodies, for which the cost associated with production in animals, followed by fractionation, purification and labeling can exceed \$10,000.

#### **4.5 CONCLUSIONS**

We developed a cost-effective sandwich ELISA system that reduces effects of optical crosstalk by confining antibodies to the bottom surfaces of assay plates in a PEG-dextran ATPS. We demonstrated that this system minimizes consumption of both capture and detection antibodies with comparable performance characteristics to conventional sandwich ELISA. Also, we showed that ATPS-ELISA significantly reduced the optical crosstalk between neighboring wells compared to conventional ELISA. Therefore, the ATPS-ELISA system described here is recommended as a cost-saving method for single protein analysis.

## CHAPTER 5      DEVELOPMENT AND CHARACTERIZATION OF A NOVEL *IN VITRO* ATPS-BASED VACCINE SCREENING PLATFORM

Materials of this chapter have been published in **Frontiers in Chemistry** and are being reproduced in this thesis with permission from the publisher Frontiers.

Teixeira AG, Kleinman A, Agarwal R, Tam NW, Jun Wang, Frampton JP (2019). Confinement of Suspension-Cultured Cells in Polyethylene Glycol/Polyethylene Oxide-Albumin Aqueous Two-Phase Systems. *Frontiers in Chemistry*, vol. 7:441.

### 5.1      ABSTRACT

Aqueous two-phase systems (ATPSs) have numerous applications in separation science, and more recently, in bioassays enabled by the solution micropatterning of cells. The most frequently used ATPS in these applications is the polyethylene glycol (PEG)-dextran system, as the polymers that form this ATPS have been extensively characterized in terms of their physicochemical properties. However, in addition to this well-known system, there exist many other ATPSs with properties that may be exploited to improve upon the PEG-dextran system for specific applications. One of these underexplored systems is the ATPS formed from PEG/polyethylene oxide (PEO) and albumin. In this article, we characterize the phase separation of PEG (35 kDa) and polyethylene oxide (PEO) (200 kDa, 900 kDa and 4,000 kDa) with bovine serum albumin (BSA). We describe the microscopic emulsion behavior of these systems in the presence of NaCl and compounds (NaHCO<sub>3</sub>, NaH<sub>2</sub>PO<sub>4</sub> and HEPES) commonly used in buffer solutions and cell culture media. We further demonstrate that PEG- and PEO-albumin systems can be used in place of the PEG-dextran system for confinement of suspension-cultured cells (Jurkat T cells and RPMI-8226 B cells). Cell viability and morphology are examined for

various polymer formulations relative to the commonly used PEG 35 kDa-dextran 500 kDa system and polymer-free cell culture medium. In addition, we examine cell activation for various phase-separating medium components by measuring IL-2 and IL-6 secretion. We demonstrate that we can confine immune cells and cytokines in the PEG-BSA system, and that this system can be employed to screen immune responses by enzyme-linked immunospot (ELISpot) assay. This new system represents a promising ATPS formulation for applications where low levels of baseline cell activation are required, for instance, when culturing immune cells.

## 5.2 INTRODUCTION

Aqueous two-phase systems (ATPSs) form when two incompatible polymers, a polymer and a salt, or a polymer and a surfactant exceed threshold concentrations in a common aqueous solvent<sup>31,115</sup>. Each system can be characterized by a phase diagram that displays the concentrations at which the solutes phase separate. A curved line called the binodal separates two areas: compositions represented by points above the binodal that give rise to phase separation and compositions represented by points below the binodal that mix to form a single phase<sup>30,31</sup>. Phase separation can be influenced by physiochemical properties such as the polymer molecular weight (MW) and concentration, temperature, pH, and ionic concentration<sup>42,95,311</sup>. For instance, higher MW polymers require lower concentrations for phase separation<sup>31</sup>. In addition, the binodal curve delineating sub-critical concentrations from supercritical concentrations becomes more asymmetrical with increasing difference in MW between the two polymers<sup>31</sup>. The system properties also influence the distribution of cells and biomolecules between the

two phases. ATPSs provide a mild non-toxic and non-denaturing environment for the partitioning of cells and biomolecules with applications ranging from isolation and recovery of antibodies<sup>83,84</sup>, proteins<sup>85,86</sup>, virus-like particles<sup>88,312</sup>, antibiotics<sup>89,90</sup>, DNA<sup>92,93</sup>, cells<sup>95,96</sup>, extracellular vesicles<sup>97</sup>, and hormones<sup>99,100</sup> to solution micropatterning of cancer cells, hepatocytes and keratinocytes<sup>82,153</sup>. The most extensively used ATPS for these applications is the polyethylene glycol (PEG)-dextran system. The cost-effectiveness and lack of acute cytotoxicity of the PEG-dextran system allows the precise positioning of cells by dispensing single-microliter or sub-microliter droplets of a cell-laden dextran solution within a PEG solution. The interfacial tension formed between the two polymer solutions confines the cells in the dextran droplets, where they can then adhere to the culture substrate. For adherent cells, the polymer solutions are removed once the cells attach to the substrate. However, confinement of suspension-cultured cells in an ATPS poses a challenge, as the polymers must remain in place for longer periods of time to maintain cell confinement. For culture periods longer than 24 hours, cytotoxicity and cellular activation can vary by polymer type and concentration.

Here, we present an under-explored system for confinement of suspension-cultured cells that utilizes a PEG/polyethylene oxide (PEO) and bovine serum albumin (BSA) ATPS. Our objectives were to characterize phase separation of this novel system, evaluate the effects of PEG, PEO and BSA on immune cell cytotoxicity and activation, and to demonstrate the utility of the PEG-BSA system for confinement of immune cells and reagents to reduce assay costs associated with the gold-standard enzyme linked immunospot (ELISpot) assay for measuring cytokine secretion from suspension-cultured cells. PEG and PEO have the same chemical structure. Industry conventions refer to low

MW ethylene glycol polymers (less than ~35,000 Da) as PEG, while ethylene glycol polymers greater than ~35,000 Da are referred to as PEO<sup>313</sup>. PEG and PEO are applied extensively in the food, cosmetic, and pharmaceutical industries. PEG and PEO are also widely used as biomaterials to alter surface properties to repel proteins<sup>314</sup>, and have been applied for biomedical applications such as coating of medical devices and nanoparticles<sup>315</sup>. As a major amphiphilic plasma protein, albumin has been used as an essential nutrient for cell culture. Albumin has also been widely used in cell culture due to its role as an antioxidant and carrier of important biomolecules<sup>316</sup>. ATPSs have been used for the extraction of BSA from biological fluids<sup>317,318</sup>. However, to the best of our knowledge, this article is the first to use BSA as an ATPS-forming polymer. We demonstrate that PEG- and PEO-albumin systems are promising ATPS formulations for confinement of suspension-cultured cells such as T cells and B cells that require low levels of baseline cell activation. This ATPS-mediated technique enables T cell and B cell culture over the course of 72 hours with minimal activation, as monitored by IL-2 and IL-6 secretion.

## **5.3 MATERIALS AND METHODS**

### **5.3.1 PEG- and PEO-BSA Binodals**

Unless otherwise noted, all polymer solutions are reported as percent weight solutions. Stock solutions of 30% BSA (Sigma-Aldrich), 20% PEG 35 kDa (Sigma-Aldrich), 10% PEO 200 kDa, 3% PEO 900 kDa, and 2.0% PEO 4,000 kDa (Dow Chemical) were dissolved in Dulbecco's Modified Eagle's Medium (DMEM; VWR).

PEO solutions were centrifuged to sediment and remove silica particles introduced by the manufacturer. Concentrated stock solutions of BSA, PEG and PEO were introduced to 96-well plates and mixed to form super-critical emulsions. Each super-critical concentration was then titrated with polymer-free culture medium until phase separation was no longer observed using methods similar to those reported previously for binodal determination in 96-well plates<sup>101</sup>. The final BSA, PEG and PEO concentrations were determined according to

$$C_i(V_i) = C_f(V_f),$$

where  $C_i$  refers to the initial concentration,  $V_i$  refers to the initial volume,  $C_f$  refers to the final concentration and  $V_f$  refers to the final volume. A Nikon Eclipse Ti microscope equipped with a 10x objective lens was used to observe microscopic emulsion characteristics.

### 5.3.2 Microdroplet Characterization

Equilibrated ATPSs composed of 15% BSA and either 7% PEG 35 kDa, 4% PEO 200 kDa, 1.5% PEO 900 kDa or 1.5% PEO 4,000 kDa were used to characterize the stability of dispensed microdroplets. PEG- and PEO-BSA systems were centrifuged at 3,000 rcf to separate the phases for collection. Once collected, the top and bottom phases were centrifuged again at 3,000 rcf to allow removal of traces of the other phase transferred during collection. For each system, a 1  $\mu$ L droplet of BSA-rich bottom phase was added to 500  $\mu$ L of the PEG- or PEO- rich top phase. After 20 minutes (to allow droplet stabilization), a Nikon Eclipse Ti microscope equipped with a 2x objective lens was used to observe the droplets.



### **5.3.3 Effects of Salt on Phase Separation**

Solutions of 15% BSA and 1.5% PEO 900 kDa were prepared in distilled, de-ionized water containing the following salts: sodium bicarbonate (Fisher Scientific), HEPES (Sigma-Aldrich), sodium phosphate monobasic (Sigma-Aldrich) and sodium chloride (Fisher Scientific). Salts were tested at the following concentrations: 2g/L, 4g/L, 6g/L, 8g/L. Microscopic emulsion characteristics in the presence of each salt were observed using a 10x objective lens on a Nikon Eclipse Ti microscope to determine the effects that individual medium components had on phase separation without extensively characterizing binodal curves for each system.

### **5.3.4 Jurkat T Cell Culture**

Jurkat T cells, clone E6-1 (ATCC: TIB-152), were cultured in a humidified incubator at 37°C under 5% CO<sub>2</sub> in RPMI 1640 medium (VWR) supplemented with 10% fetal bovine serum (FBS) and 1% antibiotics. Medium was replaced every 2-3 days and cell density was maintained below 1 X 10<sup>6</sup> cells/mL for cell propagation. Three types of plates were examined for suspension cell confinement in the PEG-BSA system: flat-bottom, round-bottom and V-bottom. Jurkat T cells were confined in the BSA phase (bottom). The BSA-phase was labelled with FITC-conjugated dextran and the cells were labelled with CellTracker Red™ CMTPIX (Life Technologies) to aid in visualization. Cells cultured in the PEG-BSA system were observed using a 4x objective lens on a Nikon Eclipse Ti microscope.

### 5.3.5 RPMI-8226 B Cell Culture

RPMI-8226 B cells, (ATCC: CCL-155), were cultured in a humidified incubator at 37°C under 5% CO<sub>2</sub> in RPMI 1640 medium (VWR) supplemented with 10% fetal bovine serum (FBS) and 1% antibiotics. Medium was replaced every 2-3 days and cell density was maintained below 1 X 10<sup>6</sup> cells/mL for cell propagation.

### 5.3.6 Cell Viability Assessment

Cells were seeded in 96-well culture plates at a density of 5 X 10<sup>3</sup> cells per well. The cells were then incubated for 72 hours in 100 µL of either the individual filter-sterilized polymer solutions or BSA at concentrations exceeding those required for phase-separation. The following polymer/BSA concentrations in RPMI 1640 medium supplemented with 10% FBS and 1% antibiotics were examined: 7% PEG 35 kDa, 2% PEO 200 kDa, 0.5% PEO 900 kDa, 0.1% PEO 4,000 kDa, 7% dextran 500 kDa (T500; Pharmacosmos) and 10% BSA. Several lots of BSA were examined including Bovine Serum Albumin (Sigma-Aldrich cat # A7906), Albumax™ I (Gibco cat # 11020-021), HyClone (GE Life Sciences cat # SH30574.02) and Collect™ Bovine Albumin Low IgG (MP Biomedicals cat # 180576). Cells were cultured in these solutions in a humidified incubator at 37°C under 5% CO<sub>2</sub> for 72 hours prior to viability assessment.

Cell viability in the presence of individual polymers was assessed by live/dead staining with Calcein-AM (C-AM, Biotium) and Propidium Iodide (PI, Sigma-Aldrich). C-AM can enter live cells, where it is hydrolyzed in the cytoplasm to calcein, producing a fluorescent signal at 530 nm upon excitation with blue light<sup>319</sup>. PI can only enter dead

cells, where it subsequently binds to nucleic acids, primarily in the nucleus<sup>320</sup>. Thus, C-AM was used to identify live cells (shown in green), whereas PI was used to identify dead cells (shown in red). A C-AM/PI stock solution (25  $\mu$ M C-AM/ 25  $\mu$ M PI) was prepared in RPMI 1640 medium. A volume of 12  $\mu$ L of the stock solution was added to each well to achieve a final concentration of 3  $\mu$ M for each dye. Cells were incubated in the presence of the dyes at 37°C under 5% CO<sub>2</sub> for 20 minutes. The cells were observed by epifluorescence microscopy using a Nikon Eclipse Ti Microscope. Images were processed using ImageJ to subtract background and adjust brightness.

### **5.3.7 Jurkat T Cell Activation**

Jurkat T cells were seeded at  $5 \times 10^5$  cells/well in 24-well plates. The cells were stimulated with phorbol-12-myristate-13-acetate (PMA) and 300ng/mL ionomycin. To determine the best PMA concentration to stimulate the cells as a positive control for cell activation, the following PMA concentrations were tested in culture medium: 25ng/mL, 50ng/mL, 100ng/mL and 200ng/mL. Supernatants from PMA/ionomycin-stimulated cells were collected at three time points: 6-, 12- and 24-hours post-stimulation. To assess Jurkat T cell activation in the presence of polymers/BSA, cells were seeded in 24-well culture plates at a density of  $5 \times 10^5$  cells/well in the following polymer and BSA solutions in RPMI 1640 medium supplemented with 10% FBS and 1% antibiotics: 7% PEG 35 kDa, 7% dextran 500 kDa, 10% BSA Sigma, 10% BSA Albumax and 10% BSA HyClone. After 6, 12, and 24 hours, supernatants were collected to measure IL-2 secretion.

### 5.3.8 RPMI-8226 B Cell Activation

RPMI-8226 B cells were seeded at  $5 \times 10^5$  cells/well in 24-well plates. The cells were stimulated with lipopolysaccharide (LPS) from *Salmonella enterica serotype minnesota* (Sigma-Aldrich). To determine the best LPS concentration to stimulate the cells as a positive control for cell activation, the following LPS concentrations were tested in culture medium: 50ng/mL, 100ng/mL, and 200ng/mL. Supernatants from LPS-stimulated cells were collected at two time points: 24- and 48-hours post-stimulation. To assess RPMI-8226 B cell activation in the presence of polymers/BSA, cells were seeded in 24-well culture plates at a density of  $5 \times 10^5$  per well in the following polymer and BSA solutions in RPMI 1640 medium supplemented with 10% FBS and 1% antibiotics: 7% PEG 35 kDa, 7% dextran 500 kDa, and 10% BSA Albumax. After 24 hours, supernatants were collected to measure IL-6 secretion.

### 5.3.9 Measurement of IL-2 and IL-6 Secretion

Concentrations of IL-2 and IL-6 in the supernatants were determined by enzyme-linked immunosorbent assay (ELISA) according to the manufacturer's instructions (R&D Systems cat # S2050 and cat # DY206) using antibody concentrations recommended by the manufacturer. Briefly, 96-well microplates were coated overnight with capture antibodies diluted in phosphate buffered saline (PBS). The next day, the plates were washed three times in PBS containing 0.2% Tween 20 (PBST) and blocked for 1 hour with 1% BSA in PBS. After blocking, the plates were washed three times in PBST and incubated with the samples and recombinant protein standards for 2 hours. Next, the plates were washed three times in PBST and incubated for 2 hours with detection

antibodies. The plates were then washed three times in PBST and incubated with streptavidin-conjugated horseradish peroxidase (HRP) for 20 minutes. Finally, the plates were washed three times in PBST and incubated with SuperSignal ELISA Pico Chemiluminescent Substrate (Thermo Fisher Scientific) for 10 minutes. All incubation and wash steps were performed at room temperature. Luminescence was measured using a FilterMax F5 microplate reader. Unknown values were determined by extrapolation from a four-parameter logistic standard curve.

### **5.3.10 Confinement of Cells in the PEG-BSA System for ELISpot Assay**

To demonstrate the utility of the PEG-BSA (Albumax) system, an optimized formulation was used to confine immune cells and reduce reagent consumption in the ELISpot assay. Briefly, 96-well ELISpot plates (Millipore Sigma) were coated with a working solution of 10  $\mu\text{g}/\text{mL}$  IL-6 capture antibody from R&D Systems cat # DY206 diluted in PBS. The plates were stored at 4°C overnight. The next day, the plates were washed with sterile water and blocked for 1 hour with complete RPMI medium for 2 hours. After blocking, the medium was removed, and RPMI-8226 B cells were added to each well at various cell seeding densities. To stimulate the RPMI-8226 B cells, a final concentration of 100 ng/mL of LPS was added to the 10% BSA solution. Next, a 20  $\mu\text{L}$  volume of the mixture was placed in each well of the ELISpot 96-well plate and covered with 80  $\mu\text{L}$  of 7% PEG solution. A conventional ELISpot assay without cell confinement in the PEG-BSA system was performed in parallel as described above, with cells and LPS mixed in RPMI medium and 100  $\mu\text{L}$  of the mixture added to each well. Following 24 hours of culture for both the ATPS-based assay and the conventional assay, the plates

were washed with PBS containing 0.01% Tween 20 and incubated with the IL-6 detection antibody (0.1 µg/mL antibody from R&D Systems cat # DY206) at 37°C for 2 hours. The plates were then washed with PBS containing 0.01% Tween 20 and incubated with streptavidin-alkaline phosphatase (Biotium) (1:1000 dilution in sterile PBS) for 45 minutes. Finally, the plates were washed with PBS containing 0.01% Tween 20, followed by three washes with PBS, and incubated with 100 µL of BCIP/NBT substrate (Sigma-Aldrich) per well for 5 to 10 minutes. Spot development was stopped by extensive washing under running tap water. Plates were left to dry overnight in the dark. IL-6 producing cell spots were counted with an ImmunoSpot S6 (Cellular Technology Limited).

### **5.3.11 Measurement of IL-6 Confinement**

IL-6 confinement was examined for two ATPS formulations: 7% PEG 35 kDa-10% BSA (Albumax) and 5% PEG 35 kDa-6.4% dextran 500 kDa. Both systems were formed in complete RPMI 1640 medium. A total of 500 pg/mL of recombinant IL-6 was added to the bottom phase of each system (i.e., in either BSA or dextran). A 50 µL volume of each bottom phase solution was added to a 200 µL microtube and covered with a 150 µL layer of either 7% PEG for the PEG-BSA system or 5% PEG for the PEG-dextran system. Both systems were left to achieve thermodynamic equilibrium at room temperature, and the phases were collected separately at three time points: 2 hours, 24 hours, and 48 hours. Three replicates were used for each system. Concentrations of recombinant IL-6 in the respective phases of the PEG-BSA and PEG-dextran systems

were measured by ELISA according to the manufacturer's instructions (R&D Systems cat # DY206) using the same ELISA procedure described above.

### 5.3.12 Statistical Analysis

Kruskal-Wallis one-way analysis of variance (ANOVA) and Tukey multiple comparison tests were conducted to compare the effects of phase-separating solutions on cell viability over 72 hours. Kruskal-Wallis ANOVA and Tukey multiple comparison tests were performed to compare the effects of PMA and LPS concentrations on cell activation. Kruskal-Wallis ANOVA and Dunn's multiple comparison tests were performed to compare the effects of phase-separating solutions on IL-2 and IL-6 secretion by Jurkat T cells and RPMI-8226 B cells, respectively, over 24 hours. One-way ANOVA and Tukey multiple comparison tests were conducted to compare IL-6 confinement ratios over time, and the number of IL-6 secreting cell spots as a function of cell density. Data are represented as mean values + standard deviations. Statistical significance was defined as \* $p < 0.05$ .

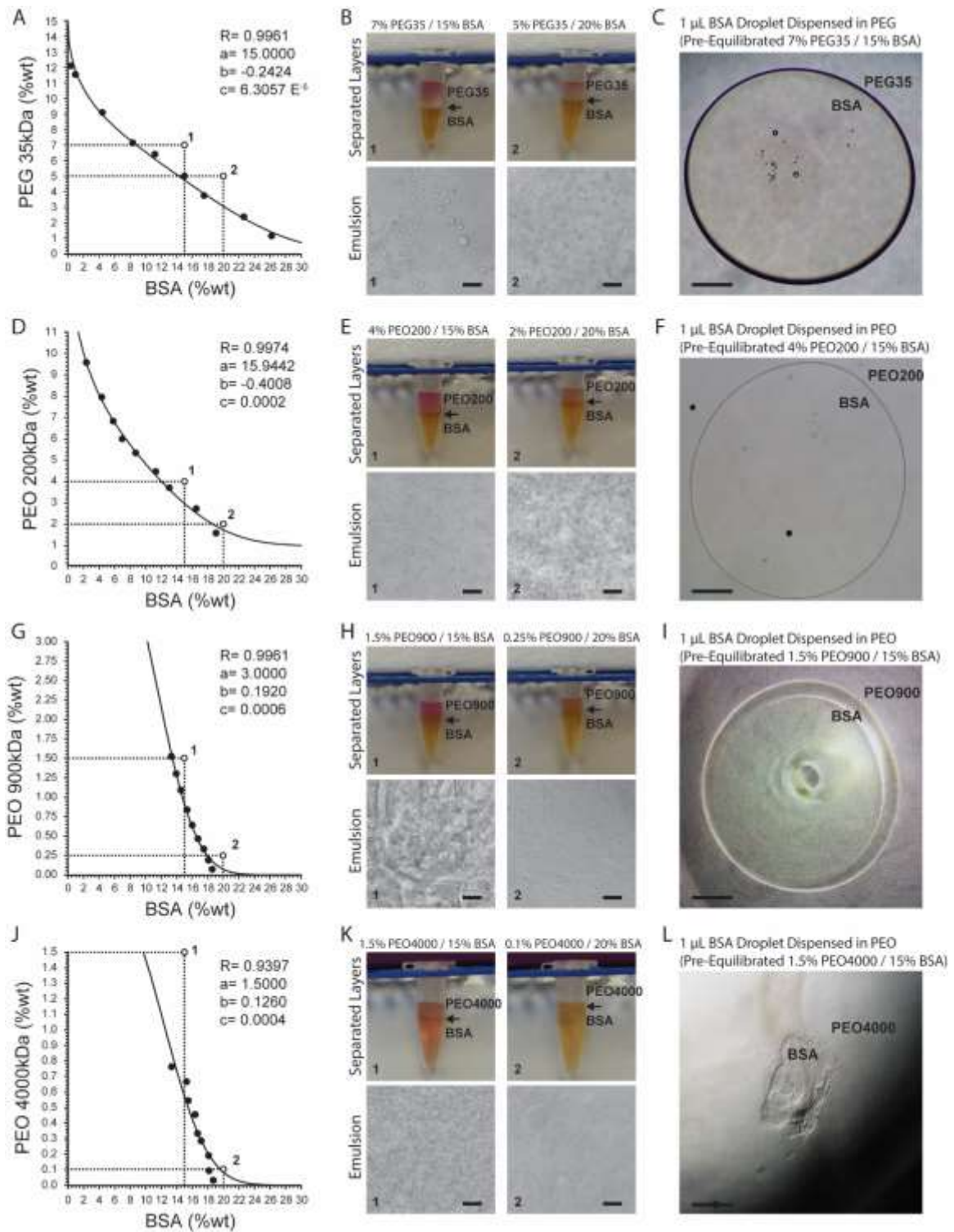
## 5.4 RESULTS AND DISCUSSION

ATPSs readily formed from mixtures of PEG and PEO with BSA (Figure 26). As expected, increasing the PEG/PEO MW and concentration favored phase separation with BSA. Thus, PEG 35 kDa and PEO 200 kDa required higher concentrations to achieve phase separation with BSA as compared to PEO 900 kDa and PEO 4,000 kDa. Binodal data were fit according to

$$y = a \exp(bx^{0.5} - cx^3),$$

where  $y$  and  $x$  are the polymer concentrations (in weight percentage), and  $a$ ,  $b$  and  $c$  represent fitting parameters<sup>321</sup>. Fitting parameters are displayed for each binodal in Figure 26. Consistent with previous observations, as the polymer MW increased (thus increasing the MW difference between PEG/PEO and BSA), the binodal curves became increasingly asymmetric. Figures 26A, D, G, and J also show two coordinates (points 1 and 2) that represent the total compositions of both phases. Figures 26B, E, H, and K display the corresponding macroscopic and microscopic images after equilibration of the phases. In Figure 26A, point 1 corresponds to a system comprised of 7% PEG and 15% BSA, and point 2 corresponds to a system comprised of 5% PEG and 20% BSA. Comparing the systems formed from points 1 and 2, one can appreciate that the relative volume of the bottom phase is greater for point 2, as would be predicted from estimation of the tie lines. Although systems on the same tie line have different total polymer concentration and different volume ratios after mixing, they should have the same final polymer concentrations in the top and bottom phases<sup>42</sup>.





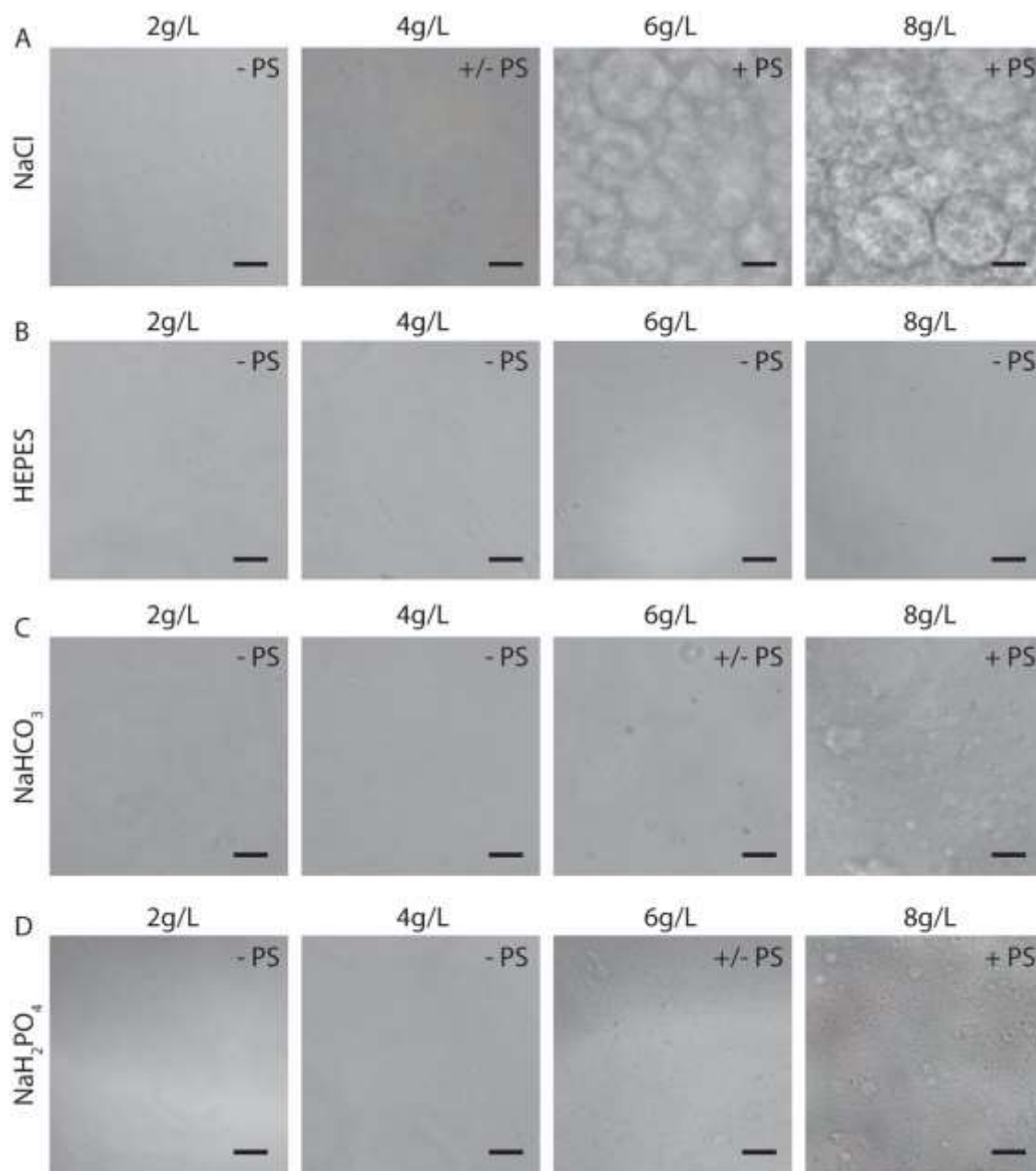
**Figure 26 Binodal curves for PEG- and PEO-BSA systems.** (A) PEG 35 kDa-BSA, (D) PEO 200 kDa-BSA, (G) PEO 900 kDa-BSA and (J) PEO 4000 kDa-BSA.  $R$  is the correlation coefficient. Fitting parameters are denoted by  $a$ ,  $b$ , and  $c$ . Points 1 and 2 correspond to formulations shown in images to the right. (B,E,H,K) show macroscopic and microscopic images of PEG, PEO, and BSA at different concentrations indicated by numbered points on the binodal graphs. Arrows indicate the location of the interface between the phases. (C,F,I,L) show microscopic images of pre-equilibrated BSA droplets dispersed in pre-equilibrated PEG and PEO solutions. Scale bars in (B,E,H,K) are  $50\mu\text{m}$ . Scale bars in (C,F,I,L) are  $500\mu\text{m}$ . Images are reproduced under a Creative Commons Attribution 4.0 International license<sup>232</sup>.

Microscopically, one can observe formation of droplet structures for supercritical concentrations of solutes, similar to oil-in-water emulsions. In an ATPS-emulsion, the phase with the greatest volume fraction forms the continuous phase. For instance, in the system composed of 5% PEG and 20% BSA (Figure 26B), the continuous phase is BSA with PEG droplets dispersed within it. Although the interfacial tension of these ATPSs is orders of magnitude lower than oil-in-water systems, the formation of droplets indicates the presence of considerable interfacial tension between the two aqueous phases <sup>79</sup>.

Increasing the molecular weight and concentration of PEG/PEO increased the viscosities of the systems, resulting in longer settling times. The relatively high viscosities of the PEO 200 kDa, PEO 900 kDa and PEO 4,000 kDa systems resulted in highly deformed microdroplets present in the emulsions (Figure 26E, H and K). The interfacial tension between the phases coupled with their viscosity can enable confinement of cells as well as select biomolecules by way of biomolecular partitioning. However, solutions of PEO 900 kDa above 1.5% and PEO 4,000 kDa above 0.7% are too viscous to experimentally analyze phase separation with BSA and display handling properties that preclude downstream applications. High viscosities of these polymer solutions make pipetting difficult, leading to inaccurate dispensed volumes. This is evident in the images of dispensed droplets of BSA-rich bottom phase into the top PEG-rich phase in Figures 26C, F, I and L. Systems composed of PEG 35 kDa, PEO 200 kDa and PEO 900 kDa offer workable viscosities that allow dispensing of BSA microdroplets into a continuous phase of PEG/PEO.

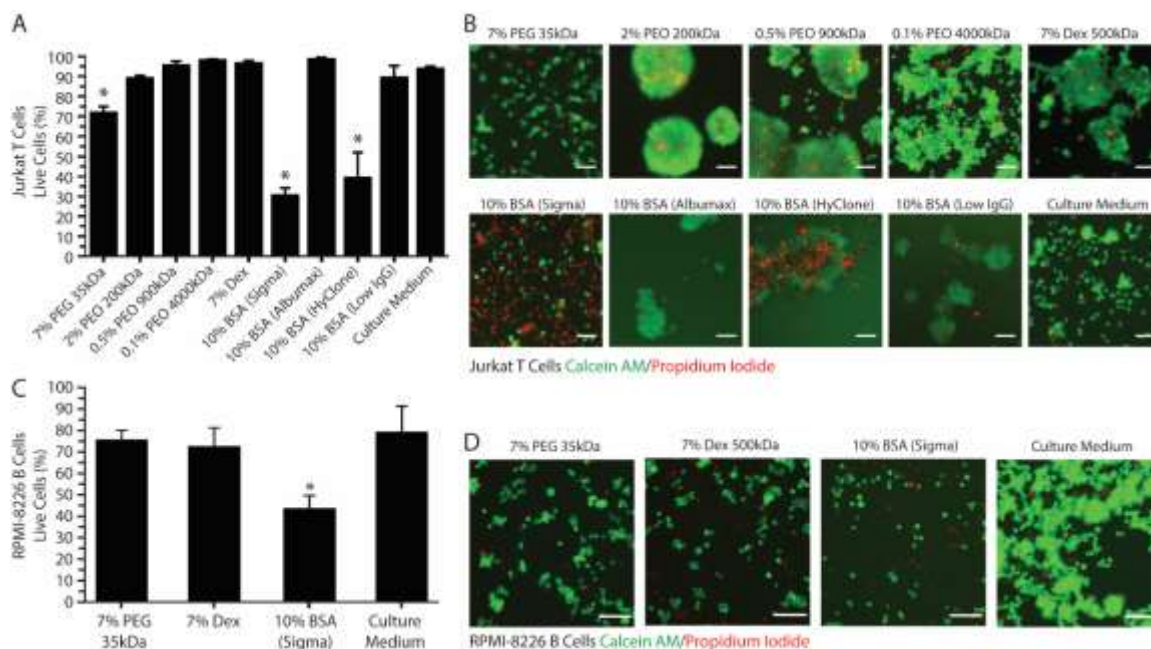
In terms of ATPS thermodynamics, the free energy of mixing must be positive for phase separation to occur, which means that the enthalpy of mixing must dominate over

the entropy of mixing<sup>322</sup>. The addition of certain salts to an ATPS is thought to decrease the entropic penalty, thereby promoting de-mixing of the system at lower polymer concentrations<sup>120,322</sup>. We reasoned that salts and buffering compounds present in various cell culture medium formulations would therefore influence phase separation of PEG/PEO-BSA ATPSs. The influence of salts such as NaCl and buffering compounds such as HEPES, NaHCO<sub>3</sub> and NaH<sub>2</sub>PO<sub>4</sub> on phase separation was therefore examined for a single ATPS formulation without extensive characterization of binodal phase diagrams (Figure 27). As shown in Figure 27A, increasing NaCl concentration promoted ATPS formation. Concentrations of NaCl in cell culture medium range from 4.5 to 7.6 g/L. Therefore, the NaCl concentration of a typical cell culture medium formulation is sufficient to promote phase separation of PEG/PEO and BSA. In contrast, HEPES, a buffering compound present in Iscove's Modified Dulbecco's Media (IMDM) at ~ 6 g/L did not promote ATPS formation (Figure 27B). Sodium bicarbonate and sodium phosphate monobasic (also present in various medium formulations at concentrations ranging from ~1.2 to 3.7 g/L, and ~ 0.100 to 0.580 g/L, respectively) had modest effects on ATPS formation as shown in Figures 27C and 27D. The type of salt added to the system also influenced the shape and size of the microdroplets. Microdroplet emulsions formed in systems containing NaCl displayed droplets that were more well-defined and rounder than droplets formed in systems containing sodium bicarbonate and sodium phosphate monobasic, indicating that addition of NaCl influences the interfacial tension by strongly favoring de-mixing of the polymers.



**Figure 27** Representative images (10X) of microdroplet emulsions in PEO 900 kDa-BSA systems with addition of NaCl (A), HEPES (B), NaHCO<sub>3</sub> (C), NaH<sub>2</sub>PO<sub>4</sub> (D). PS: no phase separation; +/- PS: near critical system/slight phase separation; + PS: super-critical system with apparent phase separation. Scale bars are 50  $\mu$ m. Images are reproduced under a Creative Commons Attribution 4.0 International license<sup>232</sup>.

Having characterized the phase separation of this novel system, we next sought to determine the effects that PEG/PEO and BSA had on cell viability and function. We evaluated the viability of Jurkat T cells in individual phase-separating solutions present in the PEG/PEO-BSA and PEG-dextran systems to assess the suitability of these polymers for long term cell culture. As shown in Figures 28A-B, culturing Jurkat T cells for 72 hours in 7% PEG, resulted in ~70% cell viability, as compared to >89% viability when the cells were cultured in the three types of PEO tested. Among the PEOs, 0.1% PEO 4,000 kDa had the least impact on cell viability with ~98% cell viability. Therefore, polymer concentration has a considerable effect on cell viability over time. Addition of either technical grade BSA from Sigma or HyClone BSA to the medium resulted in <40% cell viability. However, addition of cell culture grade Albumax BSA to the medium resulted in 98% cell viability. Addition of low IgG BSA to the medium resulted in ~90% cell viability. Cells cultured in dextran were ~97% viable. We also evaluated the viability of RPMI-8226 B cells in a selection of individual phase-separating solutions to confirm the results obtained for T cells using an additional suspension-cultured immune cell line (Figure 28C-D). Culturing RPMI B cells for 72 hours in 7% PEG 35kDa resulted in ~76% cell viability. The 7% Dex solution had a similar impact on B cell viability with ~73% cell viability. Cells cultured in the technical grade BSA (Sigma) were ~44% viable, which was significantly different compared to control (~80% cell viability). Since the impact of Sigma BSA on RPMI-8226 B cell viability was slightly lower in comparison with Jurkat T cells, we presumed that the cell culture grade Albumax BSA would not affect B cell viability. These results suggest that both PEG-BSA and PEG-dextran systems are suitable for culture of T cells and B over 72 hours.



**Figure 28 Jurkat T cell and RPMI-8226 B cell viability in ATPS-polymer solutions.** (A) Percentage of viable Jurkat T cells present for various polymer/BSA medium additives after 72 h. (B) Representative images (10X) of live Jurkat T cells (in green, stained with C-AM) and dead cells (in red, stained with PI) for various polymer/BSA medium additives after 72 h. (C) Percentage of viable RPMI-8226 B cells present for various polymer/BSA medium additives after 72 h. (D) Representative images (10X) of live RPMI-8226 B cells (in green) and dead cells (in red) for various polymer/BSA medium additives after 72 h. Scale bars are 50 $\mu$ m. Significant reductions in cell viability relative to the control are indicated by \*. Images are reproduced under a Creative Commons Attribution 4.0 International license<sup>232</sup>.

All polymer solutions examined tended to cause T cell aggregation, as shown in Figure 28B. Aggregation was most evident in the PEG, BSA, and dextran conditions. This effect can result from either excessive cell growth or immune cell activation. Therefore, we decided to investigate the effects of the phase-separating solutions on cell activation by measuring IL-2 secretion from Jurkat T cells and IL-6 secretion from RPMI-8226 B cells as these are the main cytokines secreted by these cells upon activation. As a positive control for T cell activation, Jurkat T cells were treated with PMA and ionomycin (Figure 29A). To find the optimal PMA concentration to activate the cells, we performed a dose-response experiment with PMA concentrations ranging

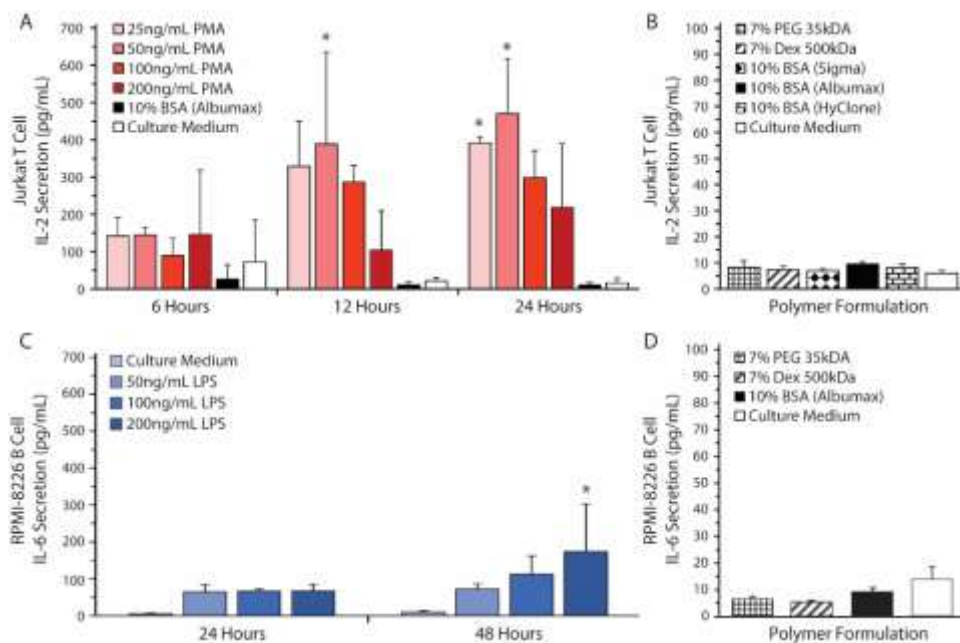
from 25 to 200 ng/mL. There were no significant differences between the four different PMA concentrations tested over the first 6 hours. After 12 hours of exposure, 50 ng/mL PMA resulted in the highest level of IL-2 secretion out of any of the concentrations tested (~390 pg/mL IL-2), reaching a peak of ~470 pg/mL IL-2 after 24 hours. As shown in Figure 29B, the polymers themselves do not stimulate IL-2 secretion over 24 hours. Activation of Jurkat T cells by PMA/ionomycin treatment in polymer/BSA-containing medium was also confirmed. Thus, although Albumax, HyClone and dextran cause cell aggregation, they do not stimulate IL-2 secretion and are therefore unlikely to have significant effects on cell activation.

To confirm that the polymer solutions did not stimulate RPMI-8626 B cells, we measured IL-6 secretion. As a positive control for B cell activation, RPMI-8226 B cells were treated with LPS (Figure 29C). To find the optimal LPS concentration to activate the cells, we performed a dose-response experiment with LPS concentrations ranging from 50 to 200 ng/mL. There were no significant differences between the four different LPS concentrations tested over the first 24 hours. After 48 hours of exposure, however, 200 ng/mL LPS resulted in the highest level of IL-6 secretion out of any of the concentrations tested (~175 pg/mL IL-6) and was significantly different from the control (~9.5 pg/mL IL-6). As shown in Figure 29D, the polymers themselves do not stimulate IL-6 secretion. Thus, Albumax, PEG and dextran solutions do not stimulate IL-6 secretion and are therefore unlikely to have significant effects on cell activation, although additional cytokines should be examined in the future to confirm this observation.

Due to the mild environment provided by ATPSs, many applications have been developed in cell biology, e.g., for cell purification and more recently for micropatterning



of cells for tissue engineering and high-throughput drug screening<sup>152,153,182</sup>. These techniques mainly use the well-known PEG-dextran system to specifically confine cells to one of the phases or to the interface between the phases<sup>155,185</sup>. Previous work has focused on applications using adherent cells where the polymers are applied acutely to confine the cells and are subsequently washed away once the cells attach or assemble into aggregates.



**Figure 29** Cytokine secretion by Jurkat T cells and RPMI-8226 B cells. (A) IL-2 levels were measured by ELISA in culture supernatants from Jurkat T cells at 6, 12, and 24 h after stimulation with 25, 50, 100, or 200 ng/mL of PMA in RPMI 1640 medium as a positive control for cell stimulation. All the stimulation conditions also received 300 ng/mL of ionomycin. The IL-2 secretion by Jurkat T-cells was also measured when the cells were cultured in 10% BSA (Albumax) without stimulation. RPMI 1640 medium was used as a negative control. Significant differences in cell activation relative to the control are indicated by \*. (B) Jurkat T cells were cultured in 10% BSA (Albumax, Sigma, or HyClone) 7 % Dex, and 7% PEG. RPMI 1640 medium was used as a control. (C) IL-6 levels were measured by ELISA in culture supernatants from RPMI-8226 B cells at 24 and 48 h after stimulation with 50, 100, or 200 ng/mL of LPS in RPMI 1640 medium as a positive control for cell stimulation. RPMI 1640 medium without LPS was used as a negative control. Significant differences in cell activation relative to the control are indicated by \*. (D) RPMI-8226 B cells were cultured in 10% BSA (Albumax) 7% Dex and 7% PEG 35 kDa. Both Jurkat T cell and RPMI-8226 B cell stimulation in various medium additives remained near baseline with no significant differences noted between polymer conditions and the culture medium control. Images are reproduced under a Creative Commons Attribution 4.0 International license<sup>232</sup>.

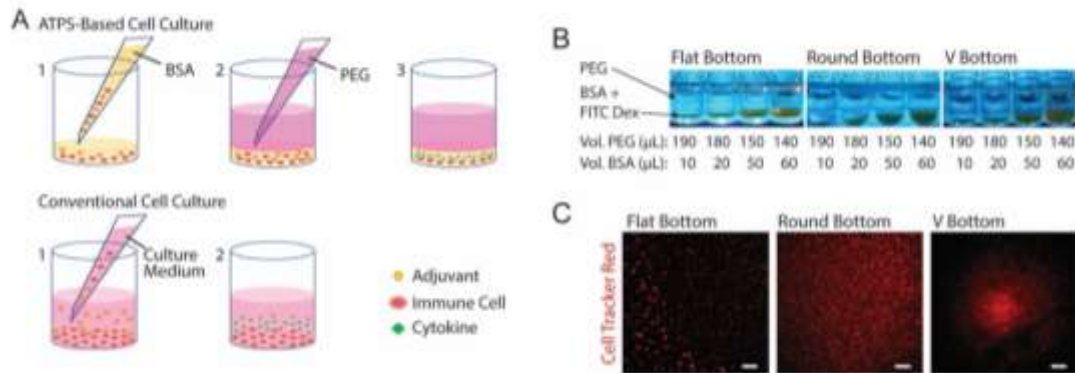


For applications involving suspension-cultured cells such as immune cells, however, the phase-separating solutions must remain in place to confine the cells over longer periods of time. Figure 30A shows a schematic diagram comparing ATPS-based immune cell culture with the conventional cell culture. The PEG-BSA system can potentially be applied for confining immune cells to reduce cell and reagent consumption in screening assays (e.g., adjuvants and antigens for vaccine development). For ATPS-based cell culture, immune cells and reagents are mixed in a BSA solution and covered with a PEG solution. Over 24 hours of stimulation, immune cells produce cytokines, which remain confined in the bottom phase. For conventional cell culture, immune cells and reagents such as adjuvants are mixed in culture medium only. Over 24 hours of stimulation, immune cells secrete cytokines that diffuse throughout the culture medium.

To begin optimizing this system, we compared the confinement of immune cells in 96-well plates with three distinct well bottom shapes: flat-bottom, round-bottom, and V-bottom. In addition, we added different volume ratios of PEG:BSA (10:190, 20:180, 50:150, 60:140) (Figure 30B). Both variables (plate type and ATPS volume ratio) were evaluated in terms of cell confinement and ability to perform microscopic imaging. To better visualize the ATPS phases and the cells, the BSA phase was labeled with FITC-dextran and the Jurkat T cells were stained with CellTracker Red™ CMTPX. As shown in Figure 30B, both PEG and BSA phases can be easily visualized in each well type. In terms of cell confinement, the V-bottom well was most effective at localizing cells to a central well region, as shown in Figure 30C, with the effect of the ATPS mainly to prevent cell disruption during medium changes and supernatant collection. All four

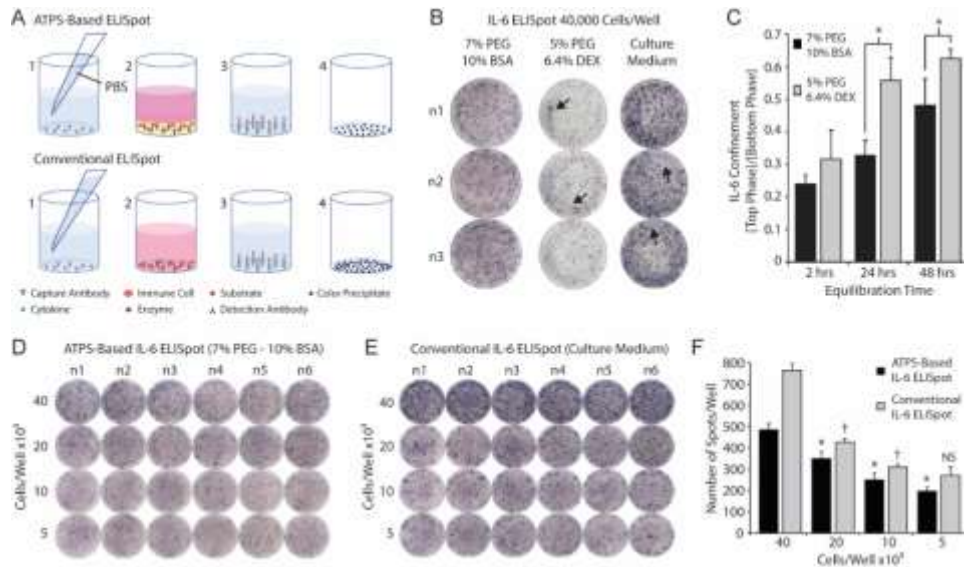
volume ratios enabled confinement and imaging of cells. Thus, the 10:190 volume ratio is the most advantageous volume ratio for minimizing cell and reagent consumption.

In order to evaluate the potential of the PEG-BSA system for screening vaccine adjuvants *in vitro*, we conducted an ATPS-based ELISpot using the PEG-BSA system. Figure 31A shows a schematic diagram comparing the ATPS-based ELISpot with the conventional ELISpot assay. Both procedures follow the same protocol, except that the ATPS-based ELISpot confines cells and cytokines in the bottom BSA phase. Figure 31B compares ELISpot results obtained from the PEG-BSA system with those obtained from the PEG-dextran system and the conventional assay system.



**Figure 30** Schematic diagram of the PEG-BSA system for compartmentalized immune cell culture. (A) Experiment setup using ATPS: (1) Immune cells are suspended in the BSA solution containing reagents (e.g., adjuvants), and 20  $\mu\text{L}$  of the mixture is added to each well of a 96-well plate. (2) An 80  $\mu\text{L}$  volume of the PEG solution is added to the well to cover the BSA-bottom phase, confining cells and reagents in the BSA solution. (3) Over 24 h of adjuvant stimulation, immune cells produce cytokines, which remain confined in the bottom phase. Conventional experiment setup: (1) Immune cells and reagents are mixed in culture medium and added to each well. (2) Over 24 h of stimulation, immune cells secrete cytokines that diffuse throughout the culture medium. (B) PEG-BSA systems in three 96-well plate geometries: flat-bottom, round bottom, and V bottom. The BSA-phase (bottom) is labeled with FITC-Dex. (C) Representative images (4X) of Jurkat T cells cultured in the PEG-BSA system in flat-bottom, round-bottom, and V-bottom 96-well plates. The cells were stained with CellTracker Red<sup>TM</sup> CMTPX. Scale bars are 100 $\mu\text{m}$ . Images are reproduced under a Creative Commons Attribution 4.0 International license<sup>232</sup>.

The PEG-BSA system produced spots that were qualitatively similar to those produced using the conventional assay protocol. Artifacts were more frequently observed for the PEG-dextran and conventional assay than in the PEG-BSA assay, as indicated by arrows pointing to line artifacts from cell movement, ring artifacts along the well edges and regions of the well devoid of spots. When the ELISpot assay was conducted using the PEG-dextran system to confine the cells, the overall signals and quality of the spots was appreciably diminished compared to the PEG-BSA and conventional assay formats. We also examined IL-6 confinement in the 7% PEG-10% BSA and 5% PEG-6.4% dextran systems by adding 150  $\mu$ L of the top phase (7% PEG or 5% PEG) on top of 50  $\mu$ L of the bottom phase (10% BSA or 6.4% dextran), with the bottom phase spiked with recombinant IL-6 (500 pg/mL). After thermodynamic equilibration at room temperature, we collected each phase separately for analysis, measured the IL-6 concentration in each phase and plotted the ratio of IL-6 concentration between the top phase and bottom phase. As shown in Figure 31C, IL-6 was more strongly confined in the BSA phase of the PEG-BSA system than in the dextran phase of the PEG-dextran system, suggesting that the PEG-BSA system is superior to the PEG-dextran phase system for confining cytokines near in the ELISpot assay and in other immunoassays used for screening cell responses. This may also partially explain why the quality of the spots in the ELISpot assay were better for the PEG-BSA system as compared to the PEG-dextran system.



**Figure 31** Screening immune cells in the PEG-BSA system by ELISpot. (A) ATPS-Based ELISpot: (1) Capture antibodies are diluted in PBS and added to each well. After overnight incubation, the capture antibodies are washed away and replaced with immune cells and adjuvants mixed in the BSA-phase. Over 24 h of stimulation, cytokines are produced by the immune cells and become confined in the BSA-phase where they bind to the capture antibodies. (2) The PEG-BSA system is washed away and it is replaced with detection antibodies mixed in PBS, followed by streptavidin-alkaline phosphatase and substrate solutions. (3) Each colored spot detected on the membrane at the bottom of each well corresponds to a cytokine-secreting cell. Conventional ELISpot: (1) Capture antibodies are mixed in PBS and added to each well of an ELISpot plate. After overnight incubation, the capture antibodies are washed away and replaced with immune cells suspended in culture medium containing adjuvants. Over 24 h of stimulation, the cytokines produced by immune cells bind to capture antibodies. (2) The culture medium is washed away and it is replaced with detection antibodies mixed in PBS, followed by enzyme and substrate solutions. (3) Each colored spot detected on the membrane at the bottom of each well corresponds to a cytokine-secreting cell. (B) Representative ELISpot results for RPMI-8226 B cells stimulated with LPS and incubated in 7% PEG-10% BSA, 5% PEG-6.4% Dex, and culture medium for 24 h. Artifacts are indicated by arrows pointing to line artifacts from cell movement, ring artifacts along the well edges, and regions of the well devoid of spots. (C) IL-6 confinement in the bulk phases of two ATPS formulations over time: 10%BSA-7%PEG and 6.4%Dex-5%PEG. \*p < 0.05 (ANOVA with Tukey post-hoc test). (D) Representative ELISpot results for RPMI-8226 B cells stimulated with LPS and incubated for 24 h in the 7% PEG-10% BSA system. (E) Representative ELISpot results for RPMI-8226 B cells stimulated with LPS and incubated for 24 h in culture medium (conventional method). (F) The spots formed within wells using both methods were counted and plotted as a function of cell density. The \* denotes significant differences from the next highest cell density for the ATPS-based method. The † denotes significant differences from the next highest cell density for the conventional method. NS denotes no significant difference from the next highest cell density. Images are reproduced under a Creative Commons Attribution 4.0 International license<sup>232</sup>.

Finally, Figure 31 D-E compares images of ATPS-based ELISpot using the PEG-BSA system and conventional ELISpot as a function of cell seeding density. Compared to the conventional technique, ATPS-based ELISpot presented less background noise and a lower frequency of spot development. As shown in Figure 31F, the number of spots developed using the ATPS-based ELISpot is smaller in comparison with the conventional assay across different cell densities. However, there is a significant difference in spot number between ATPS-based ELISpot and conventional ELISpot assay for each cell density. Interestingly, using the ATPS-based assay there is a significant difference between each cell density, whereas with the conventional method, there is no significant difference between  $10 \times 10^3$  and  $5 \times 10^3$  cells per well, suggesting that the ATPS technique may improve assay sensitivity when measuring low numbers of cytokine secreting cells.

Microscale technologies are frequently used to investigate cell-material interactions<sup>323,324</sup>, engineer and control cell shape and function<sup>325</sup>, and evaluate cell responses<sup>326</sup> in a high-throughput manner. These technologies offer tight control of the cellular microenvironment, significantly reduce the consumption of cells and reagents required to perform experiments, and in some cases, improve reaction efficiencies<sup>327</sup>. Many of these platforms rely on microfluidics to manipulate the small volumes of fluid used for cell culture and analysis. Microfluidic array platforms have been developed for high-throughput cytotoxicity screening, where three types of mammalian cell lines were screened against low and high concentrations of five toxins (digitonin, saponin,  $\text{CoCl}_2$ ,  $\text{NiCl}_2$  and acrolein)<sup>328</sup>. Another example is the sophisticated system developed by Choi and Cunningham, which integrates a 96-well microplate with microfluidic networks and biosensors to measure the binding of IgG molecules ( $20 \mu\text{L}$  IgG solution consumed) to

immobilized protein A (30  $\mu$ L protein A solution consumed)<sup>329</sup>. Although both systems are able to analyze cell viability and biomolecular interactions in a multiplex format while minimizing reagent consumption, the specialized technical expertise and equipment required to operate systems such as these limits their utility in life science laboratories.

In contrast to dextran, BSA is ionic and amphiphilic, which may intensify BSA interactions with cells and biomolecules. Our findings suggest that the PEG-BSA system has potential utility in confining immune cells in the bottom phase without significantly affecting cellular viability and activation. In addition, the BSA phase promotes a superior IL-6 confinement over time compared to the dextran phase which may be advantageous for detection by various immunoassays such as ELISpot. In terms of practical application, our ATPS-based multiplex screening does not rely on expensive and complex equipment and can be easily adapted to any laboratory familiar with commonly available liquid handling tools such as handheld micropipettes. The approach presented here can micropattern immune cells in an ATPS, while retaining high cell viability and minimizing cell activation as measured by IL-2 and IL-6 secretion.

There is considerable interest in polymers that are naturally immunostimulatory. Short cationic amphiphilic peptides are produced by several different cell types and can modulate the innate immune response, which makes them useful as adjuvants<sup>330</sup>. Polysaccharides also stimulate immune responses and have been used as adjuvants. For example, inulin-based adjuvants have been shown to activate both humoral and cellular immune responses<sup>331,332</sup>. Chitosan is another polysaccharide that elicits a cellular immune response<sup>333</sup>. We anticipate that our system may be used to confine various biomolecules and immunostimulatory polymers and particles within the BSA phase via biomolecular

partitioning for future applications in screening novel immunotherapies and adjuvant formulations. In this future work, it will be important to consider the handling properties of the ATPS-forming solutions and to more completely characterize the phenotype of cells used in experiments by assessing other types of immune cells and secreted cytokines. This cell characterization work will be particularly important in light of the cell aggregation phenomenon we observed for Jurkat T cells, since cell-cell interactions are functionally important for T cell signaling, as they are for other immune cells<sup>334</sup>. However, our data for IL-2 secretion suggest that aggregation of Jurkat T cells cultured in ATPSs does not necessarily correlate with cell activation.

Although most ATPSs used in cell culture applications have been used to biopattern adherent cells<sup>134,335</sup>, ATPS techniques have also been developed to form non-adherent cell aggregates. By exploiting the interfacial forces between PEG and dextran, Frampton et al. developed a simple method to confine cells and promote their assembly into tissue constructs<sup>185</sup>. Initially, cells were suspended in the PEG phase, which was layered on top of the dextran phase. The cells were then allowed to settle by gravity to the PEG-dextran interface. Once at the interface, cell-cell connections were formed, leading to the self-assembly of constructs over several hours. ATPS techniques have also enabled generation of tumor spheroids by confining cells within a nanoliter-volume droplet of dextran immersed in a PEG phase<sup>182,184</sup>. However, to the best of our knowledge, an ATPS has not been used to confine suspension-cultured cells such as immune cells. Confining suspension-cultured cells in an ATPS can be more challenging than adherent cells because the polymers must remain in place to continue to confine the cells.

A novel application for the PEG-BSA system is in confinement of immune cell and reagents such as adjuvants and antigens used in vaccine formulation development. ELISpot is a technique widely used for screening vaccine candidates by measuring cellular immune responses to a specific stimulus<sup>336</sup>. The ATPS-based ELISpot was used to demonstrate the application of the PEG-BSA system to confine immune cells to facilitate vaccine adjuvant screening *in vitro*. When conducting ELISpot using BSA as the bottom phase, the BSA solution reduced spot development by blocking non-specific binding and consequently improving the sensitivity of the assay. One can notice a significant difference between each cell density using the PEG-BSA system to confine cells and cytokines. However, with the conventional method, there is no significant difference between the lowest cell densities ( $10 \times 10^3$  and  $5 \times 10^3$  cells/well), which means that the ATPS-based ELISpot has potential to improve the sensitivity of this assay. Addressing how additional adjuvants and cytokines other than IL-6 partition between the PEG and BSA phase will be of paramount importance in determining the broad utility of this approach.

Finally, the ATPS-based approach described here opens up possibilities for applications beyond the culture of immune cell lines for screening applications. For example, mixtures of adherent and non-adherent cell types can potentially be co-cultured in this platform to investigate cell interactions and better understand the complexity of immune cell signaling in various tissues. Furthermore, the PEG-BSA system has potential to be applied to separate and purify biomolecules according to their affinity for each phase. The PEG/PEO-BSA system may also find applications in the encapsulation of drugs and biomolecules. Thus, characterization of this novel ATPS and preliminary



evaluation of the cytotoxicity and cellular responses to the phase-forming solutes may be valuable for exploration of a variety of future biomedical applications.

## **5.5 CONCLUSIONS**

We characterized a new ATPS and demonstrated that immune cells and cytokines can be confined in a PEG-BSA system without compromising cell viability and activation. We showed that this new system can be employed to improve the sensitivity of a conventional ELISpot assay by reducing background noise and detecting differences between small numbers of cytokine secreting cells. We anticipate that this new system will enable more robust and cost-effective multiplex screening of adjuvants and other compounds known to stimulate immune cells.

## **CHAPTER 6      SCREENING VACCINE FORMULATIONS IN THE ATPS-ELISpot ASSAY**

### **6.1      ABSTRACT**

A previously characterized ATPS composed of 7% PEG and 10% BSA was coupled with ELISpot to screen immune response from primary human peripheral blood mononuclear cells (PBMCs). This platform, so called ATPS-ELISpot, enabled the screening of vaccine formulations against influenza A H1N1 using one-fifth of the amount of reagents required by the conventional ELISpot method. The optimal influenza hemagglutinin (HA) concentration without addition of adjuvant was 10 µg/mL. This HA concentration was used to screen five Toll-like receptor (TLR)-agonists: pam3CSK4 (TLR1/TLR2), polyinosine-polycytidylic acid (poly(I:C)) (TLR-3), lipopolysaccharide (LPS) (TLR-4), imiquimod (TLR-7), and CpG oligonucleotide (TLR-9). The optimal HA-specific IFN-gamma response was achieved when PBMCs were incubated with 2.5 ng/mL pam3CSK4, 10 ug/mL poly (I:C), 5 ug/mL imiquimod, 50 ug/mL CpG, or 1 ug/mL LPS.

Therefore, this new platform can be employed to screen vaccine formulations using minimal amounts of reagents, which may facilitate the cost-effective discovery of new vaccines and accelerate their availability in the market.

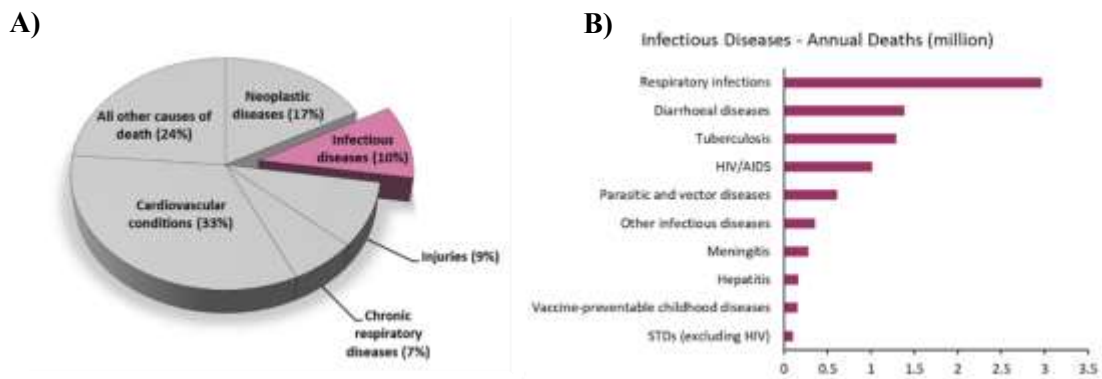
## 6.2 INTRODUCTION

Infectious diseases have posed significant threats to human health and the global economy over the last decades<sup>337,338</sup>. Emerging and re-emerging infectious diseases, including influenza, ebola, zika, and more recently, the coronavirus disease 2019 (COVID-19), continue to represent challenges to be overcome<sup>339</sup>.

Since the beginning of the 20th century, the world has faced four major influenza pandemics. The Spanish influenza (H1N1) in 1918 was the most devastating of all, causing up to 100 million deaths globally. Subsequently, the world experienced milder pandemics with Asian influenza (H2N2) in 1957, and with the Hong Kong influenza (H3N2) in 1968. In 2009, the H1N1 influenza virus re-emerged, but caused far fewer deaths compared to the 1918 virus infection<sup>340-342</sup>. The re-emergence of influenza is attributed to influenza HA glycosylation, which can allow the virus to evade antibody neutralization. However, individuals who were previously exposed to the 1918 strain developed cross-protection against the new variant, which caused milder symptoms<sup>343,344</sup>.

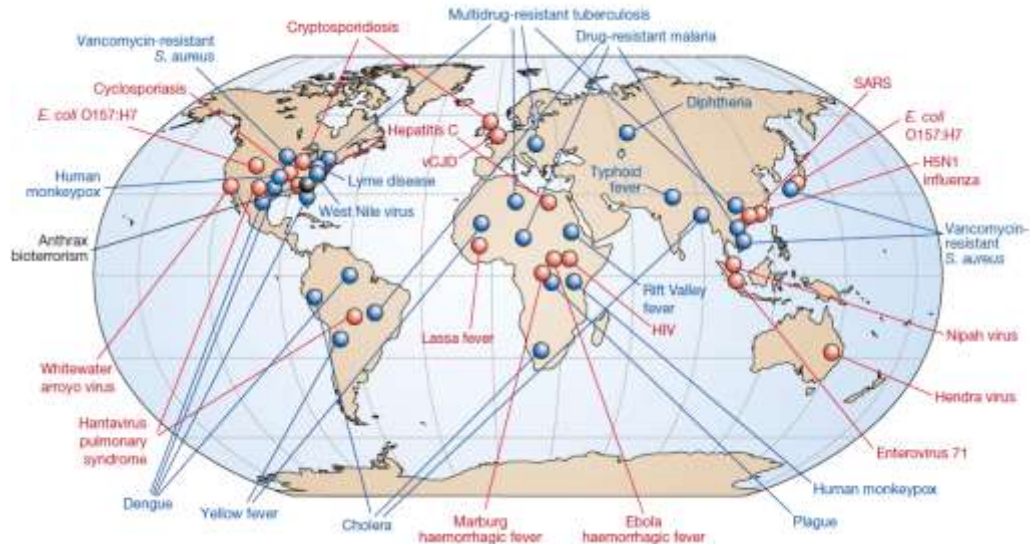
The global burden of infectious diseases remains relatively high, and it is among the leading causes of death globally, as shown in Figure 32A<sup>345</sup>. The leading cause of death among infectious diseases is respiratory infections with 3 million deaths per year (Figure 32B)<sup>346</sup>, representing a vast socioeconomic burden, a challenge that can be overcome with effective and affordable vaccines to prevent illness worldwide, especially in children, the elderly, and adults who are at high-risk<sup>347</sup>. Vaccines against influenza and severe acute respiratory syndrome coronavirus-2 (SARS-CoV-2) are the only licensed vaccines available against respiratory infections<sup>348</sup>. The scarcity of vaccines may be due to the lack of understanding immune responses against respiratory viral infections and

finding the most appropriate target antigens<sup>347,349</sup>. Also, animal models are generally inadequate at mimicking human disease or predicting the human body's response to vaccine candidates<sup>350</sup>. Therefore, there is a significant clinical need for new vaccine formulations that promote appropriate immune responses against respiratory infections<sup>349</sup>.



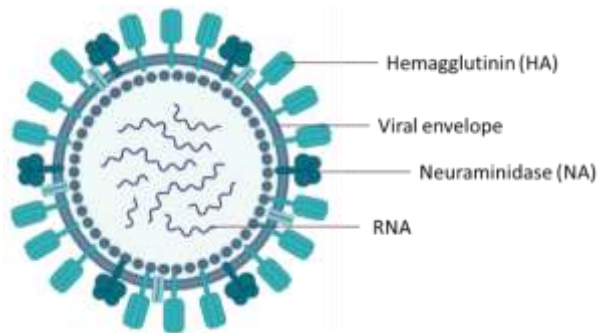
**Figure 32** Global burden of infectious diseases. A) About 10% of annual deaths worldwide are due to infectious disease. B) The deadliest infectious diseases globally.

Figure 33 shows examples of global emerging and re-emerging infectious diseases<sup>351</sup>. Newly emerging infections are the diseases that have been for the first time recognized in humans, such as the 2009 H1N1 influenza. Re-emerging infections are those that have existed before but are now rapidly increasing in incidence or geographic range, such as seasonal influenza<sup>337,345</sup>.



**Figure 33** Examples of emerging and re-emerging infectious diseases worldwide. Red indicates newly emerging diseases; blue, re-emerging diseases; black, an intentionally emerging disease. Reproduced with permission<sup>345</sup>. Copyright 2004, Nature.

Seasonal influenza normally re-emerges every year due to the ability of the influenza virus to constantly and quickly undergo small mutations, a phenomenon known as antigenic drift<sup>345,352</sup>. The influenza virus can be classified into types A, B, C, or D. Types A and B are the viruses that are responsible for causing seasonal influenza. Type A influenza virus is the only type known to cause pandemic influenza and it can be classified into subtypes based on two surface proteins: hemagglutinin (HA) and neuraminidase (NA)<sup>353</sup> (Figure 34).



**Figure 34** Influenza virus structure

The World Health Organization has estimated that seasonal influenza cause about 3 to 5 million severe illness and 290,000 to 650,000 deaths worldwide every year<sup>354</sup>. Vaccination has proved to be the most cost-effective strategy against annual seasonal influenza<sup>355,356</sup>. By exploiting the ability of the human immune system to respond to influenza virus antigens, for example, HA, vaccines can be used to induce immune responses to protect against seasonal influenza infection<sup>357</sup>. HA is the main influenza vaccine target due to its ability to bind to sialic acid molecules on the cell surface, facilitating the entry of the virus into the cell. In fact, vaccines targeting HA, specially conserved HA epitopes, are the most promising influenza vaccines currently in development<sup>358</sup>.

The antigenic component of influenza vaccines can be derived from the pathogen or produced synthetically. The influenza antigen can be either live (attenuated virus), or non-live (whole inactivated virus, a split inactivated virus, synthetic peptides, virus-like particles, DNA, or recombinant proteins)<sup>357</sup>. Live attenuated vaccines can induce a strong immune response but pose a safety risk for infants, the elderly, and individuals with compromised immune systems. On the other hand, non-live vaccines are safer but induce a weaker immune response, and for this reason, require the use of adjuvants to boost their immunogenicity<sup>359</sup>. Adjuvants are substances added to vaccines to enhance the magnitude and duration of the immune response<sup>360</sup>.

One of the main challenges in developing vaccines for infectious diseases is the identification of an appropriate adjuvant to stimulate the desired cellular and humoral adaptive immune response<sup>361</sup>. For this reason, there is a demand for improved inactivated influenza vaccines<sup>362</sup>. Successful licensed vaccines that promote long-term protective

immune responses use adjuvants that target Toll-like receptors (TLRs)<sup>363</sup>. For example, vaccines against hepatitis B virus (Fendrix™, GSK Biologicals) and human papillomavirus (Cervarix™, GSK Biologicals) contain a combination of aluminium salts and a LPS derivative, monophosphoryl lipid A (MPL), which is a TLR4 agonist<sup>364,365</sup>.

TLRs are transmembrane receptors for a range of pathogenic antigens and are expressed by cells of both the innate immune system (e.g., professional antigen-presenting cells (APCs) like macrophages and dendritic cells) and adaptive immune system (e.g., B cells and T cells). They evolved to recognize pathogen-associated molecular patterns (PAMPs) and damage-associated molecular patterns (DAMPs), stimulate the innate immune response (first line of host defense), and control the initiation of the adaptive immune response (immunological memory)<sup>366</sup>. Due to their ability to recognize conserved microbial patterns, they are called pattern-recognition receptors (PRR)<sup>367</sup>. In humans, at least ten TLRs have been identified, but the focus of this work was on TLR2/1 and TLR4, which are located on the cell surface, and TLR3, TLR7, and TLR9, which are endosomal receptors<sup>368</sup>. The lipid A portion of gram-negative bacteria LPS is recognized by TLR4, bacterial triacyl-lipoproteins are detected by TLR2/1, viral double-stranded RNA (dsRNA) is recognized by TLR3, viral single-stranded RNA (ssRNA) are detected by TLR7, and viral and bacterial CpG oligonucleotide (CpG ODN) are recognized by TLR9<sup>368,369</sup>. Upon recognition of a PAMP or DAMP, TLRs recruit Toll-interleukin-1 receptor (TIR) domain-containing adaptors, which triggers downstream signaling cascades, leading to activation of the transcription nuclear factor kappa B (NF-κB), the release of pro-inflammatory cytokines, and subsequent development of the adaptive immune response against the pathogen<sup>369,370</sup>.

TLR agonists have not been incorporated in licensed influenza vaccines yet, but they have been investigated as potential adjuvants to influenza vaccines, as shown in Table 2.

**Table 3** TLR agonists as potential adjuvants to influenza vaccines

Receptors	Agonist	Administration route (cells/animal)	Response
TLR2	Pegylated Pam2Cys	Intranasal (mouse)	Enhanced innate immunity in the lungs, increasing resistance to the subsequent challenge with influenza A virus <sup>371</sup> .
	T cell-inducing Pam2Cys-based lipopeptide	Intranasal, subcutaneous, or intramuscular (mouse)	Boosted highly specific antibodies titers, induced modest numbers of antibodies in combination with modest numbers of CD8+ T cells; induced robust cross protective CD8+ T cell responses in the absence of antibodies <sup>372</sup> .
TLR3	Rintatolimod (Ampligen®), (Poly I:Poly C <sub>12</sub> U)	Intranasal (human)	The combination of the vaccine FluMist® with rintatolimod generated specific secretory IgA responses of at least 4-fold over baseline against at least one of the vaccine strains included in the vaccine in 92% of the vaccinees. Also, it induced cross-reactive secretory IgA against highly pathogenic avian influenza virus strains H5N1, H7N9, and H7N3 with pandemic potential for humans <sup>373</sup> .



Receptors	Agonist	Administration route (cells/animal)	Response
TLR3	PIKA	Intranasal, subcutaneous, or intramuscular (mouse)	Increased influenza virus-specific antibody responses in combination with an influenza virus subunit vaccine, induced more robust immune responses compared to the unadjuvanted vaccine, provided significant antigen sparing (15-fold less antigen) <sup>374</sup> .
TLR4	Glucopyranosyl lipid adjuvant–stable emulsion (GLA-SE)	Peripheral mononuclear blood cells (PBMCs) from healthy humans (> 65 years old)	Stimulated secretion of Th1 cytokines by myeloid dendritic cells, enhanced the granzyme B response and stimulated cytotoxic T lymphocyte responses <sup>375</sup> .
	Fimbriae H protein (FimH)	Intranasal (mouse)	Increased release of IL-12 and RANTES and recruitment of neutrophils in the airway lumen <sup>376</sup> .
TLR4 and TLR7	1Z105 and 1V270, respectively	Intramuscular injection (mouse)	Induced rapid, sustained, and balanced Th1- and Th2-associated humoral responses and robust HA-specific cellular immune responses <sup>377</sup> .
TLR7	Imiquimod	Intraperitoneal injection (mouse)	Activated peritoneal B cells <i>in vitro</i> and induced stronger production of virus-antigen specific IgM and IgG against influenza A H1N1 <sup>378</sup> .
	Imiquimod	Intraperitoneal injection (mouse)	Accelerate and increased the humoral immune response against influenza A H1N1 <sup>379</sup> .
TLR9	CpG ODN	Intraperitoneal injection (mouse)	Inhibited viral replication in the lungs, and increased number of survivors <sup>380</sup> .
	CpG ODN	Subcutaneous Injection (mouse)	Increased the number of antigen-specific cytotoxic T cells <sup>381</sup> .

To effectively screen vaccine formulations *in vitro*, a cell-based assay must be designed to evaluate cellular responses to an antigen, an adjuvant, and an antigen combined with one or more adjuvants. However, limitations associated with the cost required to perform cell-based assays for screening vaccine formulations have motivated the development of modified ELISpot approaches that reduce the number of cells and reagents used per assay. In attempt to reduce assay cost, higher throughput cell-based assays have been developed. Li Pira et al. developed a platform called cell-ELISA which can be performed in 384- and 1,536-well plates with as few as  $10 \times 10^3$  PBMC per well. This approach consists of stimulating PBMCs cultured in 384- or -1,536-well tissue culture grade plates. Then, after incubation for 20 hours, cells are resuspended and transferred to a 96-well ELISpot plate to proceed with the conventional assay<sup>382,383</sup>. Although this platform reduces the number of cells used to evaluate cytokine-secreting cells, it does not miniaturize the ELISpot assay itself and requires an additional step to transfer pre-stimulated cells to an ELISpot plate. This additional step is prone to error, labor-intensive, and it may lead to cell loss during the transfer. Also, not washing the cells before adding them into the ELISpot plates can be problematic because secreted cytokines during pre-incubation may darken the membrane of the ELISpot plate when the cells are transferred which can increase background noise. To also reduce the sample size in functional T cell-based assays, Varadarajan et al. developed a microengraving-based approach that requires 100- to 1,000-fold fewer cells compared to traditional techniques such as the enzyme-linked immune absorbent spot (ELISpot)<sup>384</sup>. However, this platform requires expensive instrumentation and trained personnel that may not be available to many life sciences labs. To miniaturize the ELISpot platform, Hanson and colleagues developed an ELISpot assay

in 384-well format, which required one-third the amount of cells and reagents compared to 96-well assays. While the 96-well format required a cell suspension volume per well of 100  $\mu\text{L}$  ( $3 \times 10^5$  cells), the 384-well format only required 33  $\mu\text{L}$  of cell suspension ( $1 \times 10^5$  cells), which reduced the number of PBMC required by three-fold. However, in practice it can be difficult to accurately pipette cells and reagents into individual wells of a 384-well plate<sup>385</sup>.

Here, we developed an innovative and cost-effective platform for *in vitro* evaluation of vaccine formulations that conserves vaccine components in the ELISpot assay, using only widely available laboratory pipettes and plastic ware. This platform uses an aqueous two-phase system (ATPS) to confine immune cells and reagents in microdroplet reactors, enabling the efficient screening of antigens and adjuvants using only one-fifth of the amounts required by conventional ELISpot. More specifically, our goal was to identify adjuvant formulations suitable for influenza A H1N1 vaccines, which was achieved by evaluating synthetic TLR agonists individually or in combination with recombinant influenza A H1N1 hemagglutinin using the novel ATPS-based vaccine screening platform.

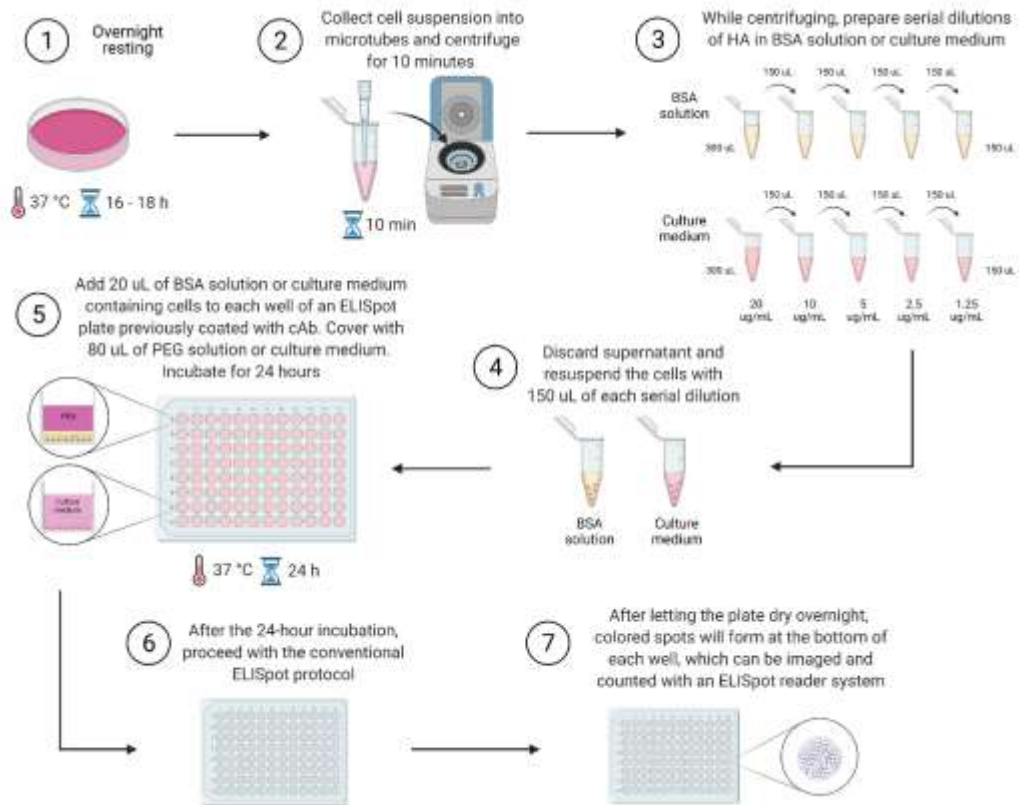
## **6.3 MATERIALS AND METHODS**

### **6.3.1 HA Titration**

To determine the optimal concentration of HA that stimulates primary human peripheral blood mononuclear cells (PBMCs), we performed a HA titration using the ATPS-ELISpot assay and the conventional ELISpot in parallel, as shown in Figure 35. Briefly, 96-well ELISpot plates (Millipore cat# MSIPS4510) were coated with a 1:60

dilution of interferon-gamma (IFN- $\gamma$ ) capture antibody from R&D Systems (cat# SEL285) diluted in sterile PBS. The plates were stored at 4°C overnight. In parallel, cryopreserved PBMCs (Lonza cat# 4W-270A) were thawed in a water bath at 37°C and seeded in a culture dish with RPMI-1640 medium with L-glutamine (Corning cat# MT10040CV) supplemented with 10% fetal bovine serum (FBS) and 1% antibiotics. PBMCs were incubated overnight (16-18 hours) at 37°C and 5% CO<sub>2</sub>. The next day, the cell suspension was collected in microtubes and centrifuged at 1,100 rpm for 10 minutes. The supernatant was removed and PBMCs was resuspended in 10% Albumax bovine serum albumin (BSA) (Gibco cat# 11020039) solution or culture medium containing influenza A H1N1 (A/California/07/2009) hemagglutinin (HA) (Sino Biological cat #11085-V08B) at various concentrations (20, 10, 5, 2.5, or 1.25  $\mu\text{g}/\text{mL}$ ). The ELISpot plates were washed with sterile water and blocked with a complete RPMI medium for 2 h. After blocking, a 20  $\mu\text{L}$  volume of the BSA solution or culture medium containing cells was placed in each well of the ELISpot plates ( $1 \times 10^5$  cells/well) and covered with 80  $\mu\text{L}$  of 7% PEG solution. Following 24 h of culture for both the ATPS-ELISpot assay and the conventional assay, the plates were washed with PBS containing 0.01% Tween 20 and incubated with the IFN- $\gamma$  detection antibody (R&D Systems cat# SEL285) with a 1:60 dilution in PBS containing 0.5% BSA at 37°C for 2 h. The plates were then washed with PBS containing 0.01% Tween 20 and incubated with streptavidin-alkaline phosphatase (Biotium cat# 29071) (1:1000 dilution in sterile PBS) for 45 min at room temperature. Finally, the plates were washed with PBS containing 0.01% Tween 20, followed by three washes with PBS only, and incubated with 100  $\mu\text{L}$  of BCIP/NBT substrate (Sigma-Aldrich cat# B1911) per well for 5–10 min at room temperature. Spot

development was stopped by extensive washing under running tap water. Plates were left to dry overnight in the dark. IFN- $\gamma$  producing cell spots were counted with an ImmunoSpot S6 reader (Cellular Technology Limited). A combination of 50 ng/mL PMA and 300 ng/mL ionomycin was used as a positive control, and the PEG-BSA system or culture medium only as a negative control.



**Figure 35** HA titration using ATPS-ELISpot versus conventional ELISpot assay.

### 6.3.2 Single Adjuvant Screening

For screening each of the TRL agonists in combination with HA, we followed the same protocol described above with slight modifications. This time, we only performed that ATPS-ELISpot. i.e., we did not run the conventional ELISpot in parallel. Briefly, in

Step 3, we prepared serial dilutions with a fixed HA concentration of 10 µg/mL with one of the five TLR agonists at the concentrations shown in Table 3. The range of concentration was defined based on data from the literature.

**Table 4** TLR agonists used in the single adjuvant screening assay

<b>TLR Agonist</b>	<b>Receptor</b>	<b>Range of Concentration</b>
Pam3CSK4 InvivoGen cat# tlr1-pms	TLR2/1	625 pg/mL – 10 ng/mL
Poly(I:C) InvivoGen cat# tlr1-picw	TLR3	625 ng/mL – 10 µg/mL
LPS Sigma-Aldrich cat# L4641	TLR4	62.5 ng/mL – 1 µg/mL
Imiquimod InvivoGen cat# tlr1-imqs	TLR7	625 ng/mL – 10 µg/mL
CpG ODN InvivoGen cat# tlr1-bw006	TLR9	6.25 µg/mL – 100 µg/mL

In addition to vaccine formulations composed of HA+TLR agonist, we evaluated formulations with TLR agonists alone at the same range of concentrations, and formulations with 10 µg/mL HA alone to assess any improvement in the immune response. A volume of 150 µL of the formulation containing HA only, or each serial dilution (HA+TLR agonist, or TLR agonist only) was added to a microtube containing the cells previously separated from supernatant. Afterward, a volume of 20 µL of each solution was added to each well of the ELISpot plates and covered with a volume of 80 µL of PEG solution, which was incubated at 37°C and 5% CO<sub>2</sub> for 24 hours. The combination of 50 ng/mL PMA + 300 ng/mL ionomycin was used as a positive control, and the PEG-BSA system or culture medium only as a negative control.

### **6.3.3 Statistical Analysis**

Analysis of variance (ANOVA) general linear model (GLM) and Tukey multiple comparison tests were conducted to compare the effects of HA on IFN- $\gamma$  secreting cell spots using ATPS-ELISpot versus conventional ELISpot over 24 hours. ANOVA GLM was also used to assess the effect of HA alone or in combination with TLR agonists on IFN- $\gamma$  secreting cell spots as a function of TLR agonist concentrations. Data are represented as mean values + standard deviations. Statistical significance was defined as \* $p < 0.05$ .

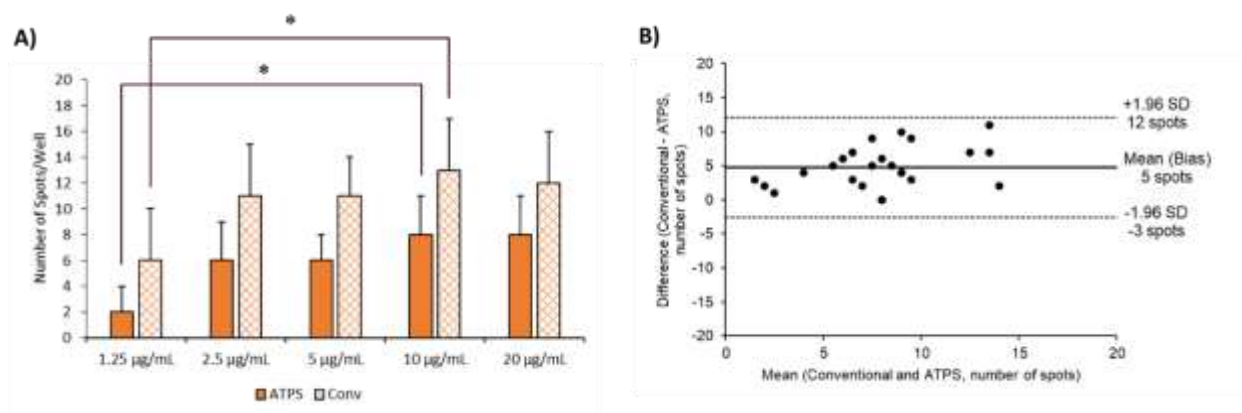
## **6.4 RESULTS AND DISCUSSION**

The novel ATPS-based assay was able to screen responses of HA alone, five TLR-agonists individually, and HA combined with each of the five TLR-agonists, using one-fifth of the vaccine reagent volumes required by the conventional method. Our previous research showed that we can confine immune cell lines and cytokines in the PEG-BSA system, and screen immune responses using an ATPS-based ELISpot<sup>273</sup>. We, therefore, optimized the system by confining primary human PBMCs to evaluate IFN- $\gamma$  secretion in the presence of hemagglutinin (HA) alone or combined with one of five TLR-agonists.

### **6.4.1 HA Titration**

Figure 36A shows the results of PBMCs exposed to serial dilutions of HA using the PEG-BSA system versus the conventional assay over 24 hours. Although the number of spots developed using the ATPS-based ELISpot is smaller compared with the

conventional assay, there is a similar trend across various HA concentrations and a significant difference in spot number between 1.25  $\mu\text{g/mL}$  and 10  $\mu\text{g/mL}$  HA for both assays. The smaller number of spots developed using ATPS-ELISpot is due to the ability of the BSA solution to block non-specific binding. Therefore, we found that the optimal HA concentration was achieved at 10  $\mu\text{g/mL}$ . We also compared ATPS-ELISpot and conventional ELISpot using Bland-Altman analysis to assess assay agreement. We found that ATPS-ELISpot and conventional ELISpot agreed more closely at medium HA concentrations as compared to lower and higher HA concentrations (Figure 36B). This may be due to slightly more consistent levels of IFN- $\gamma$  secretion within the dynamic range of the response to HA between 2.5 $\mu\text{g/mL}$  and 5  $\mu\text{g/mL}$  for both assays.



**Figure 36 Titration of HA (A) and Bland-Altman analysis of agreement between ATPS-ELISpot and conventional ELISpot (B)**

## 6.4.2 Single Adjuvant Screening

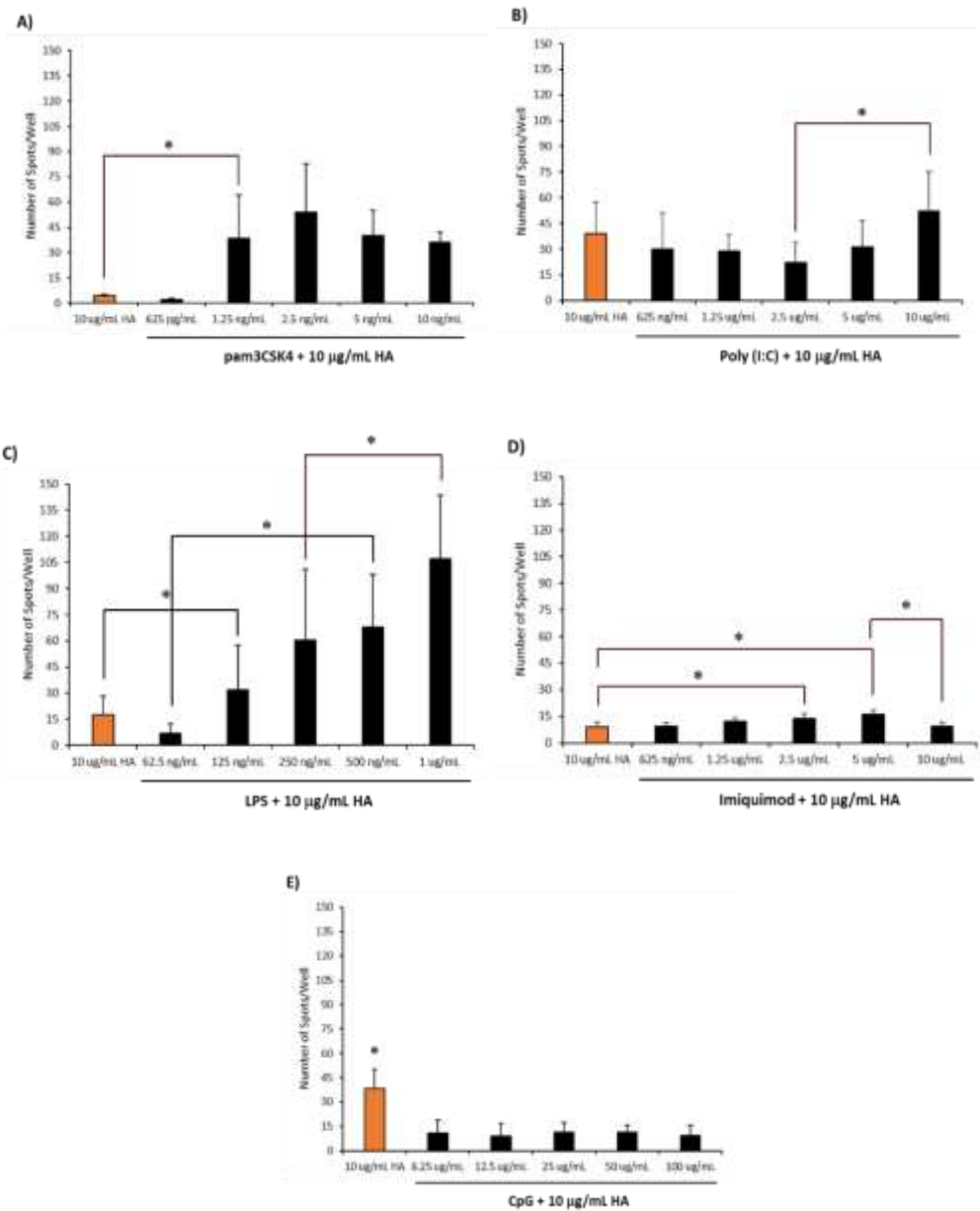
Figure 37 shows IFN- $\gamma$  ELISpot results of PBMCs treated with 10  $\mu\text{g/mL}$  HA alone or combined with TLR-agonists at various concentrations over 24 hours. Figure 38 shows the same data, but this time the graphs compare IFN- $\gamma$  secretion from PBMCs



treated with each TLR agonist alone versus each TLR agonist in combination with 10µg/mL HA.

#### **6.4.2.1 Pam3CSK4 (TLR2/1 Agonist)**

The combination of HA with 2.5 ng/mL pam3CSK4 induced the highest IFN- $\gamma$  secretion for this adjuvant, which was statistically significant compared to HA alone (Figure 37A), suggesting that pam3CSK4 makes the cellular response to HA more robust. While HA combined with 2.5 ng/mL pam3CSK4 induced the highest IFN- $\gamma$  secretion for this adjuvant, the response from 2.5 ng/mL pam3CSK4 alone was significantly lower (Figure 38A). Above the concentration of 5 ng/mL pam3CSK4 the IFN- $\gamma$  secretion was equivalent in both conditions in the presence and the absence of HA. However, the immune response triggered by the agonist alone is not HA-specific, suggesting that above 5 ng/mL, pam3CSK4 may not be an ideal vaccine adjuvant candidate for influenza A H1N1.



**Figure 37** IFN- $\gamma$  secretion from PBMCs exposed to HA alone (orange bars) or in combination with one of five TLR-agonists (black bars)

#### **6.4.2.2 Poly (I:C) (TLR3 Agonist)**

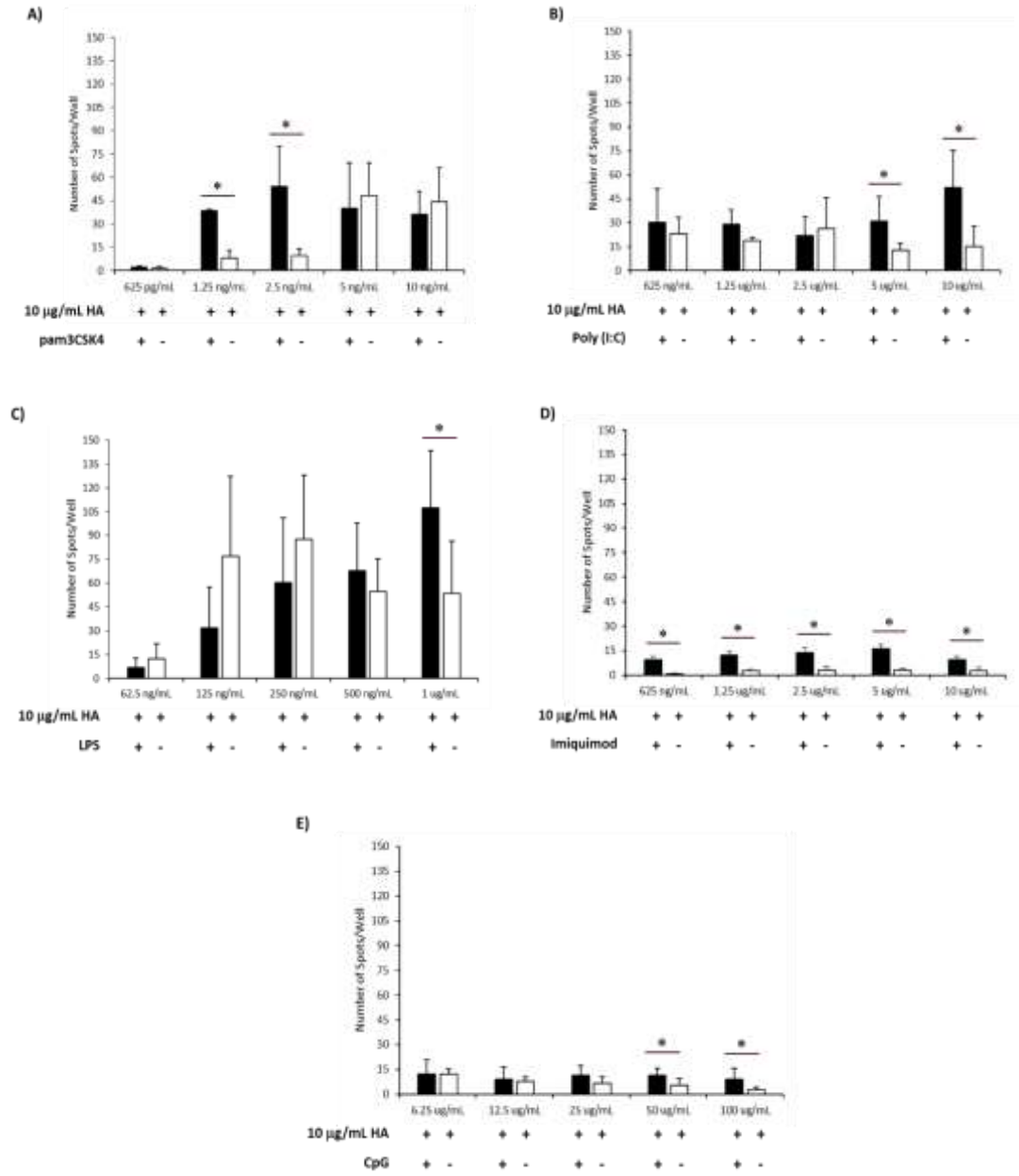
For poly(I:C), the optimal HA-specific IFN- $\gamma$  response was achieved at 10  $\mu\text{g}/\text{mL}$ , but it was not statistically different compared to HA alone (Figure 37B). The secretion of IFN- $\gamma$  from PBMCs incubated with HA and poly(I:C) at concentrations above 5  $\mu\text{g}/\text{mL}$  was significantly increased compared to poly(I:C) alone, as shown in Figure 38B. These data suggest that poly(I:C) greatly enhanced HA immune response at 5 and 10  $\mu\text{g}/\text{mL}$ . Despite the drop in IFN- $\gamma$  secretion induced by poly(I:C) alone from 5  $\mu\text{g}/\text{mL}$ , there is no statistically significant difference between poly(I:C) concentrations.

#### **6.4.2.3 LPS (TLR4 Agonist)**

In contrast to poly(I:C), treatment of the PBMCs with LPS (from 125  $\text{ng}/\text{mL}$  to 1  $\mu\text{g}/\text{mL}$ ) mediated a steady increase in IFN- $\gamma$  secretion, with statistically significant difference between LPS concentrations and HA alone (Figure 37C). These results suggest that LPS improved PBMC response against HA. LPS induced the highest IFN- $\gamma$  secretion among all the examined TLR agonists, especially in combination with HA. The optimal LPS concentration was achieved when 1  $\mu\text{g}/\text{mL}$  LPS was combined with HA, which significantly enhanced IFN- $\gamma$  secretion compared to LPS alone. From 62.5  $\text{ng}/\text{mL}$  to 250  $\text{ng}/\text{mL}$ , LPS alone promoted slightly higher secretion of IFN- $\gamma$  compared to its combination with HA, however, the increase was not statistically significant between both conditions (Figure 38C). These results suggest that LPS may be a potential vaccine adjuvant for influenza A H1N1.

#### **6.4.2.4 Imiquimod (TLR7 Agonist)**

For imiquimod, the optimal HA-specific response range was achieved when PBMCs were incubated with imiquimod concentrations between 2.5 µg/mL and 5 µg/mL combined with HA, with significant difference compared to HA alone (Figure 37D). Imiquimod induced a consistent IFN- $\gamma$  secretion across all its concentrations with and without HA. In combination with HA, imiquimod at all concentrations significantly enhanced HA response compared to imiquimod alone. These data suggest that within the range from 625 ng/mL to 10 µg/mL, imiquimod can be used as an HA-specific vaccine adjuvant (Figure 38D).



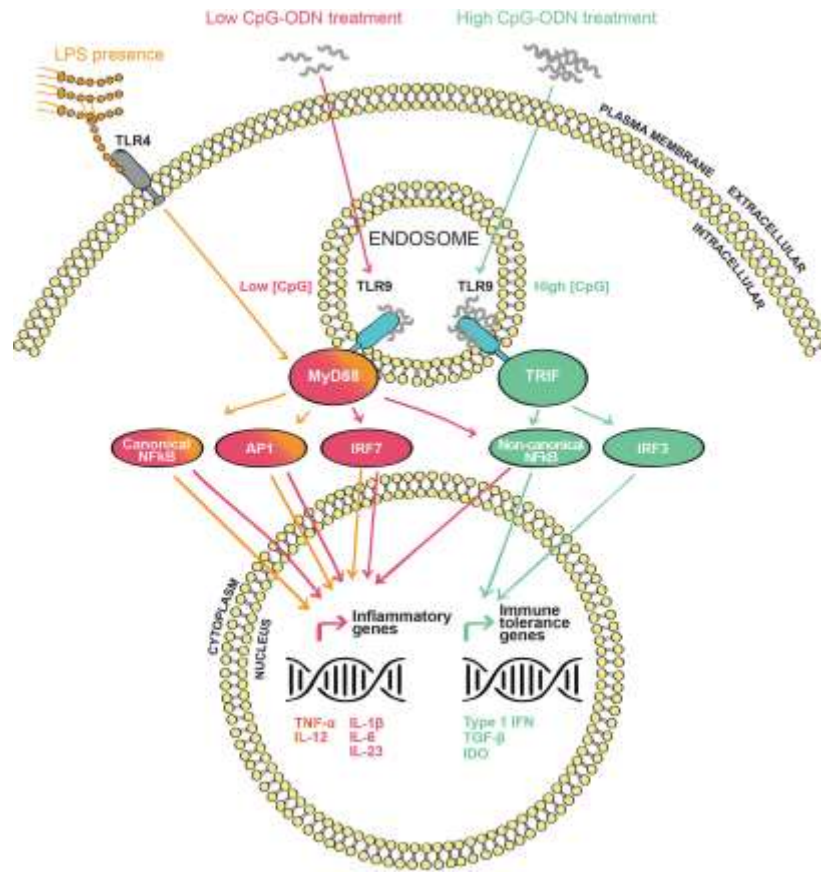
**Figure 38** IFN- $\gamma$  secretion from PBMCs in the presence (black bars) or in the absence (white bars) of HA combined with one of the five TLR-agonists

#### 6.4.2.5 CpG (TLR9 Agonist)

CpG did not improve HA immunogenicity, and it seems to decrease the PBMC responsiveness against HA regardless of its concentration (Figure 37E). Both TLR2/1 and

TLR4 bind to their ligands present in the extracellular space, which triggers downstream signaling at the cell surface. On the other hand, the ligands for TLR3, TLR7/8, and TLR9 must be first transported from outside the cell into endosomal compartments, where they will activate the intracellular TLRs and initiate signaling pathways. Therefore, signaling through the surface TLRs initiates a faster and more robust response, indicating that the spatio-temporal regulation of endosomal TLR ligands and the location of the receptors may control the signal produced<sup>386,387</sup>. In agreement with these previous studies, our results showed that incubation of PBMCs with poly(I:C), imiquimod, or CpG induced a lower response compared to pam3CSK4 or LPS. Perhaps this effect would have been less prominent if the incubation time of PBMCs with the TLR agonists was longer than 24 hours, allowing more time for ligands to reach and bind to their receptors. However, recent findings suggest that the endosomal TLRs may also appear on the cell surface of several cell types<sup>387</sup>. Interestingly, TLR9 may exist on the surface of PBMCs after incubation with LPS<sup>387</sup>, which explains why activation of TLRs 9 and 4 simultaneously has been used to enhance the immune response in mice<sup>388</sup>. Our assay was also sensitive to the suppressive effect of high doses of CpG. Our data showed that CpG at high concentrations did not enhance the pro-inflammatory response to; on the contrary, it suppressed the response to HA (Figure 37E). These results demonstrated that the ATPS-ELISpot assay can also be used to screen drugs to treat diseases that require TLR9 suppression. Previous studies have shown the potential of high doses of CpG to modulate TLR9 and its use as an adjuvant in allergen-specific immunotherapy<sup>389</sup>. Allergic bronchopulmonary aspergillosis (ABPA), for example, is an allergic reaction of the lungs to the fungus *Aspergillus fumigatus* that leads to airway inflammation. Volpi et al.<sup>390</sup>

showed that while low CpG concentrations induced a pro-inflammatory response, high CpG concentrations promoted immune regulation and tolerance. By administering two doses of 30  $\mu\text{g}$  CpG combined with *Aspergillus* antigens, they were able to induce a hypersensitivity response in the mouse lung. After 1 week of CpG treatment, the number of inflammatory cells and IgE antibodies decreased, and the typical cytokine profile of *Aspergillus* allergy was significantly attenuated. They also showed that murine splenic plasmacytoid dendritic cells p(DCs) treated with 10  $\mu\text{g}/\text{ml}$  CpG overnight and injected into recipient hosts strongly prevented allergy development. The high-dose CpG (3 $\mu\text{g}/\text{mL}$ ) in human DCs also promoted an infectious tolerance, suggesting a switch in TLR9 signaling pathways from an inflammatory myeloid differentiation factor 88 (MyD88)-dependent to an immunosuppressive TIR-domain-containing adapter-inducing interferon- $\beta$  (TRIF)-dependent response (Figure 39)<sup>389</sup>. CpG significantly enhanced HA response above 50  $\mu\text{g}/\text{mL}$  in comparison with CpG alone at the same concentrations (Figure 38E). However, as previously discussed, CpG at high concentrations promotes immune tolerance and, therefore, at these concentrations it is not an ideal vaccine adjuvant, but a potential adjuvant in allergen-specific immunotherapy.

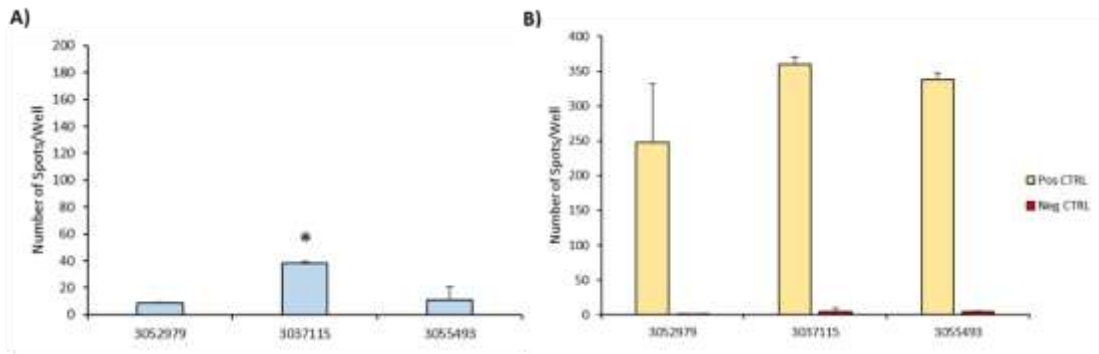


**Figure 39** Stimulation of TLR9 signaling pathways by CpG. First, CpG is internalized through endosomes where it interacts with TLR9, more specifically with the adaptor proteins MyD88 or TRIF. Low doses of CpG engage the MyD88 pathway (red) and lead to secretion of pro-inflammatory cytokines such as TNF- $\alpha$ , IL-12, IL-1 $\beta$ , IL-6, and IL-23. High doses of CpG trigger TRIF signaling (green) and lead to production of type 1 IFN and anti-inflammatory molecules such as TGF- $\beta$  and IDO. In the presence of LPS (orange), TLR4 and TLR9 signals are combined to engage MyD88 leading to enhance secretion of pro-inflammatory cytokines. Images are reproduced under a Creative Commons Attribution 4.0 International license<sup>389</sup>.

Regarding the PBMC response in each assay, it is important to emphasize that previous exposure to either influenza virus or influenza vaccine could enhance cellular response against HA, leading to high secretion of IFN- $\gamma$ . Unfortunately, it was not possible to obtain the same PBMC lot for all assays neither keep track of donor vaccine records. As we can see in Figure 40A, there was a significant difference of IFN- $\gamma$  secretion between PBMC lot 3037115 and the other two lots when exposed to HA. We



can also observe that there was a variation in response across PBMC lots when incubated with 50 ng/mL PMA + 300 ng/mL ionomycin (positive control), however, it was not statistically significant (Figure 40B). The most responsive PBMC lot was used to screen CpG and poly(I:C) adjuvanticity, followed by the lot used for screening pam3CSK4 and LPS, and finally, the lot used for HA titration and imiquimod screening. Differently, we did not see a significant difference between PBMC responses when exposed to the positive control (PMA + ionomycin), which was more consistent across lots. This can be explained by the fact that the combination of a PMA with ionomycin has been shown to non-specifically induce robust T cell activation and subsequent cytokine secretion<sup>391</sup>.

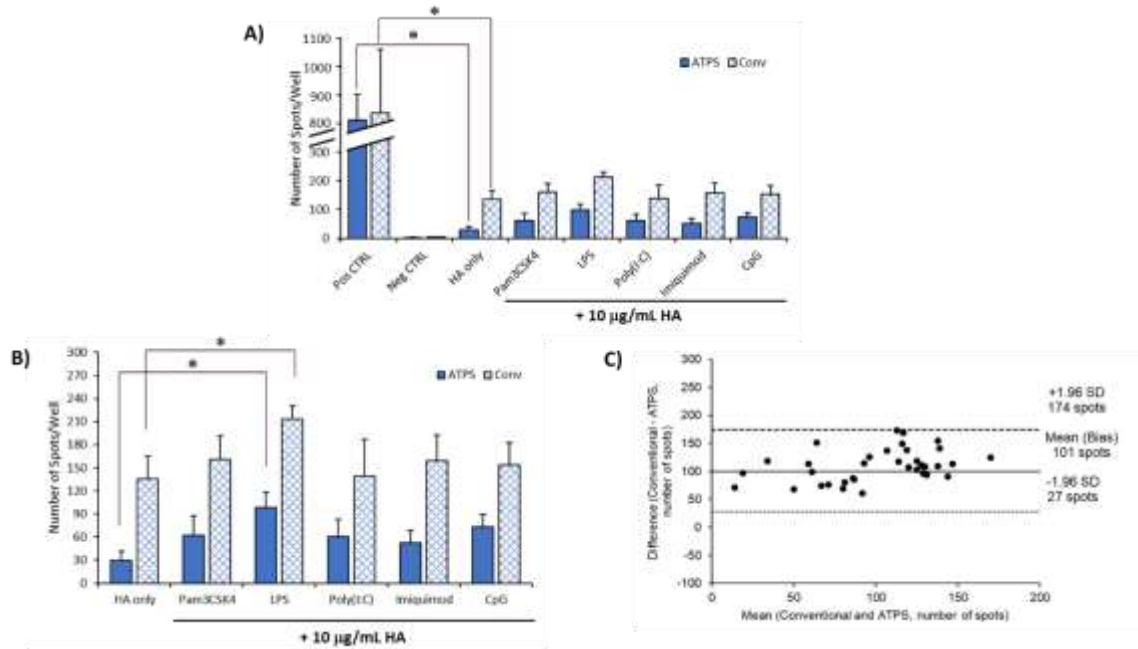


**Figure 40** Variation of IFN- $\gamma$  secretion across PBMC lots. Stimulation with HA only (A), or positive control (50 ng/mL PMA + 300 ng/mL ionomycin) versus negative control (ATPS only) (B) over 24 hours. Lot 3052979 was used for HA titration and HA+imiquimod assays, lot 3037115 was used for HA+CpG and HA+poly(I:C) assays, and lot 3055493 was used for HA+pam3CSK4 and HA+LPS assays.

### 6.4.3 Single Adjuvant Screening using ATPS-ELISpot versus Conventional ELISpot

As a positive control for PBMC stimulation, cells were treated with PMA and ionomycin. Interestingly, positive control in both methods produced very similar number of spots per well (ATPS-ELISpot=813 and conventional ELISpot=837), which differs from the pattern observed in PBMCs treated with HA only or with the HA+TLR agonists individually (Figure 11A). This must be due to the fact that PMA in combination with ionomycin consistently induces high secretion of IFN- $\gamma$  and, therefore, it is less sensitive to the blocking effect of BSA. PMA and ionomycin diffuse through the cell membrane into the cytoplasm, bypassing the receptors on the cell surface, which leads to consistent cell activation and IFN- $\gamma$  secretion. These features make PMA and ionomycin effective stimulants because they can promote a maximum response within a short time frame<sup>392</sup>.

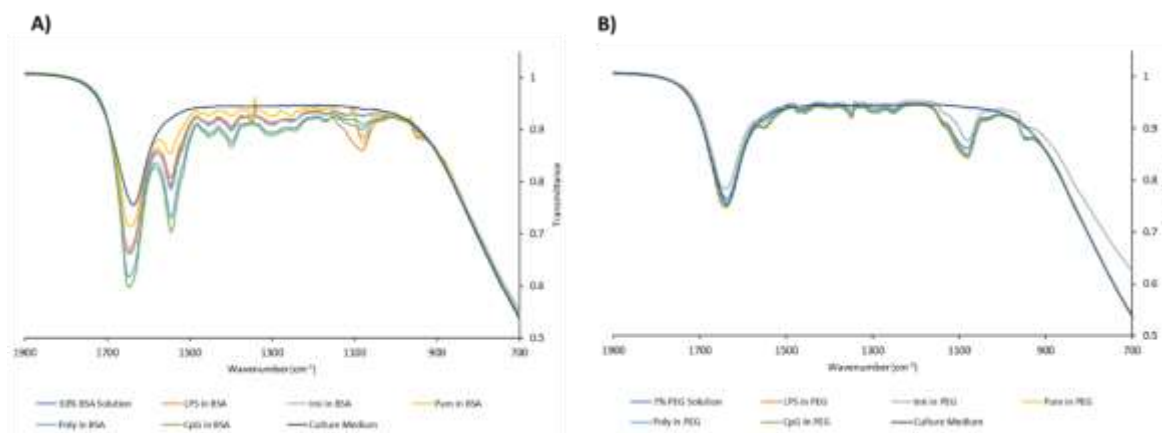
The same dataset was plotted with a different scale to better visualize the trends of both methods (Figure 41B). Consistent with previous results, the number of spots developed using the ATPS-ELISpot is smaller compared with the conventional assay. However, there is a similar trend using both methods and a significant difference in spot number between 1  $\mu\text{g/mL}$  LPS and HA only for both assays. As mentioned previously, the smaller number of spots developed using ATPS-ELISpot is due to the ability of the BSA solution to block non-specific binding. We also assessed agreement between both assays using Bland-Altman analysis, as shown in Figure 41C. The scattering points in the plot lie within the limits of agreement, which means that both methods can be used interchangeably.



**Figure 41** Single adjuvant screening using ATPS-ELISpot versus conventional ELISpot. Number of spots produced by PBMCs treated with HA only or HA combined with each TLR agonist was compared to number of spots produced by PBMCs treated with PMA + ionomycin (positive control) and ATPS or culture medium only (negative control) over 24 hours (A). The same dataset was plotted with a different scale to better visualize the trends of both methods (B). Bland-Altman analysis of agreement between ATPS-ELISpot and conventional ELISpot (C).

#### 6.4.4 Partitioning of TLR Agonists in the PEG-BSA System

Regarding partitioning of TLR agonists in the PEG-BSA system, we hypothesize that the TLR agonists studied here remain confined in the bottom phase (BSA), based on evidence from the literature (Table 3). It was not possible to prove our hypothesis and quantify the concentration of each TLR agonist in both phases. We first tried ultraviolet-visible (UV-Vis) spectroscopy in an attempt to measure the absorbance of each TLR agonist in a PEG or BSA solution. However, both PEG and BSA spectra overlapped with TLR agonist spectra. We also tried Fourier-transform infrared spectroscopy (FTIR), but we had a similar issue, as shown in Figure 42.



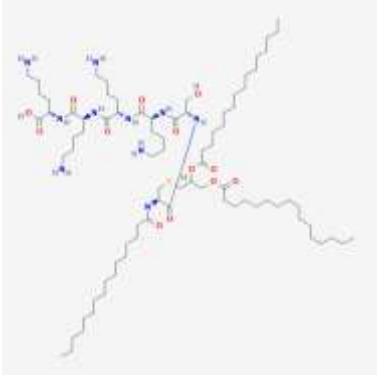

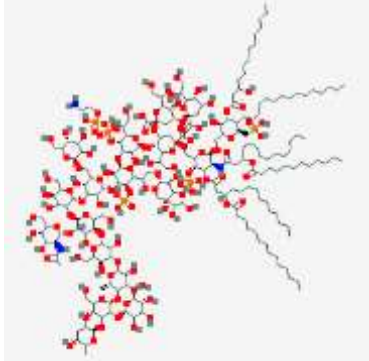
**Figure 42** FTIR spectra of TLR agonists in 10% BSA solution (A) and 7% PEG solution (B)

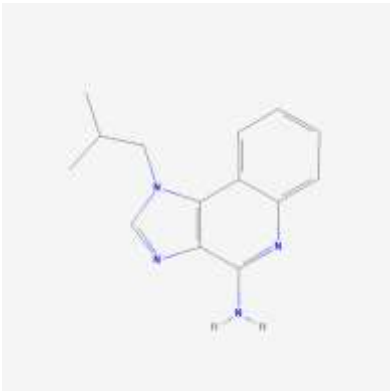
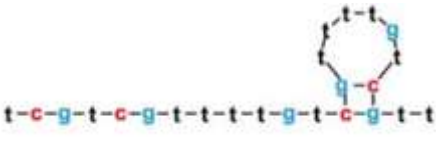
Fortunately, data from the literature support our hypothesis that the TLR agonists studied here have more affinity for the BSA phase than for the PEG phase. Pam3CSK4 is a lipoprotein and as such has a high affinity to bind serum albumin<sup>393</sup>. Serum albumin is the main fatty acid binding protein in extracellular fluids and acts as a lipid transporter in the bloodstream<sup>394</sup>. Imiquimod and poly(I:C) also have a high affinity for the BSA phase owing to the ability of both single and double-stranded oligonucleotides to form complexes with bovine serum albumin<sup>395</sup>. Albertsson investigated in detail the behavior of nucleic acids in the PEG-dextran system<sup>31</sup>. Interestingly, the partition coefficients (K values) of polyribonucleotides, such as poly(I:C), are much higher when the strands are separated as polyinosinic acid (poly I) and polycytidylic acid (poly C) than when they are mixed (poly I + poly C). The K value of the mixture is  $> 1$ , while the K values of both strands separated are  $< 0.1$  in a system composed of 5% (w/w) dextran 500 kDa, 4% (w/w) PEG 6,000 kDa, and 10 mM Na<sub>2</sub>HPO<sub>4</sub>. This behavior may be due to both the change in the nucleic acid structure itself and differences in the exposure of the bases,

which influences the nucleic acid interaction with the two phases. These results suggest that poly(I:C) has a higher affinity for the PEG phase when mixed in a PEG-dextran system. On the other hand, in a PEG-BSA system, the K value of poly(I:C) may be lower, meaning that poly(I:C) partitions to the BSA phase, considering its high affinity for albumin<sup>396</sup>, which motivates the use of BSA rather than dextran. LPS interacts with albumin through its hydrophobic portion (lipid A), which results in complexes that elicit the toxic effects of LPS<sup>397,398</sup>. CpG spontaneously binds to serum albumin<sup>399,400</sup>, a propriety that has been applied to develop albumin nanoparticles for encapsulation and controlled release of oligodeoxynucleotides<sup>401,402</sup>. In regard to HA partitioning, it is expected that HA also partitions to the BSA phase, given the affinity of albumin for glycans present on influenza HA surface<sup>403-406</sup>. The affinity of HA or TLR agonists for BSA does not seem to prevent them from interacting with their receptors. This may be due to the affinity of HA or TLR agonists for BSA is much less than the affinity for their receptors, and also, that the interaction with BSA is not specific to the receptor binding site.

In our previous study<sup>273</sup>, we demonstrated that the interfacial tension between the phases of the PEG-BSA system enabled confinement of suspension-cultured cells, such as immune cells, in the bottom phase for 24 hours. Also, for ATPS-ELISpot, immune cells confined with LPS in the BSA phase over 24 hours produced cytokines that remained confined in the bottom phase. For conventional ELISpot, immune cells and LPS were mixed with culture medium only, which favored the diffusion of LPS and secreted cytokines throughout the culture medium.

**Table 5** Hypotheses to which phase each TLR agonist may partition

TLR Agonist	Chemical structure	Partition to BSA or PEG	Supporting Information
Pam3CSK4 <sup>407</sup> (lipoprotein)		BSA	Affinity of lipids to bind albumin <sup>393</sup> . Albumin is a fatty acid transporter <sup>394</sup> .
Poly(I:C) <sup>408</sup> (analog of double-stranded RNA)		BSA	BSA forms a complex with double-stranded oligonucleotides <sup>395</sup>
LPS <sup>409</sup> (Gram-negative bacterial endotoxin)		BSA	BSA naturally interacts with LPS <sup>397</sup>

TLR Agonist	Chemical structure	Partition to BSA or PEG	Supporting Information
Imiquimod <sup>410</sup> (analog of single-stranded RNA)		BSA	BSA forms a complex with single-stranded oligonucleotides <sup>395</sup>
CpG ODN <sup>411</sup> (single-stranded DNA)		BSA	Bovine and human albumin bind to oligonucleotides <sup>399,400</sup>

#### 6.4.5 Cost-Effective ATPS-ELISpot versus Other Cell-Based Immunoassays

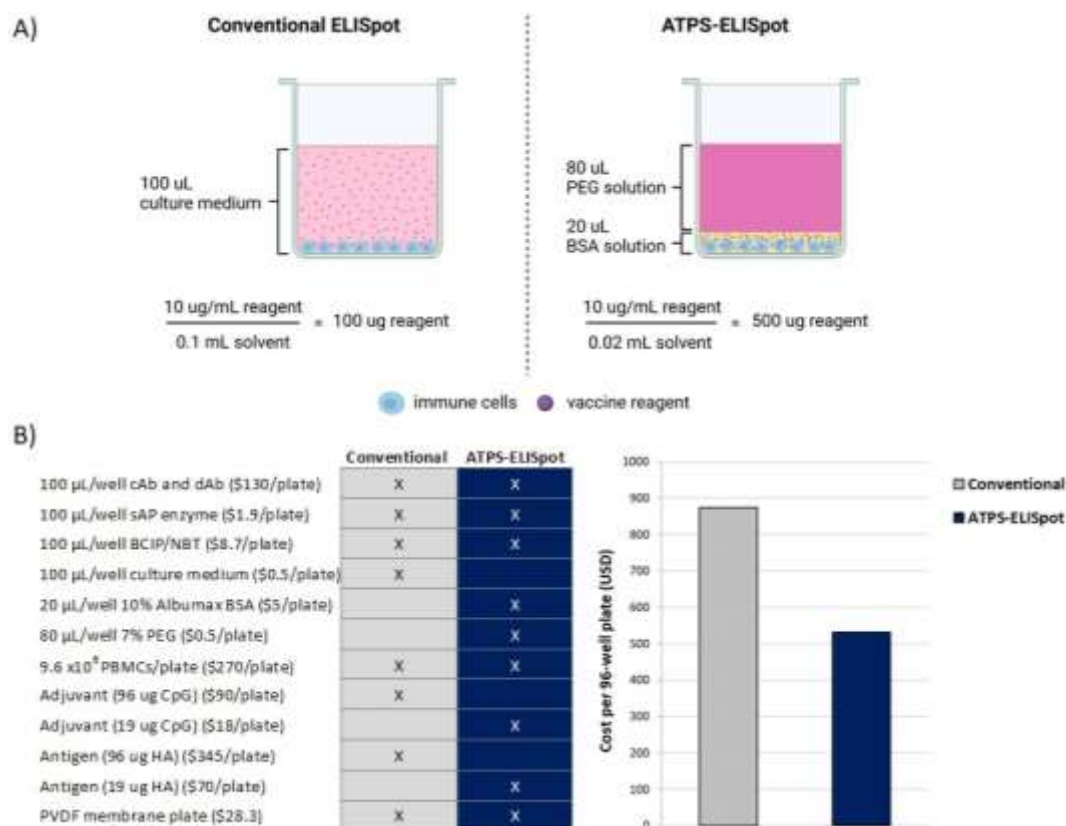
Microscale platforms have been used to evaluate immune responses *in vitro* in a high-throughput manner. These technologies have a cellular microenvironment specially designed to improve the cost-effectiveness of the assay. For example, the platform developed by Li Pira et al. is performed in 384- and 1,536-well plates, where PBMCs are stimulated for 20 hours<sup>382,383</sup>. However, this strategy does not miniaturize the ELISpot assay per se and requires an additional step to transfer pre-stimulated cells that may lead to error and cell loss. Also, there may be problems with high background for not washing the cells before adding them into the ELISpot plates. The microengraving-based approaches

developed by Varadarajan et al. requires 100- to 1,000-fold fewer cells compared to conventional ELISpot<sup>384</sup>. However, this platform requires specialized technical expertise and equipment that limit their utility in life science laboratories. The ELISpot assay developed by Hanson et al. is performed in a 384-well format, but in practice, it can be difficult to accurately pipette cells and reagents into individual wells of a 384-well plate<sup>385</sup>.

In contrast, ATPS-ELISpot does not rely on expensive equipment and personnel with training in microfluidic devices and advanced liquid handling as it only requires commonly available laboratory pipettes, plasticware and can be easily adapted to any life science laboratory. Our data showed that the PEG-BSA system can confine PBMCs in the bottom phase along with the vaccine reagents. According to the literature, the PEG-BSA is superior to the PEG-dextran system in confining TLR agonists in the bottom phase. Also, due to its high affinity for the TLR agonists studied here, the BSA phase can confine PBMCs and TLR agonists within a 20- $\mu$ L droplet, which improves the reaction efficiency of the ATPS-ELISpot by 5-fold compared to conventional ELISpot.

The differences in the cost between the optimized ATPS-ELISpot protocol and conventional ELISpot were considerable, as shown in Figure 43. Each bar in the graph (shown on the right) corresponds to a column in the table (shown on the left) and represents the costs by varying the amount of vaccine reagents, with or without ATPS polymers. These data show that the ATPS-ELISpot can save around 300 dollars per assay.





**Figure 43 Cost comparisons between ELISpot assays.** A) Schematic representation of immune cells cultured with vaccine reagents in the conventional ELISpot versus ATPS-ELISpot. In the conventional assay, cells and reagents are mixed in 100 µL culture medium, which diffuse throughout the culture medium. In ATPS-ELISpot, immune cells and reagents are mixed in 20 µL of a BSA solution and covered with 80 µL of a PEG layer, confining cells and reagents in the bottom phase. The calculation at the bottom of the diagram shows the unit mass of a reagent in the conventional assay versus in ATPS-ELISpot. In the ATPS-based assay, the reagent is concentrated by 5-fold in the BSA phase. B) Each bar in the graph (on the right) corresponds to a column in the table (on the left) and represents the costs by varying the amount of vaccine reagents, with/without ATPS polymers.

For future direction, it will be interesting to consider incubating PBMCs with TLR agonists for a longer time in the ATPS-ELISpot assay, especially with the endosomal TLR agonists. It will also be relevant to assess other cytokines, for example, interleukin 10 (IL-10), which secretion has been associated with decreased protection against influenza infection<sup>412</sup>. In addition, the ATPS-ELISpot may be applied to screen

vaccine formulations against other pathogens in combination with adjuvants to find the most appropriate immune response. Furthermore, the synergistic effect of TLR+TLR agonists or combinations of TLR+non-TLR agonists should be investigated, since targeting different receptors simultaneously may enhance immune responses<sup>366</sup>.

## **6.5 CONCLUSION**

The goal of this study was to assess the immune response of primary human PBMCs exposed to influenza A H1N1 hemagglutinin and TLR agonists, using one-fifth of the amounts of vaccine reagents compared to the conventional method. We concluded that the ATPS-ELISpot assay can be applied to identify vaccine candidates against influenza A H1N1 and potentially other pathogens, which may facilitate the cost-effective discovery of new vaccines and accelerate their availability in the market.

## CHAPTER 7 CONCLUSIONS AND FUTURE DIRECTIONS

### 7.1 SUMMARY AND CONCLUSIONS

This thesis presented the development and characterization of cost-effective ATPS-based ELISA and ELISpot assays, where ATPS was used to confine capture and detection antibodies, and immune cells and vaccine reagents respectively in microdroplets.

In Chapters 2 and 3, the emerging applications of ATPS in the Biotechnology field was critically reviewed. Even though these systems have a great potential to be used for the development of simple and cost-effective approaches, they have not been widely exploited in industrial scale yet mainly due to the lack of understanding their physicochemical properties. However, there are several other areas within the ATPS field that have shown a very promising future, including microencapsulation of biopharmaceuticals, development of artificial cells, and design of stimuli-responsive systems. These applications are currently being investigated and will be commercially available once important technological barriers and design considerations are addressed as this field matures.

In Chapter 3, the use of ATPS techniques at various scales was discussed. This chapter started highlighting applications ranging from fL to pL, where ATPS emulsions composed of PEG and dextran solutions can be formed upon supercritical concentrations and vigorous mixing. Next, examples of biomedical applications using of ATPS volumes ranging from nL to  $\mu$ L were provided. This section covered a diverse range of platforms, from microencapsulation of biomolecules and cells to development of cost-effective

immunoassays. Then, this chapter ended with several examples of ATPS applications at larger scales (mL to L). Although most of them are still at the investigation stage, they have shown remarkable potential in terms of scalability to industrial applications for purifying bioproducts.

Chapter 4 presents the development and characterization of the cost-effective single ATPS-ELISA, that exploited the interfacial tension between PEG and dextran to colocalize capture and detection antibodies in microdroplets. The colocalization technique using the PEG-dextran system minimized consumption of capture and detection antibodies in sandwich ELISA, reduced the optical crosstalk between neighboring wells, and produced comparable performance results to conventional sandwich ELISA.

Chapter 5 describes the development and characterization of the novel ATPS-ELISpot that uses the PEG and BSA system to confine immune cells and vaccine reagents together in fully aqueous environments. The results showed that the PEG-BSA system was able to confine immune cells in the bottom phase without significantly affecting cellular viability and activation. In addition, the PEG-BSA system produced spots that were comparable to those produced by the conventional assay, but with fewer artifacts.

In Chapter 6, the ATPS-ELISpot was further explored to confine primary human PBMCs with hemagglutinin (antigen) and TLR agonists (adjuvants). ATPS-ELISpot was used to screen IFN- $\gamma$  secretion by exposing PBMCs to hemagglutinin alone or in combination with a TLR agonist. ATPS-ELISpot produced comparable results to conventional ELISpot, concentrating the vaccine reagents by 5-fold.

The specific conclusions relating to the original research objectives are as follows:

- i) A cost-effective single sandwich ATPS-ELISA was successfully developed and characterized. The optimal conditions to confine capture and detection antibodies in the ATPS-ELISA were: a volume of 20  $\mu\text{L}$  of 20% (w/w%) dextran solution containing capture antibodies or 10  $\mu\text{L}$  of the same solution containing detection antibodies covered by 100  $\mu\text{L}$  of 20% (w/w%) PEG solution. Both polymers were dissolved in PBS at room temperature.
  
- ii) A cost-effective ATPS-ELISpot was successfully developed and characterized. The optimal conditions to confine immune cells and vaccine reagents in the cost-effective ATPS-ELISpot were: a volume of 20  $\mu\text{L}$  of 10% (w/w%) BSA solution containing cells and reagents covered by 80  $\mu\text{L}$  of 7% (w/w%) PEG solution. Both polymers were dissolved in culture medium at room temperature.

## **7.2 NOVEL CONTRIBUTIONS TO SCIENCE**

This study was the first to characterize the unexplored system composed of PEG/PEO and BSA, to demonstrate long-term cell culture in ATPS, and to characterize immune cell growth in these polymers. In addition, it was the first to demonstrate that immune cell responses, such as cytokine secretion, can be accurately measured from an ATPS droplet microreactor. Furthermore, this study showed the successful development of a cost-effective platform for screening vaccine formulations that utilizes ATPS rather

than microdevice-based assay miniaturization, which may contribute to the development of new vaccines and other immunotherapies.

### 7.3 RECOMMENDATIONS FOR FUTURE WORK

- Different combinations of TLR agonists with hemagglutinin should be investigated. The results obtained from screening hemagglutinin combined with TLR agonists individually are promising; however, the immune response may be more robust when combining two or more TLR agonists in the same formulation.
- More in-depth investigation of the immune response should be performed to confirm if the cytokine (IFN- $\gamma$ ) is being secreted by B or T lymphocytes. It will be also important to obtain the donors' vaccine records in future studies if they can be made available.
- Assessment of other relevant proteins secreted by PBMCs, such as granzyme B, may provide a more direct analysis of antigen-specific cytotoxic T cell responses, and complement the results obtained by measuring IFN- $\gamma$  secretion<sup>413</sup>.
- Partitioning of the TLR agonists in the PEG-BSA system should be evaluated to confirm the hypothesis that they remain confined in the BSA phase. It will be also relevant to measure the antigen partitioning between the phases to verify that these biomolecules behave as expected in the PEG-BA system or other ATPSs that may be used to promote their partitioning.
- Once the most robust vaccine formulation is defined by ATPS-ELISpot, *in vivo* studies should be performed to measure specific antibody secretion to validate the *in vitro* method.

- Vaccine formulations screened by ATPS-ELISpot should be further investigated regarding antigen sparing upon combination of antigen with adjuvants.
- Eventually, the selected vaccine formulations should be evaluated through clinical trials to effectively confirm their efficacy, safety, and dose adjustment.

## BIBLIOGRAPHY

1. Hage, D. S. Immunoassays. *Anal. Chem.* **71**, 294–304 (1999).
2. Scopus - Document search results.
3. Novanet - Web of Science.
4. Immunoassay Market by Product & Service. Global Forecast to 2023: MarketsandMarkets.
5. Immunoassay Market Size, Share, Trends. Industry Report, 2019-2025.
6. Wheeler, M. J. Immunoassay techniques. *Methods Mol. Biol.* **324**, 1–23 (2006).
7. Andersen, P. L. & Vermette, P. Intracellular insulin quantification by cell-ELISA. *Exp. Cell Res.* (2016).
8. Montserrat, M. *et al.* Detection of peanut (*Arachis hypogaea*) allergens in processed foods by immunoassay: Influence of selected target protein and ELISA format applied. *Food Control* (2015).
9. Moreno, A. *et al.* Monoclonal antibody-based ELISA for detection of antibodies against H5 avian influenza viruses. *J. Virol. Methods* (2013).
10. Ambrosi, A., Airò, F. & Merkoçi, A. Enhanced gold nanoparticle based ELISA for a breast cancer biomarker. *Anal. Chem.* (2010).
11. Rissin, D. M. *et al.* Single-molecule enzyme-linked immunosorbent assay detects serum proteins at subfemtomolar concentrations. *Nat. Biotechnol.* **28**, 595–599 (2010).
12. Ettischer-Schmid, N. & Preyer, R. ELISPOT assays and their diagnostic potential in Lyme disease and Lyme neuroborreliosis. *Clin. Exp. Immunol.* **200**, 299–301 (2020).
13. Slota, M., Lim, J. B., Dang, Y. & Disis, M. L. ELISpot for measuring human immune responses to vaccines. *Expert Review of Vaccines* (2011).
14. Spiewak, R. *et al.* Allergic contact dermatitis to nickel: Modified in vitro test protocols for better detection of allergen-specific response. *Contact Dermatitis* (2007).
15. Lindemann, M., Böhmer, J., Zabel, M. & Grosse-Wilde, H. ELISpot: A new tool for the detection of nickel sensitization. *Clin. Exp. Allergy* (2003).
16. Mazer, M. B. *et al.* A Whole Blood Enzyme-Linked Immunospot Assay for Functional Immune Endotyping of Septic Patients. *J. Immunol.* (2021).
17. Thijsen, S. *et al.* Elevated nucleoprotein-induced interferon- $\gamma$  release in COVID-19 patients detected in a SARS-CoV-2 enzyme-linked immunosorbent spot assay. *Journal of Infection* (2020).



18. Faresjö, M. Enzyme Linked Immuno-Spot; a Useful Tool in the Search for Elusive Immune Markers in Common Pediatric Immunological Diseases. *Cells* (2012).
19. Boonyaratanakornkit, J. & Taylor, J. J. Techniques to Study Antigen-Specific B Cell Responses. *Frontiers in immunology* (2019).
20. Kalyuzhny, A. E. Chemistry and Biology of the ELISPOT Assay. in *Handbook of ELISPOT - Methods and Protocols* 15–32 (Humana Press Inc., 2005).
21. Möbs, C. & Schmidt, T. Research Techniques Made Simple: Monitoring of T-Cell Subsets using the ELISPOT Assay. *Journal of Investigative Dermatology* (2016).
22. Lin, C.-C., Wang, J.-H., Wu, H.-W. & Lee, G.-B. Microfluidic Immunoassays. *JALA J. Assoc. Lab. Autom.* **15**, 253–274 (2010).
23. Han, K. N., Li, C. A. & Seong, G. H. Microfluidic Chips for Immunoassays. *Annu. Rev. Anal. Chem.* **6**, 119–141 (2013).
24. Fan, R. *et al.* Integrated barcode chips for rapid, multiplexed analysis of proteins in microliter quantities of blood. *Nat. Biotechnol.* **26**, 1373–1378 (2008).
25. Baganizi, D. R. *et al.* A Simple Microfluidic Platform for Long-Term Analysis and Continuous Dual-Imaging Detection of T-Cell Secreted IFN- $\gamma$  and IL-2 on Antibody-Based Biochip. *Biosensors* **5**, 750–767 (2015).
26. Lin, Q. *et al.* Microfluidic Immunoassays for Sensitive and Simultaneous Detection of IgG/IgM/Antigen of SARS-CoV-2 within 15 min. *Anal. Chem.* (2020).
27. Li, H., Munzar, J. D., Ng, A. & Juncker, D. A versatile snap chip for high-density sub-nanoliter chip-to-chip reagent transfer. *Sci. Rep.* (2015).
28. Pla-Roca, M. *et al.* Antibody colocalization microarray: A scalable technology for multiplex protein analysis in complex samples. *Mol. Cell. Proteomics* (2012).
29. Li, H., Bergeron, S. & Juncker, D. Microarray-to-microarray transfer of reagents by snapping of two chips for cross-reactivity-free multiplex immunoassays. *Anal. Chem.* (2012).
30. Teixeira, A. G. *et al.* Emerging Biotechnology Applications of Aqueous Two-Phase Systems. *Adv. Healthc. Mater.* (2017).
31. Albertsson, P.-Å. *Partition of cell particles and macromolecules; distribution and fractionation of cells, mitochondria, chloroplasts, viruses, proteins, nucleic acids, and antigen-antibody complexes in aqueous polymer two-phase systems.* (Wiley-Interscience, 1971).
32. Asenjo, J. A. & Andrews, B. A. Aqueous two-phase systems for protein separation: A perspective. *Journal of Chromatography A* (2011).
33. Andrews, B. A. & Asenjo, J. A. Theoretical and experimental evaluation of hydrophobicity of proteins to predict their partitioning behavior in aqueous two phase systems: A review. *Separation Science and Technology* (2010).

34. Albertsson, P.-Å. *Partitioning in Aqueous Two-Phase System*. (Academic Press, 1985).
35. Zaslavsky, B. Y. *Aqueous two-phase partitioning: physical chemistry and bioanalytical applications*. (Marcel Dekker, 1995).
36. Zaslavsky, B. Y., Ferreira, L. A., Darling, A. L. & Uversky, V. N. The solvent side of proteinaceous membrane-less organelles in light of aqueous two-phase systems. *International Journal of Biological Macromolecules* (2018).
37. Andrews, B. A., Schmidt, A. S. & Asenjo, J. A. Correlation for the partition behavior of proteins in aqueous two-phase systems: Effect of surface hydrophobicity and charge. *Biotechnol. Bioeng.* (2005).
38. Asenjo, J. A. & Andrews, B. A. Aqueous two-phase systems for protein separation: A perspective. *Journal of Chromatography A* (2011).
39. Huang, Y. & Forciniti, D. Ethylene oxide and propylene oxide random copolymer/sodium chloride aqueous two-phase systems: Wetting and adsorption on dodecyl-agarose and polystyrene. *Biotechnol. Bioeng.* **77**, 786–795 (2002).
40. Zaslavsky, B. Y., Uversky, V. N. & Chait, A. Analytical applications of partitioning in aqueous two-phase systems: Exploring protein structural changes and protein-partner interactions in vitro and in vivo by solvent interaction analysis method. *Biochimica et Biophysica Acta - Proteins and Proteomics* (2016).
41. Rahimpour, F., Feyzi, F., Maghsoudi, S. & Hatti-Kaul, R. Purification of plasmid DNA with polymer-salt aqueous two-phase system: Optimization using response surface methodology. *Biotechnol. Bioeng.* (2006).
42. Kaul, A. The Phase Diagram. in *Aqueous Two-Phase Systems: Methods and Protocols, Methods in Biotechnology, vol. 11* (ed. Hatti-Kaul, R.) 11–21 (Humana Press, 2000).
43. Cabezas, H. Theory of phase formation in aqueous two-phase systems. in *Journal of Chromatography B: Biomedical Applications* (1996).
44. Franco, T. T., Andrews, A. T. & Asenjo, J. A. Use of chemically modified proteins to study the effect of a single protein property on partitioning in aqueous two-phase systems: Effect of surface hydrophobicity. *Biotechnol. Bioeng.* (1996).
45. Ahmad, A. L., Derek, C. J. C. & Zulkali, M. M. D. Optimization of thaumatin extraction by aqueous two-phase system (ATPS) using response surface methodology (RSM). *Sep. Purif. Technol.* (2008).
46. de Vos, A. M. *et al.* Three-dimensional structure of thaumatin I, an intensely sweet protein. *Proc. Natl. Acad. Sci. U. S. A.* (1985).
47. Huddleston, J. *et al.* The molecular basis of partitioning in aqueous two-phase systems. *Trends Biotechnol.* (1991).

48. Bolognese, B., Nerli, B. & Picó, G. Application of the aqueous two-phase systems of ethylene and propylene oxide copolymer-maltodextrin for protein purification. *J. Chromatogr. B Anal. Technol. Biomed. Life Sci.* (2005).
49. Grilo, A. L., Aires-Barros, M. R. & Azevedo, A. M. Partitioning in Aqueous Two-Phase Systems: Fundamentals, Applications and Trends. *Sep. Purif. Rev.* (2016).
50. Benavides, J. & Rito-Palomares, M. Practical experiences from the development of aqueous two-phase processes for the recovery of high value biological products. *Journal of Chemical Technology and Biotechnology* (2008).
51. Ferreira, L., Madeira, P. P., Mikheeva, L., Uversky, V. N. & Zaslavsky, B. Effect of salt additives on protein partition in polyethylene glycol-sodium sulfate aqueous two-phase systems. *Biochim. Biophys. Acta - Proteins Proteomics* (2013).
52. Ferreira, L. A. *et al.* Role of solvent properties of aqueous media in macromolecular crowding effects. *J. Biomol. Struct. Dyn.* (2016).
53. Ferreira, L. A., Wu, Z., Kurgan, L., Uversky, V. N. & Zaslavsky, B. Y. How to manipulate partition behavior of proteins in aqueous two-phase systems: Effect of trimethylamine N-oxide (TMAO). *Fluid Phase Equilib.* **449**, 217–224 (2017).
54. Liu, Y., Lipowsky, R. & Dimova, R. Concentration dependence of the interfacial tension for aqueous two-phase polymer solutions of dextran and polyethylene glycol. *Langmuir* (2012).
55. MacE, C. R. *et al.* Aqueous multiphase systems of polymers and surfactants provide self-assembling step-gradients in density. *J. Am. Chem. Soc.* (2012).
56. Asenjo, J. A., Mistry, S. L., Andrews, B. A. & Merchuk, J. C. Phase separation rates of aqueous two-phase systems: Correlation with system properties. *Biotechnol. Bioeng.* (2002).
57. Sahasrabudhe, S. N., Rodriguez-Martinez, V., O'Meara, M. & Farkas, B. E. Density, viscosity, and surface tension of five vegetable oils at elevated temperatures: Measurement and modeling. *Int. J. Food Prop.* (2017).
58. Bamberger, S., Seaman, G. V. F., Sharp, K. A. & Brooks, D. E. The effects of salts on the interfacial tension of aqueous dextran poly(ethylene glycol) phase systems. *J. Colloid Interface Sci.* **99**, 194–200 (1984).
59. Forciniti, D., Hall, C. K. & Kula, M. R. Interfacial tension of polyethyleneglycol-dextran-water systems: influence of temperature and polymer molecular weight. *J. Biotechnol.* **16**, 279–296 (1990).
60. de Oliveira, C. C., Coimbra, J. S. dos R., Zuniga, A. D. G., Martins, J. P. & Siqueira, A. M. de O. Interfacial Tension of Aqueous Two-Phase Systems Containing Poly(ethylene glycol) and Potassium Phosphate. *J. Chem. Eng. Data* **57**, 1648–1652 (2012).

61. Ruiz-Ruiz, F., Benavides, J., Aguilar, O. & Rito-Palomares, M. Aqueous two-phase affinity partitioning systems: Current applications and trends. *Journal of Chromatography A* (2012).
62. Zaslavsky, B. Y. Bioanalytical Applications of Partitioning in Aqueous Polymer Two-Phase Systems. *Anal. Chem.* (1992).
63. Azevedo, A. M. *et al.* Affinity-enhanced purification of human antibodies by aqueous two-phase extraction. *Sep. Purif. Technol.* (2009).
64. Rosa, P. A. J. *et al.* Affinity partitioning of human antibodies in aqueous two-phase systems. *J. Chromatogr. A* (2007).
65. Andrews, B. A., Head, D. M., Dunthorne, P. & Asenjo, J. A. PEG activation and ligand binding for the affinity partitioning of proteins in aqueous two-phase systems. *Biotechnol. Tech.* (1990).
66. Barinaga-Rementería Ramírez, I., Mebrahtu, S. & Jergil, B. Affinity partitioning for membrane purification exploiting the biotin-NeutrAvidin interaction - Model study of mixed liposomes and membranes. *J. Chromatogr. A* (2002).
67. Gavasane, M. R. & Gaikar, V. G. Aqueous two-phase affinity partitioning of penicillin acylase from *E. Coli* in presence of PEG-derivatives. *Enzyme Microb. Technol.* (2003).
68. Cabral, J. M. S. Cell Partitioning in Aqueous Two-Phase Polymer Systems. in *Cell Separation. Advances in Biochemical Engineering/Biotechnology.* (ed. Kumar, A., Galaev I. Y., Mattiasson, B.) (Springer Berlin Heidelberg, 2007).
69. Yamada, M., Kasim, V., Nakashima, M., Eda Hiro, J. & Seki, M. Continuous cell partitioning using an aqueous two-phase flow system in microfluidic devices. *Biotechnol. Bioeng.* (2004).
70. SooHoo, J. R. & Walker, G. M. Microfluidic aqueous two phase system for leukocyte concentration from whole blood. *Biomed. Microdevices* (2009).
71. Tsukamoto, M. *et al.* Cell separation by an aqueous two-phase system in a microfluidic device. *Analyst* (2009).
72. Frampton, J. P., Lai, D., Sriram, H. & Takayama, S. Precisely targeted delivery of cells and biomolecules within microchannels using aqueous two-phase systems. *Biomed. Microdevices* (2011).
73. Tavana, H. *et al.* Nanolitre liquid patterning in aqueous environments for spatially defined reagent delivery to mammalian cells. *Nat. Mater.* (2009).
74. Abbasi, N., Navi, M. & Tsai, S. S. H. Microfluidic Generation of Particle-Stabilized Water-in-Water Emulsions. *Langmuir* (2018).
75. Watanabe, T., Motohiro, I. & Ono, T. Microfluidic Formation of Hydrogel Microcapsules with a Single Aqueous Core by Spontaneous Cross-Linking in Aqueous Two-Phase System Droplets. *Langmuir* (2019).

76. Albertsson, P.-Å. History of Aqueous Polymer Two-Phase Partition. in *Partitioning in Aqueous Two-Phase System* (ed. Walter, H.) 1–10 (Academic Press, 1985).
77. Mace, C. R. *et al.* Aqueous multiphase systems of polymers and surfactants provide self-assembling step-gradients in density. *J. Am. Chem. Soc.* **134**, 9094–9097 (2012).
78. Iqbal, M. *et al.* Aqueous two-phase system (ATPS): an overview and advances in its applications. *Biol. Proced. Online* **18**, 18 (2016).
79. Esquena, J. Water-in-water (W/W) emulsions. *Current Opinion in Colloid and Interface Science* **25**, 109–119 (2016).
80. Albertsson, P.-Å. Chromatography and partition of cells and cell fragments. *Nature* **177**, 771–774 (1956).
81. Albertsson, P.-Å. Partition of proteins in liquid polymer-polymer two-phase systems. *Nature* **182**, 709–711 (1958).
82. Frampton, J. P., White, J. B., Abraham, A. T. & Takayama, S. Cell co-culture patterning using aqueous two-phase systems. *J. Vis. Exp.* **73**, 50304 (2013).
83. Muendges, J., Zalesko, A., Górak, A. & Zeiner, T. Multistage aqueous two-phase extraction of a monoclonal antibody from cell supernatant. *Biotechnol. Prog.* **31**, 925–936 (2015).
84. Ferreira, A. M., Faustino, V. F., Mondal, D., Coutinho, J. A. & Freire, M. G. Improving the extraction and purification of immunoglobulin G by the use of ionic liquids as adjuvants in aqueous biphasic systems. *J. Biotechnol.* **236**, 166–175 (2016).
85. de Albuquerque Wanderley, M. C. *et al.* Purification and characterization of a collagenase from *Penicillium* sp. UCP 1286 by polyethylene glycol-phosphate aqueous two-phase system. *Protein Expr. Purif.* **133**, 8–14 (2017).
86. da Silva, N. R. *et al.* Analysis of partitioning of organic compounds and proteins in aqueous polyethylene glycol-sodium sulfate aqueous two-phase systems in terms of solute-solvent interactions. *J. Chromatogr. A* **1415**, 1–10 (2015).
87. Jacinto, M. J. *et al.* Optimization and miniaturization of aqueous two phase systems for the purification of recombinant human immunodeficiency virus-like particles from a CHO cell supernatant. *Sep. Purif. Technol.* (2015).
88. Ladd Effio, C. *et al.* Downstream processing of virus-like particles: Single-stage and multi-stage aqueous two-phase extraction. *J. Chromatogr. A* **1383**, 35–46 (2015).
89. Pereira, J. F. B., Santos, V. C., Johansson, H.-O., Teixeira, J. A. C. & Pessoa, A. A stable liquid–liquid extraction system for clavulanic acid using polymer-based aqueous two-phase systems. *Sep. Purif. Technol.* **98**, 441–450 (2012).

90. Marques, C. F. C. *et al.* Aqueous biphasic systems composed of ionic liquids and sodium carbonate as enhanced routes for the extraction of tetracycline. *Biotechnol. Prog.* **29**, 645–654 (2013).
91. Pereira, J. F. B. *et al.* Extraction of tetracycline from fermentation broth using aqueous two-phase systems composed of polyethylene glycol and cholinium-based salts. *Process Biochem.* **48**, 716–722 (2013).
92. Wiendahl, M., Oelmeier, S. A., Dismer, F. & Hubbuch, J. High-throughput screening-based selection and scale-up of aqueous two-phase systems for pDNA purification. *J. Sep. Sci.* **35**, 3197–3207 (2012).
93. Johansson, H.-O. *et al.* Plasmid DNA partitioning and separation using poly(ethylene glycol)/poly(acrylate)/salt aqueous two-phase systems. *J. Chromatogr. A* **1233**, 30–5 (2012).
94. Matos, T., Johansson, H.-O., Queiroz, J. A. & Bulow, L. Isolation of PCR DNA fragments using aqueous two-phase systems. *Sep. Purif. Technol.* **122**, 144–148 (2014).
95. Cabral, J. M. S. Cell partitioning in aqueous two-phase polymer systems. in *Advances in Biochemical Engineering/Biotechnology* **106**, 151–171 (2007).
96. Zimmermann, S. *et al.* High-throughput downstream process development for cell-based products using aqueous two-phase systems. *J. Chromatogr. A* **1464**, 1–11 (2016).
97. Shin, H. *et al.* High-yield isolation of extracellular vesicles using aqueous two-phase system. *Sci. Rep.* **5**, 13103 (2015).
98. Kim, J., Shin, H., Kim, J., Kim, J. & Park, J. Isolation of high-purity extracellular vesicles by extracting proteins using aqueous two-phase system. *PLoS One* (2015).
99. He, C., Li, S., Liu, H., Li, K. & Liu, F. Extraction of testosterone and epitestosterone in human urine using aqueous two-phase systems of ionic liquid and salt. *J. Chromatogr. A* **1082**, 143–149 (2005).
100. Li, N. *et al.* Determination of steroid hormones in milk using aqueous two-phase extraction coupled to liquid chromatography. *Anal. Methods* **7**, 2514–2522 (2015).
101. Ruthven, M., Ko, K. R., Agarwal, R., Frampton, J. P. & Takayama, S. Microscopic evaluation of aqueous two-phase system emulsion characteristics enables rapid determination of critical polymer concentrations for solution micropatterning. *Analyst* **142**, 1938–1945 (2017).
102. Frampton, J. P. *et al.* Aqueous two-phase system patterning of detection antibody solutions for cross-reaction-free multiplex ELISA. *Sci. Rep.* **4**, 4878 (2014).
103. Hardt, S. & Hahn, T. Microfluidics with aqueous two-phase systems. *Lab Chip* **12**, 434–42 (2012).

104. Keating, C. D. Aqueous phase separation as a possible route to compartmentalization of biological molecules. *Acc. Chem. Res.* **45**, 2114–2124 (2012).
105. Hatti-Kaul, R. Aqueous Two-Phase Systems: A General Overview. in *Aqueous Two-Phase Systems: Methods and Protocols, Methods in Biotechnology, vol. 11* (ed. Hatti-Kaul, R.) 1–10 (Humana Press, 2000).
106. Silva, D. F. C. *et al.* Determination of aqueous two phase system binodal curves using a microfluidic device. *J. Chromatogr. A* **1370**, 115–120 (2014).
107. Kojima, T. & Takayama, S. Microscale determination of aqueous two phase system binodals by droplet dehydration in oil. *Anal. Chem.* **85**, 5213–5218 (2013).
108. Vazquez-Villegas, P. *et al.* A microdevice assisted approach for the preparation, characterization and selection of continuous aqueous two-phase systems: from micro to bench-scale. *Lab Chip* **16**, 2662–2672 (2016).
109. Bamberger, S., Brooks, D., Sharp, K., Van Alstine, J. & Webber, T. Preparation of Phase Systems and Measurement of their Physicochemical Properties. in *Partitioning in Aqueous Two-Phase System* (ed. Harry Walter) 85–130 (Academic Press, 1985).
110. Lesher-Perez, S. C., Frampton, J. P. & Takayama, S. Microfluidic systems: A new toolbox for pluripotent stem cells. *Biotechnol. J.* **8**, 180–191 (2013).
111. Brooks, D. & Norris-Jones, R. Measurement of Some Physical Properties of Aqueous Two-Phase Systems. in *Aqueous Two-Phase Systems: Methods and Protocols, Methods in Biotechnology, vol. 11* (ed. Hatti-Kaul, R.) 35–45 (Humana Press, 2000).
112. Bloxham, W. H., Hennek, J. W., Kumar, A. A. & Whitesides, G. M. Fractionating Polymer Microspheres as Highly Accurate Density Standards. *Anal. Chem.* **87**, 7485–7491 (2015).
113. Almeida, M. R. *et al.* Ionic liquids as additives to enhance the extraction of antioxidants in aqueous two-phase systems. *Sep. Purif. Technol.* **128**, 1–10 (2014).
114. Kumar, A. A., Walz, J. A., Gonidec, M., Mace, C. R. & Whitesides, G. M. Combining Step Gradients and Linear Gradients in Density. *Anal. Chem.* **87**, 6158–6164 (2015).
115. Akbulut, O. *et al.* Separation of nanoparticles in aqueous multiphase systems through centrifugation. *Nano Lett.* **12**, 4060–4064 (2012).
116. Zijlstra, G. M., De Gooijer, C. D., Van Der Pol, L. A. & Tramper, J. Design of aqueous two-phase systems supporting animal cell growth: A first step toward extractive bioconversions. *Enzyme Microb. Technol.* **19**, 2–8 (1996).

117. Aumiller, W. M. & Keating, C. D. Experimental models for dynamic compartmentalization of biomolecules in liquid organelles: Reversible formation and partitioning in aqueous biphasic systems. *Advances in Colloid and Interface Science* **239**, 75–87 (2017).
118. Andes-Koback, M. & Keating, C. D. Complete budding and asymmetric division of primitive model cells to produce daughter vesicles with different interior and membrane compositions. *J. Am. Chem. Soc.* **133**, 9545–9555 (2011).
119. Antov, M. G., Peričin, D. M. & Trbojević, B. I. The effect of sulphates on partitioning of pectinases in aqueous two-phase systems. *Acta Period. Technol.* 179–186 (2004).
120. Johansson, H.-O., Feitosa, E. & Junior, A. P. Phase Diagrams of the Aqueous Two-Phase Systems of Poly(ethylene glycol)/Sodium Polyacrylate/Salts. *Polymers (Basel)*. **3**, 587–601 (2011).
121. Berggren, K., Wolf, A., Asenjo, J. A., Andrews, B. A. & Tjerneld, F. The surface exposed amino acid residues of monomeric proteins determine the partitioning in aqueous two-phase systems. *Biochim. Biophys. Acta - Protein Struct. Mol. Enzymol.* **1596**, 253–268 (2002).
122. Johansson, H. O., Karlström, G., Tjerneld, F. & Haynes, C. a. Driving forces for phase separation and partitioning in aqueous two-phase systems. *J. Chromatogr. B. Biomed. Sci. Appl.* **711**, 3–17 (1998).
123. Suga, K., Tomita, H., Tanaka, S. & Umakoshi, H. Hydrophobic properties of tRNA with varied conformations evaluated by an aqueous two-phase system. *Int. J. Biol. Sci.* **8**, 1188–1196 (2012).
124. Umakoshi, H. *et al.* Characterization of green fluorescent protein using aqueous two-phase systems. *Solv. Extr. Res. Dev. Japan* **16**, 145–150 (2009).
125. Umakoshi, H., Yoshimoto, N., Yoshimoto, M., Shimanouchi, T. & Kuboi, R. Characterization of surface properties of microbial transglutaminase using aqueous two-phase partitioning method. *Solv. Extr. Res. Dev. Japan* **15**, 111–115 (2008).
126. Ryden, J. & Albertsson, P.-Å. Interfacial tension of dextran—polyethylene glycol—water two—phase systems. *J. Colloid Interface Sci.* **37**, 219–222 (1971).
127. de Oliveira, C. C., Coimbra, J. S. dos R., Zuniga, A. D. G., Martins, J. P. & Siqueira, A. M. de O. Interfacial tension of aqueous two-phase systems containing poly (ethylene glycol) and potassium phosphate. *J. Chem. Eng. Data* **57**, 1648–1652 (2012).
128. Olivera-Nappa, A., Lagomarsino, G., Andrews, B. A. & Asenjo, J. A. Effect of electrostatic energy on partitioning of proteins in aqueous two-phase systems. in *Journal of Chromatography B: Analytical Technologies in the Biomedical and Life Sciences* **807**, 81–86 (2004).



129. Barbosa, H., Hine, A. V., Brocchini, S., Slater, N. K. H. & Marcos, J. C. Affinity partitioning of plasmid DNA with a zinc finger protein. *J. Chromatogr. A* **1206**, 105–112 (2008).
130. Schmidt, A. S., Ventom, A. M. & Asenjo, J. A. Partitioning and purification of  $\alpha$ -amylase in aqueous two-phase systems. *Enzyme Microb. Technol.* **16**, 131–142 (1994).
131. Asenjo, J. A. & Andrews, B. A. Aqueous two-phase systems for protein separation: phase separation and applications. *J. Chromatogr. A* **1238**, 1–10 (2012).
132. Molino, J. V. D., Viana Marques, D. de A., Júnior, A. P., Mazzola, P. G. & Gatti, M. S. V. Different types of aqueous two-phase systems for biomolecule and bioparticle extraction and purification. *Biotechnol. Prog.* **29**, 1343–1353 (2013).
133. SooHoo, J. R. & Walker, G. M. Microfluidic aqueous two phase system for leukocyte concentration from whole blood. *Biomed. Microdevices*, **11**, 323-9 (2009).
134. Tavana, H. *et al.* Nanoliter Liquid Patterning in Aqueous Environments for Spatially-Defined Reagent Delivery to Mammalian Cells. *Nat. Mater.* **8**, 736–741 (2009).
135. Tavana, H., Mosadegh, B. & Takayama, S. Polymeric Aqueous Biphasic Systems for Non-Contact Cell Printing on Cells: Engineering Heterocellular Embryonic Stem Cell Niches. *Adv. Mater.* **22**, 2628–2631 (2010).
136. Jacinto, M. J., Azevedo, A. M., Aires-Barros, M. R., Archinti, M. & Marzábal, P. Extraction of Zera® fusion proteins in aqueous two-phase systems. in *Bioengineering (ENBENG), 2015 IEEE 4th Portuguese Meeting on* 1–6 (IEEE, 2015).
137. Porfiri, M. C., Picó, G., Romanini, D. & Farruggia, B. *Aspergillus oryzae* alpha-amylase partition in potassium phosphate-polyethylene glycol aqueous two-phase systems. *Int. J. Biol. Macromol.*, **49**, 7-13 (2011).
138. Reddy, N. S., Nimmagadda, A. & Rao, K. R. S. S. An overview of the microbial  $\alpha$ -amylase family. *African J. Biotechnol.* **2**, 645–648 (2003).
139. Kammoun, R., Chouayekh, H., Abid, H., Naili, B. & Bejar, S. Purification of CBS 819.72  $\alpha$ -amylase by aqueous two-phase systems: modelling using response surface methodology. *Biochem. Eng. J.* **46**, 306–312 (2009).
140. Oelmeier, S. A., Ladd Effio, C. & Hubbuch, J. High throughput screening based selection of phases for aqueous two-phase system-centrifugal partitioning chromatography of monoclonal antibodies. *J. Chromatogr. A* **1252**, 104–114 (2012).
141. Oelmeier, S. A., Ladd-Effio, C. & Hubbuch, J. Alternative separation steps for monoclonal antibody purification: Combination of centrifugal partitioning chromatography and precipitation. *J. Chromatogr. A* **1319**, 118–126 (2013).

142. Azevedo, A. M., Rosa, P. A. J., Ferreira, I. F. & Aires-Barros, M. R. Integrated process for the purification of antibodies combining aqueous two-phase extraction, hydrophobic interaction chromatography and size-exclusion chromatography. *J. Chromatogr. A* **1213**, 154–161 (2008).
143. Azevedo, A. M. *et al.* Downstream processing of human antibodies integrating an extraction capture step and cation exchange chromatography. *J. Chromatogr. B Anal. Technol. Biomed. Life Sci.* **877**, 50–58 (2009).
144. Silva, D. F. C. *et al.* Design of a microfluidic platform for monoclonal antibody extraction using an aqueous two-phase system. *J. Chromatogr. A* **1249**, 1–7 (2012).
145. Langer, R. & Vacanti, J. P. Tissue engineering. *Science (80-. )*. **260**, 920–926 (1993).
146. Falconnet, D., Csucs, G., Grandin, H. M. & Textor, M. Surface engineering approaches to micropattern surfaces for cell-based assays. *Biomaterials* **27**, 3044–3063 (2006).
147. Takayama, S. *et al.* Patterning Cells and Their Environments Using Multiple Laminar Fluid Flows in Capillary Networks. *Proc. Natl. Acad. Sci. U. S. A.* **96**, 5545–5548 (1999).
148. Wright, D., Rajalingam, B., Selvarasah, S., Dokmeci, M. R. & Khademhosseini, A. Generation of static and dynamic patterned co-cultures using microfabricated parylene-C stencils. *Lab Chip* **7**, 1272–1279 (2007).
149. Ringeisen, B. R., Othon, C. M., Barron, J. A., Young, D. & Spargo, B. J. Jet-Based Methods to Print Living Cells. *Biotechnology* **1**, 930–948 (2006).
150. Koch, L. *et al.* Skin Tissue Generation by Laser Cell Printing. *Biotechnol. Bioeng.* **109**, 1855–1863 (2012).
151. Albertsson, P. A. k. *Partition of cell particles and macromolecules: separation and purification of biomolecules, cell organelles, Membranes, and cells in aqueous polymer two-phase systems and their use in biochemical analysis and biotechnology.* (Wiley, 1986).
152. Tavana, H. & Takayama, S. Aqueous Biphasic Microprinting Approach to Tissue Engineering. *Biomicrofluidics* **5**, 13404 (2011).
153. Agarwal, R., Ko, K. R., Gratzner, P. F. & Frampton, J. P. Biopatterning of Keratinocytes in Aqueous Two-Phase Systems as a Potential Tool for Skin Tissue Engineering. *MRS Adv.* **2**, 2443–2449 (2017).
154. Frampton, J. P. *et al.* Aqueous Two-Phase System Patterning of Microbubbles: Localized Induction of Apoptosis in Sonoporated Cells. *Adv. Funct. Mater.* **23**, 3420–3431 (2013).

155. Tavana, H. *et al.* Rehydration of polymeric, aqueous, biphasic system facilitates high throughput cell exclusion patterning for cell migration studies. *Adv. Funct. Mater.*, **9**, 2920-2926 (2011).
156. Fang, Y. *et al.* Rapid Generation of Multiplexed Cell Cocultures Using Acoustic Droplet Ejection Followed by Aqueous Two-Phase Exclusion Patterning. *Tissue Eng. Part C. Methods* **18**, 647–657 (2012).
157. Xu, F. *et al.* Embryonic stem cell bioprinting for uniform and controlled size embryoid body formation. *Biomicrofluidics* **5**, 22207 (2011).
158. Khademhosseini, A. *et al.* Co-culture of human embryonic stem cells with murine embryonic fibroblasts on microwell-patterned substrates. *Biomaterials* **27**, 5968–5977 (2006).
159. Tan, J. L., Liu, W., Nelson, C. M., Raghavan, S. & Chen, C. S. Simple approach to micropattern cells on common culture substrates by tuning substrate wettability. *Tissue Eng.* **10**, 865–872 (2004).
160. Khademhosseini, A. *et al.* Layer-by-layer deposition of hyaluronic acid and poly-L-lysine for patterned cell co-cultures. *Biomaterials* **25**, 3583–3592 (2004).
161. Tavana, H., Mosadegh, B., Zamankhan, P., Grotberg, J. B. & Takayama, S. Microprinted Feeder Cells Guide Embryonic Stem Cell Fate. *Biotechnol. Bioeng.* **108**, 2509–2516 (2011).
162. Kim, J., Hegde, M. & Jayaraman, A. Co-culture of epithelial cells and bacteria for investigating host-pathogen interactions. *Lab Chip* **10**, 43–50 (2010).
163. Pawelek, J. M., Low, K. B. & Bermudes, D. Tumor-targeted Salmonella as a Novel Anticancer Vector. *Cancer Res.* **57**, 4537–4544 (1997).
164. Wang, X. *et al.* Impact of biofilm matrix components on interaction of commensal *Escherichia coli* with the gastrointestinal cell line HT-29. *Cell. Mol. Life Sci. C.* **63**, 2352–2363 (2006).
165. Boudeau, J., Glasser, A.-L., Masseret, E., Joly, B. & Darfeuille-Michaud, A. Invasive Ability of an *Escherichia coli* Strain Isolated from the Ileal Mucosa of a Patient with Crohn's Disease. *Infect. Immun.* **67**, 4499–4509 (1999).
166. Yaguchi, T. *et al.* Aqueous Two-Phase System-Derived Biofilms for Bacterial Interaction Studies. *Biomacromolecules* **13**, 2655–2661 (2012).
167. Crouzet, L., and Rigottier-Gois, L. and Serror, P. Potential use of probiotic and commensal bacteria as non-antibiotic strategies against vancomycin-resistant enterococci. *FEMS Microbiol. Lett.* **362**, fnv012 (2015).
168. Zipperer, A. *et al.* Human commensals producing a novel antibiotic impair pathogen colonization. *Nature* **535**, 511–516 (2016).

169. Reynolds, L. A. *et al.* Commensal-pathogen interactions in the intestinal tract: Lactobacilli promote infection with, and are promoted by, helminth parasites. *Gut Microbes* **5**, 522–532 (2014).
170. Dwidar, M., Leung, B. M., Yaguchi, T., Takayama, S. & Mitchell, R. J. Patterning Bacterial Communities on Epithelial Cells. *PLoS One* **8**, e67165 (2013).
171. Shatzkes, K., Connell, N. D., Kadouri, D. E. Predatory bacteria: a new therapeutic approach for a post-antibiotic era. *Future Microbiol.* **12**, 469–472 (2017).
172. Johnke, Julia., Boenigk, Jens., Harms, Hauke., Chatzinotas, A. Killing the killer: predation between protists and predatory bacteria. *FEMS Microbiol. Lett.* **364**, fnx089 (2017).
173. Shamir, E. R. & Ewald, A. J. Three-dimensional organotypic culture: experimental models of mammalian biology and disease. *Nat. Rev. Mol. Cell Biol.* **15**, 647–664 (2014).
174. Mehta, G., Hsiao, A. Y., Ingram, M., Luker, G. D. & Takayama, S. Opportunities and challenges for use of tumor spheroids as models to test drug delivery and efficacy. *J. Control. Release* **164**, 192–204 (2012).
175. Shahi Thakuri, P., Ham, S. L., Luker, G. D. & Tavana, H. Multiparametric analysis of oncology drug screening with aqueous two-phase tumor spheroids. *Mol. Pharm.* **13**, 3724–3735 (2016).
176. Foty, R. A simple hanging drop cell culture protocol for generation of 3D spheroids. *J. Vis. Exp.* **20**, 4–7 (2011).
177. Tung, Y.-C. *et al.* High-throughput 3D spheroid culture and drug testing using a 384 hanging drop array. *Analyst* **136**, 473–478 (2011).
178. Fok, E. Y. L. & Zandstra, P. W. Shear-Controlled Single-Step Mouse Embryonic Stem Cell Expansion and Embryoid Body–Based Differentiation. *Stem Cells* **23**, 1333–1342 (2005).
179. Sargent, C. Y. *et al.* Hydrodynamic modulation of embryonic stem cell differentiation by rotary orbital suspension culture. *Biotechnol. Bioeng.* **105**, 611–626 (2010).
180. Eiraku, M. *et al.* Self-Organized Formation of Polarized Cortical Tissues from ESCs and Its Active Manipulation by Extrinsic??Signals. *Cell Stem Cell* **3**, 519–532 (2008).
181. Lemmo, S., Atefi, E., Luker, G. D. & Tavana, H. Optimization of aqueous biphasic tumor spheroid microtechnology for anti-cancer drug testing in 3D culture. *Cell. Mol. Bioeng.* **7**, 344–354 (2014).
182. Atefi, E., Lemmo, S., Fyffe, D., Luker, G. D. & Tavana, H. High throughput, polymeric aqueous two-phase printing of tumor spheroids. *Adv. Funct. Mater.* **24**, 6509–6515 (2014).

183. Ham, S. L., Atefi, E., Fyffe, D. & Tavana, H. Robotic Production of Cancer Cell Spheroids with an Aqueous Two-phase System for Drug Testing. *J. Vis. Exp.* **23**, 1–9 (2015).
184. Han, C., Takayama, S. & Park, J. Formation and manipulation of cell spheroids using a density adjusted PEG / DEX aqueous two phase system. *Sci. Rep.* **5**, 11891 (2015).
185. Frampton, J. P. *et al.* Rapid Self-Assembly of Macroscale Tissue Constructs at Biphasic Aqueous Interfaces. *Adv. Funct. Mater.* **25**, 1694–1699 (2015).
186. Atefi, E., Joshi, R., Mann, J. A. & Tavana, H. Interfacial Tension Effect on Cell Partition in Aqueous Two-Phase Systems. *ACS Appl. Mater. Interfaces* **7**, 21305–21314 (2015).
187. Bell, E., Ivarsson, B. & Merrill, C. Production of a tissue-like structure by contraction of collagen lattices by human fibroblasts of different proliferative potential in vitro. *Proc. Natl. Acad. Sci. U. S. A.* **76**, 1274–1278 (1979).
188. Sakota, Y., Ozawa, Y., Yamashita, H., Tanaka, H. & Inagaki, N. Collagen gel contraction assay using human bronchial smooth muscle cells and its application for evaluation of inhibitory effect of formoterol. *Biol. Pharm. Bull.* **37**, 1014–1020 (2014).
189. Moraes, C., Simon, A. B., Putnam, A. J. & Takayama, S. Aqueous two-phase printing of cell-containing contractile collagen microgels. *Biomaterials* **34**, 9623–9631 (2013).
190. Leung, B. M. *et al.* Microscale 3D Collagen Cell Culture Assays in Conventional Flat-Bottom 384-Well Plates. *J. Lab. Autom.* **20**, 138–145 (2015).
191. Ko, K. R., Agarwal, R. & Frampton, J. P. High-Throughput 3D Neural Cell Culture Analysis Facilitated by Aqueous Two-Phase Systems. *MRS Adv.* **2**, 2435–2441 (2017).
192. Wheeler, M. J. Immunoassay Techniques. in *Hormone Assays in Biological Fluids* (ed. Wheeler, M. J.) **1065**, 7–25 (2013).
193. Wild, D. Immunoassay Configurations. in *The immunoassay handbook: theory and applications of ligand binding, ELISA and related techniques* 27–242 (Elsevier, 2013).
194. Chen, Y. *et al.* Development of an enzyme-linked immunosorbent assay for detection of CDCP1 shed from the cell surface and present in colorectal cancer serum specimens. *J. Pharm. Biomed. Anal.* **139**, 65–72 (2017).
195. Sato, S. *et al.* Clinical utility of an enzyme-linked immunosorbent assay for detecting anti-melanoma differentiation-associated gene 5 autoantibodies. *PLoS One* **11**, e0154285 (2016).

196. Malíčková, K. *et al.* Serum trough infliximab levels: a comparison of three different immunoassays for the monitoring of CT-P13 (infliximab) treatment in patients with inflammatory bowel disease. *Biologicals* **44**, 33–36 (2016).
197. Frampton, J. P. Liquid-in-liquid antibody confinement provides new possibilities for multiplexed diagnostics. *Expert Rev. Mol. Diagn.* **15**, 445–447 (2015).
198. Beaudet, L. *et al.* AlphaLISA immunoassays: the no-wash alternative to ELISAs for research and drug discovery. *Nat. Methods*, **5**, an8–an9 (2008).
199. Simon, A. B. *et al.* Aqueous two-phase systems enable multiplexing of homogeneous immunoassays. *TECHNOLOGY*, **2**, 176–184 (2014).
200. Eiden, L., Yamanishi, C., Takayama, S. & Dishinger, J. F. Aqueous two-phase system rehydration of antibody-polymer microarrays enables convenient compartmentalized multiplex immunoassays. *Anal. Chem.*, **88**, 11328–11334 (2016).
201. Mosley, G. L. *et al.* Improved lateral-flow immunoassays for chlamydia and immunoglobulin M by sequential rehydration of two-phase system components within a paper-based diagnostic. *Microchim. Acta*, **184**, 4055–4064 (2017).
202. Koczula, K. M. & Gallotta, A. Lateral flow assays. *Essays Biochem.*, **60**, 111–120 (2016).
203. Land, J. A., Van Bergen, J. E. A. M., Morré, S. A. & Postma, M. J. Epidemiology of Chlamydia trachomatis infection in women and the cost-effectiveness of screening. *Hum. Reprod. Update* **16**, 189–204 (2010).
204. Mashayekhi, F., Le, A. M., Nafisi, P. M., Wu, B. M. & Kamei, D. T. Enhancing the lateral-flow immunoassay for detection of proteins using an aqueous two-phase micellar system. *Anal. Bioanal. Chem.* **404**, 2057–2066 (2012).
205. Chiu, R. Y. T., Thach, A. V, Wu, C. M., Wu, B. M. & Kamei, D. T. An aqueous two-phase system for the concentration and extraction of proteins from the Interface for detection using the lateral-flow immunoassay. *PLoS One* **10**, e0142654 (2015).
206. Jue, E., Yamanishi, C. D., Chiu, R. Y. T., Wu, B. M. & Kamei, D. T. Using an aqueous two-phase polymer-salt system to rapidly concentrate viruses for improving the detection limit of the lateral-flow immunoassay. *Biotechnol. Bioeng.* **111**, 2499–2507 (2014).
207. Mashayekhi, F. *et al.* Enhancing the lateral-flow immunoassay for viral detection using an aqueous two-phase micellar system. *Anal. Bioanal. Chem.* **398**, 2955–2961 (2010).
208. Anfossi, L., Baggiani, C., Giovannoli, C., D’Arco, G. & Giraudi, G. Lateral-flow immunoassays for mycotoxins and phycotoxins: a review. *Anal. Bioanal. Chem.* **405**, 467–480 (2013).

209. Song, S. *et al.* Multiplex lateral flow immunoassay for mycotoxin determination. *Anal. Chem.* **86**, 4995–5001 (2014).
210. Soares, R. R. G. *et al.* A simple method for point-of-need extraction, concentration and rapid multi-mycotoxin immunodetection in feeds using aqueous two-phase systems. *J. Chromatogr. A* **1511**, 15–24 (2017).
211. Stovsky, M. *et al.* Prostate-specific antigen/solvent interaction analysis: a preliminary evaluation of a new assay concept for detecting prostate cancer using urinary samples. *Urology* **78**, 601–605 (2011).
212. Klein, E. A. *et al.* The single-parameter, structure-based IsoPSA assay demonstrates improved diagnostic accuracy for detection of any prostate cancer and high-grade prostate cancer compared to a concentration-based assay of total prostate-specific antigen: a preliminary repo. *Eur. Urol.* (2017).
213. Soares, R. R. G. *et al.* Miniaturization of aqueous two-phase extraction for biological applications: From micro-tubes to microchannels. *Biotechnol. J.* **11**, 1498–1512 (2016).
214. Sia, S. K. & Whitesides, G. M. Microfluidic devices fabricated in poly (dimethylsiloxane) for biological studies. *Electrophoresis* **24**, 3563–3576 (2003).
215. Nam, K.-H. *et al.* Continuous-flow fractionation of animal cells in microfluidic device using aqueous two-phase extraction. *Biomed. Microdevices* **7**, 189–195 (2005).
216. Knight, J. B., Vishwanath, A., Brody, J. P. & Austin, R. H. Hydrodynamic focusing on a silicon chip: mixing nanoliters in microseconds. *Phys. Rev. Lett.* **80**, 3863 (1998).
217. Meagher, R. J., Light, Y. K. & Singh, A. K. Rapid, continuous purification of proteins in a microfluidic device using genetically-engineered partition tags. *Lab Chip* **8**, 527–532 (2008).
218. Hahn, T., Münchow, G. & Hardt, S. Electrophoretic transport of biomolecules across liquid–liquid interfaces. *J. Phys. Condens. Matter* **23**, 184107 (2011).
219. Hu, R. *et al.* Rapid, highly efficient extraction and purification of membrane proteins using a microfluidic continuous-flow based aqueous two-phase system. *J. Chromatogr. A* **1218**, 171–177 (2011).
220. Münchow, G., Hardt, S., Kutter, J. P. & Drese, K. S. Electrophoretic partitioning of proteins in two-phase microflows. *Lab Chip* **7**, 98–102 (2007).
221. Lu, Y., Xia, Y. & Luo, G. Phase separation of parallel laminar flow for aqueous two phase systems in branched microchannel. *Microfluid. Nanofluidics* **10**, 1079–1086 (2011).
222. Ziemecka, I. *et al.* Monodisperse hydrogel microspheres by forced droplet formation in aqueous two-phase systems. *Lab Chip* **11**, 620–624 (2011).

223. Jain, S., Yap, W. T. & Irvine, D. J. Synthesis of protein-loaded hydrogel particles in an aqueous two-phase system for coincident antigen and CpG oligonucleotide delivery to antigen-presenting cells. *Biomacromolecules* **6**, 2590–2600 (2005).
224. Moon, B.-U., Hwang, D. K. & Tsai, S. S. H. Shrinking, growing, and bursting: microfluidic equilibrium control of water-in-water droplets. *Lab Chip* **16**, 2601–2608 (2016).
225. Zhang, L. *et al.* One-Step Microfluidic Fabrication of Polyelectrolyte Microcapsules in Aqueous Conditions for Protein Release. *Angew. Chemie* **128**, 13668–13672 (2016).
226. Choi, Y. H., Song, Y. S. & Kim, D. H. Droplet-based microextraction in the aqueous two-phase system. *J. Chromatogr. A* **1217**, 3723–3728 (2010).
227. Lai, D., Frampton, J. P., Sriram, H. & Takayama, S. Rounded multi-level microchannels with orifices made in one exposure enable aqueous two-phase system droplet microfluidics. *Lab Chip* **11**, 3551–3554 (2011).
228. Sauret, A., Spandagos, C. & Shum, H. C. Fluctuation-induced dynamics of multiphase liquid jets with ultra-low interfacial tension. *Lab Chip* **12**, 3380–3386 (2012).
229. Li, Z., Mak, S. Y., Sauret, A. & Shum, H. C. Syringe-pump-induced fluctuation in all-aqueous microfluidic system implications for flow rate accuracy. *Lab Chip* **14**, 744–749 (2014).
230. Moon, B.-U., Abbasi, N., Jones, S. G., Hwang, D. K. & Tsai, S. S. H. Water-in-Water Droplets by Passive Microfluidic Flow Focusing. *Anal. Chem.* **88**, 3982–3989 (2016).
231. Shang, L., Cheng, Y. & Zhao, Y. Emerging Droplet Microfluidics. *Chem. Rev.* **117**, 7964–8040 (2017).
232. Yeredla, N., Kojima, T., Yang, Y., Takayama, S. & Kanapathipillai, M. Aqueous Two Phase System Assisted Self-Assembled PLGA Microparticles. *Sci. Rep.* **6**, 27736 (2016).
233. Ma, S. *et al.* Fabrication of Microgel Particles with Complex Shape via Selective Polymerization of Aqueous Two-Phase Systems. *Small* **8**, 2356–2360 (2012).
234. Mastiani, M., Seo, S., Jimenez, S. M., Petrozzi, N. & Kim, M. M. Flow Regime Mapping of Aqueous Two-Phase System Droplets in Flow-Focusing Geometries. *Colloids Surfaces A Physicochem. Eng. Asp.* **531**, 111–120 (2017).
235. Mytnyk, S. *et al.* Microcapsules with a permeable hydrogel shell and an aqueous core continuously produced in a 3D microdevice by all-aqueous microfluidics. *RSC Adv.* **7**, 11331–11337 (2017).
236. Cameron, D. E., Bashor, C. J. & Collins, J. J. A brief history of synthetic biology. *Nat Rev Micro* **12**, 381–390 (2014).



237. Ausländer, S. & Fussenegger, M. From gene switches to mammalian designer cells: present and future prospects. *Trends Biotechnol.* **31**, 155–168 (2017).
238. Benner, S. A. Synthetic biology: Act natural. *Nature* **421**, 118 (2003).
239. Pohorille, A. & Deamer, D. Self-assembly and function of primitive cell membranes. *Res. Microbiol.* **160**, 449–456 (2009).
240. Strulson, C. A., Molden, R. C., Keating, C. D. & Bevilacqua, P. C. RNA catalysis through compartmentalization. *Nat Chem* **4**, 941–946 (2012).
241. Dominak, L. M., Gundermann, E. L. & Keating, C. D. Microcompartmentation in artificial cells: pH-induced conformational changes alter protein localization. *Langmuir* **26**, 5697–5705 (2009).
242. Davis, B. W. *et al.* Colocalization and Sequential Enzyme Activity in Aqueous Biphasic Systems: Experiments and Modeling. *Biophys. J.* **109**, 2182–2194 (2017).
243. Zhang, Y., Wu, F., Yuan, W. & Jin, T. Polymersomes of asymmetric bilayer membrane formed by phase-guided assembly. *J. Control. Release* **147**, 413–419 (2010).
244. Norton, I. T. & Frith, W. J. Microstructure design in mixed biopolymer composites. in *Food Hydrocolloids*, 15, 543-553 (2001).
245. Song, Y. S., Choi, Y. H. & Kim, D. H. Microextraction in a tetrabutylammonium bromide/ammonium sulfate aqueous two-phase system and electrohydrodynamic generation of a micro-droplet. *J. Chromatogr. A*, 1162, 180-186 (2007).
246. Corredig, M., Sharafbafi, N. & Kristo, E. Polysaccharide-protein interactions in dairy matrices, control and design of structures. *Food Hydrocoll.*, 25, 1833-1841 (2011).
247. Tan, Y. C., Fisher, J. S., Lee, A. I., Cristini, V. & Lee, A. P. Design of microfluidic channel geometries for the control of droplet volume, chemical concentration, and sorting. *Lab Chip*, 4, 292-298 (2004).
248. Liao, Y. & Lucas, D. A literature review on mechanisms and models for the coalescence process of fluid particles. *Chemical Engineering Science*, 65, 2851-2864 (2010).
249. Di Carlo, D., Irimia, D., Tompkins, R. G. & Toner, M. Continuous inertial focusing, ordering, and separation of particles in microchannels. *Proc. Natl. Acad. Sci. U. S. A.*, 104, 18892-18897 (2007).
250. Bachmann, M. F. & Jennings, G. T. Vaccine delivery: A matter of size, geometry, kinetics and molecular patterns. *Nature Reviews Immunology*, 10, 787-796 (2010).
251. Jiang, H., Wang, Q. & Sun, X. Lymph node targeting strategies to improve vaccination efficacy. *J. Control. Release*, 267, 47-56 (2017).

252. Trevaskis, N. L., Kaminskas, L. M. & Porter, C. J. H. From sewer to saviour-targeting the lymphatic system to promote drug exposure and activity. *Nature Reviews Drug Discovery*, 14, 781–803 (2015).
253. Wiig, H. & Swartz, M. A. Interstitial fluid and lymph formation and transport: Physiological regulation and roles in inflammation and cancer. *Physiological Reviews*, 92, 1005-1060 (2012).
254. Stylianopoulos, T. *et al.* Diffusion of particles in the extracellular matrix: The effect of repulsive electrostatic interactions. *Biophys. J.*, 99, 1342–1349. (2010).
255. Rao, D. A., Forrest, M. L., Alani, A. W. G., Kwon, G. S. & Robinson, J. R. Biodegradable PLGA based nanoparticles for sustained regional lymphatic drug delivery. *J. Pharm. Sci.*, 99, 2018-2031 (2010).
256. Porter, C. J. H. & Charman, S. A. Lymphatic transport of proteins after subcutaneous administration. *Journal of Pharmaceutical Sciences*, 89, 297-310 (2000).
257. Feng, L. *et al.* Roles of dextrans on improving lymphatic drainage for liposomal drug delivery system. *J. Drug Target.*, 18, 168-78 (2010).
258. Irvine, D. J., Hanson, M. C., Rakhra, K. & Tokatlian, T. Synthetic Nanoparticles for Vaccines and Immunotherapy. *Chemical Reviews*, 115, 11109–11146 (2015).
259. Poortinga, A. T. Microcapsules from self-assembled colloidal particles using aqueous phase-separated polymer solutions. *Langmuir*, 24, 1644–1647 (2008).
260. Firoozmand, H., Murray, B. S. & Dickinson, E. Interfacial structuring in a phase-separating mixed biopolymer solution containing colloidal particles. *Langmuir*, 25, 1300–1305 (2009).
261. Nicolai, T. & Murray, B. Particle stabilized water in water emulsions. *Food Hydrocoll.*, 68, 157-163 (2017).
262. Balakrishnan, G., Nicolai, T., Benyahia, L. & Durand, D. Particles trapped at the droplet interface in water-in-water emulsions. *Langmuir*, 28, 5921–5926 (2012).
263. De Freitas, R. A., Nicolai, T., Chassenieux, C. & Benyahia, L. Stabilization of Water-in-Water Emulsions by Polysaccharide-Coated Protein Particles. *Langmuir*, 32, 1227–1232 (2016).
264. Bookstaver, M. L., Tsai, S. J., Bromberg, J. S. & Jewell, C. M. Improving Vaccine and Immunotherapy Design Using Biomaterials. *Trends in Immunology*, 39, 135-150 (2018).
265. Batty, C. J., Tiet, P., Bachelder, E. M. & Ainslie, K. M. Drug Delivery for Cancer Immunotherapy and Vaccines. *Pharm. Nanotechnol.*, 6, 232-244 (2018).
266. Jewell, C. M., Bustamante López, S. C. & Irvine, D. J. In situ engineering of the lymph node microenvironment via intranodal injection of adjuvant-releasing polymer particles. *Proc. Natl. Acad. Sci. U. S. A.*, 108, 15745-15750 (2011).

267. Vijayakumar, K., Gulati, S., Demello, A. J. & Edel, J. B. Rapid cell extraction in aqueous two-phase microdroplet systems. *Chem. Sci.*, 1, 447-452 (2010).
268. Mastiani, M., Firoozi, N., Petrozzi, N., Seo, S. & Kim, M. Polymer-Salt Aqueous Two-Phase System (ATPS) Micro-Droplets for Cell Encapsulation. *Sci. Rep.*, 9, 15561 (2019).
269. Song, Y., Sauret, A. & Shum, H. C. All-aqueous multiphase microfluidics, 7, 061301, *Biomicrofluidics* (2013).
270. Dumas, F., Benoit, J. P., Saulnier, P. & Roger, E. A new method to prepare microparticles based on an Aqueous Two-Phase system (ATPS), without organic solvents. *J. Colloid Interface Sci.*, 599, 642-649 (2021).
271. Choonara, B. F. *et al.* A review of advanced oral drug delivery technologies facilitating the protection and absorption of protein and peptide molecules. *Biotechnology Advances*, 32, 1269-1282 (2014).
272. Kvas, M., Teixeira, A. G., Chiang, B. & Frampton, J. P. Aqueous two-phase system antibody confinement enables cost-effective analysis of protein analytes by sandwich enzyme-linked immunosorbent assay with minimal optical crosstalk. *Analyst*, 145, 5458-5465 (2020).
273. Teixeira, A. G. *et al.* Confinement of Suspension-Cultured Cells in Polyethylene Glycol/Polyethylene Oxide-Albumin Aqueous Two-Phase Systems. *Frontiers in Chemistry*, 7, 441 (2019).
274. Rosa, P. A. J., Ferreira, I. F., Azevedo, A. M. & Aires-Barros, M. R. Aqueous two-phase systems: A viable platform in the manufacturing of biopharmaceuticals. *Journal of Chromatography A*, 1217, 2296-2305 (2010).
275. González-Valdez, J., Mayolo-Deloisa, K. & Rito-Palomares, M. Novel aspects and future trends in the use of aqueous two-phase systems as a bioengineering tool. *Journal of Chemical Technology and Biotechnology*, 93, 1836-1844 (2018).
276. Torres-Acosta, M. A., Mayolo-Deloisa, K., González-Valdez, J. & Rito-Palomares, M. Aqueous Two-Phase Systems at Large Scale: Challenges and Opportunities. *Biotechnology Journal*, 14, e1800117 (2019).
277. Hart, R. A., Lester, P. M., Reifsnyder, D. H., Ogez, J. R. & Builder, S. E. Large Scale, In Situ Isolation of Periplasmic IGF-I from *E. coli*. *Bio/Technology* 12, 1113-1117 (1994).
278. Magalhães, F. F., Tavares, A. P. M. & Freire, M. G. Advances in aqueous biphasic systems for biotechnology applications. *Current Opinion in Green and Sustainable Chemistry*, 27, 100417 (2021).
279. Kruse, T., Kampmann, M., Rüdgel, I. & Greller, G. An alternative downstream process based on aqueous two-phase extraction for the purification of monoclonal antibodies. *Biochem. Eng. J.*, 161, 107703 (2020).

280. Kruse, T., Schmidt, A., Kampmann, M. & Strube, J. Integrated Clarification and Purification of Monoclonal Antibodies by Membrane Based Separation of Aqueous Two-Phase Systems. *Antibodies*, 8, 40 (2019).
281. Persson, J., Andersen, D. C. & Lester, P. M. Evaluation of different primary recovery methods for E. coli-derived recombinant human growth hormone and compatibility with further down-stream purification. *Biotechnol. Bioeng.*, 90, 442-51 (2005).
282. Costa, M. J. L., Cunha, M. T., Cabral, J. M. S. & Aires-Barros, M. R. Scale-up of recombinant cutinase recovery by whole broth extraction with PEG-phosphate aqueous two-phase. *Bioseparation*, 9, 231-238 (2000).
283. Mayerhoff, Z. D. V. L., Roberto, I. C. & Franco, T. T. Purification of xylose reductase from *Candida mogii* in aqueous two-phase systems. *Biochem. Eng. J.*, 18, 217-223 (2004).
284. Mayerhoff, Z. D. V. L., Roberto, I. C. & Franco, T. T. Response surface methodology as an approach to determine the optimal activities of xylose reductase and xylitol dehydrogenase enzymes from *Candida Mogii*. *Appl. Microbiol. Biotechnol.*, 70, 761-767 (2006).
285. Azevedo, A. M. *et al.* Partitioning of human antibodies in polyethylene glycol-sodium citrate aqueous two-phase systems. *Sep. Purif. Technol.*, 65, 14-21 (2009).
286. Azevedo, A. M., Rosa, P. A. J., Ferreira, I. F. & Aires-Barros, M. R. Optimisation of aqueous two-phase extraction of human antibodies. *J. Biotechnol.*, 132, 209-217 (2007).
287. Kornmann, H. & Baer, G. Process for the purification of IL-18 binding protein. (2008).
288. Jani, I. V., Janossy, G., Brown, D. W. G. & Mandy, F. Multiplexed immunoassays by flow cytometry for diagnosis and surveillance of infectious diseases in resource-poor settings. *Lancet Infectious Diseases*, 2, 243-250 (2002).
289. Magliulo, M. *et al.* Development and validation of an ultrasensitive chemiluminescent enzyme immunoassay for aflatoxin M1 in milk. *J. Agric. Food Chem.*, 53, 3300–3305 (2005).
290. Wu, T. L. *et al.* Establishment of ELISA on 384-Well Microplate for AFP, CEA, CA 19-9, CA 15-3, CA 125, and PSA-ACT: Higher Sensitivity and Lower Reagent Cost. *J. Clin. Lab. Anal.* (2003).
291. Spies, P., Chen, G. J. & Gygax, D. Establishment of a miniaturized enzyme-linked immunosorbent assay for human transferrin quantification using an intelligent multifunctional analytical plate. *Anal. Biochem.*, 382, 35-39 (2008).
292. Ozen, M. O. *et al.* Total Microfluidic chip for Multiplexed diagnostics (ToMMx). *Biosens. Bioelectron.*, 150, 111930 (2020).

293. Yoon, J., Lee, E., Kim, J., Han, S. & Chung, S. Generation of digitized microfluidic filling flow by vent control. *Biosens. Bioelectron.*, 92, 465-471. (2017).
294. Torres Delgado, S. M. *et al.* Wirelessly powered and remotely controlled valve-array for highly multiplexed analytical assay automation on a centrifugal microfluidic platform. *Biosens. Bioelectron.*, 109, 214-223 (2018).
295. Sandetskaya, N., Isserstedt-John, N., Kölsch, A., Schattschneider, S. & Kuhlmeier, D. An integrated homogeneous SPARCL<sup>TM</sup> immunoassay for rapid biomarker detection on a chip. *Anal. Methods* 11, 2542–2550 (2019).
296. Kadimisetty, K. *et al.* Automated 4-sample protein immunoassays using 3D-printed microfluidics. *Anal. Methods*, 10, 4000-4006 (2018).
297. Ratajczak, K. & Stobiecka, M. High-performance modified cellulose paper-based biosensors for medical diagnostics and early cancer screening: A concise review. *Carbohydrate Polymers*, 229, 115463 (2020).
298. Safavieh, R. & Juncker, D. Capillarics: Pre-programmed, self-powered microfluidic circuits built from capillary elements. *Lab Chip*, 13, 4180-4189 (2013).
299. Kim, S. J., Paczesny, S., Takayama, S. & Kurabayashi, K. Preprogrammed, parallel on-chip immunoassay using system-level capillarity control. *Anal. Chem.*, 85, 6902–6907 (2013).
300. Kim, S. J., Paczesny, S., Takayama, S. & Kurabayashi, K. Preprogrammed capillarity to passively control system-level sequential and parallel microfluidic flows. *Lab Chip*, 13, 2091–2098 (2013).
301. Ngom, B., Guo, Y., Wang, X. & Bi, D. Development and application of lateral flow test strip technology for detection of infectious agents and chemical contaminants: A review. *Analytical and Bioanalytical Chemistry*, 397, 1113-1135 (2010).
302. Djoba Siawaya, J. F. *et al.* An evaluation of commercial fluorescent bead-based luminex cytokine assays. *PLoS One*, 3, e2535 (2008).
303. Lammie, P. J. *et al.* Development of a new platform for neglected tropical disease surveillance. *Int. J. Parasitol.*, 42, 797-800 (2012).
304. Anderson, J. P. *et al.* Development of a Luminex Bead Based Assay for Diagnosis of Toxocariasis Using Recombinant Antigens Tc-CTL-1 and Tc-TES-26. *PLoS Negl. Trop. Dis.* (2015).
305. Waterboer, T., Sehr, P. & Pawlita, M. Suppression of non-specific binding in serological Luminex assays. *J. Immunol. Methods* (2006).
306. Macbeath, G. Protein microarrays and proteomics. *Nature Genetics* (2002).

307. Vargaftik, N. B., Volkov, B. N. & Voljak, L. D. International Tables of the Surface Tension of Water. *J. Phys. Chem. Ref. Data* **12**, 817–820 (1983).
308. Tongdee, M. *et al.* One-incubation one-hour multiplex ELISA enabled by aqueous two-phase systems. *Analyst*, 145, 3517-3527 (2020).
309. Stobiecka, M. & Hepel, M. Effect of buried potential barrier in label-less electrochemical immunodetection of glutathione and glutathione-capped gold nanoparticles. *Biosens. Bioelectron.*, 26, 3524-3530 (2011).
310. Stobiecka, M., Chalupa, A. & Dworakowska, B. Piezometric biosensors for anti-apoptotic protein survivin based on buried positive-potential barrier and immobilized monoclonal antibodies. *Biosens. Bioelectron.*, 84:37-43 (2016).
311. Diamond, A. D. & Hsu, J. T. Aqueous two-phase systems for biomolecule separation. *Adv Biochem Eng Biotechnol*, 47, 89-135, 1992.
312. Jacinto, M. J. *et al.* Optimization and miniaturization of aqueous two phase systems for the purification of recombinant human immunodeficiency virus-like particles from a CHO cell supernatant. *Sep. Purif. Technol.* **154**, 27–35 (2015).
313. Wang, P., Tan, K. L. & Kang, E. T. Surface modification of poly(tetrafluoroethylene) films via grafting of poly(ethylene glycol) for reduction in protein adsorption. *J. Biomater. Sci. Polym. Ed.* **11**, 169–186 (2000).
314. Lee, J. H., Lee, H. B. & Andrade, J. D. Blood compatibility of polyethylene oxide surfaces. *Progress in Polymer Science* **20**, 1043–1079 (1995).
315. Aqil, A. *et al.* PEO coated magnetic nanoparticles for biomedical application. *Eur. Polym. J.* **44**, 3191–3199 (2008).
316. Francis, G. L. Albumin and mammalian cell culture: Implications for biotechnology applications. *Cytotechnology* **62**, 1–16 (2010).
317. Pei, Y., Wang, J., Wu, K., Xuan, X. & Lu, X. Ionic liquid-based aqueous two-phase extraction of selected proteins. *Sep. Purif. Technol.* **64**, 288–295 (2009).
318. Lu, Y. M., Yang, Y. Z., Zhao, X. D. & Xia, C. B. Bovine serum albumin partitioning in polyethylene glycol (PEG)/potassium citrate aqueous two-phase systems. *Food Bioprod. Process.* **88**, 40–46 (2010).
319. Weston & Parish. New fluorescent dyes for lymphocyte migration studies. Analysis by flow cytometry and fluorescence microscopy. *J. Immunol. Methods*, 133, 87-97 (1990).
320. Suzuki, T., Fujikura, K., Higashiyama, T. & Takata, K. DNA staining for fluorescence and laser confocal microscopy. *J. Histochem. Cytochem.* **45**, 49–53 (1997).
321. Merchuk, J. C., Andrews, B. A. & Asenjo, J. A. Aqueous two-phase systems for protein separation: Studies on phase inversion. *J. Chromatogr. B Biomed. Sci. Appl.*, 711, 285-293 (1998).

322. Frith, W. J. Mixed biopolymer aqueous solutions - Phase behaviour and rheology. *Adv. Colloid Interface Sci.*, 161, 48-60 (2010).
323. Khetani, S. R. & Bhatia, S. N. Microscale culture of human liver cells for drug development. *Nat. Biotechnol.*, 26, 120–126 (2008).
324. Anderson, D. G., Putnam, D., Lavik, E. B., Mahmood, T. A. & Langer, R. Biomaterial microarrays: Rapid, microscale screening of polymer-cell interaction. *Biomaterials*, 26, 4892-4897 (2005).
325. Singhvi, R. *et al.* Engineering cell shape and function. *Science*, 264, 696-698 (1994).
326. Chen, D. S. *et al.* Marked differences in human melanoma antigen-specific T cell responsiveness after vaccination using a functional microarray. *PLoS Med.*, 2, e265 (2005).
327. Chung, B. G., Kang, L. & Khademhosseini, A. Micro- and nanoscale technologies for tissue engineering and drug discovery applications. *Expert Opin. Drug Discov.*, 2, 1653-1668 (2007).
328. Wang, Z., Kim, M. C., Marquez, M. & Thorsen, T. High-density microfluidic arrays for cell cytotoxicity analysis. *Lab Chip*, 7, 740-745 (2007).
329. Choi, C. J. & Cunningham, B. T. A 96-well microplate incorporating a replica molded microfluidic network integrated with photonic crystal biosensors for high throughput kinetic biomolecular interaction analysis. *Lab Chip*, 7, 550-556 (2007).
330. Hancock, R. E. W., Haney, E. F. & Gill, E. E. The immunology of host defence peptides: Beyond antimicrobial activity. *Nature Reviews Immunology*, 16, 321-334 (2016).
331. Petrovsky, N. Novel human polysaccharide adjuvants with dual Th1 and Th2 potentiating activity. *Vaccine*, 24, S2–26-9. (2006).
332. Kumar, S. *et al.* Discovery of inulin acetate as a novel immune-active polymer and vaccine adjuvant: synthesis, material characterization, and biological evaluation as a toll-like receptor-4 agonist. *J. Mater. Chem. B*, 4, 7950-7960 (2016).
333. Moran, H. B. T., Turley, J. L., Andersson, M. & Lavelle, E. C. Immunomodulatory properties of chitosan polymers. *Biomaterials* **184**, 1–9 (2018).
334. Sabatos, C. A. *et al.* A Synaptic Basis for Paracrine Interleukin-2 Signaling during Homotypic T Cell Interaction. *Immunity* **29**, 238–248 (2008).
335. Frampton, J. P., Shi, H., Kao, A., Parent, J. M. & Takayama, S. Delivery of proteases in aqueous two-phase systems enables direct purification of stem cell colonies from feeder cell co-cultures for differentiation into functional cardiomyocytes. *Adv. Healthc. Mater.* **2**, 1440–1444 (2013).

336. Chambers, I. R., Cone, T. R., Oswald-Richter, K. & Drake, W. P. Enzyme-linked immunospot assay (ELISPOT): Quantification of Th-1 cellular immune responses against microbial antigens. *J. Vis. Exp.*, 45, e2221 (2010).
337. Morens, D. M. & Fauci, A. S. Emerging Infectious Diseases: Threats to Human Health and Global Stability. *PLoS Pathog.*, 9, e1003467 (2013).
338. Bloom, D. E. & Cadarette, D. Infectious disease threats in the twenty-first century: Strengthening the global response. *Frontiers in Immunology*, 10, 549 (2019).
339. Maslow, J. N. The cost and challenge of vaccine development for emerging and emergent infectious diseases. *The Lancet Global Health*, 6, e1266-e1267 (2018).
340. Kilbourne, E. D. Influenza pandemics of the 20th century. *Emerging Infectious Diseases*, 12, 9-14 (2006).
341. Cohen, J. What's old is new: 1918 virus matches 2009 H1N1 strain. *Science*, 327, 1563-1564 (2010).
342. Khanna, M., Saxena, L., Gupta, A., Kumar, B. & Rajput, R. Influenza pandemics of 1918 and 2009: A comparative account. *Future Virology*, 8, 335-342 (2013).
343. Wei, C. J. *et al.* Cross-neutralization of 1918 and 2009 influenza viruses: Role of glycans in viral evolution and vaccine design. *Sci. Transl. Med.*, 2, 24, 24ra21 (2010).
344. Xu, R. *et al.* Structural basis of preexisting immunity to the 2009 H1N1 pandemic influenza virus. *Science*, 328, 357-360 (2010).
345. Morens, D. M., Folkers, G. K. & Fauci, A. S. The challenge of emerging and re-emerging infectious diseases. *Nature* **430**, 242–249 (2004).
346. The World Health Organization (WHO). Global Health Estimates (GHE). (2016). Available at: [https://www.who.int/healthinfo/global\\_burden\\_disease/en/](https://www.who.int/healthinfo/global_burden_disease/en/). (Accessed: 4th April 2021)
347. Schmidt, A. C. Progress in respiratory virus vaccine development. *Seminars in Respiratory and Critical Care Medicine*, 32, 527-540 (2011).
348. Tripp, R. A. & Stambas, J. Intervention strategies for seasonal and emerging respiratory viruses with drugs and vaccines targeting viral surface glycoproteins. *Viruses*, 13, 625 (2021).
349. Chiu, C. & Openshaw, P. J. Antiviral B cell and T cell immunity in the lungs. *Nature Immunology*, 16, 18-26 (2015).
350. Hay, M., Thomas, D. W., Craighead, J. L., Economides, C. & Rosenthal, J. Clinical development success rates for investigational drugs. *Nat. Biotechnol.*, 32, 40-51 (2014).
351. Paules, C. I., Eisinger, R. W., Marston, H. D. & Fauci, A. S. What Recent History Has Taught Us About Responding to Emerging Infectious Disease Threats. *Ann. Intern. Med.* **167**, 805–811 (2017).



352. Jung, H. E. & Lee, H. K. Host Protective Immune Responses against Influenza A Virus Infection. *Viruses* **12**, (2020).
353. Centers for Disease Control and Prevention (CDC). Types of Influenza Viruses. (2019). Available at: <https://www.cdc.gov/flu/about/viruses/types.htm>. (Accessed: 4th April 2021)
354. The World Health Organization (WHO). Influenza (Seasonal). (2018). Available at: [https://www.who.int/en/news-room/fact-sheets/detail/influenza-\(seasonal\)](https://www.who.int/en/news-room/fact-sheets/detail/influenza-(seasonal)). (Accessed: 15th February 2021)
355. The World Health Organization (WHO). Immunization. (2019). Available at: <https://www.who.int/news-room/facts-in-pictures/detail/immunization>. (Accessed: 15th February 2021)
356. The World Health Organization (WHO). Smallpox. (2019). Available at: [https://www.who.int/health-topics/smallpox#tab=tab\\_1](https://www.who.int/health-topics/smallpox#tab=tab_1). (Accessed: 15th February 2021)
357. Sridhar, S., Brokstad, K. A. & Cox, R. J. Influenza Vaccination Strategies: Comparing Inactivated and Live Attenuated Influenza Vaccines. *Vaccines* **3**, 373-389 (2015).
358. Nachbagauer, R. *et al.* A chimeric hemagglutinin-based universal influenza virus vaccine approach induces broad and long-lasting immunity in a randomized, placebo-controlled phase I trial. *Nat. Med.*, **27**, 106-114 (2021).
359. Pollard, A. J. & Bijker, E. M. A guide to vaccinology: from basic principles to new developments. *Nature Reviews Immunology*, **21**, 83-100 (2020).
360. Pulendran, B., S. Arunachalam, P. & O'Hagan, D. T. Emerging concepts in the science of vaccine adjuvants. *Nature Reviews Drug Discovery*, **20**, 454-475 (2021).
361. Moser, B. A. *et al.* Increased vaccine tolerability and protection via NF- $\kappa$ B modulation. *Sci. Adv.*, **6**, eaaz8700 (2020).
362. Shi, S. *et al.* Vaccine adjuvants: Understanding the structure and mechanism of adjuvanticity. *Vaccine*, **37**, 3167-3178 (2019).
363. Kang, S. M. & Compans, R. W. Host responses from innate to adaptive immunity after vaccination: Molecular and cellular events. *Molecules and Cells*, **27**, 5-14. (2009).
364. Garçon, N. & Di Pasquale, A. From discovery to licensure, the Adjuvant System story. *Human Vaccines and Immunotherapeutics*, **13**, 19-33 (2017).
365. Garçon, N., Leroux-Roels, G. & Cheng, W. F. Vaccine adjuvants. *Perspect. Vaccinol.*, **1**, 89-113 (2011).
366. Duthie, M. S., Windish, H. P., Fox, C. B. & Reed, S. G. Use of defined TLR ligands as adjuvants within human vaccines. *Immunol. Rev.*, **239**, 178-196 (2011).

367. Medzhitov, R. Toll-like receptors and innate immunity. *Nature Reviews Immunology*, 1, 135-145 (2001).
368. Akira, S. & Takeda, K. Toll-like receptor signalling. *Nature Reviews Immunology*, 4, 499-511 (2004).
369. Kawai, T. & Akira, S. Signaling to NF-kappaB by Toll-like receptors. *Trends Mol. Med.* **13**, 460–469 (2007).
370. Janeway, C. A. & Medzhitov, R. Innate immune recognition. *Annual Review of Immunology*, 20,197-216 (2002).
371. Tan, A. C. L. *et al.* Intranasal administration of the TLR2 agonist pam2Cys provides rapid protection against influenza in mice. *Mol. Pharm.*, 9, 2710-2718 (2012).
372. Cobbin, J. C. A., Zeng, W., Jackson, D. C. & Brown, L. E. Different arms of the adaptive immune system induced by a combination vaccine work in concert to provide enhanced clearance of influenza. *PLoS One*, 9, e115356 (2014).
373. Overton, E. T. *et al.* Intranasal seasonal influenza vaccine and a TLR-3 agonist, rintatolimod, induced cross-reactive IgA antibody formation against avian H5N1 and H7N9 influenza HA in humans. *Vaccine*, 32, 5490-5495 (2014).
374. Lau, Y.-F., Tang, L.-H., McCall, A. W., Ooi, E.-E. & Subbarao, K. An Adjuvant for the Induction of Potent, Protective Humoral Responses to an H5N1 Influenza Virus Vaccine with Antigen-Sparing Effect in Mice. *J. Virol.*, 84, 8639-8649 (2010).
375. Behzad, H. *et al.* GLA-SE, a synthetic toll-like receptor 4 agonist, enhances T-cell responses to influenza vaccine in older adults. *J. Infect. Dis.*, 205, 466-473 (2012).
376. Abdul-Careem, M. F. *et al.* FimH, a TLR4 ligand, induces innate antiviral responses in the lung leading to protection against lethal influenza infection in mice. *Antiviral Res.*, 92, 346-355 (2011).
377. Goff, P. H. *et al.* Synthetic Toll-Like Receptor 4 (TLR4) and TLR7 Ligands as Influenza Virus Vaccine Adjuvants Induce Rapid, Sustained, and Broadly Protective Responses. *J. Virol.*, 89, 3221-3235 (2015).
378. Li, C. *et al.* Costimulation with TLR7 agonist imiquimod and inactivated influenza virus particles promotes mouse B cell activation, differentiation, and accelerated antigen specific antibody production. *Front. Immunol.*, 9, 2370 (2018).
379. Zhang, A. J. X. *et al.* Toll-like receptor 7 agonist imiquimod in combination with influenza vaccine expedites and augments humoral immune responses against Influenza A(H1N1)pdm09 Virus Infection in BALB/c mice. *Clin. Vaccine Immunol.*, 21, 570-579 (2014).
380. Jiang, T. *et al.* CpG oligodeoxynucleotides protect against the 2009 H1N1 pandemic influenza virus infection in a murine model. *Antiviral Res.*, 89, 124-126 (2011).

381. Soema, P. C. *et al.* Influenza T-cell epitope-loaded virosomes adjuvanted with CpG as a potential influenza vaccine. *Pharm. Res.*, 32, 1505-1515 (2015).
382. Li Pira, G., Ivaldi, F., Bottone, L. & Manca, F. High throughput functional microdissection of pathogen-specific T-cell immunity using antigen and lymphocyte arrays. *J. Immunol. Methods*, 326, 22-32 (2007).
383. Li Pira, G. *et al.* Miniaturized and high-throughput assays for analysis of T-cell immunity specific for opportunistic pathogens and HIV. *Clin. Vaccine Immunol.*, 21, 488-495 (2014).
384. Varadarajan, N. *et al.* Rapid, efficient functional characterization and recovery of HIV-specific human CD8 + T cells using microengraving. *Proc. Natl. Acad. Sci. U. S. A.*, 109, 3885-3890 (2012).
385. Hanson, J. *et al.* ELISPOT Assays in 384-Well Format: Up to 30 Data Points with One Million Cells. *Cells*, 4, 71-83 (2015).
386. Blasius, A. L. & Beutler, B. Intracellular Toll-like Receptors. *Immunity*, 32, 305-315 (2010).
387. Mielcarska, M. B., Bossowska-Nowicka, M. & Toka, F. N. Cell Surface Expression of Endosomal Toll-Like Receptors - A Necessity or a Superfluous Duplication? *Frontiers in Immunology*, 11, 620972 (2021).
388. Raman, V. S. *et al.* Applying TLR Synergy in Immunotherapy: Implications in Cutaneous Leishmaniasis. *J. Immunol.*, 185, 1701-1710 (2010).
389. Montamat, G., Leonard, C., Poli, A., Klimek, L. & Ollert, M. CpG Adjuvant in Allergen-Specific Immunotherapy: Finding the Sweet Spot for the Induction of Immune Tolerance. *Frontiers in Immunology*, 12, 590054 (2021).
390. Volpi, C. *et al.* High doses of CpG oligodeoxynucleotides stimulate a tolerogenic TLR9-TRIF pathway. *Nat. Commun.* 4, 1852 (2013).
391. Crawford, T. Q., Jalbert, E., Ndhlovu, L. C. & Barbour, J. D. Concomitant evaluation of PMA+ionomycin-induced kinase phosphorylation and cytokine production in T cell subsets by flow cytometry. *Cytom. Part A*, 85, 268-276 (2014).
392. Ai, W., Li, H., Song, N., Li, L. & Chen, H. Optimal method to stimulate cytokine production and its use in immunotoxicity assessment. *Int. J. Environ. Res. Public Health*, 10, 3834-42 (2013).
393. Liu, H. *et al.* Structure-based programming of lymph-node targeting in molecular vaccines. *Nature*, 507, 519-522 (2014).
394. van der Vusse, G. J. Albumin as fatty acid transporter. in *Drug Metabolism and Pharmacokinetics*, 24, 300-307 (2009).

395. Xia, Y., Chen, E. & Liang, D. Recognition of single - And double-stranded oligonucleotides by bovine serum albumin via nonspecific interactions. *Biomacromolecules*, 11, 3158-3166 (2010).
396. Albertsson, P. Å. Partition studies on nucleic acids. I. Influence of electrolytes, polymer concentration and nucleic acid conformation on the partition in the dextran-polyethylene glycol system. *BBA Sect. Nucleic Acids Protein Synth.*, 103, 1-12 (1965).
397. Das, D., Sidiq, S. & Pal, S. K. A simple quantitative method to study protein-lipopolsaccharide interactions by using liquid crystals. *ChemPhysChem*, 16, 753-60 (2015).
398. David, S. A., Balaram, P. & Mathan, V. I. Characterization of the interaction of lipid A and lipopolysaccharide with human serum albumin: Implications for an endotoxin carrier function for albumin. *J. Endotoxin Res.*, 2, 99-106 (1995).
399. Geselowitz, D. A. & Neckers, L. M. Bovine Serum Albumin Is a Major Oligonucleotide-Binding Protein Found on the Surface of Cultured Cells. *Antisense Res. Dev.*, 5, 213 - 217 (1995).
400. Rykova, E. Y., Pautova, L. V., Yakubov, L. A., Karamyshev, V. N. & Vlassov, V. V. Serum immunoglobulins interact with oligonucleotides. *FEBS Lett.*, 344, 96-98 (1994).
401. Arnedo, A., Espuelas, S. & Irache, J. M. Albumin nanoparticles as carriers for a phosphodiester oligonucleotide. *Int. J. Pharm.*, 244, 59-72 (2002).
402. Patel, N. *et al.* The effect of antisense to NF- $\kappa$ B in an albumin microsphere formulation on the progression of left-ventricular remodeling associated with chronic volume overload in rats. *J. Drug Target.*, 22, 796-804 (2014).
403. Rondeau, P. & Bourdon, E. The glycation of albumin: Structural and functional impacts. *Biochimie*, 93, 645-658 (2011).
404. Pongprayoon, P. & Mori, T. The critical role of dimer formation in monosaccharides binding to human serum albumin. *Phys. Chem. Chem. Phys.*, 20, 3249-3257 (2018).
405. Chen, J. R., Ma, C. & Wong, C. H. Vaccine design of hemagglutinin glycoprotein against influenza. *Trends in Biotechnology*, 29, 426-34 (2011).
406. Wang, C. C. *et al.* Glycans on influenza hemagglutinin affect receptor binding and immune response. *Proc. Natl. Acad. Sci. U. S. A.*, 106, 18137-18142 (2009).
407. Compound Summary - Pam3CSK4. Available at: <https://pubchem.ncbi.nlm.nih.gov/compound/21121326>. (Accessed: 12th August 2021)
408. Compound Summary - Poly I:poly C. Available at: <https://pubchem.ncbi.nlm.nih.gov/compound/135478809>. (Accessed: 12th August 2021)

409. Compound Summary - Lipopolysaccharide. Available at: <https://pubchem.ncbi.nlm.nih.gov/compound/11970143>. (Accessed: 12th August 2021)
410. Compound Summary - Imiquimod. Available at: <https://pubchem.ncbi.nlm.nih.gov/compound/57469>. (Accessed: 12th August 2021)
411. Ingelsson, B. *et al.* Lymphocytes eject interferogenic mitochondrial DNA webs in response to CpG and non-CpG oligodeoxynucleotides of class C. *Proc. Natl. Acad. Sci. U. S. A.*, 115, E478-E487 (2018).
412. McElhaney, J. E. *et al.* T Cell Responses Are Better Correlates of Vaccine Protection in the Elderly. *J. Immunol.*, 176, 6333-63339 (2006).
413. Malyguine, A. M., Strobl, S., Dunham, K., Shurin, M. R. & Sayers, T. J. ELISPOT Assay for Monitoring Cytotoxic T Lymphocytes (CTL) Activity in Cancer Vaccine Clinical Trials. *Cells* (2012).
414. Tsai, M.-C., Teixeira, A. G. & Frampton, J. Microfluidic control of droplet formation from stable emulsions formed by aqueous two-phase systems. *Proc SPIE 10491, Microfluidics, BioMEMs, and Medical Microsystems XVI* (2018).

# APPENDIX A: COPYRIGHT PERMISSION LETTERS

8/11/2021

RightsLink Printable License

## JOHN WILEY AND SONS LICENSE TERMS AND CONDITIONS

Aug 11, 2021

---

This Agreement between Dalhousie University -- Alyne Teixeira ("You") and John Wiley and Sons ("John Wiley and Sons") consists of your license details and the terms and conditions provided by John Wiley and Sons and Copyright Clearance Center.

License Number 5125320298454

License date Aug 10, 2021

Licensed Content  
Publisher John Wiley and Sons

Licensed Content  
Publication Advanced Healthcare Materials

Licensed Content  
Title Emerging Biotechnology Applications of Aqueous Two-Phase Systems

Licensed Content  
Author John P. Frampton, Brendan M. Leung, Jessica Grant-Burt, et al

Licensed Content  
Date Dec 27, 2017

Licensed Content  
Volume 7

Licensed Content  
Issue 6

Licensed Content  
Pages 19

8/11/2021

RightsLink Printable License

Type of use	Dissertation/Thesis
Requestor type	Author of this Wiley article
Format	Print and electronic
Portion	Full article
Will you be translating?	No
Title	DEVELOPMENT OF MICROSCALE IMMUNOASSAYS USING AQUEOUS TWO-PHASE SYSTEMS
Institution name	Dalhousie University
Expected presentation date	Sep 2021
Requestor Location	Dalhousie University 5981 University Ave. PO box 15000 Halifax, NS B3H 4R2 Canada Attn: Dalhousie University
Publisher Tax ID	EU826007151
Total	0.00 CAD
Terms and Conditions	

#### TERMS AND CONDITIONS

This copyrighted material is owned by or exclusively licensed to John Wiley & Sons, Inc. or one of its group companies (each a "Wiley Company") or handled on behalf of a society with which a Wiley Company has exclusive publishing rights in relation to a particular work (collectively "WILEY"). By clicking "accept" in connection with completing this licensing transaction, you agree that the following terms and conditions apply to this transaction (along with the billing and payment terms and conditions established by the Copyright Clearance Center Inc., ("CCC's Billing and Payment terms and conditions"), at the time that

<https://s100.copyright.com/CustomerAdmin/PLF.jsp?ref=b7939626-18ea-4299-81c5-26ee385b6f5f>

2/6

you opened your RightsLink account (these are available at any time at <http://myaccount.copyright.com>).

### Terms and Conditions

- The materials you have requested permission to reproduce or reuse (the "Wiley Materials") are protected by copyright.
- You are hereby granted a personal, non-exclusive, non-sub licensable (on a stand-alone basis), non-transferable, worldwide, limited license to reproduce the Wiley Materials for the purpose specified in the licensing process. This license, and any CONTENT (PDF or image file) purchased as part of your order, is for a one-time use only and limited to any maximum distribution number specified in the license. The first instance of republication or reuse granted by this license must be completed within two years of the date of the grant of this license (although copies prepared before the end date may be distributed thereafter). The Wiley Materials shall not be used in any other manner or for any other purpose, beyond what is granted in the license. Permission is granted subject to an appropriate acknowledgement given to the author, title of the material/book/journal and the publisher. You shall also duplicate the copyright notice that appears in the Wiley publication in your use of the Wiley Material. Permission is also granted on the understanding that nowhere in the text is a previously published source acknowledged for all or part of this Wiley Material. Any third party content is expressly excluded from this permission.
- With respect to the Wiley Materials, all rights are reserved. Except as expressly granted by the terms of the license, no part of the Wiley Materials may be copied, modified, adapted (except for minor reformatting required by the new Publication), translated, reproduced, transferred or distributed, in any form or by any means, and no derivative works may be made based on the Wiley Materials without the prior permission of the respective copyright owner. For STM Signatory Publishers clearing permission under the terms of the [STM Permissions Guidelines](#) only, the terms of the license are extended to include subsequent editions and for editions in other languages, provided such editions are for the work as a whole in situ and does not involve the separate exploitation of the permitted figures or extracts, You may not alter, remove or suppress in any manner any copyright, trademark or other notices displayed by the Wiley Materials. You may not license, rent, sell, loan, lease, pledge, offer as security, transfer or assign the Wiley Materials on a stand-alone basis, or any of the rights granted to you hereunder to any other person.
- The Wiley Materials and all of the intellectual property rights therein shall at all times remain the exclusive property of John Wiley & Sons Inc, the Wiley Companies, or their respective licensors, and your interest therein is only that of having possession of and the right to reproduce the Wiley Materials pursuant to Section 2 herein during the continuance of this Agreement. You agree that you own no right, title or interest in or to the Wiley Materials or any of the intellectual property rights therein. You shall have no rights hereunder other than the license as provided for above in Section 2. No right, license or interest to any trademark, trade name, service mark or other branding ("Marks") of WILEY or its licensors is granted hereunder, and you agree that you shall not assert any such right, license or interest with respect thereto
- NEITHER WILEY NOR ITS LICENSORS MAKES ANY WARRANTY OR REPRESENTATION OF ANY KIND TO YOU OR ANY THIRD PARTY, EXPRESS, IMPLIED OR STATUTORY, WITH RESPECT TO THE MATERIALS



OR THE ACCURACY OF ANY INFORMATION CONTAINED IN THE MATERIALS, INCLUDING, WITHOUT LIMITATION, ANY IMPLIED WARRANTY OF MERCHANTABILITY, ACCURACY, SATISFACTORY QUALITY, FITNESS FOR A PARTICULAR PURPOSE, USABILITY, INTEGRATION OR NON-INFRINGEMENT AND ALL SUCH WARRANTIES ARE HEREBY EXCLUDED BY WILEY AND ITS LICENSORS AND WAIVED BY YOU.

- WILEY shall have the right to terminate this Agreement immediately upon breach of this Agreement by you.
- You shall indemnify, defend and hold harmless WILEY, its Licensors and their respective directors, officers, agents and employees, from and against any actual or threatened claims, demands, causes of action or proceedings arising from any breach of this Agreement by you.
- IN NO EVENT SHALL WILEY OR ITS LICENSORS BE LIABLE TO YOU OR ANY OTHER PARTY OR ANY OTHER PERSON OR ENTITY FOR ANY SPECIAL, CONSEQUENTIAL, INCIDENTAL, INDIRECT, EXEMPLARY OR PUNITIVE DAMAGES, HOWEVER CAUSED, ARISING OUT OF OR IN CONNECTION WITH THE DOWNLOADING, PROVISIONING, VIEWING OR USE OF THE MATERIALS REGARDLESS OF THE FORM OF ACTION, WHETHER FOR BREACH OF CONTRACT, BREACH OF WARRANTY, TORT, NEGLIGENCE, INFRINGEMENT OR OTHERWISE (INCLUDING, WITHOUT LIMITATION, DAMAGES BASED ON LOSS OF PROFITS, DATA, FILES, USE, BUSINESS OPPORTUNITY OR CLAIMS OF THIRD PARTIES), AND WHETHER OR NOT THE PARTY HAS BEEN ADVISED OF THE POSSIBILITY OF SUCH DAMAGES. THIS LIMITATION SHALL APPLY NOTWITHSTANDING ANY FAILURE OF ESSENTIAL PURPOSE OF ANY LIMITED REMEDY PROVIDED HEREIN.
- Should any provision of this Agreement be held by a court of competent jurisdiction to be illegal, invalid, or unenforceable, that provision shall be deemed amended to achieve as nearly as possible the same economic effect as the original provision, and the legality, validity and enforceability of the remaining provisions of this Agreement shall not be affected or impaired thereby.
- The failure of either party to enforce any term or condition of this Agreement shall not constitute a waiver of either party's right to enforce each and every term and condition of this Agreement. No breach under this agreement shall be deemed waived or excused by either party unless such waiver or consent is in writing signed by the party granting such waiver or consent. The waiver by or consent of a party to a breach of any provision of this Agreement shall not operate or be construed as a waiver of or consent to any other or subsequent breach by such other party.
- This Agreement may not be assigned (including by operation of law or otherwise) by you without WILEY's prior written consent.
- Any fee required for this permission shall be non-refundable after thirty (30) days from receipt by the CCC.
- These terms and conditions together with CCC's Billing and Payment terms and conditions (which are incorporated herein) form the entire agreement between you and WILEY concerning this licensing transaction and (in the absence of fraud) supersedes

all prior agreements and representations of the parties, oral or written. This Agreement may not be amended except in writing signed by both parties. This Agreement shall be binding upon and inure to the benefit of the parties' successors, legal representatives, and authorized assigns.

- In the event of any conflict between your obligations established by these terms and conditions and those established by CCC's Billing and Payment terms and conditions, these terms and conditions shall prevail.
- WILEY expressly reserves all rights not specifically granted in the combination of (i) the license details provided by you and accepted in the course of this licensing transaction, (ii) these terms and conditions and (iii) CCC's Billing and Payment terms and conditions.
- This Agreement will be void if the Type of Use, Format, Circulation, or Requestor Type was misrepresented during the licensing process.
- This Agreement shall be governed by and construed in accordance with the laws of the State of New York, USA, without regards to such state's conflict of law rules. Any legal action, suit or proceeding arising out of or relating to these Terms and Conditions or the breach thereof shall be instituted in a court of competent jurisdiction in New York County in the State of New York in the United States of America and each party hereby consents and submits to the personal jurisdiction of such court, waives any objection to venue in such court and consents to service of process by registered or certified mail, return receipt requested, at the last known address of such party.

## WILEY OPEN ACCESS TERMS AND CONDITIONS

Wiley Publishes Open Access Articles in fully Open Access Journals and in Subscription journals offering Online Open. Although most of the fully Open Access journals publish open access articles under the terms of the Creative Commons Attribution (CC BY) License only, the subscription journals and a few of the Open Access Journals offer a choice of Creative Commons Licenses. The license type is clearly identified on the article.

### The Creative Commons Attribution License

The [Creative Commons Attribution License \(CC-BY\)](#) allows users to copy, distribute and transmit an article, adapt the article and make commercial use of the article. The CC-BY license permits commercial and non-

### Creative Commons Attribution Non-Commercial License

The [Creative Commons Attribution Non-Commercial \(CC-BY-NC\) License](#) permits use, distribution and reproduction in any medium, provided the original work is properly cited and is not used for commercial purposes.(see below)

### Creative Commons Attribution-Non-Commercial-NoDerivs License

The [Creative Commons Attribution Non-Commercial-NoDerivs License \(CC-BY-NC-ND\)](#) permits use, distribution and reproduction in any medium, provided the original work is properly cited, is not used for commercial purposes and no modifications or adaptations are made. (see below)

**Use by commercial "for-profit" organizations**

Use of Wiley Open Access articles for commercial, promotional, or marketing purposes requires further explicit permission from Wiley and will be subject to a fee.

Further details can be found on Wiley Online Library  
<http://olabout.wiley.com/WileyCDA/Section/id-410895.html>

**Other Terms and Conditions:**

**v1.10 Last updated September 2015**

Questions? [customercare@copyright.com](mailto:customercare@copyright.com) or +1-855-239-3415 (toll free in the US) or +1-978-646-2777.

---

## Request permission to reuse article

---

Nicole Harris <nicoleh@spie.org>  
To: "alynegteixeira@gmail.com" <alynegteixeira@gmail.com>

Wed, Aug 11, 2021 at 2:28 PM

Dear Alyne,

Thank you for seeking permission from SPIE to reprint material from our publications. SPIE shares the copyright with you, so as author you retain the right to reproduce your paper in part or in whole.

Publisher's permission is hereby granted under the following conditions:

- (1) the material to be used has appeared in our publication without credit or acknowledgment to another source;
- and
- (2) you credit the original SPIE publication. Include the authors' names, title of paper, volume title, SPIE volume number, and year of publication in your credit statement.

Please let me know if I may be of any further assistance.

Best regards,

Nicole

Nicole Harris  
Conference Proceedings Coordinator, SPIE  
1000 20th St.  
Bellingham, WA 98225  
[nicoleh@spie.org](mailto:nicoleh@spie.org)

**JOHN WILEY AND SONS LICENSE  
TERMS AND CONDITIONS**

Aug 11, 2021

---

This Agreement between Dalhousie University -- Alyne Teixeira ("You") and John Wiley and Sons ("John Wiley and Sons") consists of your license details and the terms and conditions provided by John Wiley and Sons and Copyright Clearance Center.

License Number 5125871148880

License date Aug 11, 2021

Licensed Content  
Publisher John Wiley and SonsLicensed Content  
Publication Angewandte Chemie International EditionLicensed Content  
Title One-Step Microfluidic Fabrication of Polyelectrolyte Microcapsules in Aqueous Conditions for Protein ReleaseLicensed Content  
Author Liyuan Zhang, Li-Heng Cai, Philipp S. Lienemann, et alLicensed Content  
Date Sep 26, 2016Licensed Content  
Volume 55Licensed Content  
Issue 43Licensed Content  
Pages 5



8/11/2021

RightsLink Printable License

Type of use	Dissertation/Thesis
Requestor type	University/Academic
Format	Print and electronic
Portion	Figure/table
Number of figures/tables	1
Will you be translating?	No
Title	DEVELOPMENT OF MICROSCALE IMMUNOASSAYS USING AQUEOUS TWO-PHASE SYSTEMS
Institution name	Dalhousie University
Expected presentation date	Sep 2021
Portions	Figure 1 parts a and d (Microfluidic fabrication of polyelectrolyte capsules in aqueous conditions). Page 13471.
Requestor Location	Dalhousie University 5981 University Ave. PO box 15000  Halifax, NS B3H 4R2 Canada Attn: Dalhousie University
Publisher Tax ID	EU826007151
Total	0.00 CAD

Terms and Conditions

#### TERMS AND CONDITIONS

<https://s100.copyright.com/CustomAdmin/PLF.jsp?ref=9a0d0aff-4bod-4b37-b1f2-42526a7d5135>

2/6

This copyrighted material is owned by or exclusively licensed to John Wiley & Sons, Inc. or one of its group companies (each a "Wiley Company") or handled on behalf of a society with which a Wiley Company has exclusive publishing rights in relation to a particular work (collectively "WILEY"). By clicking "accept" in connection with completing this licensing transaction, you agree that the following terms and conditions apply to this transaction (along with the billing and payment terms and conditions established by the Copyright Clearance Center Inc., ("CCC's Billing and Payment terms and conditions"), at the time that you opened your RightsLink account (these are available at any time at <http://myaccount.copyright.com>).

### Terms and Conditions

- The materials you have requested permission to reproduce or reuse (the "Wiley Materials") are protected by copyright.
- You are hereby granted a personal, non-exclusive, non-sub licensable (on a stand-alone basis), non-transferable, worldwide, limited license to reproduce the Wiley Materials for the purpose specified in the licensing process. This license, and any CONTENT (PDF or image file) purchased as part of your order, is for a one-time use only and limited to any maximum distribution number specified in the license. The first instance of republication or reuse granted by this license must be completed within two years of the date of the grant of this license (although copies prepared before the end date may be distributed thereafter). The Wiley Materials shall not be used in any other manner or for any other purpose, beyond what is granted in the license. Permission is granted subject to an appropriate acknowledgement given to the author, title of the material/book/journal and the publisher. You shall also duplicate the copyright notice that appears in the Wiley publication in your use of the Wiley Material. Permission is also granted on the understanding that nowhere in the text is a previously published source acknowledged for all or part of this Wiley Material. Any third party content is expressly excluded from this permission.
- With respect to the Wiley Materials, all rights are reserved. Except as expressly granted by the terms of the license, no part of the Wiley Materials may be copied, modified, adapted (except for minor reformatting required by the new Publication), translated, reproduced, transferred or distributed, in any form or by any means, and no derivative works may be made based on the Wiley Materials without the prior permission of the respective copyright owner. **For STM Signatory Publishers clearing permission under the terms of the [STM Permissions Guidelines](#) only, the terms of the license are extended to include subsequent editions and for editions in other languages, provided such editions are for the work as a whole in situ and does not involve the separate exploitation of the permitted figures or extracts, You may not alter, remove or suppress in any manner any copyright, trademark or other notices displayed by the Wiley Materials. You may not license, rent, sell, loan, lease, pledge, offer as security, transfer or assign the Wiley Materials on a stand-alone basis, or any of the rights granted to you hereunder to any other person.**
- The Wiley Materials and all of the intellectual property rights therein shall at all times remain the exclusive property of John Wiley & Sons Inc, the Wiley Companies, or their respective licensors, and your interest therein is only that of having possession of and the right to reproduce the Wiley Materials pursuant to Section 2 herein during the continuance of this Agreement. You agree that you own no right, title or interest in or to the Wiley Materials or any of the intellectual property rights therein. You shall have no rights hereunder other than the license as provided for above in Section 2. No right,

license or interest to any trademark, trade name, service mark or other branding ("Marks") of WILEY or its licensors is granted hereunder, and you agree that you shall not assert any such right, license or interest with respect thereto

- NEITHER WILEY NOR ITS LICENSORS MAKES ANY WARRANTY OR REPRESENTATION OF ANY KIND TO YOU OR ANY THIRD PARTY, EXPRESS, IMPLIED OR STATUTORY, WITH RESPECT TO THE MATERIALS OR THE ACCURACY OF ANY INFORMATION CONTAINED IN THE MATERIALS, INCLUDING, WITHOUT LIMITATION, ANY IMPLIED WARRANTY OF MERCHANTABILITY, ACCURACY, SATISFACTORY QUALITY, FITNESS FOR A PARTICULAR PURPOSE, USABILITY, INTEGRATION OR NON-INFRINGEMENT AND ALL SUCH WARRANTIES ARE HEREBY EXCLUDED BY WILEY AND ITS LICENSORS AND WAIVED BY YOU.
- WILEY shall have the right to terminate this Agreement immediately upon breach of this Agreement by you.
- You shall indemnify, defend and hold harmless WILEY, its Licensors and their respective directors, officers, agents and employees, from and against any actual or threatened claims, demands, causes of action or proceedings arising from any breach of this Agreement by you.
- IN NO EVENT SHALL WILEY OR ITS LICENSORS BE LIABLE TO YOU OR ANY OTHER PARTY OR ANY OTHER PERSON OR ENTITY FOR ANY SPECIAL, CONSEQUENTIAL, INCIDENTAL, INDIRECT, EXEMPLARY OR PUNITIVE DAMAGES, HOWEVER CAUSED, ARISING OUT OF OR IN CONNECTION WITH THE DOWNLOADING, PROVISIONING, VIEWING OR USE OF THE MATERIALS REGARDLESS OF THE FORM OF ACTION, WHETHER FOR BREACH OF CONTRACT, BREACH OF WARRANTY, TORT, NEGLIGENCE, INFRINGEMENT OR OTHERWISE (INCLUDING, WITHOUT LIMITATION, DAMAGES BASED ON LOSS OF PROFITS, DATA, FILES, USE, BUSINESS OPPORTUNITY OR CLAIMS OF THIRD PARTIES), AND WHETHER OR NOT THE PARTY HAS BEEN ADVISED OF THE POSSIBILITY OF SUCH DAMAGES. THIS LIMITATION SHALL APPLY NOTWITHSTANDING ANY FAILURE OF ESSENTIAL PURPOSE OF ANY LIMITED REMEDY PROVIDED HEREIN.
- Should any provision of this Agreement be held by a court of competent jurisdiction to be illegal, invalid, or unenforceable, that provision shall be deemed amended to achieve as nearly as possible the same economic effect as the original provision, and the legality, validity and enforceability of the remaining provisions of this Agreement shall not be affected or impaired thereby.
- The failure of either party to enforce any term or condition of this Agreement shall not constitute a waiver of either party's right to enforce each and every term and condition of this Agreement. No breach under this agreement shall be deemed waived or excused by either party unless such waiver or consent is in writing signed by the party granting such waiver or consent. The waiver by or consent of a party to a breach of any provision of this Agreement shall not operate or be construed as a waiver of or consent to any other or subsequent breach by such other party.
- This Agreement may not be assigned (including by operation of law or otherwise) by you without WILEY's prior written consent.



- Any fee required for this permission shall be non-refundable after thirty (30) days from receipt by the CCC.
- These terms and conditions together with CCC's Billing and Payment terms and conditions (which are incorporated herein) form the entire agreement between you and WILEY concerning this licensing transaction and (in the absence of fraud) supersedes all prior agreements and representations of the parties, oral or written. This Agreement may not be amended except in writing signed by both parties. This Agreement shall be binding upon and inure to the benefit of the parties' successors, legal representatives, and authorized assigns.
- In the event of any conflict between your obligations established by these terms and conditions and those established by CCC's Billing and Payment terms and conditions, these terms and conditions shall prevail.
- WILEY expressly reserves all rights not specifically granted in the combination of (i) the license details provided by you and accepted in the course of this licensing transaction, (ii) these terms and conditions and (iii) CCC's Billing and Payment terms and conditions.
- This Agreement will be void if the Type of Use, Format, Circulation, or Requestor Type was misrepresented during the licensing process.
- This Agreement shall be governed by and construed in accordance with the laws of the State of New York, USA, without regards to such state's conflict of law rules. Any legal action, suit or proceeding arising out of or relating to these Terms and Conditions or the breach thereof shall be instituted in a court of competent jurisdiction in New York County in the State of New York in the United States of America and each party hereby consents and submits to the personal jurisdiction of such court, waives any objection to venue in such court and consents to service of process by registered or certified mail, return receipt requested, at the last known address of such party.

#### WILEY OPEN ACCESS TERMS AND CONDITIONS

Wiley Publishes Open Access Articles in fully Open Access Journals and in Subscription journals offering Online Open. Although most of the fully Open Access journals publish open access articles under the terms of the Creative Commons Attribution (CC BY) License only, the subscription journals and a few of the Open Access Journals offer a choice of Creative Commons Licenses. The license type is clearly identified on the article.

#### The Creative Commons Attribution License

The [Creative Commons Attribution License \(CC-BY\)](#) allows users to copy, distribute and transmit an article, adapt the article and make commercial use of the article. The CC-BY license permits commercial and non-

#### Creative Commons Attribution Non-Commercial License

The [Creative Commons Attribution Non-Commercial \(CC-BY-NC\) License](#) permits use, distribution and reproduction in any medium, provided the original work is properly cited and is not used for commercial purposes.(see below)

**Creative Commons Attribution-Non-Commercial-NoDerivs License**

The [Creative Commons Attribution Non-Commercial-NoDerivs License](#) (CC-BY-NC-ND) permits use, distribution and reproduction in any medium, provided the original work is properly cited, is not used for commercial purposes and no modifications or adaptations are made. (see below)

**Use by commercial "for-profit" organizations**

Use of Wiley Open Access articles for commercial, promotional, or marketing purposes requires further explicit permission from Wiley and will be subject to a fee.

Further details can be found on Wiley Online Library  
<http://olabout.wiley.com/WileyCDA/Section/id-410895.html>

**Other Terms and Conditions:**

v1.10 Last updated September 2015

Questions? [customercare@copyright.com](mailto:customercare@copyright.com) or +1-855-239-3415 (toll free in the US) or +1-978-646-2777.



This is a License Agreement between Alyne G. Teixeira / Dalhousie University ("User") and Copyright Clearance Center, Inc. ("CCC") on behalf of the Rightsholder identified in the order details below. The license consists of the order details, the CCC Terms and Conditions below, and any Rightsholder Terms and Conditions which are included below.

All payments must be made in full to CCC in accordance with the CCC Terms and Conditions below.

Order Date	11-Aug-2021	Type of Use	Republish in a thesis/dissertation
Order License ID	1139798-1	Publisher	Royal Society of Chemistry
ISSN	2041-6539	Portion	Image/photo/illustration

## LICENSED CONTENT

Publication Title	Chemical science	Rightsholder	Royal Society of Chemistry
Article Title	Rapid cellextraction in aqueous two-phase microdroplet systems	Publication Type	e-Journal
Author/Editor	Royal Society of Chemistry (Great Britain)	Start Page	447
Date	01/01/2010	Issue	4
Language	English	Volume	1
Country	United Kingdom of Great Britain and Northern Ireland	URL	<a href="http://www.rsc.org/Publishing/journals/SC/Index.asp">http://www.rsc.org/Publishing/journals/SC/Index.asp</a>

## REQUEST DETAILS

Portion Type	Image/photo/illustration	Distribution	Canada
Number of images / photos / illustrations	2	Translation	Original language of publication
Format (select all that apply)	Print, Electronic	Copies for the disabled?	No
Who will republish the content?	Academic institution	Minor editing privileges?	No
Duration of Use	Life of current edition	Incidental promotional use?	No
Lifetime Unit Quantity	Up to 499	Currency	CAD
Rights Requested	Main product		

## NEW WORK DETAILS

Title	DEVELOPMENT OF MICROSCALE IMMUNOASSAYS USING AQUEOUS TWO-PHASE SYSTEMS	Institution name	Dalhousie University
Instructor name	Dr. John Frampton	Expected presentation date	2021-09-29

## ADDITIONAL DETAILS



Order reference number	N/A	The requesting person / organization to appear on the license	Alyne G. Teixeira / Dalhousie University
------------------------	-----	---------------------------------------------------------------	------------------------------------------

## REUSE CONTENT DETAILS

Title, description or numeric reference of the portion(s)	Figure 1 (Schematic illustrating device design), page 449. Figure 4 (Cells with Ab-NIPAM conjugate in DEX at a microfluidic T-junction), page 450.	Title of the article/chapter the portion is from	Rapid cellextraction in aqueous two-phase microdroplet systems
Editor of portion(s)	Vijayakumar, Kalpana; Gulati, Shelly; deMello, Andrew J.; Edel, Joshua B.	Author of portion(s)	Vijayakumar, Kalpana; Gulati, Shelly; deMello, Andrew J.; Edel, Joshua B.
Volume of serial or monograph	1	Issue, if republishing an article from a serial	4
Page or page range of portion	447	Publication date of portion	2010-09-07

## CCC Terms and Conditions

1. Description of Service; Defined Terms. This Republication License enables the User to obtain licenses for republication of one or more copyrighted works as described in detail on the relevant Order Confirmation (the "Work(s)"). Copyright Clearance Center, Inc. ("CCC") grants licenses through the Service on behalf of the rightsholder identified on the Order Confirmation (the "Rightsholder"). "Republication", as used herein, generally means the inclusion of a Work, in whole or in part, in a new work or works, also as described on the Order Confirmation. "User", as used herein, means the person or entity making such republication.
2. The terms set forth in the relevant Order Confirmation, and any terms set by the Rightsholder with respect to a particular Work, govern the terms of use of Works in connection with the Service. By using the Service, the person transacting for a republication license on behalf of the User represents and warrants that he/she/it (a) has been duly authorized by the User to accept, and hereby does accept, all such terms and conditions on behalf of User, and (b) shall inform User of all such terms and conditions. In the event such person is a "freelancer" or other third party independent of User and CCC, such party shall be deemed jointly a "User" for purposes of these terms and conditions. In any event, User shall be deemed to have accepted and agreed to all such terms and conditions if User republishes the Work in any fashion.
3. Scope of License; Limitations and Obligations.
  - 3.1. All Works and all rights therein, including copyright rights, remain the sole and exclusive property of the Rightsholder. The license created by the exchange of an Order Confirmation (and/or any invoice) and payment by User of the full amount set forth on that document includes only those rights expressly set forth in the Order Confirmation and in these terms and conditions, and conveys no other rights in the Work(s) to User. All rights not expressly granted are hereby reserved.
  - 3.2. General Payment Terms: You may pay by credit card or through an account with us payable at the end of the month. If you and we agree that you may establish a standing account with CCC, then the following terms apply: Remit Payment to: Copyright Clearance Center, 29118 Network Place, Chicago, IL 60673-1291. Payments Due: Invoices are payable upon their delivery to you (or upon our notice to you that they are available to you for downloading). After 30 days, outstanding amounts will be subject to a service charge of 1-1/2% per month or, if less, the maximum rate allowed by applicable law. Unless otherwise specifically set forth in the Order Confirmation or in a separate written agreement signed by CCC, invoices are due and payable on "net 30" terms. While User may exercise the rights licensed immediately upon issuance of the Order Confirmation, the license is automatically revoked and is null and void, as if it had never been

8/11/2021 <https://marketplace.copyright.com/rs-ui-web/mp/license/84e58877-0647-4890-9db9-9200291c5b9a/7b6be915-4367-4c47-9a13-abdc7d0...>  
issued, if complete payment for the license is not received on a timely basis either from User directly or through a payment agent, such as a credit card company.

- 3.3. Unless otherwise provided in the Order Confirmation, any grant of rights to User (i) is "one-time" (including the editions and product family specified in the license), (ii) is non-exclusive and non-transferable and (iii) is subject to any and all limitations and restrictions (such as, but not limited to, limitations on duration of use or circulation) included in the Order Confirmation or invoice and/or in these terms and conditions. Upon completion of the licensed use, User shall either secure a new permission for further use of the Work(s) or immediately cease any new use of the Work(s) and shall render inaccessible (such as by deleting or by removing or severing links or other locators) any further copies of the Work (except for copies printed on paper in accordance with this license and still in User's stock at the end of such period).
- 3.4. In the event that the material for which a republication license is sought includes third party materials (such as photographs, illustrations, graphs, inserts and similar materials) which are identified in such material as having been used by permission, User is responsible for identifying, and seeking separate licenses (under this Service or otherwise) for, any of such third party materials; without a separate license, such third party materials may not be used.
- 3.5. Use of proper copyright notice for a Work is required as a condition of any license granted under the Service. Unless otherwise provided in the Order Confirmation, a proper copyright notice will read substantially as follows: "Republished with permission of [Rightsholder's name], from [Work's title, author, volume, edition number and year of copyright]; permission conveyed through Copyright Clearance Center, Inc. " Such notice must be provided in a reasonably legible font size and must be placed either immediately adjacent to the Work as used (for example, as part of a by-line or footnote but not as a separate electronic link) or in the place where substantially all other credits or notices for the new work containing the republished Work are located. Failure to include the required notice results in loss to the Rightsholder and CCC, and the User shall be liable to pay liquidated damages for each such failure equal to twice the use fee specified in the Order Confirmation, in addition to the use fee itself and any other fees and charges specified.
- 3.6. User may only make alterations to the Work if and as expressly set forth in the Order Confirmation. No Work may be used in any way that is defamatory, violates the rights of third parties (including such third parties' rights of copyright, privacy, publicity, or other tangible or intangible property), or is otherwise illegal, sexually explicit or obscene. In addition, User may not conjoin a Work with any other material that may result in damage to the reputation of the Rightsholder. User agrees to inform CCC if it becomes aware of any infringement of any rights in a Work and to cooperate with any reasonable request of CCC or the Rightsholder in connection therewith.
4. Indemnity. User hereby indemnifies and agrees to defend the Rightsholder and CCC, and their respective employees and directors, against all claims, liability, damages, costs and expenses, including legal fees and expenses, arising out of any use of a Work beyond the scope of the rights granted herein, or any use of a Work which has been altered in any unauthorized way by User, including claims of defamation or infringement of rights of copyright, publicity, privacy or other tangible or intangible property.
5. Limitation of Liability. UNDER NO CIRCUMSTANCES WILL CCC OR THE RIGHTSHOLDER BE LIABLE FOR ANY DIRECT, INDIRECT, CONSEQUENTIAL OR INCIDENTAL DAMAGES (INCLUDING WITHOUT LIMITATION DAMAGES FOR LOSS OF BUSINESS PROFITS OR INFORMATION, OR FOR BUSINESS INTERRUPTION) ARISING OUT OF THE USE OR INABILITY TO USE A WORK, EVEN IF ONE OF THEM HAS BEEN ADVISED OF THE POSSIBILITY OF SUCH DAMAGES. In any event, the total liability of the Rightsholder and CCC (including their respective employees and directors) shall not exceed the total amount actually paid by User for this license. User assumes full liability for the actions and omissions of its principals, employees, agents, affiliates, successors and assigns.
6. Limited Warranties. THE WORK(S) AND RIGHT(S) ARE PROVIDED "AS IS". CCC HAS THE RIGHT TO GRANT TO USER THE RIGHTS GRANTED IN THE ORDER CONFIRMATION DOCUMENT. CCC AND THE RIGHTSHOLDER DISCLAIM ALL OTHER WARRANTIES RELATING TO THE WORK(S) AND RIGHT(S), EITHER EXPRESS OR IMPLIED, INCLUDING

<https://marketplace.copyright.com/rs-ui-web/mp/license/84e58877-0647-4890-9db9-9200291c5b9a/7b6be915-4367-4c47-9a13-abdc7d0de900>

3/4

WITHOUT LIMITATION IMPLIED WARRANTIES OF MERCHANTABILITY OR FITNESS FOR A PARTICULAR PURPOSE. ADDITIONAL RIGHTS MAY BE REQUIRED TO USE ILLUSTRATIONS, GRAPHS, PHOTOGRAPHS, ABSTRACTS, INSERTS OR OTHER PORTIONS OF THE WORK (AS OPPOSED TO THE ENTIRE WORK) IN A MANNER CONTEMPLATED BY USER; USER UNDERSTANDS AND AGREES THAT NEITHER CCC NOR THE RIGHTSHOLDER MAY HAVE SUCH ADDITIONAL RIGHTS TO GRANT.

7. Effect of Breach. Any failure by User to pay any amount when due, or any use by User of a Work beyond the scope of the license set forth in the Order Confirmation and/or these terms and conditions, shall be a material breach of the license created by the Order Confirmation and these terms and conditions. Any breach not cured within 30 days of written notice thereof shall result in immediate termination of such license without further notice. Any unauthorized (but licensable) use of a Work that is terminated immediately upon notice thereof may be liquidated by payment of the Rightsholder's ordinary license price therefor; any unauthorized (and unlicensable) use that is not terminated immediately for any reason (including, for example, because materials containing the Work cannot reasonably be recalled) will be subject to all remedies available at law or in equity, but in no event to a payment of less than three times the Rightsholder's ordinary license price for the most closely analogous licensable use plus Rightsholder's and/or CCC's costs and expenses incurred in collecting such payment.

8. Miscellaneous.

8.1. User acknowledges that CCC may, from time to time, make changes or additions to the Service or to these terms and conditions, and CCC reserves the right to send notice to the User by electronic mail or otherwise for the purposes of notifying User of such changes or additions; provided that any such changes or additions shall not apply to permissions already secured and paid for.

8.2. Use of User-related information collected through the Service is governed by CCC's privacy policy, available online here: <https://marketplace.copyright.com/rs-ui-web/mp/privacy-policy>

8.3. The licensing transaction described in the Order Confirmation is personal to User. Therefore, User may not assign or transfer to any other person (whether a natural person or an organization of any kind) the license created by the Order Confirmation and these terms and conditions or any rights granted hereunder; provided, however, that User may assign such license in its entirety on written notice to CCC in the event of a transfer of all or substantially all of User's rights in the new material which includes the Work(s) licensed under this Service.

8.4. No amendment or waiver of any terms is binding unless set forth in writing and signed by the parties. The Rightsholder and CCC hereby object to any terms contained in any writing prepared by the User or its principals, employees, agents or affiliates and purporting to govern or otherwise relate to the licensing transaction described in the Order Confirmation, which terms are in any way inconsistent with any terms set forth in the Order Confirmation and/or in these terms and conditions or CCC's standard operating procedures, whether such writing is prepared prior to, simultaneously with or subsequent to the Order Confirmation, and whether such writing appears on a copy of the Order Confirmation or in a separate instrument.

8.5. The licensing transaction described in the Order Confirmation document shall be governed by and construed under the law of the State of New York, USA, without regard to the principles thereof of conflicts of law. Any case, controversy, suit, action, or proceeding arising out of, in connection with, or related to such licensing transaction shall be brought, at CCC's sole discretion, in any federal or state court located in the County of New York, State of New York, USA, or in any federal or state court whose geographical jurisdiction covers the location of the Rightsholder set forth in the Order Confirmation. The parties expressly submit to the personal jurisdiction and venue of each such federal or state court. If you have any comments or questions about the Service or Copyright Clearance Center, please contact us at 978-750-8400 or send an e-mail to [support@copyright.com](mailto:support@copyright.com).



**SPRINGER NATURE LICENSE  
TERMS AND CONDITIONS**

Aug 11, 2021

---

---

This Agreement between Dalhousie University -- Alyne Teixeira ("You") and Springer Nature ("Springer Nature") consists of your license details and the terms and conditions provided by Springer Nature and Copyright Clearance Center.

License Number	5125370289114
License date	Aug 10, 2021
Licensed Content Publisher	Springer Nature
Licensed Content Publication	Nature
Licensed Content Title	The challenge of emerging and re-emerging infectious diseases
Licensed Content Author	David M. Morens et al
Licensed Content Date	Jul 8, 2004
Type of Use	Thesis/Dissertation
Requestor type	academic/university or research institute
Format	print and electronic
Portion	figures/tables/illustrations
Number of figures/tables/illustrations	1

High-res required no

Will you be translating? no

Circulation/distribution 1 - 29

Author of this Springer Nature content no

Title DEVELOPMENT OF MICROSCALE IMMUNOASSAYS USING AQUEOUS TWO-PHASE SYSTEMS

Institution name Dalhousie University

Expected presentation date Sep 2021

Portions Figure 1: Global examples of emerging and re-emerging infectious diseases, some of which are discussed in the main text. Page 243.

Requestor Location Dalhousie University  
5981 University Ave.  
PO box 15000  
Halifax, NS B3H 4R2  
Canada  
Attn: Dalhousie University

Total 0.00 CAD

Terms and Conditions

**Springer Nature Customer Service Centre GmbH  
Terms and Conditions**

This agreement sets out the terms and conditions of the licence (the **Licence**) between you and **Springer Nature Customer Service Centre GmbH** (the **Licensor**). By clicking 'accept' and completing the transaction for the material (**Licensed Material**), you also confirm your acceptance of these terms and conditions.

**1. Grant of License**



1. 1. The Licensor grants you a personal, non-exclusive, non-transferable, world-wide licence to reproduce the Licensed Material for the purpose specified in your order only. Licences are granted for the specific use requested in the order and for no other use, subject to the conditions below.

1. 2. The Licensor warrants that it has, to the best of its knowledge, the rights to license reuse of the Licensed Material. However, you should ensure that the material you are requesting is original to the Licensor and does not carry the copyright of another entity (as credited in the published version).

1. 3. If the credit line on any part of the material you have requested indicates that it was reprinted or adapted with permission from another source, then you should also seek permission from that source to reuse the material.

## 2. Scope of Licence

2. 1. You may only use the Licensed Content in the manner and to the extent permitted by these Ts&Cs and any applicable laws.

2. 2. A separate licence may be required for any additional use of the Licensed Material, e.g. where a licence has been purchased for print only use, separate permission must be obtained for electronic re-use. Similarly, a licence is only valid in the language selected and does not apply for editions in other languages unless additional translation rights have been granted separately in the licence. Any content owned by third parties are expressly excluded from the licence.

2. 3. Similarly, rights for additional components such as custom editions and derivatives require additional permission and may be subject to an additional fee. Please apply to [Journalpermissions@springernature.com](mailto:Journalpermissions@springernature.com)/[bookpermissions@springernature.com](mailto:bookpermissions@springernature.com) for these rights.

2. 4. Where permission has been granted free of charge for material in print, permission may also be granted for any electronic version of that work, provided that the material is incidental to your work as a whole and that the electronic version is essentially equivalent to, or substitutes for, the print version.

2. 5. An alternative scope of licence may apply to signatories of the [STM Permissions Guidelines](#), as amended from time to time.

## 3. Duration of Licence

3. 1. A licence for is valid from the date of purchase ('Licence Date') at the end of the relevant period in the below table:

Scope of Licence	Duration of Licence
Post on a website	12 months
Presentations	12 months
Books and journals	Lifetime of the edition in the language purchased

#### 4. Acknowledgement

4. 1. The Licensor's permission must be acknowledged next to the Licenced Material in print. In electronic form, this acknowledgement must be visible at the same time as the figures/tables/illustrations or abstract, and must be hyperlinked to the journal/book's homepage. Our required acknowledgement format is in the Appendix below.

#### 5. Restrictions on use

5. 1. Use of the Licensed Material may be permitted for incidental promotional use and minor editing privileges e.g. minor adaptations of single figures, changes of format, colour and/or style where the adaptation is credited as set out in Appendix 1 below. Any other changes including but not limited to, cropping, adapting, omitting material that affect the meaning, intention or moral rights of the author are strictly prohibited.

5. 2. You must not use any Licensed Material as part of any design or trademark.

5. 3. Licensed Material may be used in Open Access Publications (OAP) before publication by Springer Nature, but any Licensed Material must be removed from OAP sites prior to final publication.

#### 6. Ownership of Rights

6. 1. Licensed Material remains the property of either Licensor or the relevant third party and any rights not explicitly granted herein are expressly reserved.

#### 7. Warranty

IN NO EVENT SHALL LICENSOR BE LIABLE TO YOU OR ANY OTHER PARTY OR ANY OTHER PERSON OR FOR ANY SPECIAL, CONSEQUENTIAL, INCIDENTAL OR INDIRECT DAMAGES, HOWEVER CAUSED, ARISING OUT OF OR IN CONNECTION WITH THE DOWNLOADING, VIEWING OR USE OF THE MATERIALS REGARDLESS OF THE FORM OF ACTION, WHETHER FOR BREACH OF CONTRACT, BREACH OF WARRANTY, TORT, NEGLIGENCE, INFRINGEMENT OR OTHERWISE (INCLUDING, WITHOUT LIMITATION, DAMAGES BASED ON LOSS OF PROFITS, DATA, FILES, USE, BUSINESS OPPORTUNITY OR CLAIMS OF THIRD PARTIES), AND WHETHER OR NOT THE PARTY HAS BEEN ADVISED OF THE POSSIBILITY OF SUCH DAMAGES. THIS LIMITATION SHALL APPLY NOTWITHSTANDING ANY FAILURE OF ESSENTIAL PURPOSE OF ANY LIMITED REMEDY PROVIDED HEREIN.

#### 8. Limitations

8. 1. **BOOKS ONLY:** Where 'reuse in a dissertation/thesis' has been selected the following terms apply: Print rights of the final author's accepted manuscript (for clarity,

NOT the published version) for up to 100 copies, electronic rights for use only on a personal website or institutional repository as defined by the Sherpa guideline ([www.sherpa.ac.uk/romeo/](http://www.sherpa.ac.uk/romeo/)).

8. 2. For content reuse requests that qualify for permission under the [STM Permissions Guidelines](#), which may be updated from time to time, the STM Permissions Guidelines supersede the terms and conditions contained in this licence.

## 9. Termination and Cancellation

9. 1. Licences will expire after the period shown in Clause 3 (above).

9. 2. Licensee reserves the right to terminate the Licence in the event that payment is not received in full or if there has been a breach of this agreement by you.

### Appendix 1 — Acknowledgements:

#### **For Journal Content:**

Reprinted by permission from [the Licensor]: [Journal Publisher (e.g. Nature/Springer/Palgrave)] [JOURNAL NAME] [REFERENCE CITATION (Article name, Author(s) Name), [COPYRIGHT] (year of publication)]

#### **For Advance Online Publication papers:**

Reprinted by permission from [the Licensor]: [Journal Publisher (e.g. Nature/Springer/Palgrave)] [JOURNAL NAME] [REFERENCE CITATION (Article name, Author(s) Name), [COPYRIGHT] (year of publication), advance online publication, day month year (doi: 10.1038/sj.[JOURNAL ACRONYM])]

#### **For Adaptations/Translations:**

Adapted/Translated by permission from [the Licensor]: [Journal Publisher (e.g. Nature/Springer/Palgrave)] [JOURNAL NAME] [REFERENCE CITATION (Article name, Author(s) Name), [COPYRIGHT] (year of publication)]

**Note: For any republication from the British Journal of Cancer, the following credit line style applies:**

Reprinted/adapted/translated by permission from [the Licensor]: on behalf of Cancer Research UK: : [Journal Publisher (e.g. Nature/Springer/Palgrave)] [JOURNAL NAME] [REFERENCE CITATION (Article name, Author(s) Name), [COPYRIGHT] (year of publication)]

#### **For Advance Online Publication papers:**

Reprinted by permission from The [the Licensor]: on behalf of Cancer Research UK: [Journal Publisher (e.g. Nature/Springer/Palgrave)] [JOURNAL NAME] [REFERENCE CITATION (Article name, Author(s) Name), [COPYRIGHT] (year of publication), advance online publication, day month year (doi: 10.1038/sj.[JOURNAL ACRONYM])]

#### **For Book content:**

Reprinted/adapted by permission from [the Licensor]: [Book Publisher (e.g.

8/11/2021

RightsLink Printable License

Palgrave Macmillan, Springer etc) [Book Title] by [Book author(s)]  
[COPYRIGHT] (year of publication)

**Other Conditions:**

Version 1.3

Questions? [customercare@copyright.com](mailto:customercare@copyright.com) or +1-855-239-3415 (toll free in the US) or  
+1-978-646-2777.

---

---



---

## Request permission to reuse figure

---

**Szandra Sebok (Frontiers Application Support)** <support@frontiersin.org>  
Reply-To: Frontiers Application Support <support@frontiersin.org>  
To: Alyne Teixeira <alynegteixeira@gmail.com>

Thu, Aug 12, 2021 at 12:33 PM

-- Please type your reply above this line --



Your request (573043) has been solved. To reopen this request, reply to this email.

---

**Szandra Sebok (Frontiers Application Support)**

Aug 12, 2021, 17:33 GMT+2

Dear Alyne G. Teixeira,

Thank you for your email and we are delighted that you help make our articles more widely available. However, I do not believe that you need our individual permission or a blanket permission. Our articles are published under CC-BY terms, meaning that commercial re-publication is permitted.

The right to re-produce is subject to any copyright notices appearing in respect of third-party graphics, and is in any case subject to our terms and conditions (<http://www.frontiersin.org/TermsandConditions.aspx>) - notably the requirement to attribute the original publication to Frontiers.

This means that you do not need to ask our individual permission for each article but you do need to check for third-party copyright notices. We are trying to ensure that such notices are kept to a minimum and, hopefully, eliminated.

Best regards,

Szandra Sebok

Application Support Analyst